## *Lifecycle of the Antibacterial Triclosan*

MARIE ANNA SHACKLEFORD

# Lifecycle of the Antibacterial TC

*A thesis submitted in partial fulfilment of the requirements for the degree of Doctor of Philosophy in Durham University by*

Marie Anna Shackleford


Department of Chemistry

Durham University

December 2016

## Abstract

With the rise of liquid soaps, and consumers becoming more environmentally conscious manufacturers have two duties of care; one being to ensure adequate bug inhibition and the other to ensure that an excessive burden is not placed on the environment by any benefit agent.[1,2] Recently there have been concerns about the excessive use of certain benefit agents.[3] It is key to deliver the right amount of TC (TC) to the right place at the right time so that at least the Minimum Inhibitory Concentration is delivered but not to over deliver which causes waste. The antibacterial TC has been studied as a model active ingredient in surfactant systems and on its own to contribute to the understanding of the lifecycle of active ingredients when used in soap formulations.

The effect of TC in sodium dodecyl sulphate (SDS) and sodium laurate (SL) systems has been investigated using a range of physical chemistry techniques including UV-Vis and NMR to determine the increased solubility of TC in surfactant micelles. The effect of TC on the size and shape of SDS micelles has been examined using small angle neutron scattering. The surface tension of TC/ surfactant mixtures was studied to find the effects of TC on the critical micelle concentration (CMC) of the surfactant solutions: TC decreases the CMC of SDS and the effect is pH dependant.

The partitioning of the poorly water soluble TC is dependent on pH as well as the concentration of surfactant. It is important to understand the partitioning in these soap system to understand factors such as bioavailability and deposition. I have proposed a model for partitioning between free TC and TC in micelles, and between anionic and neutral forms based on an NMR study. The phenol form of TC partitions much more strongly into micelles than the phenolate: when there is 1% SDS, there is 700 times more phenol in the micelles than in the bulk, whereas the proportion of phenolate in bulk and micelles is nearly the same.

The partitioning of TC into supported lipid bilayers as models for cell membranes has been investigated by Total Internal Reflection Raman spectroscopy. In these experiments, TC was inserted into the bilayer at high pH and rinsed with low pH buffer. In these conditions TC is very resistant to rinsing from the bilayer. When bilayers with mixtures of lipids close to those found in bacterial cells were treated with TC, the bilayers were removed from the surface.

The work described in this thesis has contributed to the investigation of surfactant systems in combination with TC and can be applied to other active ingredients in similar formulations as part of product development. I have investigated the state of the active ingredient TC in surfactant formulations through dilution and to delivery to one of the sites of action using appropriate physical chemistry techniques for each stage of the investigation.

## Acknowledgements

I would like to thank my supervisor Colin, for his support and guidance. I would like to thank the Bain group for the supportive and fun work environment; in particular I would like to thank the other TIR-Raman users, Mario Possiwan, Elin Eis and Celine Mercier for their help, training and guidance. Here's hoping that we will not be in Durham to celebrate the spectrometer's 20$^{th}$ birthday! Also in Durham, I would like to recognise Margarita Staykova and Liam Stubbington for their help with fluorescent imaging of supported lipid bilayers.

From Unilever, I would like to thank my supervisors Ian Tucker and Katherine Thompson for their direction and guidance. I would also like to thank Radka Petkova and Andrew Buckley for their help setting up surface tension experiments and SANS experiments.

I would also like to thank all the friends and housemates who have made my time in Durham enjoyable and helped me feel so settled here. I thank my family for their support, care and regular visits to see me and the North East.

## Declaration

I declare that this thesis and the work presented in it are my own and have been generated by me as a result of my original research. Where assistance has been given by others, they are attributed and their contribution to the work is made clear.

## Copyright

## Publications

The following publication was made in the course of this thesis:

M.A. Shackleford, K.M. Thompson, I.M. Tucker, C.D. Bain, Lifecycle of the Antibacterial TC: Understanding partitioning in SDS systems at The Australian Colloid and Interface Society Conference, February 2015

A number of other publications are in preparation based on the work contained in this thesis.

## Abbreviations and Terminology

| Abbreviation | Name |
|---|---|
| **2,4-DCP** | 2,4-Dichlorophenol |
| **2,8-DCDD** | 2,8-Dichlorodibenozo-p-dioxin |
| ***A*** | Absorbance |
| **AFM** | Atomic force microscopy |
| **AI** | Active ingredient |
| $A_m$ | Area per molecule |
| ***B. cerus*** | *Bacillus cereus* |
| ***B. subtilus*** | *Bacillus subtilus* |
| **Brij-58** | Polyethylene glycol hexadecyl ether |
| $C_{12}E_6$ | Hexaethylene glycol monododecyl ether |
| $C_{12}E_8$ | Octaethylene glycol monododecyl ether |
| $C_{12}$**TAB** | Dodecyltrimethylammonium bromide |
| $CaCl_2$ | Calcium chloride |
| **CCD** | Charge-coupled device |
| **Cd** | Cyclodextrin |
| $CDCl_3$ | Deuterated chloroform |
| **CF** | 5(6)-Carboxyfluorescein |
| **Chol** | Cholesterol |
| **CMC** | Critical micelle concentration |
| **CMOS** | Complementary metal-oxide semiconductor |
| **COSY** | Correlation spectroscopy |
| **CSAC** | Critical supramicellar assembly concentration |
| **CTAB** | Certyl trimethyl ammonium bromide |
| $D_2O$ | Deuterium oxide |
| **DAD** | Diode array detector |
| **DEPE** | 1,2-Dielaidoyl-*sn*-glycero-3-phosphoethanolamine |
| **DLS** | Dynamic light scattering |
| **DMPC** | 1,2-Dimyristoyl-*sn*-glycero-3-phosphocholine |
| **DMPG** | 1,2-Dimyristoyl-*sn*-3-[phospho-rac-glycerol] |
| **DOESY** | Diffusion ordered spectroscopy |
| **DOPC** | 1,2-Dioleoyl-*sn*-glycero-3-phosphocholine |
| **DPPC** | 1,2-Dipalmitoyl-*sn*-glycero-3-phosphocholine |

| | |
|---|---|
| **DRM** | Detergent resistant membrane |
| **$Dy(PPP)_2$** | Dysprosium bis-triphosphate |
| ***E. coli*** | *Escherichia coli* |
| **FabI** | Enoyl-acyl carrier protein reductase I |
| **GC** | Gas chromatography |
| **HCl** | Hydrochloric acid |
| **HDPE** | High density polyethene |
| **HEPES** | 4-(2-Hydroxyethyl)-1-piperazineethanesulfonic acid |
| **HMBC** | Hetronuclear multiple-bond correlation spectroscopy |
| **HOMO** | Highest occupied molecule orbital |
| **HPLC** | High performance liquid chromatography |
| **HPβCd** | Hydroxypropyl-β-cyclodextrin |
| **HSQC** | Hetronuclear single quantum coherence |
| **IFT** | Interfacial tension |
| **IR** | Infra-red |
| $K_-$ | Phenolate partition coefficient |
| $K_+$ | Phenol partition coefficient |
| **KCl** | Potassium chloride |
| **KOH** | Potassium hydroxide |
| **LC** | Liquid chromatography |
| **LUMO** | Lowest unoccupied molecular orbital |
| **LUV** | Large unilamellar vesicle |
| **$MDC_{50}$** | Concentration required for 50% membrane damage |
| $m_i$ | The molar concentration of species i |
| **MIC** | Minimum inhibitory concentration |
| **MLV** | Multilamellar vesicle |
| **MS** | Mass spectrometry |
| **$Na_2CO_3$** | Sodium carbonate |
| **$NaHCO_3$** | Sodium hydrogen carbonate |
| **NaOAc** | Sodium acetate |
| **NaOH** | Sodium hydroxide |
| **NMR** | Nuclear magnetic resonance |
| **OAc** | Acetate |
| **PBS** | Phosphate buffered saline |
| **PC** | Phosphatidylcholine |
| **PDA** | Photo diode array |
| **PDMS** | Polydimethylsiloxane |
| **PE** | Phosphatidylethanolamine |
| **PEO** | Polyethylene oxide |
| **PG** | Phospho-(1'-*rac*-glycerol) |
| **pMβCd** | Permethylated-β-cyclodextrin |
| **POPC** | 1-Palmitoyl-2-oleoyl-*sn*-glycero-3-phosphocholine |
| **POPE** | 1-Hexadecanoyl-2-(9Z-octadecenoyl)-*sn*-glycero-3-phosphoethanolamine |
| **POPG** | 1-Hexadecanoyl-2-(9Z-octadecenoyl)-*sn*-glycero-3-phospho-(1'-*rac*-glycerol) |

| | |
|---|---|
| **PPO** | Polypropylene oxide |
| **PVA** | Polyvinyl acetate |
| **PXRD** | Powder X-ray diffraction |
| **QCM** | Quartz crystal microbalance |
| **Rh-DPPE** | Rhodamine B-1,2-dihexadecanoyl-sn-glycero-3-phosphoethanolamine |
| **RMSA** | Refined mean spherical approximation |
| ***S. aureus*** | *Staphylococcus aureus* |
| ***S. epidermis*** | *Staphylococcus epidermis* |
| ***S. mutans*** | *Staphylococcus mutans* |
| **SA** | Supramolecular assemblies |
| **SANS** | Small angle neutron scattering |
| **SDBS** | Sodium dodecyl benzene sulphate |
| **SDS** | Sodium dodecyl sulphate |
| **$SDS_{(mic)}$** | Micellar SDS |
| **SL** | Sodium dodecanoate (Sodium Laurate) |
| **SLB** | Supported lipid bilayer |
| **SLD** | Scattering length density |
| **SM** | Hexadecanoyl Sphingomyelin |
| **SUV** | Small unilamellar vesicle |
| **TC** | TC |
| **$TC_{aq}$** | Aqueous TC in the phenol form |
| **$TC^-_{aq}$** | Aqueous TC in the phenolate form |
| **$TC_{mic}$** | Micellar TC in the phenol form |
| **$TC^-_{mic}$** | Micellar TC in the phenolate form |
| **TEM** | Transmission electron microscope |
| **TGA** | Thermogravimetric analysis |
| **TIR** | Total internal reflection |
| **$T_m$** | Melting transition, the transition from gel phase to fluid phase |
| **Tris** | Tris(hydroxymethyl)aminomethane |
| **Tris.HCl** | Tris(hydroxymethyl)aminomethane hydrochloride |
| **TX-100** | Triton-X100, 4-(1,1,3,3-tetramethylbutyl)phenyl-polyethylene glycol |
| **UV/Vis** | Ultra-violet and visible |
| **WWTP** | Waste water treatment plant |
| $\gamma$ | Interfacial tension |
| $\Gamma_i$ | The surface excess of species i |
| $\delta_i$ | The NMR shift in ppm of species i |
| $\delta_{obs}$ | The observed NMR shift in ppm |
| $\lambda_{max}$ | The wavelength of maximum absorbance |

# Contents

# 1 Introduction

## 1.1 The Importance of Triclosan

### 1.1.1 Introduction

Many different chemicals make up modern consumer products such as soaps, washing powders and cleaning products. Some chemicals are specific to the function of personal care products, whereas others improve the desirability of the product through appearance, fragrance and texture. When these chemicals are combined in the final product, numerous interactions will occur. Multiple questions arise: when there is a low concentration of the active ingredient, where will it interact during the different stages of its lifetime and which parts of the formulations will it reside in preferentially? These will have an impact on the efficacy of the final product. As always, questions of economics come into this as well: how can the smallest amount of product provide the required efficacy?

There is a wide range of different routes this project could have taken, as there are many different active ingredients in any formulation, with specific targets and limitations. The focus has been on Triclosan (TC) (Figure 1.1), a common antimicrobial used in soaps, toothpastes, plastics and deodorants. No one method will be able to fully describe the lifecycle, even for one specific compound, due to the wide range of concentrations and phases. In this project, a variety of different techniques have been used to probe various stages of the 'lifecycle'; from looking at where the active ingredient (AI) goes when applied, to the interactions that occur in the bottle before it reaches the consumer. NMR has been used to calculate partitioning of the active ingredient between bulk and micelles at a range of concentrations, and the rate of exchange. TIR-Raman has been used to study the effect of the active ingredient on models for cell membranes and several techniques have been used to study the effect of TC on the surfactant systems and the properties of TC and surfactant mixtures.

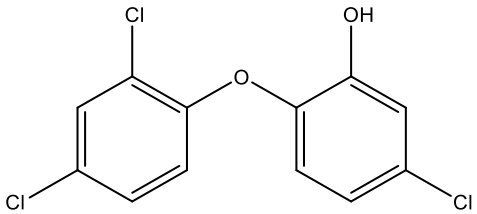


**Figure 1.1 The structure of Triclosan**

TC has an estimated usage around 5 mg per day for Americans[4] and has been used in personal care products since 1968.[5] In Sweden, up to 2 tons of TC a year are used in toothpaste.[6] Other commonly used antibacterial agents include chloroxyphenol,[7] triclocarban[8] and benzalkonium chloride.[9] TC is mildly acidic with a pKa of 7.9[10] and is lipophilic with the log of the octanol/ water partition coefficient (LogP or $K_{o/w}$) being 4.53.[11] The melting point of TC is relatively low at around 56°C.[10] The solid state structure of TC has been determined by two separate authors[7,12–14] to be $P3_1$ (Figure 1.2). TC has the greatest efficacy against gram positive bacteria[15] such as *Staphylococcus aureus*, with a minimal inhibitory concentration (MIC) in the range of 0.01-100 μg/ml, but it is known to be effective against certain strains of gram negative bacteria as well.[16]

Gram-Positive bacteria have been termed such due to the retention of crystal violet dye during gram staining, although there are more common features to this type of bacteria. They have a thick cell wall made up of sheets of peptidoglycan tethered by teichoic acid (Figure 1.3). Gram-negative bacteria have two membranes, an outer membrane and inner membrane with a single peptidoglycan layer between.[17]

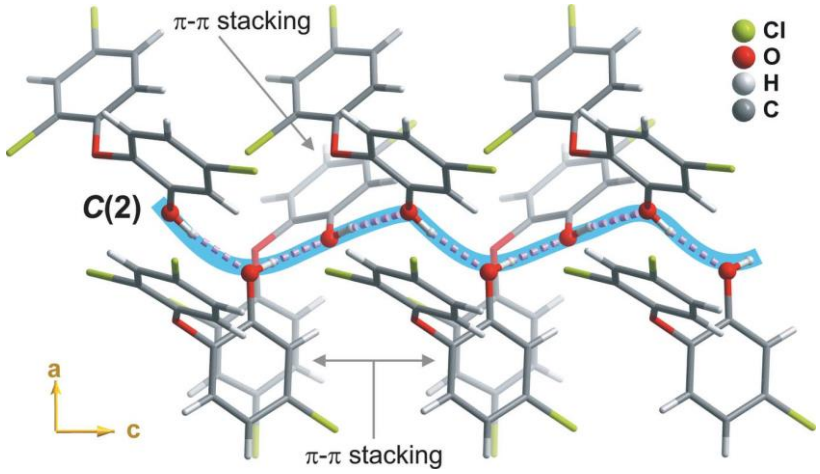


**Figure 1.2 Schematic representation of the O—H--O hydrogen-bonding interactions (dashed lines) connecting adjacent TC molecules along the [001] direction of the unit cell, leading to a supramolecular chain described as a C(2) graph-set motif. The presence of π-π stacking interactions between adjacent molecular units is emphasized.[12] Reproduced with permission of the International Union of Crystallography**

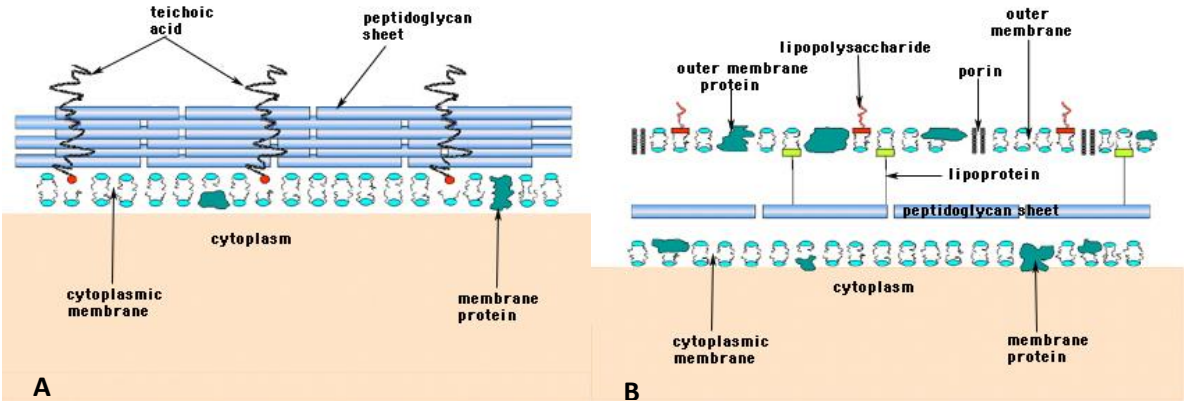


**Figure 1.3 The structure of the Gram-positive (a) and the Gram-negative (b) cell wall.[17]**

### 1.1.2 Mode of Action

A number of investigations have been carried out on the mode of action of TC. It is widely reported that the antibacterial activity of TC is against the enzyme enoyl–acyl carrier protein reductase (FabI),[18–20] which is involved in bacterial fatty acid biosynthesis, which included work by A. Slabbas at Durham.[21] The paper by McMurray[22] was the first to report this mechanism and has been cited 571 times by March 2016 according to Web of Knowledge.[23] The minimum inhibitory concentration (MIC) for FabI is given as 2 µM (0.58 µg/ml) and under experimental conditions with pure FabI in phosphate buffer in solution, catalysis was not observed after three minutes from the addition of TC.[18,24] FabI activity was observed using absorbance at 340 nm. The crystal structure of the TC-FabI complex shows that TC interacts with FabI through the phenol group (Figure 1.4).[25] FabI catalyses the regulatory step of fatty acid synthesis, which is important for cell growth and function.[18]

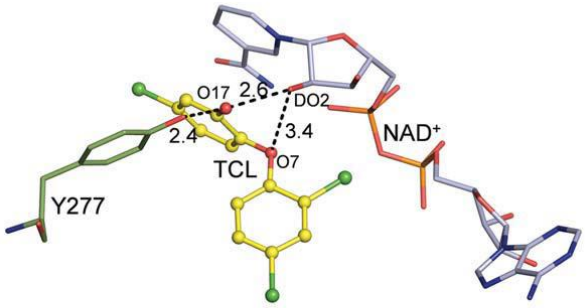


**Figure 1.4 Interactions made by TC with FabI. TC is shown in the ball and stick format (yellow). NAD1 (blue) and amino acid residues (green) of the protein are shown in stick format and water molecules in sphere. The hydrogen bond distances shown in the pictures are in the Å.[25]**

Before the discovery of Heath, Levy and collegues of the activity against FabI,[18,21] it was believed that the major contributor to the bacteriostatic activity of TC was the effect on cell membranes.[16,20] The activity of TC against membranes has been studied in cell membrane models, such as liposomes, and in living cells.[16,20,26–29]

Using models for cell membranes, the gel to liquid-crystalline phase transition temperature for DMPC, DMPG and DEPE decreased in the presence of TC and the main transition was almost eliminated at 30 mol% TC in Lipid.[30] In the liposomes prepared by Jones and colleagues[31–33] the liquid-crystalline transition ($T_m$) was affected by the presence of TC, where at molar ratios of TC to lipid above 0.6, no transition was observed in DPPC. There was improved permeability towards glucose at lower temperatures, due to the increased fluidity of the membranes in the presence of TC.

Lygre[26] used DSC on aqueous liposome suspensions of phosphatidylcholines (PC) to probe the interaction of TC combined with the copolymer polyvinylmethyl ether/ maleic acid and found similar results with the $T_m$ suppressed and noted some domain formation. A magic angle NMR study[34] was used to determine the orientation of TC in multilamellar vesicles of egg yolk lecithin, where the TC hydroxyl group resides close to the headgroup and the rest of the molecule was aligned almost perpendicular with respect to the phospholipid molecule, *i.e.* parallel to the plane of the bilayer.

A molecular dynamics study by Orsi, Noro and Essex[35] used a combination of coarse-grain models of the lipids and water and atomistic models for TC, to find that TC resides at the interface between the headgroup and the glycerol region and orients parallel to the plane of the bilayer in an approximately random distribution (Figure 1.5). They also found that the internal pressure, which contributes to the bilayer area, was affected by the presence of TC at concentrations above 17 mol%, where it appeared that TC acted in a similar way to surfactants in the headgroup region by decreasing the surface tension of the bilayer.

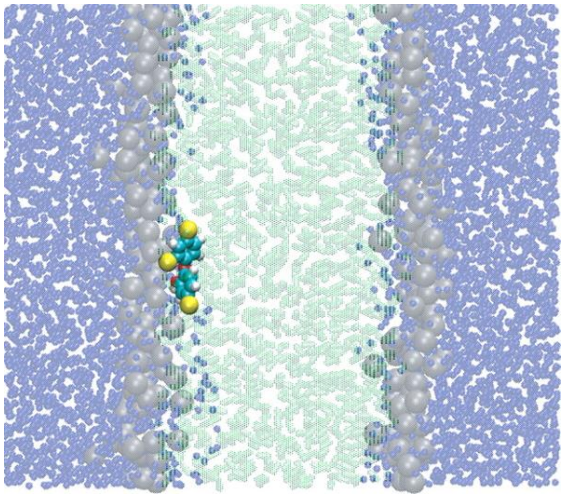

**Figure 1.5 Simulation snapshots from dual-resolution z-constraint simulations. The antimicrobial TC is constrained at a distance of 1.3 nm from the bilayer centre in the lipid glycerol region so the orientation (order parameter) can be determined. CG colour code: water molecules are transparent blue; lipid headgroups are transparent grey; lipid tails are transparent green. AL solute colour code: carbon is cyan; hydrogen is white; oxygen is red; chlorine is yellow.[35]**

Jones, Francis *et al.*[31] found that the TC in proteoliposomes targeted to biofilms inhibited growth of bacteria to a greater extent than free TC where they found that the inhibition effects depended on the concentration of TC available. At low concentrations, liposomes were more effective and at higher concentrations, free TC had a greater inhibition effect.[33]

The direct effect of TC on biofilms models for plaque has been investigated by Corbin[27] using an "*in vitro flow cell oral biofilm model*", where leaching of green fluorescent dye from bacterial cells (*Streptococcus oralis, Streptococcus gordonii* and *Actinomyces naeslundii*) treated with TC was observed. The time taken for the fluorescence to fall to half its intensity was 19 ±13 min when an initial concentration of 0.3 mg/ mL TC at pH 7.4 was used. In this system, some of the TC was delivered in solid form because the total concentration of TC was above the solubility limit in water.

Singh[28] used rapid analysis to find the concentration of agent required for 50% membrane damage of *Bacillus subtilis.* This method uses two separate dyes, one that stains damaged membranes red and another that stains whole cells green. By comparing the two emissions, the ratio of dead to living cells was determined, drug treatment of between 15 and 30 minutes gave 50% membrane damage at 4 µg/mL TC. TC was shown to be membrane active in cells of *E. coli* causing membrane damage to over 50% of the cells at the MIC. The effect of TC on the release of components from human gingival cells was observed by Zukerbraun,[29] where release of lactic acid dehydrogenase was measured and a TC concentration of 1.45 mg/ mL was sufficient to cause 50% leakage. TC was delivered in solutions with ethanol at concentrations below cytotoxic levels. Cell growth was halted at concentrations of TC above 4 µg/mL. The activity of TC against bacterial cell is at lower concentrations that the activity against human cells, which is advantageous when TC is applied. The different cell types will have different cell membrane structures and contain different mixtures of phospholipids. The concentrations at which TC causes membrane damage are slightly higher than the MIC of FabI but are close to the values of MIC quoted by McDonnell[15] and Bhargava.[16]

The effect of TC on biofilms in the aquatic environment has also been studied. The environmental contamination, at levels that are much lower than the MIC of the bacteria noted in the review by Bhargava,[16] between 0.21-280 ng/mL, was sufficient to have an effect on natural biofilms. The

biofilms had decreased surface adhesion and reduced division rates in the presence of TC. A reduced growth rate is the result.[36]

The biofilm structure of dental plaque as observed using an electron microscope is generally compact, heterogeneous and colonial. It consists of many gram-positive cells, the major target of TC. Biofilms can be beneficial in the mouth; for example as pH controllers, reducing the acidity of the environment through the arginine deiminase system and urease, producing ammonia.[37] Some channels in the structure allow transport of molecules through the biofilm, although the distribution is not even.[38] For example, pH has been shown to vary greatly across the mixed biofilms,[39] which may have implications on the activity of TC, a pH-sensitive molecule. Free bacteria and biofilm bacteria of the same species behave differently. One of the key differences is the increased resistance of biofilms to antimicrobials in comparison to free bacteria.[38]

A number of studies have looked at the activity of TC applied directly to the body, on the skin or orally. For example, Loftsson *et al.*[40] investigated the salivary concentration of TC with time and suggested two possible models for the decline of the agent based on previous literature. The first model was based on simple first order kinetics

$$m_t = m_0 e^{-\left(\frac{Ft}{V}\right)} \qquad \text{Equation 1.1}$$

Where $m_0$ is the initial concentration, $F$ is the flow rate and $V$ is the volume of saliva in the mouth. The other suggested model is based on a two-compartment open model

$$m_t = Ae^{-\alpha t} + Be^{-\beta t} \qquad \text{Equation 1.2}$$

where $m_0 = A + B$, $\alpha$ is the hybrid rate constant for the distribution phase and $\beta$ is the rate constant for the elimination of TC by saliva. The two compartments are the distribution phase and the elimination phase. The distribution phase includes the initial rapid contributions from the adsorption and adsorption of TC into oral mucosa and the elimination of TC through the saliva. The elimination phase is the decline in salivary concentration after equilibrium has been reached after the initial distribution. For toothpaste formulations with TC, β-cyclodextrin and carboxylmethyl cellulose, the TC concentration profile within saliva fitted best to the two compartment model, where the TC became distributed across the mouth in 20 minutes and was eliminated with a half-life of around one and a half hours. TC applied in toothpaste formulations without cyclodextrin (Cd) had around 25% retention in the mouth after brushing, with a half-life of 20 min in oral biofilms.[41] Similarly, in saliva TC was still detectable for at least 8 hours after application of TC containing toothpaste.[42]

TC is retained in the mouth after cleaning teeth and rinsing. For antibacterial protection to remain between brushings, sufficient TC must remain in the mouth to prevent bacteria growth. TC in the mouth must be resistant to rinsing through drinking, for example, and resistant to dissolution and removal in the saliva. TC has low water solubility and partitions strongly into lipophilic environments, which will prevent rapid removal of TC from the mouth. TC is stored in the mouth either in the lipophilic environments such as cell membranes, or as small crystals of the solid form.

Nole *et al.*[43] used a variety of methods to establish the efficacy of TC as an ingredient in hand lotion. They found that through the application of a TC-containing lotion, there were detectable amounts of TC on the skin, even after washing the skin a number of times with soap. Hagedorn-Leweke and

Lippold[11] looked directly at the penetration of TC on the skin, and found the permeability to be 0.076 ±0.026 cm $h^{-1}$. The availability of TC between applications is as important on the skin as it is in the mouth for the efficacy and bacterial inhibition during and between applications.

### 1.1.3 TC Solubility

The aqueous solubility of TC is quoted variously as 0.002-0.004 mg/ mL[10] and 0.01 mg/ mL,[44] which is below the MIC for some bacteria.[16] Table 1.1 shows the solubility in different solvents; the highest solubility is in ethanol and chloroform.[45]

**Table 1.1 Experimental solubility of TC in solvents as mole fraction at 25°C.[45]**

| Solvent | Solubility of TC (mole fraction) |
|---|---|
| Ethanol | 0.449 |
| Chloroform | 0.412 |
| Isopropyl mistrate | 0.0475 |
| Octanol | 0.0250 |
| Heptane | 0.286 |

One of the techniques used to improve the solubility of TC in aqueous media, to improve the efficacy, is the use of natural and modified Cd. It is reported that the use of Cd does not affect the ability of TC to interact with the bacterial membranes[8] or improves it.[40] TC most readily forms complexes with βCd as opposed to αCd or γCd (Table 1.2), most likely due to the relative size of the internal cavities, with little interaction seen between TC and γCd.[10,44] The solubility increases to 0.08 mg/ mL at 1% βCd concentration.

Water-soluble polymers have been thought to improve the efficiency of formation for complexes with Cd.[8] For example, in toothpastes, βCd was a slightly poorer solubilizer than the more water soluble derivative, 2-hydroxypropyl-β-cyclodextrin, when used in combination with carboxymethylcelluose.[40] Loftsson[40] reported that use of carboxymethylcelluose in combination with βCd increased the initial concentration and the active lifetime of TC in the mouth. Du Preez[10] showed that for certain bacteria types, TC and βCd had a greater inhibition effect than TC alone, although the authors were not specific as to whether this was simply due to a higher concentration.

Encapsulation is another method suggested in the literature to increase the concentration of TC in solution. For example, Rannard and co-workers[46] used nanoparticles of PVA and SDS and saw an increase activity of TC as compared to aqueous solutions. Elsewhere, chitosan/gelatine microcapsules have been used as carriers of TC, with the release rate being controlled by the amount of chitosan in the walls.[47]

**Table 1.2 Stability constant for the interaction of TC with natural and hydroxypropylated cyclodextrins in water at 25°C (a) increase in TC solubility relative to water.[44]**

| Cyclodextrin | $K_{1:1}$/ $M^{-1}$ | Solubilizing efficiency[a.] |
|---|---|---|
| αCd | 390 | 10.5 |
| βCd | 750 | 6.0 |
| γCd | 20 | 1.5 |
| HPαCd | 3500 | 68.5 |
| HPβCd | 8100 | 123.2 |
| HPγCd | 3970 | 74.2 |

Huang,[48] using micellar electrokinetic chromatography and microemulsion electrokinetic chromatography, noted that the retention time of TC was strongly dependent on the amount of SDS present. There was strong association between TC and the micelles or the microemulsion oil phase, affecting the retention time.

Chiappetta[49] used TC-loaded poloxamine micelles with the idea of enhancing topical activity. TC was combined with the poloxamine T1107 ($M_W$ = 15,000 Da, 70 wt% PEO), which is a branched block copolymer made of blocks of polyethylene oxide (PEO) and polypropylene oxide (PPO) in the pattern PEO-PPO-PEO. This polymer has temperature susceptibility and pH sensitivity. A range of techniques were used to examine the effect the inclusion on the micelle behaviour, such as CMC calculations, dynamic light scattering (DLS) and transmission electron microscopy (TEM). The group[49] found that the size of micelles (at pH 7.4) increased upon TC saturation and with an increase in the concentration of T1107. Micelle fusion occurred in TC saturated systems at 5-10% poloxamine, with much larger aggregates of around 500 nm being observed through DLS. The authors believe that this phenomenon occurs particularly in saturated solutions, where the TC content in the micelles is at the capacity limit.

Chiappetta[49] also reported that, above the CMC, there was a higher drug/core affinity at low pH.[49] This behaviour was ascribed to the formation of hydrogen bonds with the ether linkages in the polymer. At higher pH, when the phenolate is present, these H-bonds do not form and the affinity is decreased. This explanation is in agreement with the work of Mahugo Santana,[50] when studying the extraction of chlorophenol derivatives into a non-ionic surfactant solution. The lower affinity also has implications on the efficacy of TC against FabI, which is shown to be partially through hydrogen bonds.

Du Preez[10] studied a range of solubilizers and their ability to increase the solubility of TC; N-methylglucamine was the most effective solubilizer, surpassing SDS and βCd. N-methylglucamine was thought to form complexes with TC, which was responsible for the improved solubility. The authors also found that mixtures with the best solubilizes did not show the same increase in the bacteriostatic activity. The solubilizers that improved the solubility of TC through micellar trapping caused a partial inactivation of TC. They increase the solubility of TC but not the chemical potential. There was more TC available in the system but the energetics of the interaction with bacteria were not improved to the same extent as other solubilizers.

In Wang's review[51] of the bioavailability of organic compounds in non-ionic surfactant micelles, he concluded that organic compounds solubilized in micelles are not directly available to microbes but

that the improved dissolution of the organic compound leads to increased rates of biotransformation.[52–54] Guha and Jaffé[55] have previously discussed the increased bioavailability of polycyclic aromatic compounds in the presence of non-ionic surfactants above their CMC and proposed a different model. Two separate factors contribute to the increased bioavailability. First, the surfactant increases the solubility of the target and second, the filled surfactant micelles form a hemi-micelle layer on the surface of cells, which allows the solute to diffuse into the cell from the surface. In the experiments by Du Preez[10] with TC in micelles, the micelles behaved in a similar way to the systems reviewed by Wang[51] rather than the system described by Guha and Jaffé.[55] However, in the surfactant/ TC system, the method of application will affect the bioavailability. TC may be applied in a concentrated surfactant solution at a high concentration, which will be diluted upon rinsing in the handwashing process to below the critical micelle concentration which will release TC from the micelles. The excess TC will be unstable in solution and will either crystallise or partition into other lipophilic environments.

There is some data available on the solubility of TC at different pH. The study by Loftsson *et al*.[8] looked at the solubility of TC when combined with βCd with different concentrations of ammonia. When 1 M ammonia solution (pH 11.2) was used, the maximum solubilisation of TC/βCd complex was seen, of 40 mg/ mL. Loftsson[8] measured solubility after samples were left to equilibrate for 6 days and filtered before analysing by HPLC-DAD (High Pressure Liquid Chromatography with Diode Array Detection) in a mixture of acetonitrile and water. They also noted a change in the solubility of TC, when fully ionized in ammonia above pH 10 the inherent solubility increased to 7 mg/ mL. Caution should be used when considering the solubility of TC in ammonia, as Du Preez[10] showed that TC formed complexes with amines which increased the solubility of TC, so the observed solubility enhancement at high pH in ammonia may be caused by several contributing factors and not simply due to full ionisation of TC. Elsewhere, the solubility of TC at pH 12 in PBS solution has been reported as around 1.4 mg/ mL calculated from UV-Vis measurements based on a calibration in methanol.[49]

### 1.1.4 Methods of Detection of TC

A wide range of different methods have been developed for the determination of TC concentration in solution. These have been used at the concentrations appropriate to soap formulations during the active lifetime, and can be adapted as appropriate.

A number of different authors have published studies where HPLC with UV-Vis detection has been used as the principal method of determination.[8,40,56–61] TC has an absorbance maximum around 281 nm in unbuffered water. The wavelength of maximum absorbance of the TC peak ($\lambda_{max}$) depends on the pH of solution, the phenol has a lower $\lambda_{max}$ (283 nm) than the phenolate form (295 nm) (Figure 1.6).[6,8] The peak observed at intermediate pH, when there are both forms of TC in solution, is at an average position depending on the ratio of phenol and phenolate.

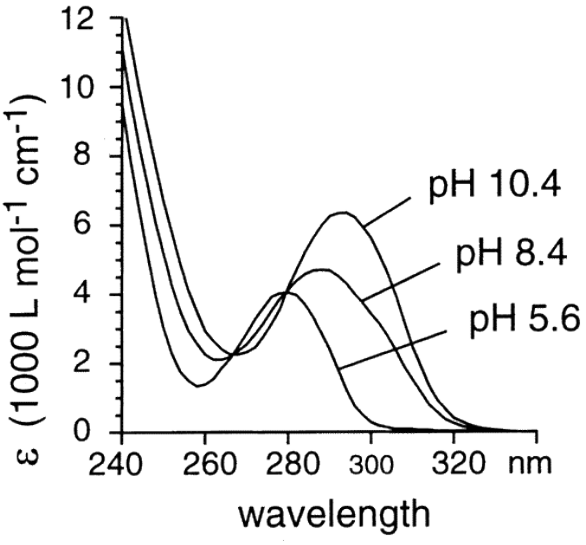


**Figure 1.6 UV spectra of TC at pH 5.6, 8.4, and 10.4. At pH 10.4, the majority of TC is in the phenolate form, whereas at pH 5.6, there is mostly only the phenol form present. Reprinted with permission from Lindström, 2002. Copyright 2002 American Chemical Society.[6]**

Over time methods have been developed to detect lower concentrations of TC in waste water in relations to environmental contamination. These methods generally rely on functionalising TC. One such method involved attaching an azo-group to TC and gave a limit of detection of 0.079 mg/ mL.[59] This method was further developed by Cabaleiro and co-workers[58] to extract the azo-derivative into an ionic liquid and carried out microvolume UV-Vis Spectrophotometry. Using two slightly different methods they could detect concentrations between 0.05-200 µg/ml and 0.02-0.18 µg/ml. A similar method was used by Kysliak and Smyk[62] as an attempt to make the reaction more selective towards TC.

Silva et al.[63] developed the use of stir bar sorptive extraction and liquid desorption followed by HPLC-DAD. Stir bar sorptive extraction is used for sampling a liquid phase based upon sorption of the target onto a coated magnetic stirrer bar, where the partitioning of the target is proportional to the octanol/ water partition coefficient. Stir bars coated with polydimethylsiloxane were placed in waste water or cosmetic samples and the TC was adsorbed by the stir bar. The bar was then removed and placed in a desorption solvent. HPLC-DAD analysis was carried out on the desorption solvent.

These methods are complex and more adapted for detecting low concentrations of TC. These techniques which involve TC functionalisation are less useful for understanding how TC behaves naturally in relation to other formulation ingredients. At the concentrations of TC used in personal care products, simple UV-Vis experiments in water are sufficient to measure the concentration and remove the technical difficultly and errors associated with functionalising or extracting TC.

Mura, Cirri et al.[44] used the fluorescence spectra of TC, with excitation and emission peaks at 325 nm and 365 nm, as an alternative to absorbance measurements to quantify the increased solubility of TC in the presence of cyclodextrins. Aufiero, Butler and Jaser[56] used an excitation wavelength of 290 nm and the emission wavelength 340 nm for fluorescence spectroscopy, with a detection limit of 0.02 mg/ mL.

### 1.1.5 The Synthesis of TC

The patent of Lourens[64] from the Dow Chemical company describes two synthetic methods used to produce TC. Lourens described a synthesis from 1,4-dichlororbenzene and 2,4-dichlorophenol via 1-(5-chloro-2-dichlorophenoxy)phenyl)ethanone. The process contains four major steps: acylation of the para-dichlorobenzene, an Ulman ether synthesis, a Baeyer-Villager esterification and transesterification. An earlier synthesis which was proposed by Schreiber and Marky from Ciba-Geigy Corparation[65] which went from the same starting products via 5-chloro-2-(2',4'-dicholorphenoxy)aniline. TC produced using the Ciba-Geigy process is harder to purify than the Lourens TC, requiring up to six extractions, distillation and crystallisation.[66] Another advantage to the Lourens process is that no dibenzofurans are produced, which are produced in the Ciba-Geigy process (Table1.3).[64,66] Dibenzofurans are toxic and possible carcinogens.[67]

**Table 1.3 Comparison of two different patented methods to produce TC a. Schreiber and Markey 1983[65] b. Lourens 1999.[64]**

| Process | Ciba-Geigy[a.] | Lourens[b.] |
|---|---|---|
| Staring materials | 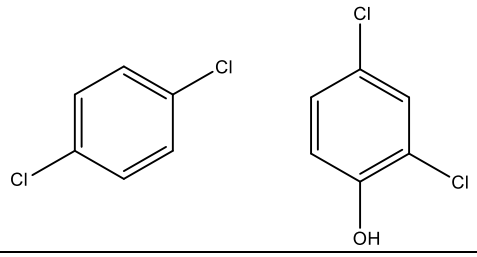 | 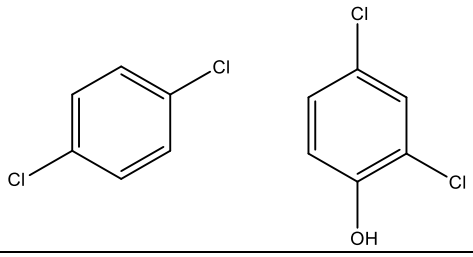 |
| Key intermediates | 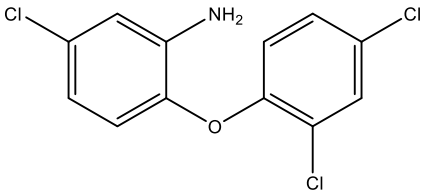 | 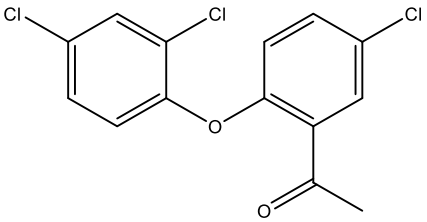 |
| Side Products | 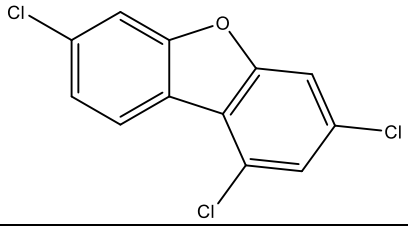 | 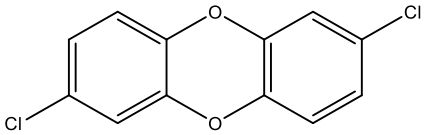 |

### 1.1.6 The Future of TC

During the course of this project, international opinion of TC in personal care products has changed and markets are moving away from using TC in soaps and cleansing products. Unilever released a statement in 2013 stating that, whilst there was no basis to stop using antibacterial ingredients, TC was to be phased out of soaps by the end of 2015 and should be removed from oral care products by the end of 2017.[68]

In 2014, the state of Minnesota issued a ban on TC containing products that "*are used for hand or body cleansing*" starting in January 2017.[3] Following this, a number of other states have issued bans for TC containing products, including Iowa.[69] These bans do not include products approved by the FDA for consumer use, such as TC containing toothpastes. The EU withdrew the approval for TC from 16th February 2016.[70]

In response to these bans, Colegate issued a report through their professional dentistry network to refute some of the safety worries cited in Minnesota.[71] The report was also designed to defend the continued use of TC in Colegate Total toothpaste products, where there have been proven health benefits.[42] In the report, Colegate state that many of the worries about TC overuse are unfounded. For example, there are concerns about the build-up of TC in humans due to long term exposure. However, TC absorbed into the body is almost completely eliminated by the kidneys and the half-life is between 10 and 20 hours. TC has not been shown to accumulate in humans and no adverse clinical effects have been observed.[72,73] A recent article by Yueh,[74] reported that TC is a liver tumour promoter based on experiments with mice combined at high concentrations, 0.2 mg/mL in all water consumed, with a known carcinogen. It was widely publicised[75,76] and in an article on the NHS website[77] the impact of the article was investigated further and the results were summarised for a lay audience. The response from the NHS stated that the testing scenario was different to the route of human exposure to TC and that mice are a useful research models for mammals but results collected in mice are not directly comparable to human biology.

Another risk of overuse of TC is the possibility of antibacterial resistance, although in domestic and clinical setting TC has not been shown to increase resistance.[72,78,79] In some laboratory experiments with TC, a number of resistant bacteria have developed, *E.coli* being a commonly studied one.[80] A number of other bacteria use efflux pumps and membrane permeability barriers to reduce the effect of TC. However, naturally occurring *Staphylococci* do not appear to show strong resistance to TC.[20] The 2011 review by Dann and Hontela[73] contains several useful tables of information from studies carried out on the effects of TC, included aquatic concentrations, the concentrations of TC detected in aquatic organisms, the effect of TC on aquatic organisms and a summary of the investigations into the endocrine-disrupting effects of TC.

Environmental contamination of TC and its degradation products has been a concern for a number of years, with small amounts of TC detected in many natural water sources.[5,6,81–83] TC enters the environment mostly through effluent from waste-water treatment plants. In the study by Tixier,[84] 6% of the TC that entered waste water treatment plant plants in the Lake Greifensee area in Switzerland left in the effluent at a concentration of 42 ng $dm^{-3}$. 79% of the input TC was biologically degraded and 15% sorbed onto the sludge. Environmental contamination is a cause for concern from TC overuse, as it is for any chemical that enters waste water.

TC in the environment is degraded in a number of ways. For example, up to 12% TC is degraded in river water by surface sunlight to 2,8-dichlorodibenzo-p-dioxin (2,8-DCDD).[82] 2,8-DCDD is a chemical of concern due to toxicity.[82,85] Methyl-TC is another major photoproduct of TC.[6] Methyl-TC is also a major biodegradation product, which occurs in aerobic conditions with bacteria such as *Sphingomonas sp.*, that are not disrupted by TC.[5,86,87] In their review, Bedoux *et al.*[5] created a lifecycle of TC in the aquatic environment (Figure 1.7), showing the route TC takes after home use and how it can re-enter drinking water.

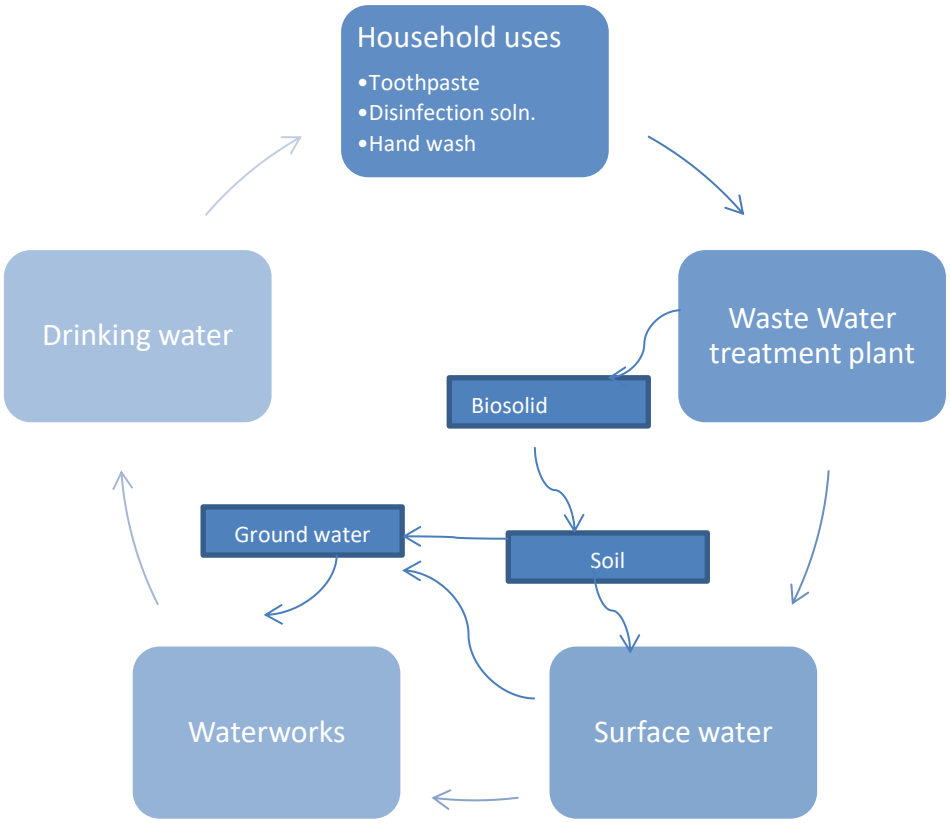


**Figure 1.7 Lifecycle of TC in the aquatic environment. Adapted from Bedoux 2012.[5]**

There is debate about the effectiveness of TC containing household soaps when they are compared to plain soaps. One of the most recent papers on this subject[88] showed no significant difference in the bactericidal activity of plain soaps compared to TC containing soaps with the results reported by a number of news sources and discussed by the general public.[89,90] A number of other authors have found similar results in studies on both rates of infection in groups using different soap types[91] and in bacterial counts on hands.[92,93] Levy[94] published a comprehensive review in 2007, where five out of nine studies showed a reduction in the bacterial counts upon handwashing with TC but the studies that looked at disease outcomes from community intervention studies showed no significant difference between soap types. It should be noted, in clinical settings when used at 1% in soap formulations, TC has proven efficacy.[95] The efficacy of TC in consumer hand soaps is inconclusive. Whilst it may lower bacterial counts on hands after treatment, this does not necessarily transfer to reduced disease outcomes. It remains that the most effective way to prevent spread of disease through basic hygiene practises is to scrub hands with any soap, for 20 s, rinse and dry.[96]

In the next few years, TC use globally will decrease, although TC will continue to be used in toothpastes and in clinical settings. However, much of the research into the efficacy and effects of TC should be used when considering replacements. For example, many of the techniques detailed and developed in this thesis can be used to study other antimicrobials with similar structures. The results can also be used to inform research and development programs when formulating with antibacterial compounds and inform the formulation of new antibacterial soaps. It is clear that the whole lifecycle of chemical should be considered when it is released for mass consumer use to prevent the issues caused by TC overuse such as environmental contamination.

## 1.2 Surfactant Systems

The suggested formulation space for TC in personal care products is at 0.1% weight in 1% sodium dodecyl sulphate (SDS) or 1% sodium laurate (SL), as these are often the concentrations in complete formulations (Figure 1.8).[97] Generally, in personal care products, the concentration of SDS is limited to 2.5% and the EU imposed a limit of 0.3% TC in domestic washes and gels,[72] so concentrations above these limits are less relevant to the real life applications. At these concentrations, both surfactants are in the micelle phase.[98,99] Cellulose-based polymers are used to improve the final rheology of liquid soap products to give their distinctive feel.[100]

Toothpastes have a wide range of pHs depending on the active and added ingredients. Largely, the pH is formulated to be between pH 7 and pH 10.[101] A study in the year 2000 of nine whitening toothpastes showed a range of pH values between 4.2 and 8.4.[102] In Colegate Total (Colegate Palmolive) products, where the active ingredients are sodium fluoride and TC, the pH is formulated to remain around 7, although across their product range the pH of toothpastes varies between 5.6 and 8.9.[103]

On the U.S. Department of Health website there are 441 listed personal care products that contain SDS and it is commonly used in soap products in a liquid or paste form.[104] Sodium laurate has many fewer references on the Department of Health's website, with only 14 listed personal care products, of which almost all are solid soap bars.[105]

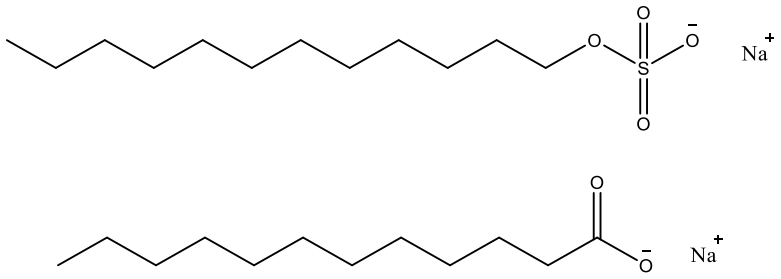


**Figure 1.8 The structures of SDS and SL**

The critical micelle concentration (CMC) is the concentration range at which the surfactant molecules begin to form small aggregates in solution, called micelles. Moroi defines the CMC as

> *"the narrow concentration range over which surfactant solutions show an abrupt change in physiochemical properties."*[106]

Other authors define the CMC differently. Williams and Phillips[107] use two separate definitions, the first is the concentration at which the two straight lines above and below the CMC intersect with one another and the second is the concentration at which the change in gradient in the solution properties is highest. Corrin[108] used a CMC defined as the total surfactant concentration at which a small defined amount of surfactant is in the aggregated form. Israelachvili[109] used the definition as the concentration at which the concentration of micellar surfactant was equal to the monomer concentration.

### 1.2.1 Sodium Dodecyl Sulphate

Sodium dodecyl sulphate (SDS) is an anionic surfactant used in shampoos, hand washes and toothpastes.[100,103] The pKa of the conjugate acid of SDS is 3.3.[110] The CMC of SDS in water is around

8 mM.[111] When salt is present, the CMC of SDS decreases and the micelle size increases.[112,113] For anionic systems such as SDS, the electrostatic interactions between the headgroups limit the adsorption at the interface and the area per molecule. In salt solutions, the electrostatic interactions are shielded so that the surfactant can become closer packed on the surface. Increasing the salt in anionic surfactant solutions increases the efficiency of the surfactant and decreases the CMC.[114] The shape of the micelles similarly depends on the concentration of salt. At low concentrations of salt, SDS micelles are spherical and as the concentration of salt increases, the micelles become ellipsoidal or rodlike.[115,116] Most commercial samples of SDS are contaminated with dodecanol, which affects properties such as the CMC and surface tension of SDS solutions.[111,117] A number of methods have been developed to remove the excess dodecanol for laboratory experiments to improve measurement accuracy.[111,112,118–120] The phase diagram of SDS in water is shown below (Figure 1.9 and Figure 1.10). Below 40 wt%, SDS is in the micellar phase. Between 39% and 57%, SDS is in the hexagonal phase and above 87% SDS is in the crystal phase. At higher temperatures, above 50°C, the lamellar phase forms for concentrations of SDS above 70%.

Uses of SDS other than in personal care products include biological applications such as lysing cells and unravelling proteins in SDS-PAGE gels. SDS has also been approved for use in pesticides and food products as an emulsifying agent.[121,122]

SDS is synthesised from dodecanol which is obtained from palm kernel oil and coconut oil by hydrogenation. The fatty acids are treated with sulphur trioxide and neutralised with sodium hydroxide.[123–125]

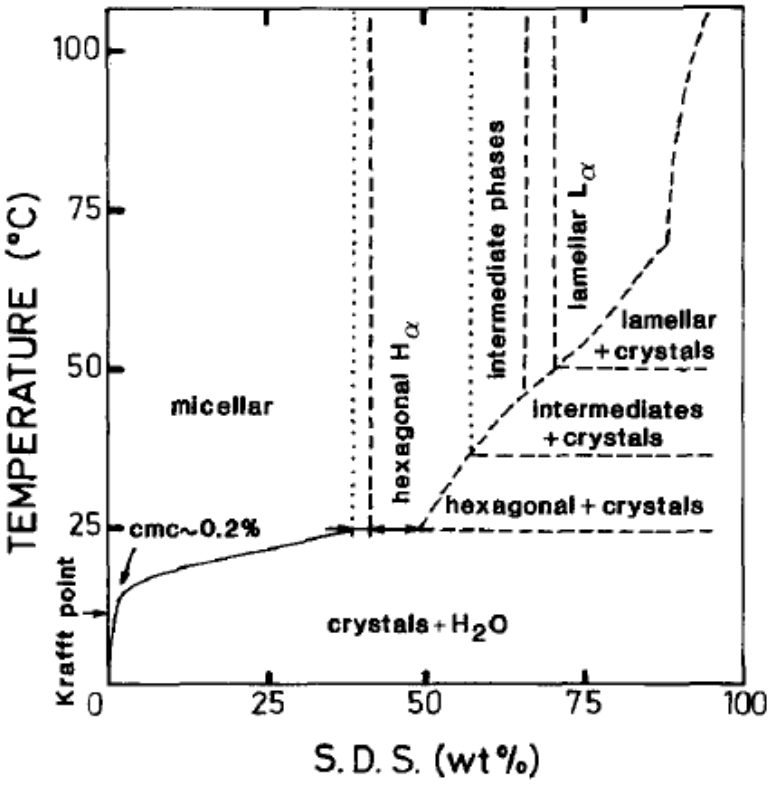


**Figure 1.9 Phase diagram for the SDS water system as determined by calorimetry and NMR.[126]**

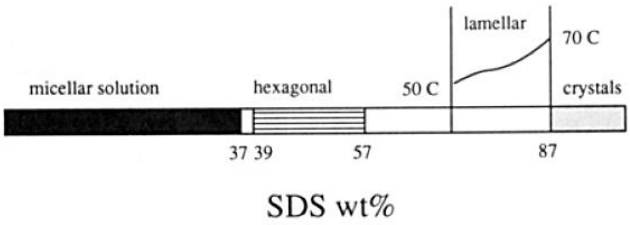


**Figure 1.10 Surfactant-water phase diagram for SDS at 40°C.Blank areas correspond to two phase regions. The lamellar phase at higher than 50°C is also show. Reprinted with permission from Marques 1993. Copyright 1993 American Chemical Society.[99]**

### 1.2.2 Sodium Laurate

Sodium Laurate is another anionic surfactant with a 12 carbon length tail. It is also used in soaps and shampoos[105,127] and has been mentioned in a number of patents as a skin disinfectant.[128,129] In the literature, a wide range of values for the CMC of SL have been reported. Jackson[130] suggests that one of the causes in the uncertainty of the CMC is the precipitation of impurities such as lauric acid around the CMC. The CMC has been reported as 20 mM.[131]

SL is sensitive to pH. In general an alkanoate can dissociate in water into the alkanoic acid and the neutral soap based on the following equilibria:

$$Z^- + H_2O \rightleftharpoons HZ + OH^-$$

$$HZ + 2Z^- + 2M^+ \rightleftharpoons MZ + MHZ_{2\,(aq)}$$

$$MHZ_{2\,(aq)} \rightleftharpoons MHZ_{2\,(S)}$$

$Z^-$ is the alkanoate anion, $M^+$ the metal cation, HZ the alkanoic acid, MZ the neutral soap and $MHZ_2$ the acid soap.[132]

The pKa of SL measured by Kanicky[133] in a 2 mM solution, a factor of 10 lower than the CMC, was 7.48. At pH values around the pKa, SL solutions show maximum foam stability and foam height. The surface tension of SL solutions increases with pH as the solubility of sodium salt is higher than the acid and the salt is less surface-active. Around the pKa of SL, a molecular complex forms between the alkanoic acid and the alkanoate to form the acid soap.[132] As the concentration of SL decreases, the pH decreases (Figure 1.11).[130] At the lowest concentrations of SL, no precipitates are observed when there is 10 mM salt. When the concentration of SL increases to between 0.25 and 7 mM, there is some lauric acid precipitate observed. At concentrations of SL higher than 7 mM, the precipitate is a 1:1 complex of lauric acid and sodium laurate.[132] A phase diagram for SL is shown in Figure 1.12. Below 50°C and 30 wt%, SL is in the micellar phase. Between 35 wt% and 40wt%, SL is in the hexagonal phase and above 40 wt% SL the solution is in two phases: the hemihydrate phase with excess water as a liquid. At temperatures above 60°C, SL can form a lamellar phase above 55 wt%.

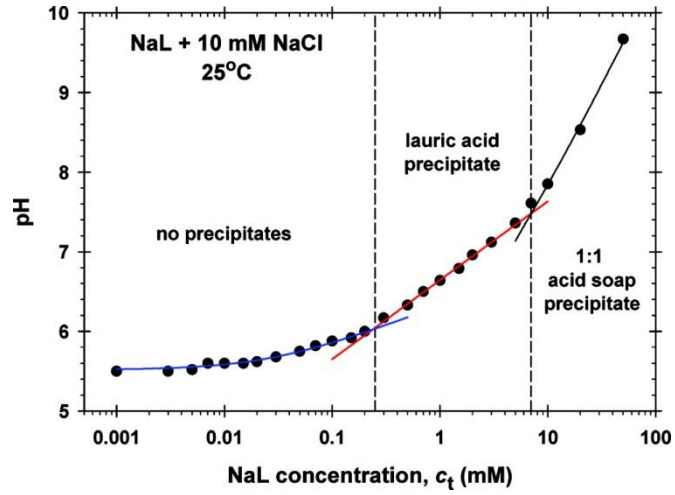


**Figure 1.11 Plot of pH of SL solutions against the total concentration of SL in 10 mM NaCl at 25°C. The dashed lines are theoretical boundaries between zones of different precipitates. Reprinted with permission from Kralchevsky 2007. Copyright 2007 American Chemical Society.**[132]

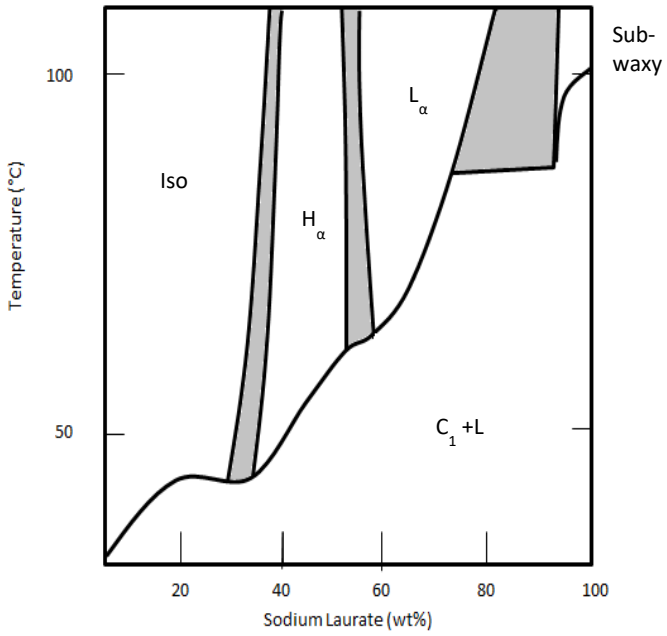


**Figure 1.12 Temperature against concentration phase diagram of a mixture of sodium laurate and water**[98]

At high concentrations of sodium ions, SL gels in water. These gels are formed from cylindrical nanofibres where the inside of the fibres are structurally similar to rod-like micelles (Figure 1.13) and the sodium ions are free to move through the continuous water phase.[134,135]

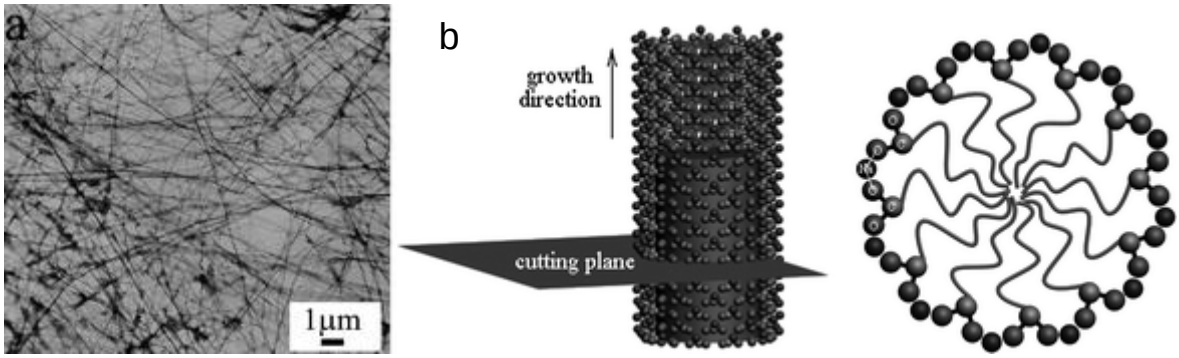


**Figure 1.13 (a) TEM image of the gel for 50 mM SL, 250 mM NaCl in $H_2O$ system. (b) Schematic view of a cylindrical nanofibre formed by SL molecules. The left is a front view and the right is a sectional view of the nanofiber. Grey lines are hydrocarbon chains, the carbon atoms, oxygen atoms, and sodium atoms are denoted by spheres with different grey scaling. Adapted from Yuan 2008.[134]**

Sodium laurate is synthesised from lauric acid which is obtained from coconut oil and synthesised either by the precipitation method or the fusion method.[136–138] Commercial samples of sodium laurate often contain additional lauric acid.[138]

### 1.2.3 Micelle Breakdown and Formation

A range of different process that can occur when a surfactant solution is diluted. Micelle kinetics can be described by the Aniansson and Wall model (Figure 1.14 and Figure 1.15).[139,140] The authors base the model on the assumption that the breakdown or formation micelles occur when single monomers combine with aggregates (or leave aggregates). There are several different relaxation processes that occur after the system is changed; the first is the fast exchange of the surfactant between the bulk and the micellar phase (Figure 1.14). The timescale for the fast process tends range from nano to microseconds ($\tau_1$). The second process is slower, in the micro to millisecond range ($\tau_2$) and is linked to the breakdown or formation of complete micelles (Figure 1.15)). In some experiments, the rearrangement of counter ions can be observed at very short times.[141] As this is faster than the other processes, generally, it is assumed to be almost instantaneous and excluded from calculations.

$$A_1 + A_1 \underset{k_2^d}{\overset{k_2^a}{\rightleftharpoons}} A_2$$

$$A_1 + A_g \underset{k_g^d}{\overset{k_g^a}{\rightleftharpoons}} A_{g+1}$$

**Figure 1.14 Mechanism for fast monomer loss in the Aniansson and Wall model: the $\tau_1$process.**

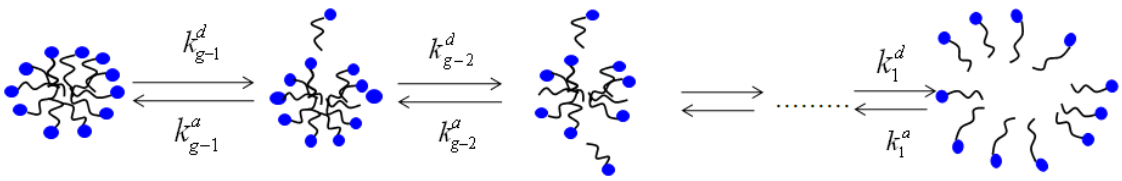


**Figure 1.15 Mechanism for sequential monomer loss, slow micelle breakdown in the Aniansson and Wall model: the $\tau_2$ process.[142]**

For SDS at the CMC, $\tau_1$ is 29 µs and $\tau_2$ is 2.3 ms as determined by shock tube and pressure jump experiments respectively.[143] Both $\tau_1$ and $\tau_2$ are dependent on the monomer concentration, chain length and ionic strength. The residence time of SDS in micelles is around $10^{-5}$ s.[144] The dissociation rate constant, $k^d_g$ is strongly dependent on the surfactant, with an extra methyl group reducing it by up to three times.[144]

The distribution of surfactant in micellar solutions includes monomers as well as micelles. The intermediate or pre-micelles, *i.e.* dimers, trimers and oligomers, are rare (Figure 1.16).[145] Above the CMC, the equilibrium concentration of monomers is approximately the CMC.

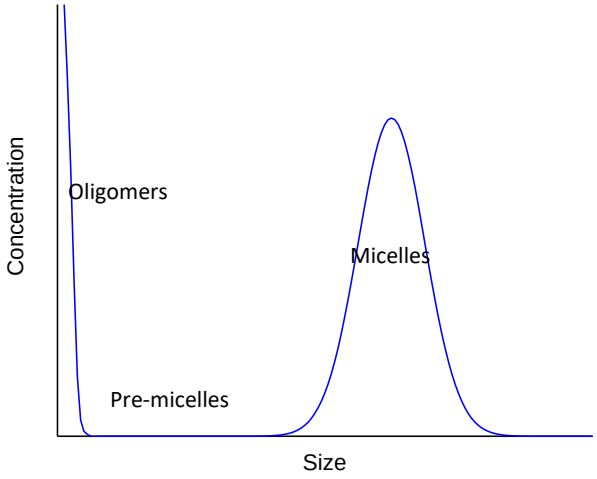


**Figure 1.16 Simplified model for the micelle size distribution of polydisperse micelles.[146]**

The Bain group[147] has added to the theory of micelle breakdown, specifically with the non-ionic surfactant $C_{12}E_8$, octaethylene glycol monododecyl ether, although the theory is relevant to most surfactant systems. An additional route of micelle re-equilibration is suggested; the formation of super micelles through fusion of smaller aggregates (Figure 1.17). The super micelles then decompose to standard micelles via stepwise monomer release, and the process is much faster overall than if monomer loss alone takes place.

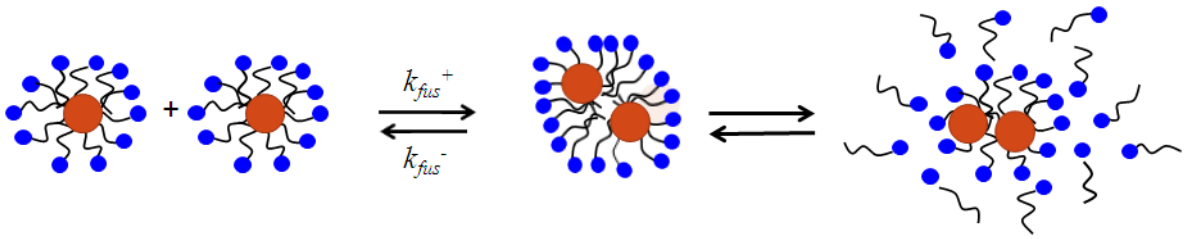


**Figure 1.17 The fusion-Becker-Döring mechanism for micelle breakdown, and the reverse process[142]**

Upon dilution of a surfactant system, for example when rinsing an SDS and TC containing soap during handwashing, the timescale and mechanism of micelle redistribution is important and will affect the relative concentrations of TC in bulk and micelles.

### 1.2.4 The Effect of Additives on Micelles

The above systems only consider the re-equilibration of unloaded micelles. However, it is clear that the presence of solutes within the micelles affects the structures formed after dilutions, especially as the CMC is approached and just below the CMC. At longer times of measurement, *i.e.* longer than $\tau_2$ and the surfactant has equilibrated, it is likely to be these structures that are observed when saturated micelles are diluted and the individual micelle breakdown process.

Zhu and Reed[148] have used a model made of three components to describe the structures observed at low ratios of solute to surfactant when the concentration of surfactant is just above the CMC. Supramolecular Assemblies (SA) have been observed through their light scattering peak since around 1955. Around the CMC, the authors[148] believe large metastable structures form when hydrophobic compounds are incorporated into a system; whereas when the system is well above the CMC, regular micelles form encapsulating the solute. In the system studied by Zhu and Reed, the solute was either dodecanol or dodecane and the surfactants were SDS and dodecyl trimethyl ammonium bromide ($C_{12}$TAB). A number of factors influence the onset of formation of large aggregates including the concentration of solute and the ionic strength of the medium. Other authors[117] have previously thought that the particles are adducts with the structure ROH:2SDS. The SDS straight from the bottle shows these light scattering peaks as well due to the residual dodecanol from the manufacturing process.

In the work of Zhu and Reed,[148,149] the models work for low ratios of solute to surfactant. The first model the authors propose has SDS in three different forms: monomeric SDS ($SDS_{aq}$), SDS in micelles ($SDS_{mic}$) and in supra molecular assemblies. Dodecanol (Do) is separated likewise. The four concentration regimes are shown in Figure 1.18. In $C_1$, there are no SAs, in $C_2$ the concentration of surfactant is above the CMC and there are SAs. In $C_3$, the concentration of surfactant is below the CMC but there are SAs and $C_4$ is below the CMC and below the limit for SAs to form.

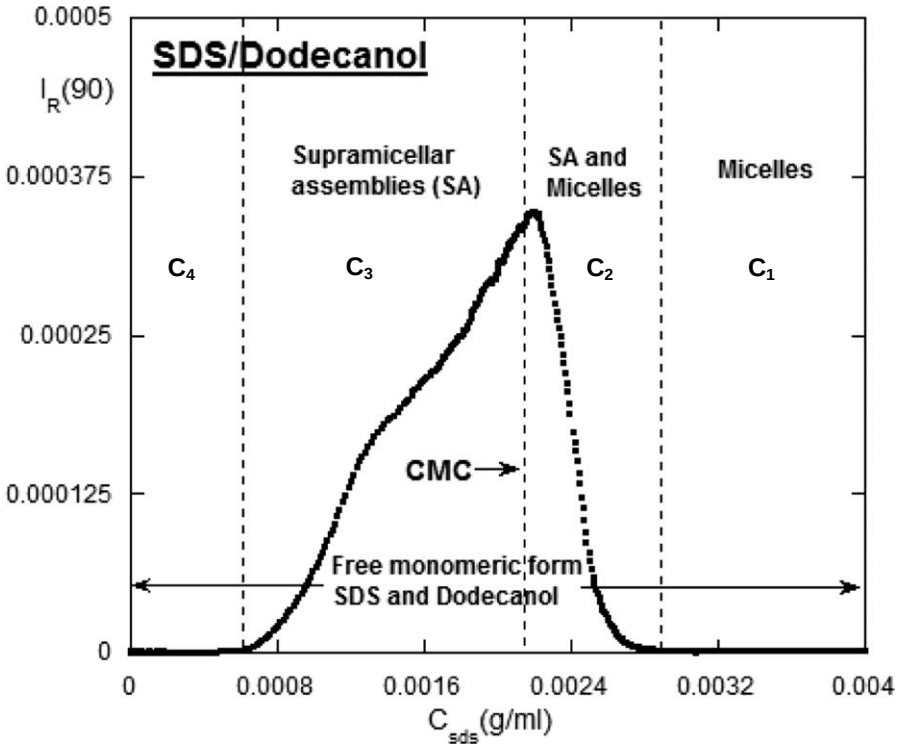


**Figure 1.18 Light scattering peak from SDS and dodecanol at *R*=0.023 and [NaCl]=0. The different concentration regimes are indicated.** Reprinted with permission from Zhu 2013. Copyright 2013 American Chemical Society.[148]

In $C_1$ region, stable micelles solubilize the dodecanol, the concentration of free SDS is around the CMC and the concentration of supramolecular assemblies is effectively 0. The loading of the micelles is given by:

$$r = \frac{m_{Do(mic)}}{m_{Surf(mic)}} = \frac{Rm_{Surf(tot)} - m_{Do(aq)}}{m_{Surf(tot)} - CMC_R}$$ Equation 1.3

where *R* is the concentration of solute over the concentration of surfactant, $CMC_R$ is the CMC at the specific *R*, $m_{Do(mic)}$ and $m_{surf(mic)}$ are the concentrations of dodecanol and surfactant in micelles, $m_{Surf(tot)}$ is the total concentration of surfactant and $m_{Do(aq)}$ is the concentration of aqueous dodecanol.

In the $C_2$ region, the micelles are saturated and there is a small concentration of SA. As $C_2$ decreases, the concentration of micelles drops and the concentration of aggregates increases. In the $C_3$ regime, the concentration of SA decreases. SA will only exist above the saturation level of dodecanol in the solvent. In $C_4$, only monomeric surfactant and dodecanol exist. The point where the solubility of dodecanol in aqueous solution is reached ($C_e$) is where aggregates start to assemble (the critical supramicellar assembly concentration (CSAC)). From their study, these supramicelles do not fit to a spherical model and the authors postulate that the micelles are disk-like or worm like.

This light scattering phenomenon might be seen in other systems where there is a more hydrophobic solute in surfactant micelles, such as TC and SDS when they are diluted. However, SDS/dodecanol forms a lamellar phase so the details will be different in a SDS/TC system.

### 1.2.5 Loaded Micelles

A variety of different methods have been used to determine characteristics of loaded micellar solutions such as partition coefficients and solubility. Shah *et al.*[150] used conductance data to determine the partition coefficients of potential-sensitive dyes in sodium dodecyl benzene sulphate (SDBS) solutions. The solubilisation is controlled by the hydrophobic interaction; the water affinity of the dye is important for partitioning. For example, if the dye is mildly hydrophilic, a water shell is taken into the micelle with the dye.

The CMC of SDBS decreased when dye was added. The observed CMC decrease can be used to determine the partition coefficient in combination with absorbance data, where the absorbance of the dyes increases with increasing SDBS. There are two factors that lead to a reduction in the CMC in the presence of additives. Firstly, there is an increase in entropy due to the mixing of the surfactant and solute. Secondly, the amount electrical work is decreased due to the lower surfactant charge density.

The partition coefficient, the ratio of the mole fraction of the dye in micelles to the mole fraction in bulk ($K_C$), can be determined from the Kawamura relationship:

$$\frac{1}{\Delta A} = \frac{1}{K_c \Delta A_\infty \left(m_{dye} + m_{surf\,(mic)}\right)} + \frac{1}{\Delta A_\infty} \qquad \text{Equation 1.4}$$

where $\Delta A$ is the change in absorbance and $\Delta A_\infty$ is the change in absorbance at infinite concentration of surfactant, $m_{dye}$ is the total concentration of dye and $m_{surf(mic)}$ is the concentration of surfactant in micelles.[151]

Alonso, Harris and Kenwright, at Durham University and CNRS,[152] investigated the solubilisation of short chain (n=3-6) alcohols and amines in CTAB micelles and found that these molecules reside preferentially in the palisade layer, towards the head groups and the surface. $^{13}C$ NMR of the additive alkyl chains were sensitive to the conformational changes arising from a change in the environment of a carbon chain in the micelles. The addition of the alcohols and amines reduced the CMC of the CTAB. The additives are in fast equilibrium between the bulk and the micelle leading to an average signal. NMR can be used to measure the rate of exchange rates between two species or put a limit on rates that are faster or slower than the measurable range.

1D and 2D-DOESY NMR spectroscopy was used to find the solubilisation capacity of SDS micelles for the insoluble drug molecules artemisinin and curcumin.[153] The signals in the DOESY spectra were a mixture of the drug in micelles and free in solution: the exchange was faster than the NMR timescale. The solubilisation ratio can be calculated from the linear regression of solubility of drug against concentration of SDS. The solubility was calculated from the proton signal integration and compared to the reference trimethylsilane.

The observed pKa of solutes changes in micellar media where a portion of the solute resides preferentially in the micelles. The pKa change can be investigated by NMR.[154–156] The observed pKa of a solute in a micellar system depends on the electrostatic potential of the charged interface and the relative partitioning of the acid and base into micelles. If the base partitions more strongly into the micelles, the observed pKa will decrease and if the acid partitions more strongly into the micelles, the observed pKa will increase.[155] With a negatively charged interface, like that of SDS or

SL, the anions of an acid are repelled by the negatively charged interface meaning that the acid form partitions more strongly into the micelle, which leads to an increase in the observed pKa of the solute. Jaiswal *et al.*[154] found that the pKas of the maleic acids tested were very similar in SDS micelles to the pKa of the acids in solution. In cationic surfactant solution the pKa was reduced due to the positively charged micelle surface strongly attracting the acid anion and causing a strain on the acid molecule leading to dissociation.

## 1.3 Supported Lipid Bilayers

Supported lipid bilayers (SLB) were first described in literature by Tamm and McConnell[157] and have been used as models of cell membranes. Once formed, SLBs are stable and accessible to surface sensitive techniques such as atomic force microscopy (AFM), quartz crystal microbalance (QCM) and total internal reflection Raman (TIR-Raman).[158] A lipid bilayer is formed of two lipid leaflets supported on a solid substrate with a thin water layer between the bilayer and the substrate which means that the bilayer retains lateral fluidity (Figure 1.19).[157,159] The bilayer width is approximately 40 Å and the water layer thickness is between 10 and 20 Å.[158,159]

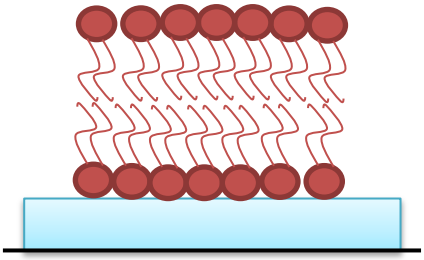

**Figure 1.19 Schematic of a supported lipid bilayer with a water layer between the substrate and the bilayer**

The first SLBs were prepared using a Langmuir-Blodgett technique with the sequential transfer of two monolayers from the air-water interface onto the solid substrate.[157] One advantage of this technique is that it allows the formation of asymmetric bilayers. After formation, the SLB is kept in aqueous solution because SLBs restructure when they pass through the air-water interface.[160] Vesicle fusion is often used instead of Langmuir-Blodgett because of its simplicity.[161] Common support surfaces include fused silica, mica, silicon and borosilicate glass.[157,162–164] A vesicle suspension is formed either by sonication or extrusion and passed over the solid support. The vesicles adsorb to the solid support from the bulk. The vesicles fuse with one another, rupture to form disks on the surface and fuse to other disks on the surface to form a continuous bilayer (Figure 1.20).[165] Vesicles in contact with each other fuse and once the vesicle reaches the critical size, it fuses into a bilayer disk.[166] Membrane fusion occurs at all pH and ionic charge for neutral and positively charged vesicles whereas negatively charged vesicles do not fuse at high pH or low ionic strength on glass.[162] Divalent protons such as $Mg^{2+}$ and $Ca^{2+}$ are well known to promote vesicle attachment and bilayer formation.[167]

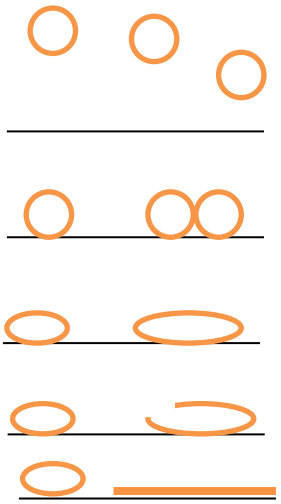

Figure 1.20 Schematic of supported lipid bilayer formation by vesicle fusion[168]

Supported lipid bilayers have been used as models to understand membrane bound proteins[169] and the interaction of small molecules with lipid bilayers. One area of interest has been to understand the interaction between anaesthetic molecules and the cell membrane.[170–174] Other researchers have used SLBs to investigate the interaction between bilayers and alcohols,[175] cationic surfactants[176] and drug molecules.[177] In this thesis, SLBs formed of different phospholipid mixtures have been used as models to investigate the partitioning of TC into cell membranes using TIR-Raman spectroscopy.

## 1.4 TIR-Raman Spectroscopy

One of the experimental techniques used in my project is Total Internal Reflection Raman spectroscopy (TIR-Raman). The current set-up was developed by previous members of the Bain group and has been continually improved, most recently by M. Possiwan and E. Eis to include imaging. The details of the set-up are well described elsewhere[178,179] and are summarised in Section 4.2.2. TIR-Raman is a surface-sensitive technique and results can be obtained in a matter of seconds.

Raman scattering is inelastic and associated with transitions between vibrational and rotational levels. The molecule is excited to a virtual state by the laser input and relaxes to a different vibrational level releasing a photon at a slightly lower or higher energy, Stokes or anti-Stokes emission (Figure 1.21). The Raman Effect was first described in literature by C.V. Raman and K. S. Krishnan,[180] with the first spectra recorded in early 1928.[181] Vibrational spectra are dependent on the conformation of the molecule so this method is useful for studying the orientation and fluidity.[182] The gross selection rule for Raman transitions is that the polarizability of the molecule should change as the molecule vibrates and the specific selection rule is $\Delta v = \pm 1$.[183]

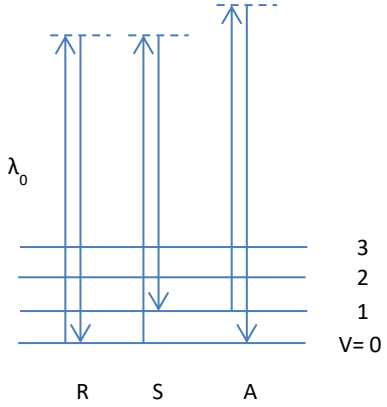


**Figure 1.21 The energy level changes in Raman spectra where the transitions shown are the Rayleigh line (R), where the emitted light is the same wavelength as the input ($\lambda_0$), the stokes line (S), where the emitted light is at a shorter wavelength and the anti-stokes line (A), where the emitted light is at a longer wavelength than the emitted light.**

In TIR-Raman, the incident light excitation is an evanescent electric field rather than a transmitted laser beam directly applied, which means Raman scattering remains in a targeted area of interest. Across an interface there is no transmission of energy above the critical angle, when the beam is totally internally reflected. Boundary conditions require an electric field across the interface: this is termed the evanescent wave. The evanescent wave decays exponentially with distance from the interface. The evanescent wave generates Raman scattering. Typically in my experiments using a silica hemisphere probing the water-silica interface the light is sent to the hemisphere at an angle of 73°. For the silica/water interface the evanescent wave penetrates 200 nm and the Raman scattering has a sample depth of half of the penetration depth (100 nm) (Figure 1.22).[182,184,185] The critical angle for 532 nm radiation at the silica/water interface is 67°, calculated from Snell's law

$$\theta_{crit} = \arcsin\left(\frac{n_1}{n_2}\right) \qquad \text{Equation 1.5}$$

where $n_1$ is the refractive index of the medium with the lower refractive index and $n_2$ is the refractive index of the medium with the higher refractive index. The refractive index of silica is 1.46 and the refractive index of water is 1.34.[178]

The electric field decays with the length

$$l = \frac{\lambda_o}{2\pi n_2}\left(\left(\frac{n_1}{n_2}\right)^2 \sin^2\theta - 1\right)^{-\frac{1}{2}} \qquad \text{Equation 1.6}$$

where $\lambda_o$ is the wavelength of the input light and $\theta$ is the angle of incidence.

The evanescent wave causes Raman scattering from the thin film at the interface. Different polarisations of the light change the direction of the electric field. Signals observed with S polarised light are in the plane of the surface and P polarised components are in and out of plane, except at $\theta_{crit}$. Supported lipid bilayers can be formed at the silica/ water interface and be probed using TIR-Raman. Comparing the relative intensities of peaks from S and P light allows some insight into the orientation of the lipid chains.[182,184,185] When Lee[184] looked at spectra of DMPC with temperature, he

observed the average chain tilt decreased as the temperature decreased from the comparison of the lipid peak changes in both S and P light.

TIR-Raman has also been used to study the adsorption of surfactants to the silica water interface.[178,186] Tyrode[187] studied the monotonic adsorption of CTAB to the silica-water interface where the conformational order was found to be independent of surface excess. Tyrode[188] also used TIR-Raman to probe the structure of water in contact with a silane monolayer. The Smith group[189,190] at Iowa State University have used a Plasmon waveguide resonance interface in their TIR-Raman experiments on silane monolayers, polystyrene films and gold films with monolayers of small molecules. Other researchers have used different substrates. For example, the thickness of thin films of isotropic polystyrene films on a polypropylene substrate have been measured using TIR-Raman techniques[191] as has sulphate adsorption to haematite surfaces.[192] Greene[193] used TIR-Raman to examine the wax layer on barley leaves. Praveena[194] developed a TIR-Raman tribometer to investigate friction-induced material transfer *in situ*.

Supported phospholipid bilayers can be useful models for cell membranes and TIR-Raman is a useful technique to study the effect that changes to the environment can have on the bilayer structure. Changes in the cell outer bilayer structure can perturb normal cell function and one of the mechanisms where TC is known to inhibit bacteria is through membrane disruption.[43]

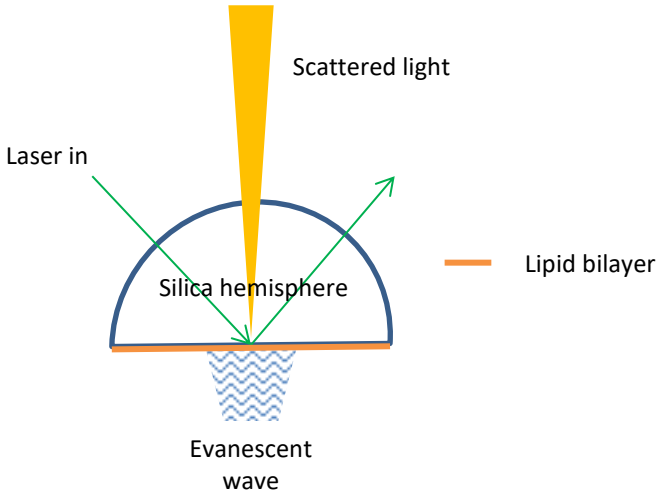


**Figure 1.22 Schematic showing the evanescent wave and scattered Raman light**

## 1.5 Project Outline

My experimental work is separated into three chapters which describe different techniques used to probe different stages in the lifecycle of TC. Each chapter contains a materials and methods section rather than this thesis having a single materials and methods chapter because in each chapter different techniques are used to explore different aspects of the lifecycle of TC.

The first chapter describes the effect of TC on the behaviour of SDS and SL micellar systems. In this section, I aim to show how the presence of TC affects the behaviour of SDS and SL using a number of different techniques. UV-Vis spectroscopy has been used to probe the concentration of TC in surfactant solutions and whether the phenol or phenolate is present. Stopped flow and particle

tracking analysis experiments have been used to investigate the changes that occur in model systems when they are diluted and the particles that form as TC crystallises from solution. I have probed the effect of TC on the CMC of the surfactants using surface tension experiments. Small Angle Neutron Scattering (SANS) has been used to study effect of TC on the size and shape of SDS micelles using data collected by SANS.

In the second experimental chapter, I detail work carried out to calculate the partitioning of TC between micelles and bulk as phenol and phenolate using proton NMR. One of the major contributions to the observed shift is the presence of TC in several phases (phenol and phenolate forms both in and outside micelles) in rapid equilibrium. I have used NMR analysis to look at the observed shift of TC proton peaks in SDS and SL micellar systems at a range of pH. From the observed NMR shift, I have calculated the partition coefficients of TC between micelles and aqueous solution for the phenolate form of TC ($K_-$) and the phenol form ($K_+$). I have also investigated the effect of more than one TC molecule per micelle has on the observed shift and how that affects the fitting. In my $^1$H NMR experiments, changes in the shift of TC proton peaks have varied with concentration of TC, concentration of surfactant and pH. I have also used NMR analysis to calculate the solubility ratio of TC in SDS and SL.

In the third section of this thesis, I will describe my experiments using TIR-Raman to study the effect of TC on supported phospholipid bilayers. Bilayers are supported on silica within a cell where the environment around the bilayer can be changed and the bilayer signal indicates the structure and phase of the bilayer. POPC bilayers were used initially and then different lipids and lipid mixture were used to change the conditions and model different cell types. Interesting behaviour has been found when the bilayers were treated with TC. The TC peaks at 3075 cm$^{-1}$ and 1600 cm$^{-1}$ were used to calculate the concentration of TC in the bilayer and the effect of rinsing on the concentration within the bilayer. Experimental work include using different lipid mixtures that are good models for bacterial membranes and detergent resistant membranes, which have different phase behaviour to POPC bilayers.

At the end of the thesis, I will present my conclusions and describe how each of the different sections contributes to the further understanding of the lifecycle of TC.

# 2 Triclosan in SDS and SL micellar systems

## 2.1 Introduction

The aim of this chapter is to investigate the effect of Triclosan on the aggregation of SDS and SL in the bulk and at the surface. I have investigated the effect of TC on the critical micelle concentration (CMC) of the surfactants and the interfacial tension of the solutions with TC and surfactant. The size and shape of SDS micelles with and without TC have been explored by small angle neutron scattering (SANS).

UV-Vis spectroscopy has been used to determine the presence of either the phenol or the phenolate in solution. The UV-Vis experiments were initially used to determine solubility and I investigated the change in molar extinction coefficient and the wavelength of maximum absorbance with surfactant. I have also used stopped flow methods with UV-Vis absorbance detection to begin to understand the processes that occur when the concentrated solutions of surfactant and TC are diluted, as the concentration of surfactant approaches the CMC, as a model for the dilution effects that occur upon handwashing. I have investigated the particle concentration and size by NanoSight analysis in these diluted solutions and in the more concentrated surfactant solutions.

Some of the technicalities of the different methods are described below, to aid data interpretation. I have also summarised some of the results on TC collected by other authors using similar techniques.

### 2.1.1 Interfacial Tension

Interfacial tension measurements are commonly used in surfactant science to understand the properties of the surfactant system. For example, the shape and wettability of droplets are dependent on the interfacial tension. Young's equation is used to describe the balance of tensions at the three-phase contact line of a droplet on a solid surface:

$$\gamma_{sv} - \gamma_{sl} = \gamma_{lv} \cos\theta \qquad \text{Equation 2.1}$$

where $\gamma_{sv}$ is the solid-vapour interfacial tension, $\gamma_{sl}$ is the solid-liquid interfacial tension, $\gamma_{lv}$ is the liquid-vapour interfacial tension, commonly referred to as the surface tension, and $\theta$ is the contact angle. When $\theta$ is 180° the droplet is non-wetting, for 0°<$\theta$<180°, the droplet is partially wetting and when $\theta$ is 0°, there is complete wetting (Figure 2.1).

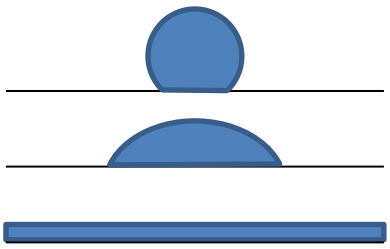

**Figure 2.1 Schematic of droplet shape with a high contact angle which is poorly wetting, a low contact angle which shows intermediate wetting and a fully wetted surface where the contact angle is 0°**

Interfacial tension is the free energy change associated with increasing the surface area of a medium by unit area, which is the equivalent to the minimum work of separating two half unit areas from contact to infinity

$$\gamma_{LV} = -\frac{1}{2} W_{coh}$$ Equation 2.2

where $W_{coh}$ is the work of cohesion. For the liquid-vapour interface the conventional SI units for the interfacial tension, $\gamma_{LV}$, are mN m$^{-1}$.[114,195–198]

Interfacial tension is dependent on the species adsorbed at the interface. In two component mixtures, there will be preferential adsorption of one of the components at the surface if that leads to a decrease in the surface energy, reducing the observed interfacial tension. For example in surfactant-water mixtures, the surfactant will preferentially adsorb to the liquid-vapour interface with the hydrophobic tails orientated towards the air and the hydrophilic head-groups in the water.[114,195,196]

The interfacial tension changes with concentration of surfactant. At very low concentrations of surfactant, the interfacial tension of the solution is dominated by the interfacial tension of the bulk liquid. As the concentration of surfactant increases, more becomes adsorbed onto the surface and the interfacial tension decreases with concentration of surfactant. The interfacial tension stops decreasing at the CMC, above the CMC the interfacial tension remains constant and the extra surfactant forms micelles.[114] The CMC is described in Section 1.2 and is the concentration range at which the surfactant molecules begin to form micelles in solution. An example interfacial curve with the surfactant SDS is shown in Figure 2.2.

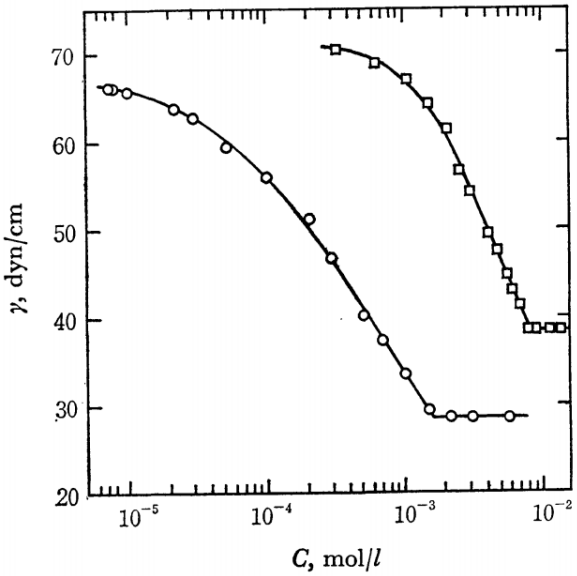


**Figure 2.2 Interfacial tension at the liquid-vapour interface against concentration of tritiated SDS solutions (□) in salt free solution and (○) excess salt.[120]**

Below the CMC, the tangent of the curve of interfacial tension against the natural log of concentration (ln*m*) can be used to calculate the Gibbs surface excess concentration, so long as ideal dilute assumptions hold. The surface excess remains constant in the region where interfacial tension is linear with log concentration and the changes in interfacial tension are caused by the change in surfactant activity in the bulk solution.[199–201] The surface excess is calculated using the Gibbs equation

$$\Gamma_{surf} = -\frac{1}{nRT}\left(\frac{d\gamma}{d\ln(m_{surf})}\right)$$ Equation 2.3

where $m_{surf}$ is the concentration of surfactant and $n$ is 2 for ionic surfactants unless there is excess salt when $n$ is 1. $n$ is 1 for non-ionic surfactants. From the surface excess, the minimum area occupied by the surfactant absorbed at the interface ($A_m$) can be calculated using

$$A_m = \frac{1}{\Gamma N_a}$$ Equation 2.4

Tajima,[120,202,203] using tritiated SDS found an area per molecule of 38.4 Å$^2$ for SDS in 0.115 M NaCl. Tajima used tritiated SDS to confirm the validity of the fit to the Gibbs equation by counting β-rays. In water, without any salt, the area per molecule is higher, around 44 Å$^2$,[111,204] where there is strong electrostatic repulsion between the SDS headgroups.[200,205] For anionic systems such as SDS, the electrostatic interactions between the headgroups limit the adsorption at the interface and the area per molecule. In salt solutions, the electrostatic interactions are shielded so that the surfactant can become closer packed on the surface. Increasing the salt in anionic surfactant solutions increases the efficiency of the surfactant and decreases the CMC.[114]

For surfactant mixtures, the interfacial tension depends on the relative surface activity of each surfactant and the interaction of the two surfactants. Simply, the most hydrophobic surfactant is the most abundant on the surface.[114] In my work, I have explored the influence of TC on the interfacial tension of SDS solutions and examined the impact of TC on the CMC of SDS. TC has very low solubility in water so there is likely to be significant portion of TC incorporated into the surfactant monolayer at the air-water interface.

Interfacial tension at the liquid-vapour interface has been measured by two different methods: Wilhelmy plate and drop shape analysis. In Wilhelmy plate measurements, the tension of the surface is directly measured by pulling a platinum plate from the liquid surface. The contact angle is zero, to allow accurate readings. The interfacial tension is calculated from the force measurement, $f$

$$\gamma_{lv} = \frac{f\cos\theta}{2(l+t)}$$ Equation 2.5

where $\theta$ is the contact angle, $l$ is the length of the plate and $t$ is the thickness of the plate.

Drop shape measurements were also used to calculate the interfacial tension of solutions. If a droplet is a sphere deformed only by gravity, then the interfacial tension can be calculated using the Young-Laplace equation:

$$\Delta p = \gamma_{lv}\left(\frac{1}{R_1}+\frac{1}{R_2}\right) = \rho g h$$ Equation 2.6

where $\Delta p$ is the pressure difference between the outside and the inside of the drop, $R_1$ and $R_2$ are radii of curvature, $g$ is the gravitational constant, $\rho$ is the density of the fluid and $h$ is the z position in the drop. The interface will assume the shape of a minimal surface.[206] Droplets with high interfacial tension are more spherical than droplets with low interfacial tension which are elongated and more

deformed by gravity.[196] The Bond number, or Eötvös number, in all the droplets used for pendant drop is approximately 1:

$$Bo = \frac{\rho g d^2}{\gamma}$$ Equation 2.7

where *d* is the z diameter of the droplet. Droplets with low Bond numbers are spherical and droplets with high Bond numbers do not have a stable drop shape. The Bond number describes the relative importance of gravity and interfacial tension on a droplet; when the Bond number is 1, the shape of the drop is distorted which allows *γ* to be calculated.[207]

### 2.1.2 Small Angle Neutron Scattering

Small angle neutron scattering (SANS) is a useful technique for studying the structure of small particles and aggregates in solution such as micelles, proteins and polymers. Neutrons penetrate matter further than X-rays and interact via the nucleus rather than the electric field. Several types of scattering can occur in solution. Coherent scattering is when the neutron wave interacts with the sample and waves from different nuclei interact with one another, which provides information about structure. Elastic coherent scattering provides information about the equilibrium structure and inelastic coherent scattering provides information about the motions of the atoms. Incoherent scattering is when the neutron wave interacts with nuclei independently and provides information on atomic diffusion.[208]

The output of a scattering experiment is a plot of intensity of scattering against the scattering vector Q, which is related to the momentum transfer

$$Q = \frac{4\pi \sin(\theta/2)}{\lambda}$$ Equation 2.8

where $\theta$ is the scattering angle and $\lambda$ is the neutron wavelength. The intensity of scattering depends on the contrast and the structure. Many models have been developed to fit the scattering pattern, including the Hayter-Penfold model for core shell micelles.[209,210]

The scattered intensity for micelles, in the decoupling approximation is

$$I(Q) = n\left[ S(Q)\left|\langle F(Q)\rangle_Q\right|^2 + \left\langle |F(Q)|^2 \right\rangle_Q - \left|\langle F(Q)\rangle_Q\right|^2 \right]$$ Equation 2.9

where the averages, $\langle Q \rangle$, are over particles sizes and orientation, *n* is the micelle number density, *S(Q)* is the structure factor and *F(Q)* is the form factor. The form factor denotes the micelle structure and for the core and shell model, the form factor is

$$F(Q) = V_1(\rho_1 - \rho_2)F_0(QR_1) + V_2(\rho_2 - \rho_s)F_0(QR_2)$$ Equation 2.10

where $R_1$ is the radius of the core and $R_2$ is the radius of the micelle, $V_i = \frac{4\pi R_i^3}{3}$, $F_0(QR_i) = \frac{3J_1(QR_i)}{(QR)} \approx 3\frac{\sin(QR) - QR\cos(QR)}{(QR)^3}$, $\rho_1$, $\rho_2$, and $\rho_s$ are the scattering length densities of the

micelle core, the micelle shell and the solvent, respectively, and $j_1(QR_i)$ is a first order spherical Bessel function, which has a mathematical approximation in terms of sin($QR$) and cos($QR$).[211,212]

The scattering length is the strength of the interaction between the incident wave and the point centre, which is the nucleus in neutron scattering.[213] The strength of the neutron-nucleus interaction is related to the cross-section of the nucleus, and different isotopes have different scattering lengths. The scattering length density (SLD) is determined by the number of nuclei per unit volume. For scattering to occur, there must be a contrast between the object of interest and the surrounding solution. One of the most exploited variations is hydrogen/ deuterium substitution to ensure that scattering comes from the objects of interest. The scattering length of hydrogen is -0.374 x$10^{-12}$ cm and the scattering length of deuterium is 0.667 x$10^{-12}$ cm. SANS data is often collected in deuterated solvent with the target hydrogen labelled. Contrast matching is used to highlight particular parts of structure. For example, the core of a micelle can be deuterium labelled in a contrast-matched solvent so that only the shell is observed or the shell can be labelled so that only the core is observed (Figure 2.3). This is an advantage over X-ray scattering, where the scattering length changes with atomic number and the contrast cannot be manipulated in the same way. If there is no scattering length density difference, there is no scattering. The SLD can be calculated

$$\rho_N = \frac{\rho_m N_A}{M_w} \sum_i n_i b_i \qquad \text{Equation 2.11}$$

from the density, $\rho_m$, the molecular weight, $M_w$, and the sum of the scattering lengths of the nuclei, $b_i$, where $n_i$ is the number of nuclei of type $i$ in the molecule. There are a number of scattering length density calculators online, such as the one produced by NIST.[214] This was used to calculate the SLD of SDS, TC and $D_2O$ (Table 2.1). In this thesis, SANS has been used to study the change in the size and shape of SDS micelles with TC.

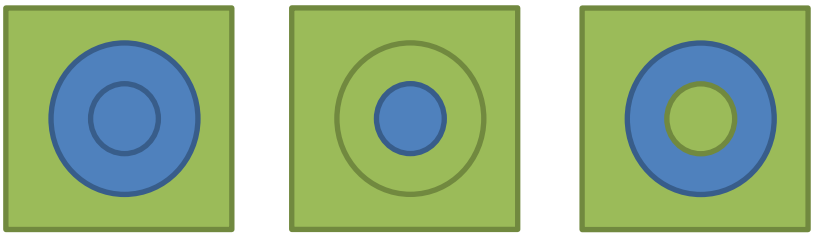


**Figure 2.3 Examples of different contrast settings for SANS: (A) In a deuterated solvent, scattering from the entire micelle is observed, (B) with a deuterated shell and contrast matched solvent, scattering from the core is observed and (C) with a deuterated core and contrast matched, scattering from the shell is observed.**

**Table 2.1 Calculated scattering length densities from a 1 Å neutron source[214]**

| Molecule | SLD (x$10^{-6}$ Å$^{-2}$) |
|---|---|
| SDS | 0.333 |
| TC | 1.954 |
| $D_2O$ | 5.759 |

### 2.1.3 UV-Visible Spectroscopy

In UV-Visible spectroscopy, absorbance is measured. According to the Beer-Lambert law the absorbance, A, is

$$A = \log \frac{I_0}{I} = \varepsilon c l$$ Equation 2.12

where $I$ is the transmitted intensity of the sample and $I_0$ is the transmitted intensity of the background, $\varepsilon$ is the molar extinction coefficient, $c$ is the concentration of the absorbing species and $l$ is pathlength. It is common for UV-Vis to be used to calculate the concentration of solute from a concentration curve using the extinction coefficient.

The selection rules for absorbance in the UV-Visible region are that active transitions involve a change in the dipolar charge distribution and the transition moment is non-zero.[183] The transition of an electron from the HOMO in a linear conjugated system to the LUMO is allowed, but there are common forbidden transitions are the π*←n band around 300 nm in ketones and the 260 nm band (π*←π) in benzene. The intensity of the absorbance is a dependent on the probability of the transition or its "allowedness".[215] The $\varepsilon$ for the π*←π transition of aromatic systems is often between 1 000 and 10 000 $mol^{-1}$ $cm^2$ because the transition is forbidden due to the symmetry of the ground and excited states but is weakly allowed due to spin-orbit coupling or vibronic coupling.

A Jablonski diagram is often used to show the electronic transitions a molecule undergoes after absorbing light (Figure 2.4). The molecule goes from the singlet ground state to the singlet excited state after photon absorbance and the molecule decays back to the ground state either by radiative decay, such as fluorescence or by internal conversion. The excited singlet may undergo intersystem crossing to the triplet state before radiative decay to the ground state, phosphorescence. During an electronic transition the atoms do not move according to the Frank-Condon principle.

The extinction coefficient and the wavelength of maximum absorbance ($\lambda_{max}$) are dependent on many factors including the solvent and the molecular charge. For example, when TC is in the phenol form, $\lambda_{max}$ for the π*←π transition is 280 nm, whereas the absorbance of the phenolate form of TC is red-shifted with $\lambda_{max}$ at 291 nm (Figure 1.6).[6] Based on the work of Lindström,[6] it appears that TC has an isobestic point at around 270 nm. At the isobestic point, the absorption intensity remains constant with pH. Changing the solvent can induce a change in $\lambda_{max}$. For example, changing the solvent from hexane to ethanol can induce a red shift for the π*←π transition.[215]

The phenolate form of TC is the more photo-reactive and upon absorbance of a photon the electron density moves from the phenolate ring onto the dichloro-ring (Figure 2.5).[81–83,216–219] From the $S_1$ state, the phenolate can undergo many photochemical transformations (see Section 2.1.4).

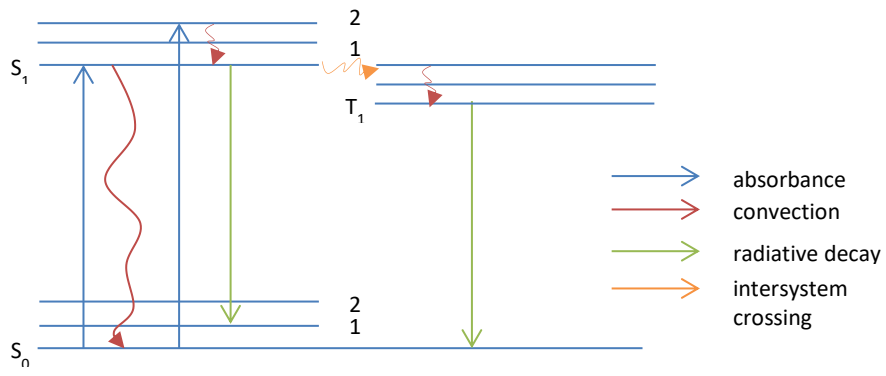


Figure 2.4 Jablonski diagram of electronic transitions

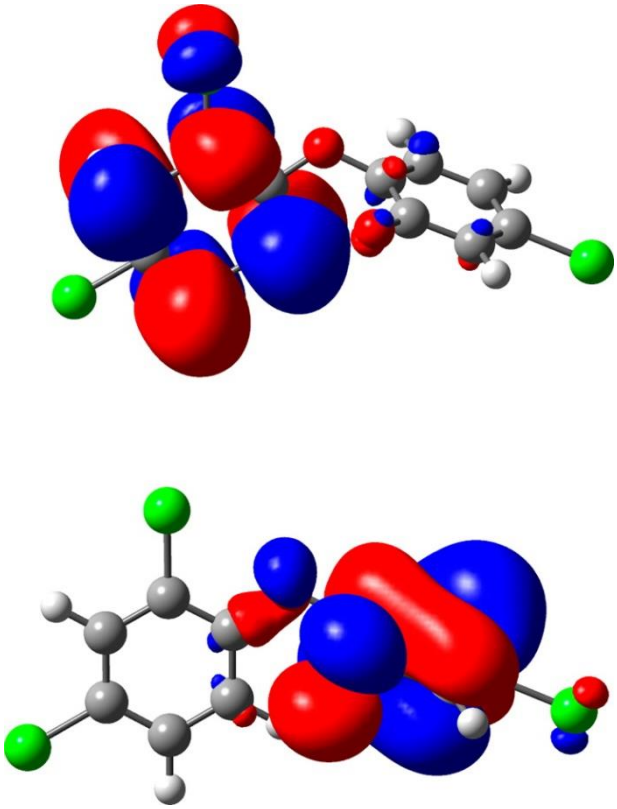

**Figure 2.5 Electron density plots of the LUMO (above) and the HOMO (below) orbitals of TC. Reprinted with permission from Kliegman 2013. Copyright 2013 American Chemical Society.[216]**

### 2.1.4 Photochemistry of TC

It is important to understand how the much TC photodegrades under the measurement conditions. The TC degradation rate in natural sunlight is higher at pH 8 than at pH 5.6,[6] due to both the increased photo-reactivity of the phenolate and the increased overlap of the adsorption spectrum of TC with the emission spectra of sunlight.[81] When using TC at levels appropriate to environmental contamination at 0.001 µg/ml and pH 8.0 in direct sunlight for an hour, the concentration of TC dropped to less than 10% of the initial amount.[6] Other researchers found that the half-life of TC exposed to midsummer sun was 2.5 hours.[82]

The photo-degradation of TC was further probed in the work of Wong-Wah-Chung;[57] the effect of photolysis is seen as a general increase in the absorbance spectrum. TC appeared to disappear completely within half an hour when exposed to a 6 W Philips TUV light at 254 nm (Figure 2.6). The authors also found that oxygen present in solution decreased the rate of photolysis.

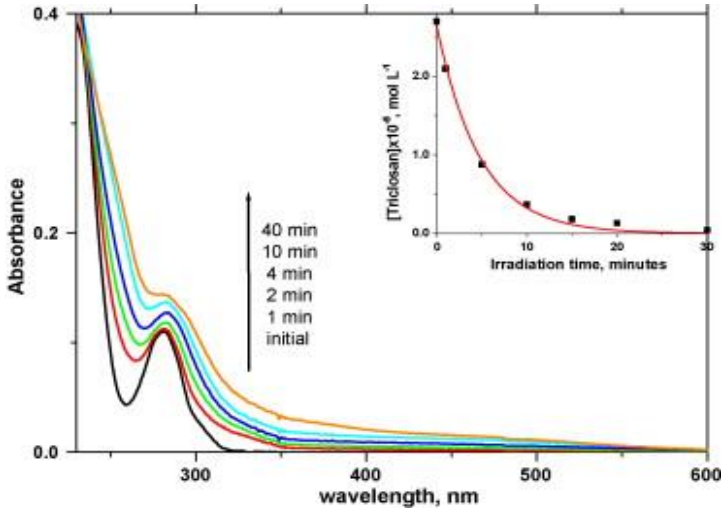


**Figure 2.6 Evolution of the absorption spectrum of an aerated aqueous solution of TC upon irradiation at 254 nm (pH 6.4). The TC concentration was measured using HPLC with MS and DAD with the absorbance at 250 nm.[57]**

A number of authors[6,82,217,218] have used techniques such as HPLC-UV, GC-MS, LC-MS and NMR to determine the photoproducts of TC, some of which are shown in Figure 2.7. The majority of authors have been particularly interested in photo-degradation as a route of TC decay in the natural environment when released at low concentrations from waste water treatment plants (WWTPs).

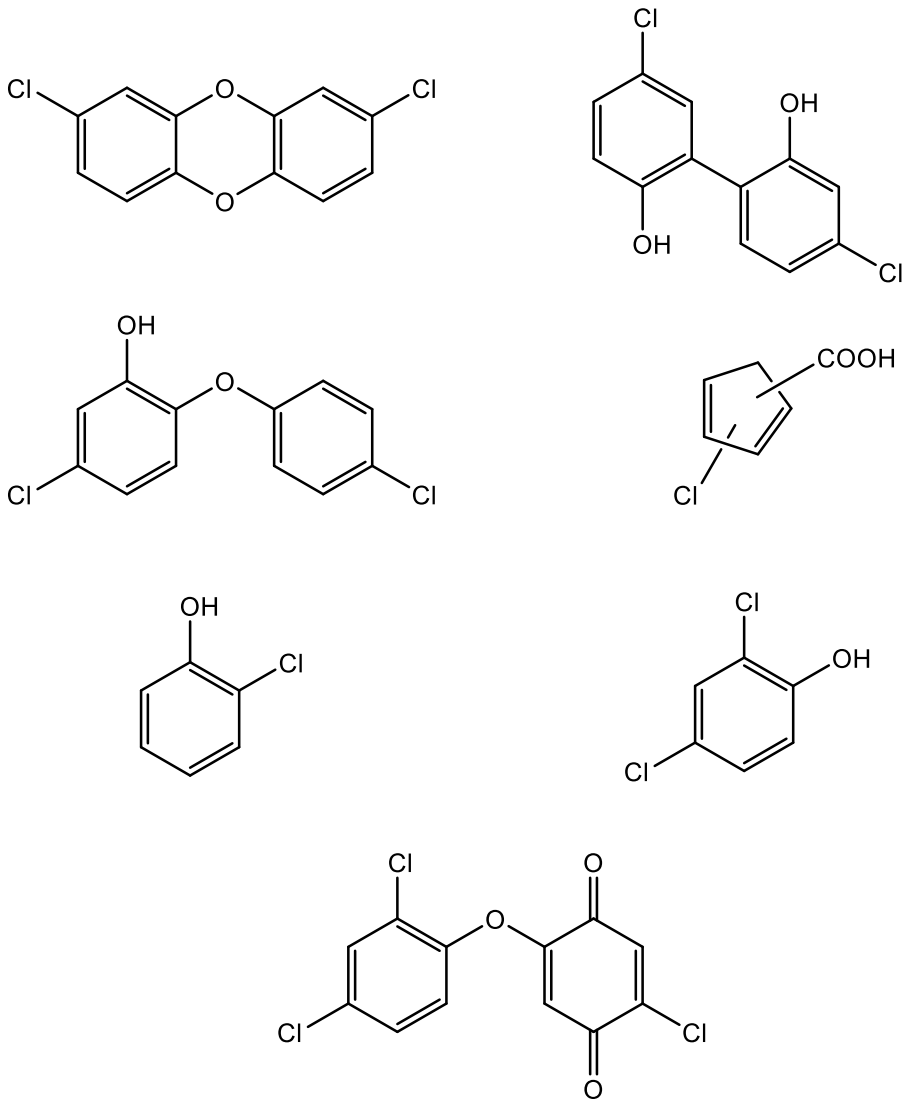


**Figure 2.7 Various photoproducts of TC, clockwise from top right: 5,6'-dichloro[1,1'biphenyl]-2,3'-diol, chloro-cyclopentadiene-1-carboxylic acid, 2,4-dicholorphenol, 2-chloro-5-(2,4-dichlorophenoxy)-2,5-cyclohexadiene, 2-chlorophenol, 5-chloro-2-(4-chlorophenoxy)phenol and 2,8-dichlorodibenzo-*p*-dioxin.** [5,81–83,216–218,220]

For example, Latch *et al.*[217] looked at samples with TC concentrations 0.001-0.022 mg/ mL irradiated under a 450 W Hg-Vapour lamp with various cut-off filters. They found that TC disappeared in the first five minutes. 2,8-dichlorodibenzo-*p*-dioxin (2,8-DCDD) concentration increased at the same rate as TC was degraded in a first order fit, after 5 minutes, the fit was lost due to the formation of light screening products. From their calculation of quantum yields, they conclude that the phenolate is the photoreactive species and the phenol is photostable.

This conclusion is in agreement with the work by Tixier,[81] where the pH was adjusted so that either the phenol was present (pH=5.9) or the phenolate was present (pH=11.5) and the sample was irradiated at $\lambda_{max}$. The quantum yield was calculated and was higher for the phenolate. Tixier used the following model to describe the phototransformation process:

$$k_{photolysis} = 2.303 \int_{\lambda} \varepsilon(\lambda)\phi(\lambda)\frac{dI(\lambda)}{d\lambda}d\lambda \qquad \text{Equation 2.13}$$

$\varepsilon(\lambda)$ is the molar absorption coefficient in $m^2mol^{-1}$ at $\lambda$, $\varphi(\lambda)$ is the reaction quantum yield in mol Einstein$^{-1}$ at $\lambda$ and $\frac{dI(\lambda)}{d\lambda}$ is the irradiation spectrum in Einstein $m^{-2}$ $nm^{-1}$.

Chen *et al*.[218,219] attribute the increased reactivity of the phenolate to two factors. The first is that the phenolate is more reactive than the phenol, as shown by Kliegman[216] where the excited state of the phenolate is more likely to undergo C-Cl bond cleavage than the phenol excited state. The other factor that must be considered is the higher molar extinction coefficient at higher pH, 6150 $mol^{-1}dm^3cm^{-1}$ compared to 4670 $mol^{-1}dm^3cm^{-1}$.[218]

A number of the products detected are actually intermediates which further react if left exposed to the light source. For example, 2,4-DCP has a low formation yield because the rate of decay is on a comparable timescale to the rate of formation so only steady state concentrations are observed.[82] In the presence of singlet oxygen, quinone has been detected as an intermediate between TC and 2,4-dichlorophenol (2,4-DCP).[82] The absorbance spectra of 2,4 DCP has $\lambda_{max}$ at 306 nm and half peak width of 30 nm (Figure 8.4).

The presence of surfactants has an effect on the degradation of TC. Degradation is dependent on which surfactant is used. All surfactants tested in the study by Chen[218] reduced the degradation rate but Triton-X100 was more protective than SDS and CTAB due to the absorbance in the same range as TC. The mixture of products was different when surfactants were present as compared to the photodegradation of aqueous TC, with no polymers detected when TC was irradiated with surfactant.

Latch[82] and Chen[218] noted when higher pH samples were irradiated, the absorbance at around 330 nm increased with time. They put this down to photo-yellowing caused by humification and mineralisation including the formation of polymers and oligomers. The formation of polymer is favoured in high concentration samples where the pH is kept slightly above the pKa.[219]

In the phototransformation of TC, the reaction proceeds via radical intermediates, based on the observed products. Kliegman[216] suggests the bi-radical as the most likely pathway for C-Cl bond cleavage (Figure 2.8) leading to lower chlorinated derivatives.

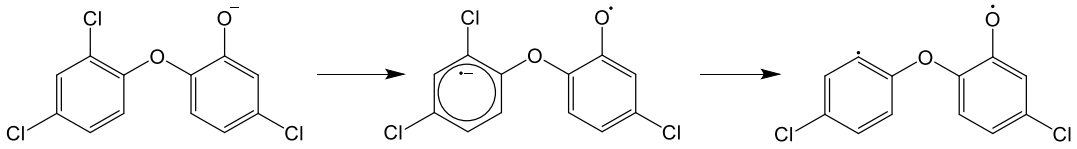


**Figure 2.8 Biradical routes for photochemical decay of the phenolate form of TC.**

All of this poses questions about the reliability of testing TC under UV light, for example when determining concentration. Caution should be taken over the amount of UV light TC is exposed to during measurements to avoid photodegradation. This is investigated in Section 2.3.4 using a stopped flow set-up.

## 2.2 Materials and Methods

### 2.2.1 Materials

TC (Igrasan ≥ 97%), sodium dodecyl sulphate (≥ 99%), sodium laurate (sodium dodecanoate 99-100%), sodium acetate, Trizma base, Trizma HCl and sodium carbonate (≥ 99.5%) were purchased from Sigma Aldrich (St Loius, MO, USA). Potassium chloride, sodium chloride, sodium hydroxide, potassium hydroxide, pH 4.4 acetate buffer, pH 7.4 phosphate buffer tablets and pH 9.2 borate buffer tablets were purchased from Fisher Scientific (Loughborough, UK). Deuterium oxide (≥ 99.9%) was purchased from Cambridge Isotopes (Andover, MA, USA) and sodium hydrogen carbonate was purchased from BDH Laboratory supplies (Poole, UK). The chemicals were all used without any further purification, except in the interfacial tension experiments and SANS experiments, where the SDS was recrystallized three times in ethanol. The purity of the recrystallized SDS was confirmed by measuring the surface tension of 1 mM SDS using pendant drop analysis and comparing the value found to the results by Hines.[111]

### 2.2.2 Methods

#### *2.2.2.1 Interfacial Tension Measurements*

Interfacial tension measurements were carried out using a Krüss force tensiometer K100 with a platinum Wilhelmy plate on the liquid-vapour interface. Forty dilutions were used starting from an initial concentration of 1 x$10^4$ mg/ L SDS down to 0.1 mg/ L with an average time per measurement of 8 minutes and a total of 40 measurements. Samples were prepared by sonication. The glassware used was cleaned in Deacon solution and rinsed five times before use.

Equilibrium interfacial tensions were measured by the pendant drop in air, where an average of eleven measurements was taken using a First Ten Angstroms FTA 200. Software (FTA32 Video 2.1) was used to measure interfacial tension based on the drop shape. The interfacial tension can be calculated using the Young-Laplace equation (Equation 2.6).

#### *2.2.2.2 Small Angle Neutron Scattering*

SANS measurements were made on the SANS-2D at the ISIS pulsed neutron source at the Rutherford Appleton Laboratory in November 2015. The measurements on SANS-2D were made using the white beam time-of-flight method, giving a $Q$ range of 0.004−1 $Å^{-1}$. The samples were contained in Starna 2 mm path length quartz spectrophotometer cells and maintained at a temperature of 25 °C. The data were corrected for background scattering, detector response, and the spectral distribution of the incident neutron beam, and converted to an absolute scattering cross section ($I(Q)$ in $cm^{-1}$) using standard procedures. Samples were prepared by sonication.

Data was fitted by I. Tucker using the methods described in Penfold 2002,[221] Petkov 2010[212] and Bradbury 2013.[211]

#### *2.2.2.3 UV-Vis of TC*

UV-Vis was used to measure the concentration of TC in solution, and determine its solubility. To allow optimum solubilisation of TC the appropriate amounts of TC and surfactant were dissolved in the minimum amount of methanol, which was removed under vacuum to leave a thin film. The film was re-dissolved in MilliQ water or appropriate buffer. The solution was then filtered through 0.45 µm nylon filters.

An absorbance calibration curve at 280 nm was carried out using solutions of TC in methanol with concentrations between 0.003-0.1 mg/ mL. For samples containing surfactant, a background with surfactant only was subtracted from the spectra. UV-Vis was carried out on a Perkin-Elmer Lambda 9000 UV-Vis spectrometer using UV WinLabL800/900 and analysed in Excel.

The pH was measured on a Hanna Instruments HI931410 pH meter and a Cole-Parmer calomel electrode (5990-35), calibrated daily using standard buffer solutions at pH 9, pH 7 and pH 4.

#### 2.2.2.4 Stopped-Flow analysis

Stopped flow analysis was carried out on an Applied Photophysics SX20 stopped flow spectrometer with a photodiode array (PDA) in the absorbance configuration. For kinetic measurements, 50:50 mixing was carried out with appropriate solvent and the average of seven to ten runs were taken. Analysis was carried by plotting the absorbance at $\lambda_{max}$ against time. Samples were prepared using rotary evaporation to form a thin film which was then dissolved in MilliQ water

#### 2.2.2.5 Nanosight Analysis

Nanosight tracks the Brownian motion of individual particles based on the scattering of the particles in a laser beam. With a 20 x objective connected to a CCD camera, the scattering from the particles can be seen and tracked.[222] The distance travelled by each particle allows the hydrodynamic diameter ($d$) to be calculated based on the Stokes-Einstein equation:

$$\frac{\overline{(x,y)}^2}{4} = Dt = \frac{Tk_B}{3\pi\eta d} \qquad \text{Equation 2.14}$$

where $T$ is the temperature, and $\eta$ is the dynamic viscosity. This gives high resolution particle distribution. Sample concentrations should be $10^7$-$10^9$ particles per ml.[223] Samples were prepared by rotary evaporation as above or mixed directly with MilliQ water and dissolved by sonication in a sonicator bath.

#### 2.2.2.6 pH Experiments

pH measurements were carried out on a Hanna Instruments (HI931410) pH meter in pH mode using a Cole-Parmer calomel electrode (5990-35) and a Malvern Ag/AgCl electrode (SEN0106). Calibrations were carried out on the same day as experiments with Hanna Instruments pH calibration solutions pH 4.010, pH 7.010 and pH 10.010. It is also considered good practise to measure the sample at the same temperature that the calibration was carried out.[224] Measurements were either carried out at room temperature (20°C ±1°C) or in a water bath set to 25°C

## 2.3 Results and Discussion

### 2.3.1 IFT Measurements of SDS and SL

I have carried out a set of experiments to observe the effect of TC on surfactant solutions. First, I ran experiments to determine the effect of TC on the CMC of SDS to find the proportion of SDS in micelles at different concentrations, and the effect of TC on the interfacial tension of SDS solutions, especially below the CMC. The CMC of SDS has been previously reported by many authors,[111] and is known to be affected by the concentration of salt[112,113] and organic solutes.[225] It is common for a hydrophobic solute to decrease the CMC. I used the CMC calculations to determine the concentration of surfactant in micelles so I could understand the amount of surfactant available to

solubilize TC. Below the CMC, excess TC will crystallise out of solution due to its low solubility. The solubility limit for TC in aqueous solution is much lower than the solubility limit in micellar surfactant solution, as initially mentioned in Section 1.1.3.

Interfacial tension at the air-water interface was measured using a platinum Wilhelmy plate. The purity of SDS was checked by finding the interfacial tension at 1 mM using pendant drop analysis. The interfacial tension was within error of the value found by Hines[111] for chemically pure SDS. The interfacial tension was plotted against concentration of SDS, when solutions of SDS and TC were made at a fixed weight ratio and diluted in 0.1 M NaCl, 0.01 M NaOAc (Figure 2.9). No pH control was used. TC causes a number of changes to the interfacial tension curves of SDS: a change in interfacial tension above the CMC, a change in the CMC and a change in the gradient below the CMC.

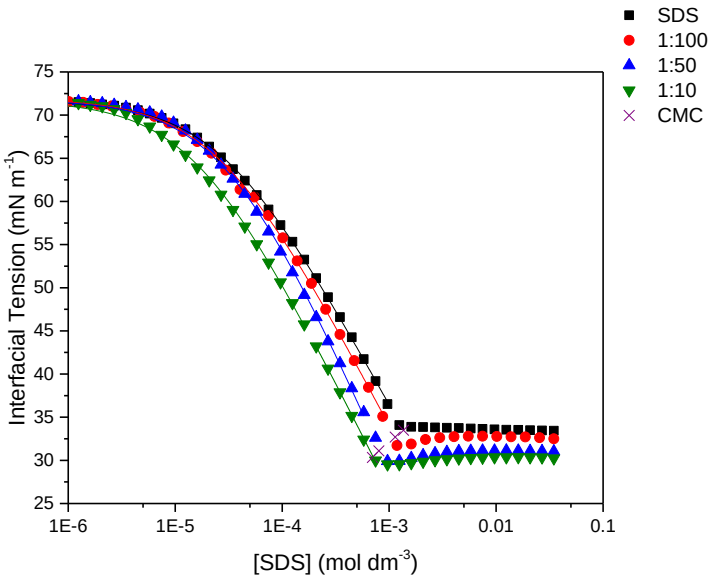


**Figure 2.9 The curves of the air/water interfacial tension against concentration of SDS in 0.1 M NaCl, 0.01 M NaOAc with different ratios of TC recorded using a force tensiometer with a Whilhelmy plate. TC to SDS in 1:10 wt ratio (green triangle), 1:50 wt ratio (blue triangle) and 1:100 wt ratio (red circle), and SDS alone (black square). The solid lines show the Szyszkowski fits, the parameters are in Table 2.2**

**Table 2.2 Parameters for Szyszkowski fits shown in Figure 2.9 for SDS in 0.1 M NaCl, 0.01 M NaOAc a. from the points above the solubility limit of TC b. from the points below the solubility limit of TC.**

| Surfactant system | $\gamma_0$/ mN m$^{-1}$ | $\Gamma_\infty$ / 10$^{-6}$ mol m$^{-2}$ | A/ 10$^{-5}$ mol dm$^{-3}$ |
|---|---|---|---|
| SDS | 71.7 ±0.1 | 4.01 ±0.02 | 2.97 ±0.06 |
| 1:100 TC/SDS | 71.9 ±0.1 | 4.19 ±0.04 | 2.69 ±0.08 |
| 1:50 TC/SDS | 71.8 ±0.1 | 5.04 ±0.04 | 3.2 ±0.4 |
| 1:10 TC/SDS[a.] | 71.7 ±0.1 | 4.48 ±0.02 | 1.72 ±0.03 |
| 1:10 TC/SDS[b.] | 71.7 ±0.1 | 4.5 ±0.1 | 1.7 ±0.1 |

Table 2.3 The critical micelle concentration of SDS (CMC) in mM, the interfacial tension above the CMC in mN $m^{-1}$ and the gradient of the line of the interfacial tension against log $C_{SDS}$ in mN $m^{-1}$.

| Ratio of TC to SDS | CMC/ mM | ST at 0.035 M SDS/ mN $m^{-1}$ | $\frac{d\gamma}{d \ln m_{SDS}}$ at the CMC/ mN $m^{-1}$ |
|---|---|---|---|
| 1 to 10 | 0.70 ±0.04 | 30.24 ±0.06 | -10.8 ±0.1 |
| 1 to 50 | 0.80 ±0.04 | 31.05 ±0.07 | -12.0 ±0.2 |
| 1 to 100 | 1.14 ±0.06 | 32.50 ±0.05 | -10.1 ±0.1 |
| SDS | 1.36 ±0.07 | 33.43 ±0.05 | -9.7 ±0.1 |

TC in a 1:10 ratio lowered the interfacial tension of 0.035 M SDS to 30.24 ±0.03 mN $m^{-1}$ from 33.43 ±0.05 mN $m^{-1}$. The decrease in interfacial tension is associated with a decrease in the work needed to transport the surfactant to the surface and a lower surface energy film formed by the absorbed surfactant and TC.[199] TC partitions to the interface because it is hydrophobic, so it causes the decrease in interfacial tension.

As the concentration of SDS decreased towards the CMC, the interfacial tension dipped in way characteristic of hydrophobic impurities within the surfactant system.[201] In this concentration region, there are fewer micelles, so there is more TC per micelle leading to a higher chemical potential in solution, which leads to a higher concentration in the monolayer to equate the chemical potentials and a lower $\gamma$. A similar effect is seen on the interfacial tension curves of SDS when the concentration of the impurity dodecanol is sufficiently high.

The CMC is the break point between the two regions of the surface tension curve, where the interfacial tension decreases with increasing concentration of surfactant and the region where increasing the concentration of surfactant does not decrease the interfacial tension. The region of the curve where the interfacial tension decreases with surfactant concentration can be fitted to the Szyszkowski equation

$$\gamma = \gamma_0 - RT\Gamma^{\infty} \ln\left(1+\frac{m_{SDS}}{A}\right) \qquad \text{Equation 2.15}$$

where $\gamma_0$ is the interfacial tension of water in the absence of SDS, $\Gamma^{\infty}$ is the saturation adsorption and $A$ is the Langmuir-Von Szyszkowski constant.[226,227] The Szyszkowski equation neglects interactions between molecules, and is designed to fit to systems with only one surfactant present, rather than systems where there is a co-surfactant.

Below the CMC, in the systems with SDS alone and 1:100 TC/SDS, the ratio of concentrations of TC to SDS was fixed because the concentration of TC was below the solubility limit in water. In the systems where the ratio of TC to SDS was higher, at some points below the CMC, the total concentration of TC in the system was above the solubility limit and a portion of TC was not in solution so that the effective concentration of TC was 1 x$10^{-5}$ M and excess TC crystallised out of solution. For the system with 1:50 TC/SDS, for all the points below 7 x$10^{-4}$ M SDS, the concentration of TC was below the solubility limit and the data was fitted to a Szyszkowski curve. For the system with 1:10 TC/SDS, for all of the data points collected above 1.4 x$10^{-4}$ M to the CMC, the concentration of TC in solution was constant, at the solubility limit, assuming supersaturation did not occur, because the total

amount of TC in the system was above the solubility limit. The data points with saturated TC, and below the saturation limit were fitted separately to the Szyszkowski equation, where the parameters found from fitting below the solubility limit were within error of the fit for the region of the curve where TC was above the solubility limit (Table 2.2).

The Szyszkowski curve fits the data collected with just SDS very well, but for the data collected with 1:50 TC/SDS, the data fit is poorer at higher concentrations of SDS. I chose to fit the data to Szyszkowski plots as they capture the shape of the surface tension curve over the whole concentration range up to the CMC rather than using a linear fit against $\ln m_{SDS}$ to part of the curve. If a linear fit was used, error would be added by the choice of points to include and exclude from the linear fit. However, Szyszkowski plots are designed for systems where there is no co-surfactant, so in the systems where $\Gamma_{TC}$ is high, the data deviates from a Szyszkowski plot and the quality of the fit is limited, as demonstrated in the 1:50 data set.

The CMC of the four systems was found by the intercept of the Szyszkowski curves with the average interfacial tension of the 5 points below 0.035 M, well above the CMC. With hydrophobic dopants, which decrease $\gamma$ just above the CMC, the accuracy of determining the CMC from interfacial tension plots is limited due to the difficulty in finding $\gamma$ at the CMC. The accuracy of $\gamma$ at the CMC in this experiment is limited by the number of measurements used to find the average $\gamma$ above the CMC. However, as the method used to find the CMC is the same for each of the data sets in Figure 2.9, the effect of TC on the CMC can still be found, even if there is uncertainty in the absolute values. The error is consistent between measurements.

As the ratio of TC to SDS increased, the CMC decreased, to counter the free energy cost of TC in the bulk rather than the more favourable hydrophobic micelle centre. The decrease in CMC with concentration of TC was not linear. In both the 1:50 and 1:100 TC/SDS systems, the concentration of TC at the CMC was above the solubility limit. At concentrations just above the CMC, where there was very little surfactant in micelles to solubilize TC, any excess TC crystallised out of solution. Therefore at concentrations of SDS just above the CMC, the concentration of TC in solution was similar in the 1:50 and 1:100 TC/SDS systems, when at other points on the curve there was a larger difference in the concentration of TC, hence the similar CMC values.

Below the CMC, the gradient of the interfacial tension with concentration can be used to find the surface excess concentration, $\Gamma_i$, using the Gibbs equation (Equation 2.3). In the experiments shown in Figure 2.9, there is excess salt and both TC and SDS contribute to the observed gradient so that

$$\frac{d\gamma}{d\ln m_{SDS}} = -RT\Gamma_{SDS} - RT\Gamma_{TC} \qquad \text{Equation 2.16}$$

This equation only applies below the solubility limit of TC. From the Szyszkowski plots, $\frac{d\gamma}{d\ln m_{SDS}}$ can be calculated at the CMC. The effective surface excess at the CMC, calculated from the Szyszkowski fit, which contains contributions from SDS and TC is

$$\Gamma_{obs} = \Gamma^{\infty}\frac{m_{SDS}}{A + m_{SDS}} \qquad \text{Equation 2.17}$$

The gradients of interfacial tension against ln$m_{SDS}$ at the CMC are shown in Table 2.3. The gradients of the plots increased as the ratio of TC to SDS increased suggesting an increase in the Gibbs surface excess. From the surface excess, the minimum area occupied by the surfactant absorbed at the interface ($A_m$) can be calculated using Equation 2.4.

When TC was included in the system, the gradient was higher than the system with SDS alone, suggesting a decrease in the area per molecule. The area per molecule for SDS can be calculated when the concentration of TC is constant. When the concentration of TC is constant, the gradient of $\gamma$ against ln$m_{SDS}$ gives the surface excess of SDS. For SDS, the area per molecule was 42 ± 2 Å$^2$ which is very similar to the results given by Tajima,[120,202,203] from interfacial tension experiments using tritiated SDS where the area per molecule of SDS in 0.115 M NaCl was 38.4 Å$^2$ (Figure 2.2). For the 1:10 TC/SDS system, for the points above the solubility limit of TC but below the CMC, $\mu_{TC}$ is constant so the slope of the Gibbs plot is due solely to $\Gamma_{SDS}$. From the gradient of $\gamma$ against ln$m_{SDS}$, the surface excess of SDS can be calculated. The area per molecule of SDS when the total concentration of TC was above the solubility limit in the 1:10 TC/SDS experiment was 38 ±2 Å$^2$.

It was not possible to find the area per molecule of surfactant alone from the data collected with 1:100 and 1:50 TC/SDS because the gradient of interfacial tension against ln$m_{SDS}$ contained contributions from the surface excess of SDS and TC. To determine $\Gamma_{SDS}$ and $\Gamma_{TC}$ separately, one has to vary $m_{SDS}$ at constant $m_{TC}$, and $m_{TC}$ at constant $m_{SDS}$, respectively, in the dilute regime. The interfacial tension at 4.4 x10$^{-5}$ mol dm$^{-3}$ SDS, against concentration of TC has been plotted in Figure 2.10, taken from the data in Figure 2.9. If the concentration of TC on the surface is at the dilute limit, then a plot of interfacial tension against surface excess of TC should have the gradient $-RT$ because

$$\gamma_o - \gamma = -\Gamma RT \qquad \text{Equation 2.18}$$

The surface excess of TC is proportional to the concentration in bulk so that

$$\Gamma_{TC} = -\frac{m_{TC}}{RT}\left(\frac{d\gamma}{dm_{TC}}\right)_{m_{SDS}} \qquad \text{Equation 2.19}$$

Based on the data shown in Figure 2.10 at 4.4 x10$^{-5}$ mol dm$^{-3}$ SDS, which is fitted to two straight line curves, TC is in the dilute limit in all solutions, except at the highest concentration. From the gradient of the plot, the surface excess over the concentration of TC $\left(\frac{\Gamma_{TC}}{m_{TC}}\right)$ is 7.0 ±0.4 x10$^{-4}$ m. If the surface monolayer has a thickness of 1 nm, the partition coefficient between the bulk and the surface monolayer is 700 000. As there are only a few data points, it is difficult to say with certainty if the highest concentration of TC is outside the dilute limit. If the final point was included in the fit, the partition coefficient is 500 000.

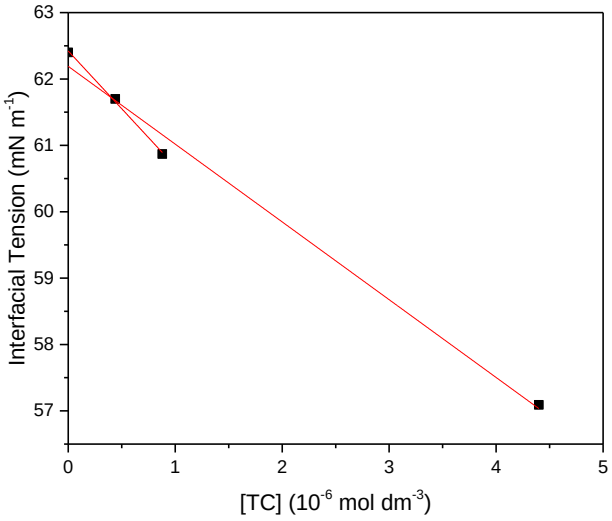


**Figure 2.10 The interfacial tension at 4.4 x10$^{-5}$ mol dm$^{-1}$ SDS against the concentration of TC The red lines are linear fits with gradient -1.15 ±0.07 x10$^{6}$ mN m$^{-1}$ mol$^{-1}$ dm$^{3}$ when all points are included in the linear fit and -1.73 ±0.09 x10$^{6}$ mN m$^{-1}$ mol$^{-1}$ dm$^{3}$ when only the first three points are included in the linear fit.**

The effect of TC on the interfacial tension curves of SDS was investigated further in a data set collected with a constant concentration of TC. The concentration of TC was kept constant in the buffer and the concentration of SDS changed, rather than the ratio of TC to SDS remaining constant (Figure 2.11). The solubility of the phenolate TC is higher than the phenol form of TC (Table 2.8) so the pH was increased with 0.1 M NaOH so that sufficient TC could be dissolved. The phenolate form of TC has a much smaller effect on the interfacial tension above the CMC: at 0.035 M SDS, there was no significant different between the observed interfacial tensions with and without TC (Table 2.5) and there was a smaller decrease in the observed CMC with the phenolate compared to the phenol. The data collected below the CMC was fitted to the Szyszkowski equation and the data fit was better than for the previous experiment where the surface excess of TC changed. The gradient of the plot of interfacial tension against ln*m* at the CMC was calculated and used to find the area per molecule.

The gradient of interfacial tension against ln$m_{SDS}$ was shallower for the data collected with 0.05% TC than for SDS alone, with a slightly higher area per molecule of SDS (Table 2.5). This was the opposite of the effect of the phenol on the area per molecule of SDS and is due to repulsive interactions between the negatively charged surfactant and the negatively charged TC. $\gamma_0$ of 0.05 % TC in 0.1 M NaOH, 0.01 M NaOAc was significantly lower than the interfacial tension of water.

The interfacial tension of the saturated solutions of the phenol (in water) and the phenolate (in 0.1 M NaOH) were measured using pendant drop. $\gamma$ of the saturated phenol was 71.6 ±0.2 mN m$^{-1}$ and the saturated phenolate solution had $\gamma$ of 50.9 ±0.1 mN m$^{-1}$. The phenol form of TC only caused a slight decrease to the interfacial tension of water. The saturated phenol alone showed a smaller decrease in the $\gamma$ of water than when it was combined with SDS below the solubility limit. TC/SDS in 1:10 ratio lowered the surface tension by 5.3 mN m$^{-1}$ at 4.4 x10$^{-5}$ mol dm$^{-3}$ SDS, where TC was below the saturation limit, as compared to SDS alone. The interfacial tension of saturated TC$^{-}$ was much lower than $\gamma_0$ of 0.05 % TC in SDS.

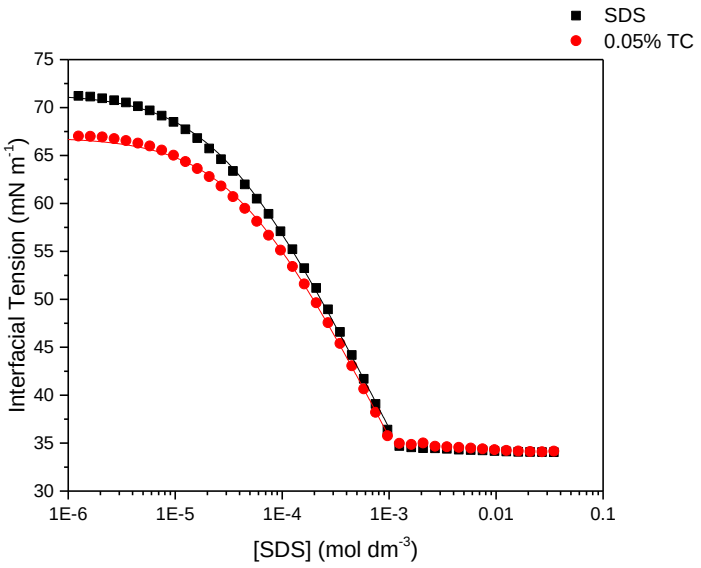


**Figure 2.11 The curves of the air/water interfacial tension against concentration of SDS in 0.1 M NaOH, 0.01 M NaOAc with different concentrations of TC: 0.05% TC (red circles) and SDS alone (black square). The solid lines show the Szyszkowski fits, the parameters are in Table 2.4. Curves were recorded using a force tensiometer with a Whilhelmy plate**

**Table 2.4 Parameters for Szyszkowski fits shown in Figure 2.11 for SDS in 0.1 M NaOH, 0.01 M NaOAc**

| Surfactant system | $\gamma_0$/ mN m$^{-1}$ | $\Gamma_\infty$ / 10$^{-6}$ mol m$^{-2}$ | A/ 10$^{-5}$ mol dm$^{-3}$ |
|---|---|---|---|
| SDS | 71.4 ±0.1 | 3.92 ±0.02 | 2.85 ±0.08 |
| 0.05% TC and SDS | 66.9 ±0.1 | 3.90 ±0.03 | 4.1 ±0.1 |

**Table 2.5 The critical micelle concentration of SDS (CMC) in mM, the interfacial tension above the CMC and at 0.1 mg/ mL TC in mN m$^{-1}$, the gradient of the line of the interfacial tension against log [SDS] in mN m$^{-1}$ and the area per molecule of SDS in Å$^2$ for data collected in 0.1 M NaOH, 0.01 M NaOAc.**

| [TC]/ % | CMC/ mM | ST at 0.035 M SDS/ mN/m | $\frac{d\gamma}{d \ln m_{SDS}}$ at the CMC/ mN m$^{-1}$ | Area per molecule/ Å$^2$ |
|---|---|---|---|---|
| 0.05 | 1.17 ±0.02 | 34.16 ±0.04 | -9.3 ±0.2 | 44 ±2 |
| SDS | 1.31 ±0.02 | 34.05 ±0.06 | -9.5 ± 0.2 | 43 ±2 |

An experiment was run to calculate the CMC of SL in 0.1 M KCl and 0.01 M NaOAc using pendant-drop tensiometry (Figure 2.12 and Table 2.6). Kanicky[133] found that the area per molecule of 0.05% SL was very dependent on pH and showed a minimum at pH 7.5 of 56.7 Å$^2$ using Wilhelmy plate tensiometry. The data shown below is not of sufficient quality to calculate $\Gamma_{SL}$. The CMC was 13 ±5 mM. There is a significant dip in the interfacial tension curve indicating that SL is not pure.

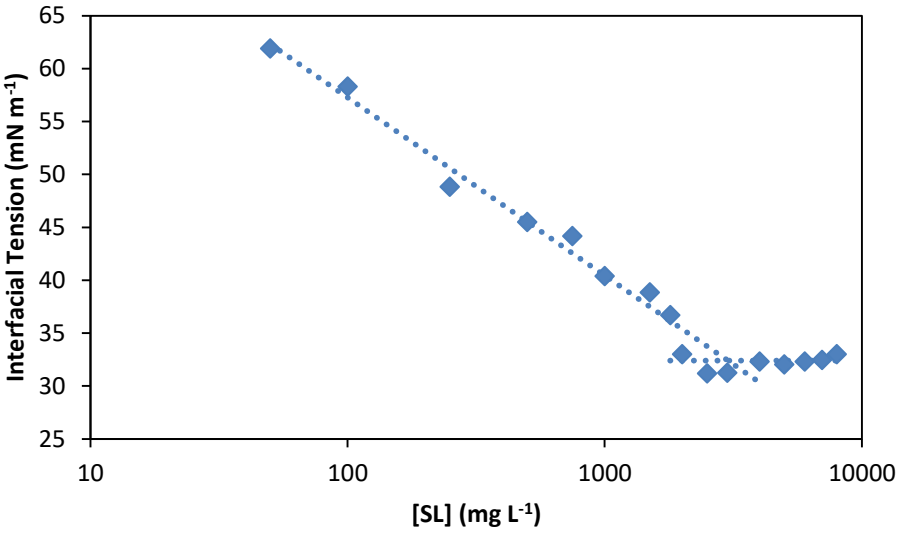


**Figure 2.12 Interfacial tension in mN $m^{-1}$ against concentration of SL in 0.1 M KCl and 0.01 M NaOAc measured by pendant-drop. The two blue lines were where the data was fit to curves below the CMC y=−7.3ln(x)+91 and above the CMC y=32.4 ±0.4.**

**Table 2.6 The critical micelle concentration of SL (CMC) in mM and the interfacial tension above the CMC in mN $m^{-1}$.**

| | CMC/ mM | ST above CMC/ mN $m^{-1}$ |
|---|---|---|
| SL | 13 ±5 | 32.4 ±0.4 |

### 2.3.2 SANS Analysis of SDS and TC Solutions

Small Angle Neutron Scattering was used in a small study to investigate the change in the size and shape of SDS micelles with TC at different ratios. Samples were prepared with a total solute concentration of 69.3 mM and the ratio of TC to SDS was varied from 1:9, 1:19 and 1:99 in 0.1 M NaCl, 0.01 M NaOAc. Data was fitted to the Hayter-Penfold core and shell model[209,210,228] with polydispersity and screened Yukawa potential.[229] The model was similar to the model by Penfold, Staples and Tucker[221] used to model hexadecane in SDS and $C_{12}E_6$ micelles. The inter-particle interactions depend on the surface charge, micelle number density and the Debye-Hückel inverse screening length and diameter. The inter-particle interactions and their contribution to the structure factor are modelled using a refined mean spherical approximation (RMSA).[209,210]

Data fitting was carried out by Dr I. Tucker and is summarised in Table 2.7 and Figure 2.13. The scattering intensity against scattering vector, *Q,* for 2% SDS and fit are plotted in Figure 2.15. The fits of the other samples and additional fitting parameters are in the appendix, Section 8.2.1. The inner core ($R_1$) is represented by alkyl chains only and is constrained. It plays no role in the Coulomb potential. The outer shell ($R_2$) contains additional alkyl chain, the head-groups and radius of hydration. Fitting was first optimised around the parts of the curve at the lowest values of Q and the part of the curve where I(Q) starts to curve with Q. The model did not invoke polydispersity but instead included a Shultz distribution of the radius and focussed on including the ellipticity of the micelles. There may be more ellipticity in the micelles than the fit allows. The model first tried included TC in the core but gave unreasonable numbers for aggregation number and unphysical answers for the radius of the core; the core cannot be any larger than the SDS chain length. The

model used with TC included in the shell gave more reasonable numbers for the radius and aggregation number.

The radius of the micelle core remained constant with increasing concentration of TC but the radius of the outer shell increased, suggesting that TC resides in the shell, rather than the core (Figure 2.14). The fit of the sample with 0.1% TC, 1.9% SDS is poor (appendix Figure 8.12) and the fitting parameters are not comparable to those from the other samples. The aggregation number ($N_{agg}$), which is the average number of molecules of SDS per micelle, increased with concentration of TC and the ellipticity of the micelle decreased. The scattering data for TC to SDS in 1:99 ratio and 1:19 ratio are very similar to the data with just SDS, but when TC is included at the 1:9 ratio, there is a large increase in the size of the micelles (Figure 2.14), with TC residing in the shell, rather than the core. It is known that fluorocarbon surfactants in mixed micelles with hydrocarbon surfactants show demixing,[230] and it may be that at high concentrations the chlorocarbon TC shows similar demixing in the micelle headgroup region.

**Table 2.7 Summary of selected fitting parameters for SANS data**

| SDS/ % | TC/ % | Core Radius, $R_1$/ Å | Total Radius, $R_2$/ Å | $N_{agg}$ | Electronic charge per micelle/ e | Ellipticity |
|---|---|---|---|---|---|---|
| 2 | 0 | 16.7 ±0.5 | 18.6 ±0.5 | 120 ±10 | 7.9 | 1.2 ±0.1 |
| 1.98 | 0.02 | 17.5 ±0.5 | 21.1 ±0.5 | 120 ±10 | 7.3 | 1.2 ±0.1 |
| 1.9 | 0.1 | 15.9 ±0.5 | 17.9 ±0.5 | 150 ±10 | 5 | 1.3 ±0.1 |
| 1.8 | 0.2 | 21.1 ±0.5 | 41.3 ±0.5 | 600 ±60 | 11 | 1.0 ±0.1 |

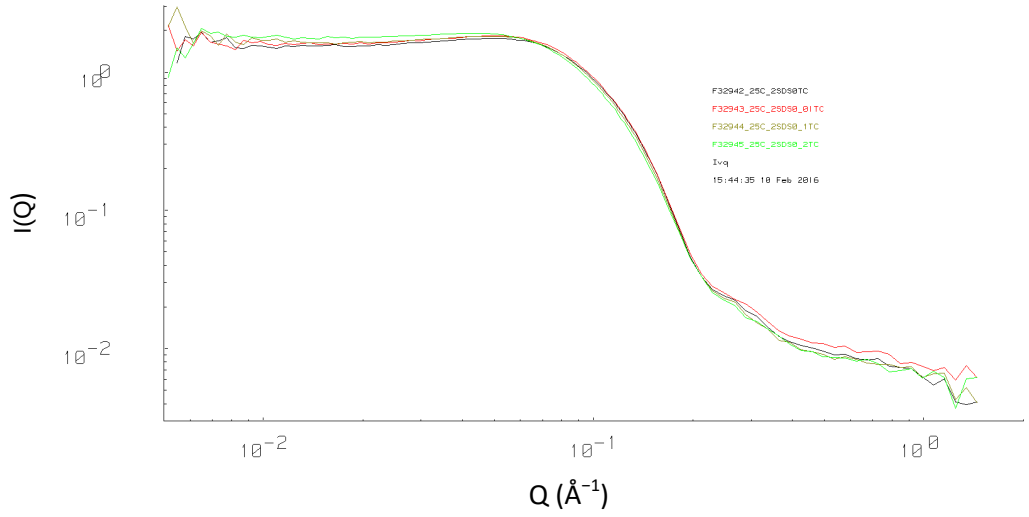


**Figure 2.13 Normalized scattering intensity, I(Q), against scattering vector, Q, in Å$^{-1}$ of 2% SDS in 0.1 M NaCl, 0.01 M NaOAc (black), of 0.02% TC 1.98% SDS in 0.1 M NaCl, 0.01 M NaOAc (red) of 0.1% TC 1.9% SDS in 0.1 M NaCl, 0.01 M NaOAc (brown) and of 0.2% TC 1.8% SDS in 0.1 M NaCl, 0.01 M NaOAc (green)**

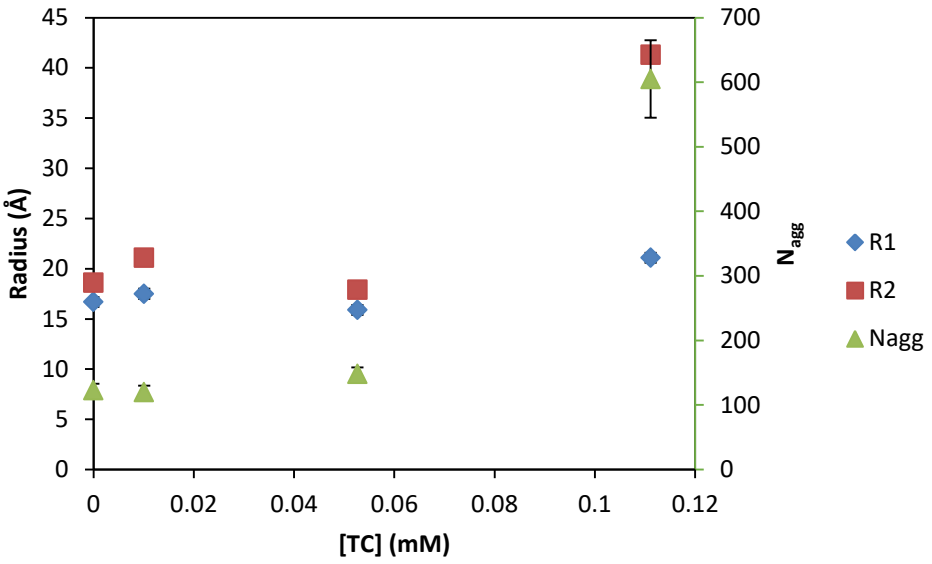


**Figure 2.14 Radius of the inner core, R1, and the total radius, R2, of SDS micelles and the calculated aggregation number against the ratio of TC to SDS when the total concentration of TC and SDS is 69.3 mM.**

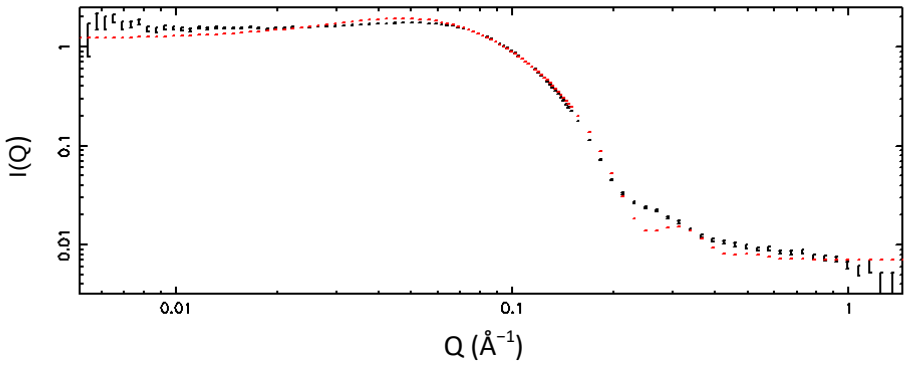


**Figure 2.15 Normalized Scattering intensity, I(Q), of 2% SDS in 0.1 M NaCl, 0.01 M NaOAc (black) against scattering vector, Q in Å$^{-1}$ and fitting (red)**

To improve the quality of the fitting, data could be collected with more contrasts, using per-deuterated SDS to find the location of TC in the micelles and using deuterated TC to find the SDS core and shell radius. Experiments could also be carried out with a chlorinated surfactant to test whether de-mixing occurs or not. These further experiments were not carried out in this work due to time constraints. This SANS study was planned as investigation to find the aggregation number of the surfactant, rather than designed to fully characterise the system. The aggregation numbers are larger than those predicted in the model used by Laguerre[231]

$$N_{agg} = 164(0.27m_{SDS_{tot}} + 0.73m_{SDS_{aq}} + m_{salt})^{1/4} \qquad \text{Equation 2.20}$$

which at 2% SDS gives $N_{agg}$ as 98 in 0.11 M total salt.

### 2.3.3 Determination of the Concentration of TC in Solution by UV-Vis Absorption spectroscopy

TC has an absorbance maximum around 281 nm in unbuffered water. The maximum of the TC peak ($\lambda_{max}$) depends on the pH of solution: the phenol has a lower $\lambda_{max}$ than the phenolate form.[6] The aim of these UV-Vis experiments was to determine the concentration of TC in solution based on the absorbance at 280 nm and to determine the proportions of phenol and phenolate in micelles and in the bulk. Absorbance measurements were used to determine the solubility of TC with and without surfactants and at different pH.

The $\lambda_{max}$ of the phenol form of TC is 281 nm and the $\lambda_{max}$ of the phenolate is 291 nm. The molar absorbance coefficient is higher for the phenolate than the phenol at $\lambda_{max}$, although the molar extincion coefficient at 280 nm is similar regardless of the form of TC present (see Figure 1.6).[6,8] The peak position observed in UV-Vis at intermediate pH, when there are both forms of TC in solution is at a weighted average of the peak of the phenol and the phenolate. The molar extinction coefficient at 280 nm was determined when TC was below the solubility limit in surfactant solutions. The wavelength of maximum absorbance ($\lambda_{max}$) was used to understand whether the phenol or phenolate form of TC was predominant in solution.

The UV-Vis spectrum in Figure 2.16 is a saturated solution of the phenol form of TC in water in a 1 cm pathlength cell and 0.05 mg/ml of the phenolate in 0.1 M NaOH in a 1 mm pathlength cell. Excess solid TC was removed by filtration through a 0.45-µm nylon syringe filter. The calculated concentration in solution is proportional to the absorbance at 281 nm, from the Beer-Lambert law, Equation 2.12. The solubility of the phenol was determined as 0.004±0.001 mg/ mL (Figure 2.16), based on a calibration in methanol (Figure 2.17) which is comparable to the values found by other researchers.[10]

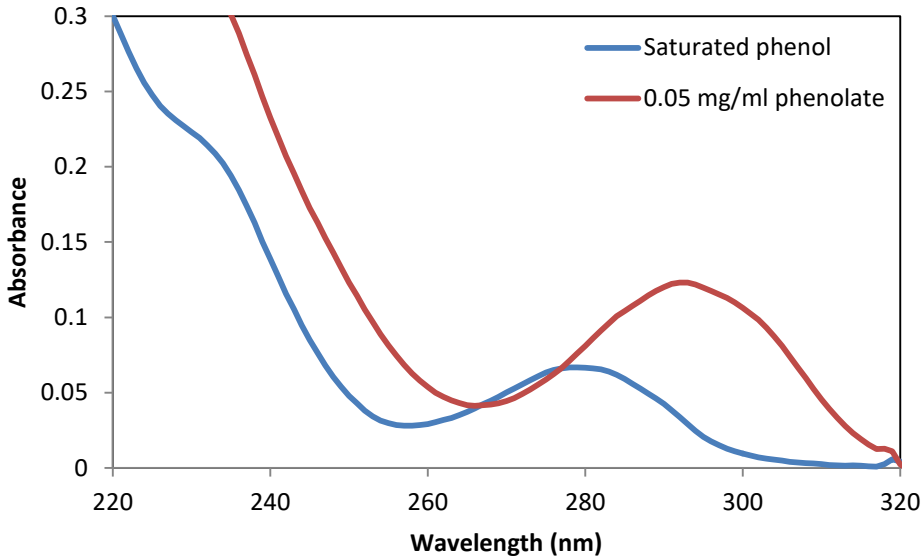


**Figure 2.16 Absorbance (A) against wavelength (λ) in nm for saturated TC in water, cuvette pathlength was 1 cm (blue) and 0.05 mg/ mL TC in 0.1 M NaOH, cuvette pathlength was 1 mm.**

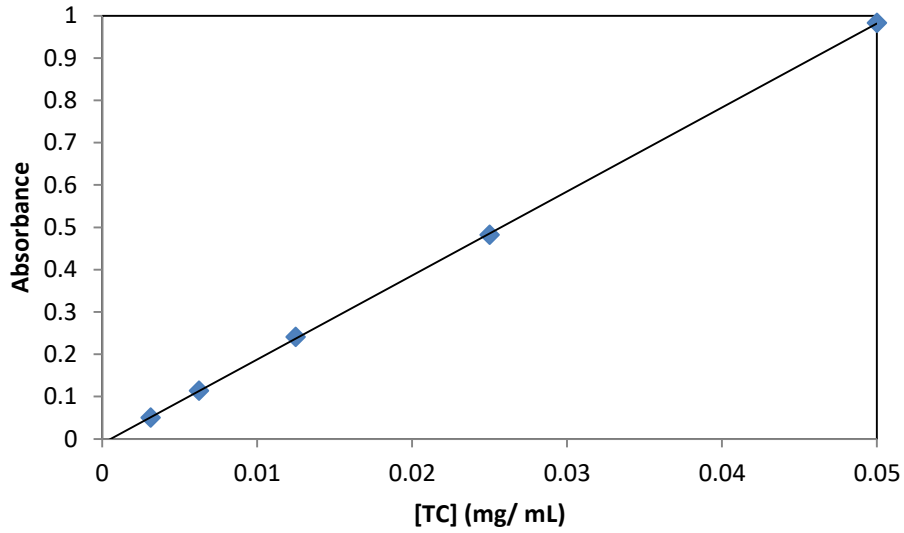


**Figure 2.17 Absorbance (A) at 280 nm against concentration of TC in methanol. The line of best fit is shown in black, with a gradient of 19.91±0.03 ml/mg and intercept of -0.01±0.02. The molar extinction coefficient was 5.76 ±0.09 x10$^3$ mol$^{-1}$dm$^3$cm$^{-1}$. Cuvette pathlength 1 cm.**

The concentration of TC dissolved in a saturated solution in 0.1 M NaOH was measured and 0.68 ±0.08 mg/ mL was in solution, with $\lambda_{max}$ of 292 nm (Figure 2.16). The concentration curve used to calculate the concentration of the phenolate was TC in 0.1 M NaOH based on the absorbance at 280 nm (Figure 2.18). The extinction coefficient at 280 nm of the phenolate, 4 900 ± 100 mol$^{-1}$dm$^3$cm$^{-1}$, was lower than that of the phenol in methanol, 5 760 ±90 mol$^{-1}$dm$^3$cm$^{-1}$.

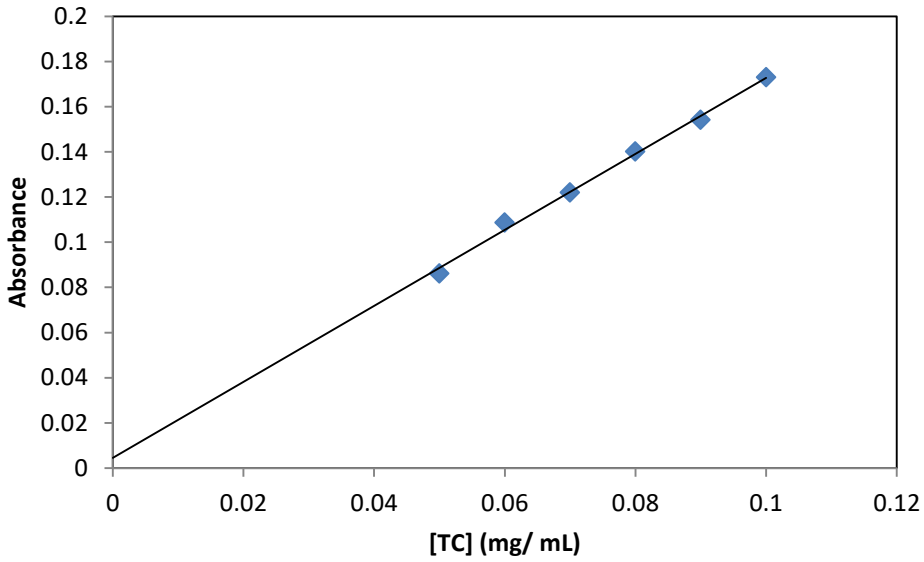


**Figure 2.18 Absorbance (A) at 280 nm against concentration of TC in 0.1 M NaOH in mg/ mL. The line of best fit is shown in black, with a gradient of 1.68 ± 0.05 ml/mg and intercept of 0.005 ± 0.004. The molar extinction coefficient was calculated as 4.9 ± 0.1 x10$^3$ mol$^{-1}$dm$^3$cm$^{-1}$. Cuvette pathlength was 1 mm.**

Surfactants such as SDS and SL are known to increase the solubility of TC in solution above the CMC.[10] UV-Vis was used to determine the concentration of TC dissolved in samples with 1% surfactant. At 1%, all of the surfactants are in the micelle phase.[232,233] The SL and SDS systems were

compared to $C_{12}TAB$ and $C_{12}E_8$, a cationic and non-ionic surfactant respectively, to investigate the effect of surfactant charge on the observed spectra (Figure 2.19 and Table 2.8). $C_{12}TAB$ is dodecyltrimethylammonium bromide, a cationic surfactant with a CMC of 0.015 M;[234] $C_{12}E_8$ is octaethylene glycol monododecyl ether which has a CMC of 7 x$10^{-5}$ M.[235] Samples were filtered through a 0.45-µm filter before measurement to remove any excess TC and left overnight to equilibrate. Initially samples were made up using 1 mg/ mL TC and 1% (wt/wt) soap, and the absorbance was too high to measure in 10 mm pathlength cells, so 1 mm pathlength cuvettes were used (Figure 2.19).

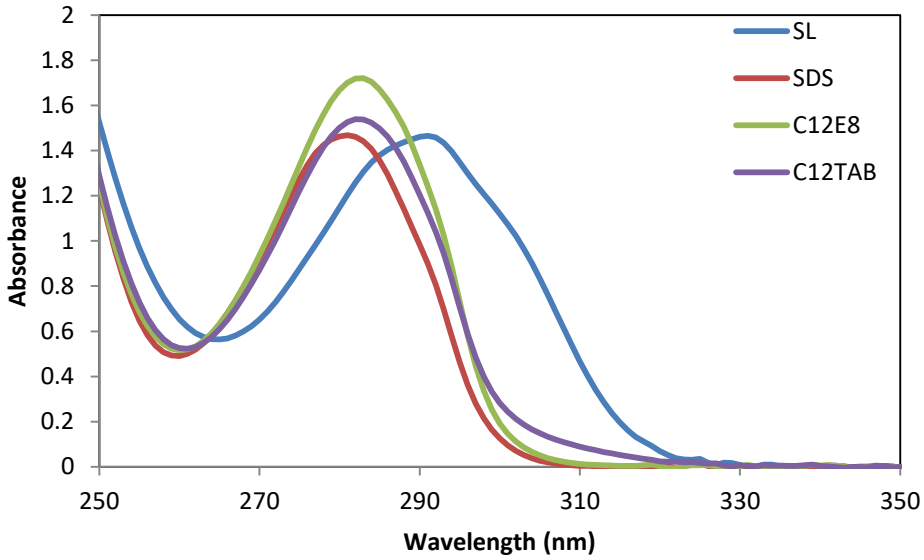


**Figure 2.19 Absorbance against wavelength for 1% surfactant, 1 mg/ mL TC in water using a 1 mm pathlength cuvette.**

**Table 2.8 The molar extinction coefficients and maximum absorbance of TC in different surfactants (1% w/w) and when 0.1% TC is initially added. The cuvette pathlength was 1 mm.**

| Surfactant | ε at 280 nm/ $mol^{-1}dm^3cm^{-1}$ | $\lambda_{max}$/nm |
|---|---|---|
| SDS | 4 200 ±100 | 281 |
| SL | 3 300 ±100 | 291 |
| $C_{12}TAB$ | 4 300 ±100 | 282 |
| $C_{12}E_8$ | 4 800 ±100 | 283 |

The spectra shown have the surfactant background subtracted. In these samples, it was assumed that TC was below the solubility limit and all of the TC was dissolved, based on concentration calculations using the extinction coefficient of the phenolate. The absorbance was used to calculate $\varepsilon$ of TC in the surfactant solutions. The extinction coefficients for TC in surfactant are lower (Table 2.8) than the extinction coefficient of the phenolate in water. The extinction coefficient in $C_{12}TAB$ and $C_{12}E_8$ was higher than the extinction coefficients of TC in spherical micelles of SDS and SL. The extinction coefficients were lower than either TC in methanol or the phenolate alone because of the surfactant interaction with TC and the change in the environment of TC. The extinction coefficient varied with solvent (Table 2.9). The extinction coefficient was highest in methanol and lowest in SL micelles. Depending on the orientation and partitioning of TC in the micelles, TC is solvated differently, causing a decrease in the observed $\varepsilon$.

$\lambda_{max}$ was found to be 280 nm for SDS solutions, 291 nm for SL solutions and 282 nm for $C_{12}$TAB solutions. The absorbance peak for TC in $C_{12}$TAB solution was broader than the peak in SDS and showed significant absorbance at higher wavenumbers, when in SDS the absorbance had returned to the baseline, suggesting that TC had undergone some photochemistry and the peak at 310 nm may be from some of the photoproducts of TC or other impurities in solution such as 2,4-DCP. When tested, the pH of the 1% SL with 0.05 mg/ mL TC solution was around 10.5, whereas the pH of the similar SDS solution was much lower at around 6. The pKa of TC is 7.9,[236] so the spectra collected in 1% SL was the phenolate form of TC and the spectra collected in SDS was the phenol form of TC.

TC in $C_{12}$TAB and $C_{12}E_8$ had a slightly higher $\lambda_{max}$ than in SDS, but the absorbance spectrum was still dominated by the phenol rather than the phenolate. $C_{12}$TAB alone has a peak with $\lambda_{max}$ at 263 nm (Figure 8.5), so the absorbance is not caused by the surfactant. The shape of the peaks at 260 nm was the same for the surfactant mixtures with the phenol.

**Table 2.9 The molar extinction coefficients and maximum absorbance of TC in different solvents a. taken from Wong-Wah-Chung.[57]**

| Solvent | $\varepsilon$ at 280 nm/ $mol^{-1}dm^3cm^{-1}$ | $\lambda_{max}$/ nm |
|---|---|---|
| Methanol | 5 760 ±90 | 281 |
| Heptane | 4 200 ±200 | 278 |
| Chloroform | 3 700 ±200 | 279 |
| Water[a.] | 4 200 | 281 |

I studied the effect of pH on solutions 0.05 mg/ mL TC and SDS at 1% in different buffer solutions (Figure 2.20). In these solutions, the wavelength of maximum absorbance did not change significantly with pH: $\lambda_{max}$ varied between 279-282 nm, indicating that the dominant form of TC in all these solutions was the phenol in solution. This method was insensitive to a small amount of the phenolate, otherwise the observed $\lambda_{max}$ would change. At pH 9.2, based on the pKa, there is twenty times the phenolate to phenol. Whilst there is some difference in wavenumber from the different forms of TC, when the bin size on the spectrometer was 1 nm and the error in $\lambda_{max}$ was ± 1nm, it was difficult to use the absorbance spectra to calculate the relative concentrations of the phenol and the phenolate especially when $\lambda_{max}$ depends on the environment. The background at pH 4.4 was high, suggesting that there may be particles scattering light and causing the increase in absorbance. For particles to form after filtering, TC in SDS and this buffer solution must not stable.

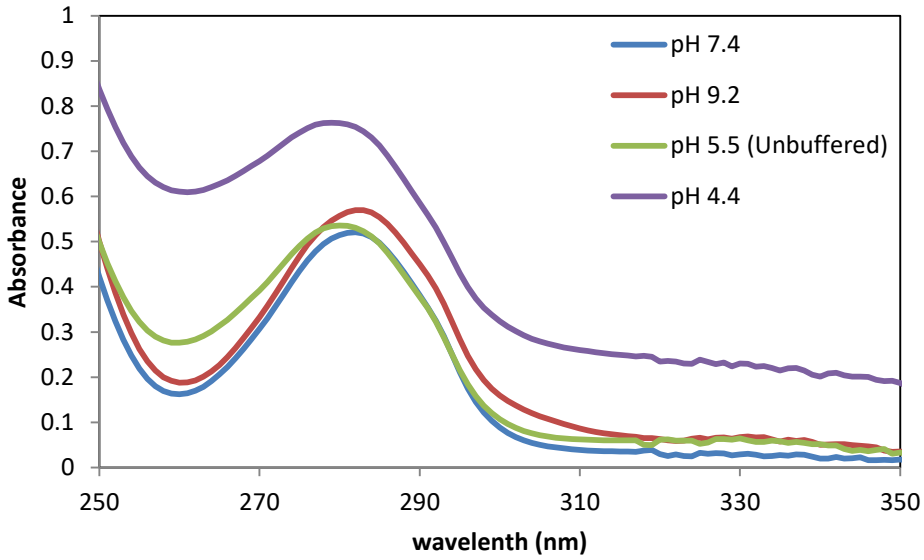


**Figure 2.20 Absorbance (A) against wavelength (λ) in nm for 0.05 mg/ mL TC with 1 % SDS at pH 9.2 (red), pH 7.0 (blue), unbuffered pH 5.5 (green) and pH 4.4 (purple). $\lambda_{max}$ was 279 nm at pH 9.2, 280 nm at pH 5.5, 282 nm at pH 7.4, 280 nm at pH 5.5, and 279 nm at pH 4.4. The cuvette pathlength was 10 mm.**

In the solutions studied, there was a difference in the peak shape for samples when TC was in different surfactant phases and a difference in the molar extinction coefficient. However, it is difficult to use this data to determine the proportion of TC inside and outside the micelles or the relative proportions of $TC^-$ and TC. Through UV-Vis alone, it is difficult to get a full picture of exactly how much TC is in the system and where it is located. TC is fully dissolved in the surfactants at the standard concentrations used in a personal care product formulation of 1% surfactant, 0.1% TC, increasing the solubility of TC by a thousand as compared to the solubility of the phenol alone in water. In the solutions with 1% SL, TC was predominantly in the phenolate form due to the high pH, whereas in 1% SDS, TC was predominantly in the phenol form. In the solutions of TC used with 1% surfactant, all of the TC was dissolved when added at 0.1% and another method should be used to determine solubility of TC in 1% surfactant where the detection range is higher, such as NMR which is used in Chapter 3.

### 2.3.4 Stopped Flow Experiments

Stopped flow analysis was carried out by diluting solutions containing varying amounts of surfactant and TC. The aim of this was to understand what happens to TC in the SDS and SL micelles when diluted below the CMC *i.e.* when applied during a washing process for example to study how the partitioning changes and the length of time to reach equilibrium. To start with, experiments were run using 50% dilution into either water or soap solutions.

Stopped flow analysis was carried out through diluting solutions containing varying amounts of soap and TC. The aim of this was to understand what happens to TC in the SDS and SL micelles when diluted below the CMC. As micelle breakdown occurs, TC molecules are released into solution. As the solution becomes saturated with TC, two processes may occur. Either TC forms aggregates, which grow and may perhaps be stabilised by surfactant, or a portion of the TC enters the remaining micelles to form supersaturated micelles. These supersaturated micelles will possibly breakdown further.

The relaxation processes of micellar solutions need to be considered to understand some of the changes seen in the absorbance upon dilution. Micelle kinetics can be described by the Aniansson and Wall model with simple monomer exchange between bulk and aggregates (see Section 1.2.3).[139,140]

For SDS at the CMC, the lifetime of monomer exchange between bulk and micelles, $\tau_1$, is 29 μs and the breakdown/ formation of complete micelles, $\tau_2$, is 2.3 ms as determined by shock tube and pressure jump experiments respectively.[143] Both $\tau_1$ and $\tau_2$ are dependent on the monomer concentration, chain length and ionic strength.[145]

Previous members of the Bain group observed the change in fluorescence to study the redistribution of fluorescent molecules in micelles of $C_{12}E_8$ upon dilution.[142,147,237] They observed the change in the ratio of fluorescence from dimers, in micelles containing more than one fluorophore and the fluorescence from monomers. The number of micelles reached equilibrium at the new concentration within five seconds at 5°C. We were interested whether a similar effect could be seen with TC in SDS and SL micelles. With TC, there are limitations to following the weak fluorescence, so the absorbance with time was observed instead.

There appears to be a change in the absorbance of peaks with time in a 50% dilution with water (Figure 2.21). For 1% SDS, across the spectrum, there was an increase in the absorbance with time. After 1000 s of exposure to the Xe lamp, the spectra of TC lost its distinctive shape. The local minimum at 260 nm disappeared and there was an increase in the intensity at higher wavelengths. Some of the TC in solution underwent photochemical reactions and formed some of the photoproducts detailed in Figure 2.7. Some of the absorbance at higher wavelengths may come from the photoproduct 2,4-dichlorophenol (2,4-DCP), which is a known photoproduct of TC and absorbs at around 300 nm (Figure 8.4). TC in SL also showed an increase in absorbance with time and a significant change in the absorbance spectrum with time (Figure 2.22). In the first 50 s of exposure to the lamp, the local minimum at around 260 nm changed shape significantly and there was a significant increase in the absorbance at wavelengths higher than 330 nm. The phenolate is the more photoreactive form of TC and is the dominant form in the SL solution, and so TC photodegrades to a greater extent in SL solutions.

Whilst some of the change was from photoreactivity of TC,[6,57] when looking at times less than 100 s, the increase in absorbance with time was less significant due to photoreactivity. There was a clear difference in the absorbance at 281 nm when mixed with water as compared to just mixing with itself (Figure 2.23). If the changes observed were from the photoreactivity, the effects observed in both samples would be the same. The change of absorbance with time for the sample diluted 50% in water suggests that the effects observed are due to the redistribution of TC in the micellar system. When comparing the first and the final spectrum collected for SDS and SL after being exposed to light for 90 s, to separate out the photo-degradation from the kinetics, there are some changes in the spectra (Figure 2.24). For SDS, there was a slight increase in intensity during the experiment. For SL, the change in spectra was more significant because the phenolate form of TC is more photoreactive than the phenol.[216] Latch[82,217,218] noticed a similar effect, with the absorbance at higher wavelengths increasing with time under a lamp, which they put down to a humification effect such the formation of higher molecular weight species such as oligomers and short chain polymers.

Some of the increase at around 320-330 nm could be due to the formation of 2,4-DCP, which has a higher $\lambda_{max}$ than TC in solution and absorbs at 320 nm (Figure 8.4).[238]

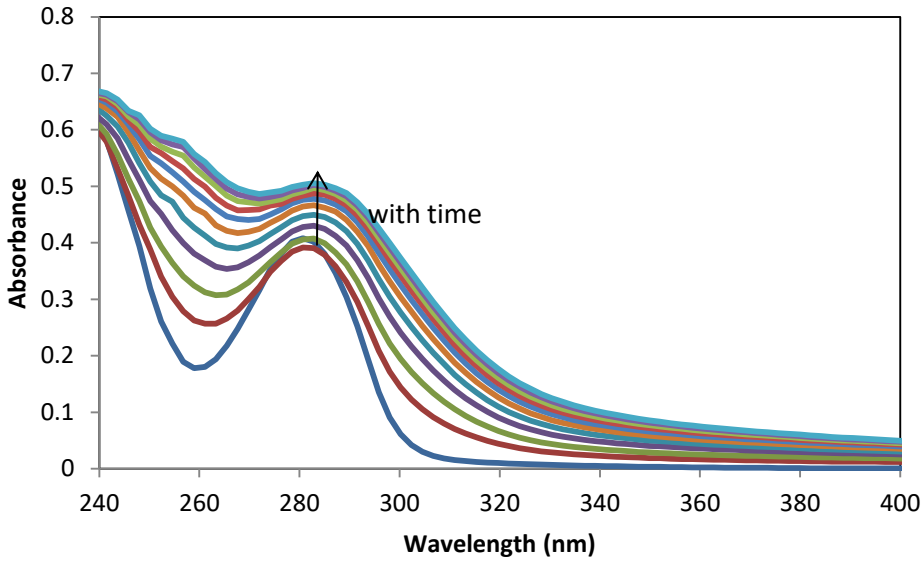


**Figure 2.21 Absorbance against wavelength (nm) for 1% SDS containing 0.1% TC diluted 50:50 with water at 25°C. Spectra shown are taken every 100 s for 1000s.**

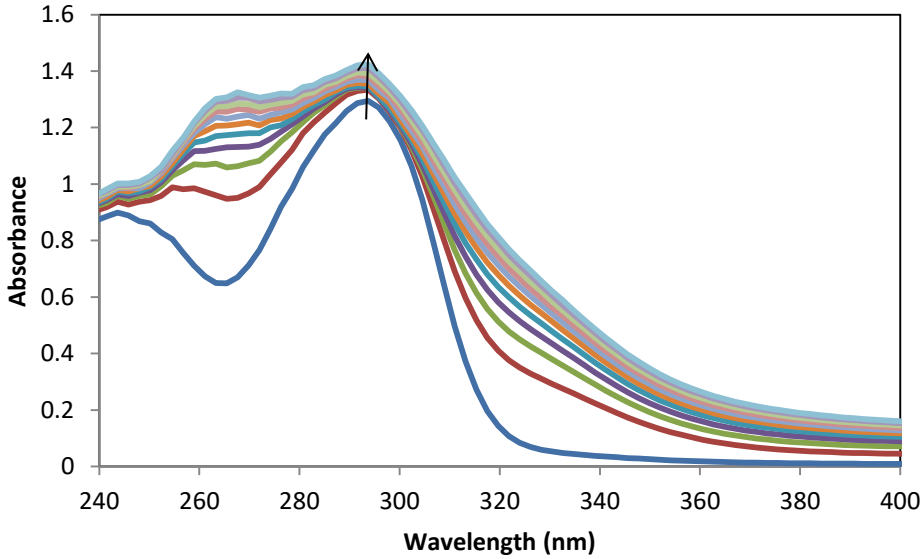


**Figure 2.22 Absorbance against wavelength (nm) for 1% SL containing 0.05% TC diluted 50:50 with water at 25°C. The spectra shown are taken every 50 s for a total of 500s. The arrows indicate the change in absorbance with time.**

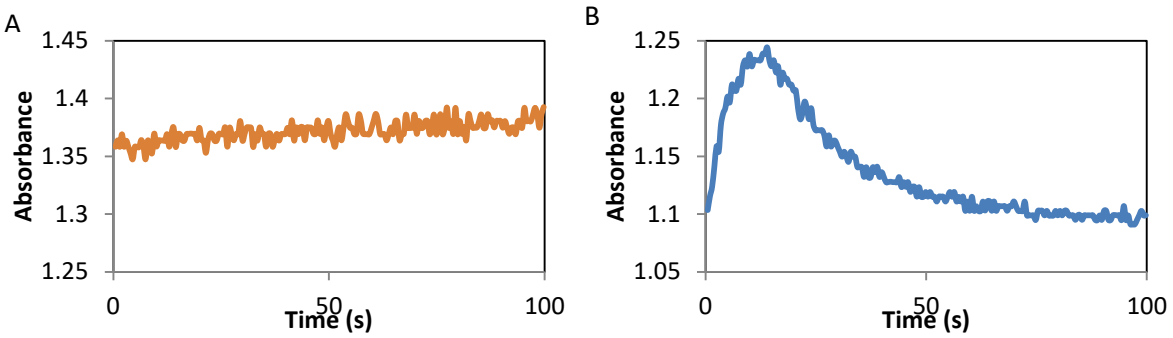


**Figure 2.23 Absorbance at 281nm against time (s) for several runs of 0.75% SDS with 0.1% TC without mixing (A) and diluted 50:50 with water (B).**

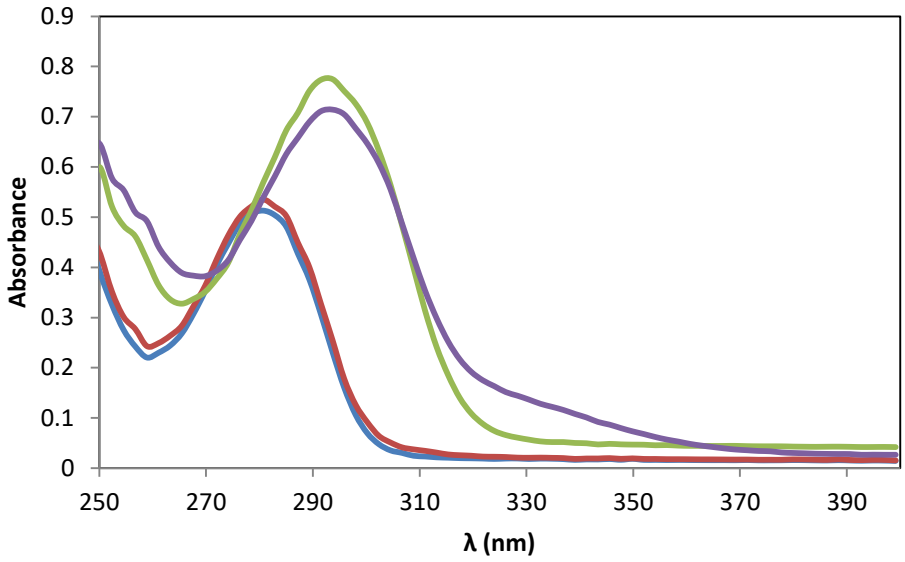


**Figure 2.24 Absorbance against wavelength (nm) for 1% SDS 0.05% TC at 0.45 s (blue) and 90.22 s (red) compared to 1% SL 0.05% TC at 0.45 s (green) and 90.22 s (purple)**

In some experiments, it was noticed that the sample was cloudy after dilution, where TC had crystallised, especially as the concentration of SDS approached the CMC. From eyesight observations, this process is complete within a couple of seconds and likely to contribute to the absorbance observed. Due to the difference between experiments run on different days with the same formulations, the absorbance changes observed are more likely due to errors and a combination of many factors in the experiment rather than simple kinetic processes taking place. Further results are summarised in Section 8.2.3 but are complicated and not repeatable. When the experiment with 0.75% SDS, 0.1% TC diluted 50:50 in water was repeated (Figure 8.9), the change in absorbance with time observed was a different shape to data shown in Figure 2.23, with a much broader peak.

There is also some variation in the initial value of absorbance, for example in Figure 2.23, the sample where there was no mixing has absorbance levels only slightly higher than the sample where there is mixing and the concentration of TC is half of the original.

The lifetimes of monomer exchange and complete breakdown and formation of SDS micelles are significantly shorter than the absorbance changes observed in these experiments where experiments were measured over 100 s.

In the stopped flow experiments, many different effects contributed to the change in absorbance. In some experiments there was TC degradation, caused by the light. TC underwent a number of photo reactions and underwent degradation with the shape of the absorption spectrum changing significantly over 1000s. In other samples, some of the TC crystallised from solution causing scattering and increasing the absorbance, especially as the concentration of surfactant approached the CMC. Whilst this was taken into account by subtracting the absorbance at 320 nm from the absorbance at $\lambda_{max}$, there was still a lack of repeatability. The changes in absorbance should not be caused by the simple rearrangement of SDS as the lifetimes of the surfactant exchange and the breakdown of micelles are less than 1 s.[143]

There are several causes for the observed change in absorbance, which make it difficult to determine the rate of transfer of TC between micelles and bulk from simply following the change in absorbance with time. The change in absorbance with time has not been investigated further and other techniques have been used to get a broader understanding of the lifecycle of TC.

### 2.3.5 Nanosight Analysis

Nanosight analysis was carried out on TC and surfactant solutions diluted to the concentrations used in the Stopped Flow Experiments to understand the size of the TC crystals formed from solution around the CMC. Solutions of 1:10 TC to surfactant were diluted to 0.03% which was well below the CMC of the surfactant. TC solidified from solution and formed small particles with a diameter around 150 nm and a high polydispersity (Figure 2.25). Particles smaller than 50 nm are too small to observe using Nanosight analysis. It is likely the particles observed in the Nanosight are the same particles observed in the stopped flow experiment causing the solutions to become cloudy and contributing to the increase in absorbance.

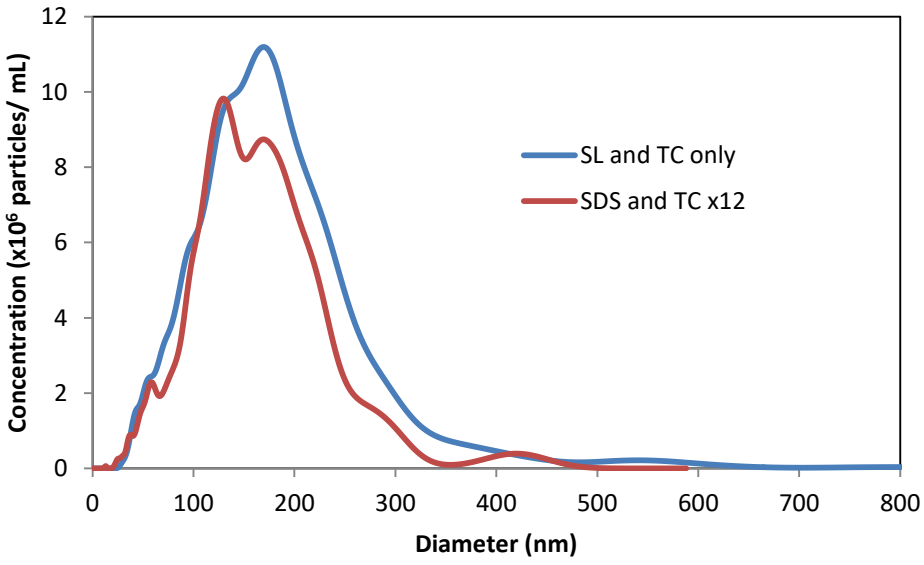


**Figure 2.25 Nanosight analysis of TC and surfactant in 1: 10 ratio at 0.03% surfactant. The intensity the SDS and TC peak has been multiplied by a factor of 12 so that the intensities are comparable.**

Particle distribution was measured for samples with 1% SDS and 0.1% TC prepared both by rotary evaporation and by sonication. Any of the particles measured are most likely to be small particles of TC not completely in solution. The day they were made, the concentration of particles was not high enough to measure, but the following day measurements were taken. The peaks had maximums around the same value: 152 nm for the sonicated sample and 147 nm for the sample prepared using a rotary evaporator (Figure 2.26). In these samples, the concentration of SDS was 30 times the concentration of TC and as shown in the UV-Vis experiments, at 0.1% TC is below the solubility limit in 1% SDS.

During the timescale of only a couple of hours, the particle distribution did not change (see Figure 8.14), so that these samples are stable over a few hours, but the particle growth over a number of days and weeks has not been investigated.

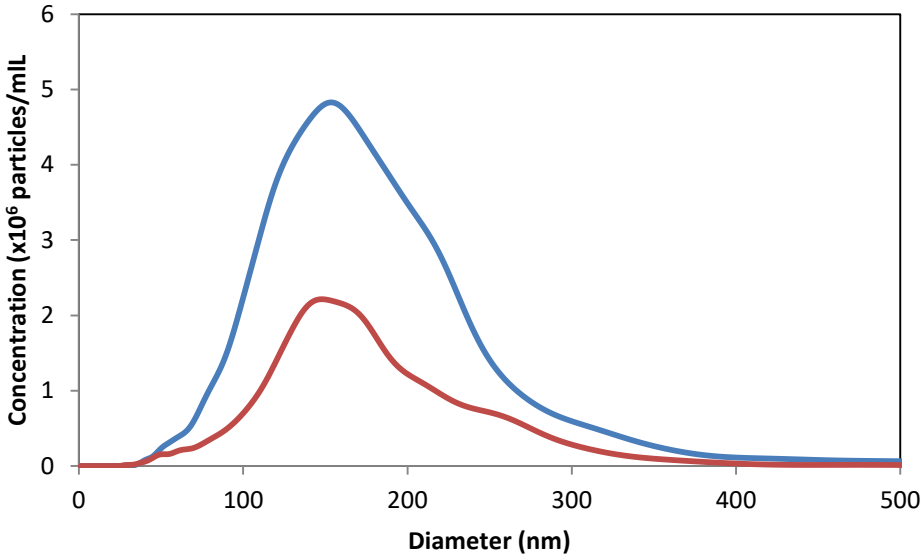


**Figure 2.26 Plot of the concentration of particles (x10$^6$/ml) vs. diameter (nm) for samples of 1% SDS and 0.1% TC prepared either by sonication (blue) or rotary evaporation (red). For the sample prepared by sonication, the mode is 152 nm and the average is 182 nm. For the sample prepared by rotary evaporation the mode is 147 nm and the average is 188 nm.**

Samples were prepared with different concentration of TC and SDS in the 1:10 ratio by diluting down the stock solution of SDS and TC (Figure 2.27). Samples were measured the day after they were prepared so that any large particles above the measurement range of the Nanosight settled out of solution. The rate of settling can be calculated using Stokes's Law where the terminal velocity of a sphere with the density $\rho_p$ and diameter d is

$$V = \frac{1}{18}\frac{d^2 g}{\nu}\left(\frac{\rho_p}{\rho_f} - 1\right) \qquad \text{Equation 2.21}$$

in a fluid with the density $\rho_f$, $\nu$ is the dynamic viscosity of the fluid over the density and $g$ is the gravitational constant.[239] If the sample height is 5 cm, a particle of TC with a diameter 200 nm will have a terminal velocity of 1.07 x10$^{-8}$ ms$^{-1}$ and will settle in 1300 hours. If samples are left to settle for around 18 hours, the largest particles that would not have reached the bottom have a diameter of 1.7 µm.

The samples measured by Nanosight and composed of a mixture of SDS and TC had a single broad peak somewhere between 150 and 250 nm. For most of the samples prepared above the CMC, the total concentration of particles was towards the lower limit of the Nanosight machine, where the recommended particle concentration is $10^7$-$10^9$ particles per ml.[222]

There was no clear pattern of particle distribution with concentration (Figure 2.27). Nevertheless, the sample with 0.1% SDS has a much higher particle average diameter. This sample was around the CMC, so the vast majority of the TC had crystallised from solution. The CMC of SDS alone in water is 8 mM (see Section 1.2.1),[111] and at the 1:10 ratio, TC halves the CMC of SDS (see Table 2.3), so the CMC with 1:10 TC/SDS is approximately 4 mM or 0.1% SDS. The sample at 0.1% SDS was very cloudy once it was prepared, but after sitting overnight most of the larger particles settled to the bottom of the vial. The sample prepared to 0.05% SDS has a lower concentration of particles than the sample with 0.1% SDS. The concentration of TC was lower so there was less TC to form particles and the concentration of surfactant was below the CMC so some TC formed particles larger than the detection range of the Nanosight.

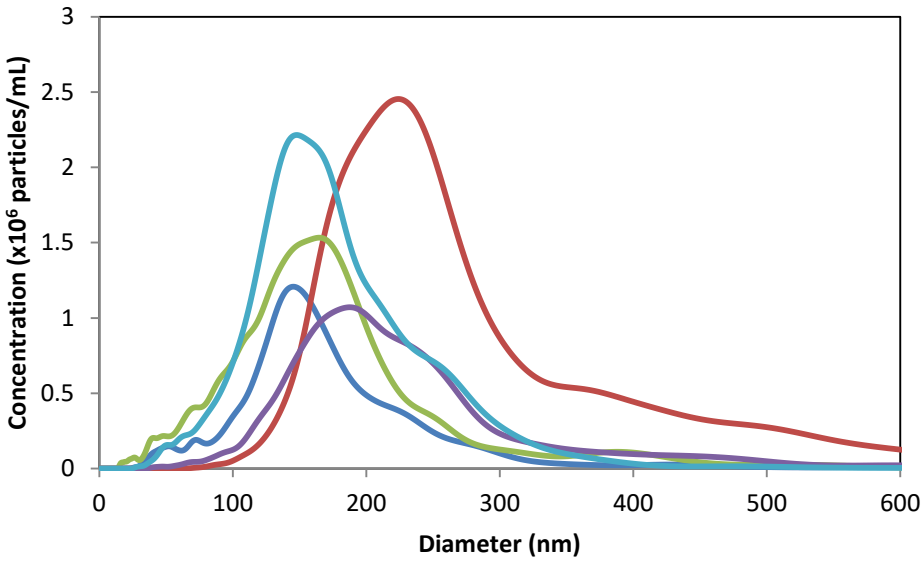


**Figure 2.27 Concentration of particles (x$10^6$/ml) against diameter (nm) for samples with different concentrations of SDS (0.05% (dark blue), 0.1% (red), 0.25% (green), 0.75% (purple), 1% (light blue)) when the molar ratio of SDS: TC is 10:1.**

Further measurements were carried out just above and below the CMC of SDS (Figure 9.15). The samples became cloudy as soon as they were made and had to be left overnight to allow particles above the size range of the Nanosight to settle out before measurement. At concentrations of SDS close to the CMC, the number of micelles available to solubilize TC is small, so excess TC crystallises out of solution. Many of the particles that formed were larger than the detection range of the Nanosight. The particles that were suspended in both solutions were the same size showing that there was no increase in particle size in this size range at the CMC. The excess unsolubilized TC in the sample below the CMC may have formed excess particles that were above the detection range of the Nanosight.

Differences between the curves did not show a clear pattern such as increasing size or concentration with time. For the SDS samples around the CMC, clouding of the solutions was seen straight after

dilution with water: well before the sample could be measured by Nanosight. As mentioned previously, these cloudy solutions had to be left overnight before enough particles had settled for the sample to be measured.

One flaw in Nanosight measurements is that only a very small area of the solution is measured and although in the data shown is an average of three separate sections of solution, they may not be representative of the bulk of solution. Large particles also affect the ability to measure particle distribution, large particles scatter light more strongly than small particles so they can dominate the measurement tracks. Using the Nanosight setup it is not possible to track the particle distribution as mixing occurs and can only be carried out at least a minute after mixing.

In the samples studied above, there were particles larger than 2 µm, above measurement range of the Nanosight which settle overnight. There was another set of particles with a size around 200 nm which do not settle in the measurement time and do not change size or concentration. There are very few particles in the intermediate range. When soap solutions with TC and SDS are diluted, different size particles of TC form below the CMC of the surfactant. Some of these particles will settle on surface such as the skin and provide a well of TC between handwashing increasing the bacteriostatic lifetime of TC from to after handwashing is complete.

### 2.3.6 The pH of SL Solutions

The pH of SL solutions against concentration has been measured at concentrations relevant to this study without TC. The pH of unbuffered sodium laurate in 0.1 M KCl and 0.01 M NaCl was measured using two separate electrodes and an average value used. I did this to compare the SL used in further experiments in this thesis to the data collected by Kralchevsky.[132] TC is a pH sensitive molecule so understanding the pH of the system is important for understanding the form of TC present. The SL surfactant system is sensitive to the presence of impurities such as the acid soap and as SL was used as received, it was important to understand the relationship between concentration and pH for this SL and to compare it to the data collected with purified SL by Kralchevsky.

The pH decreased with concentration of SL (Figure 2.28), and was mostly in agreement with the data collected by Kralchevsky *et al.*[132] (Figure 1.12) which showed a linear relationship between pH and $\log C_{SL}$ between 7 and 100 mM and a separate linear relationship concerning pH and $\log m_{SL}$ between 0.12 and 7 mM. The model used by Kralchevsky is shown in Figure 2.28 as the blue dashed lines. The two models showed most agreement at the highest concentration of SL.

The data was fitted to two separate curves, between 22 mM and 45 mM. Data fit well to a linear plot with gradient of 20 ±0.1 $mol^{-1}$ $dm^3$ and intercept of 9.65 ±0.03 and between 18 mM and 4.4 mM, the data fit to a linear log concentration plot with gradient of 2.3 ±0.1 and intercept of 14.0 ±0.2.

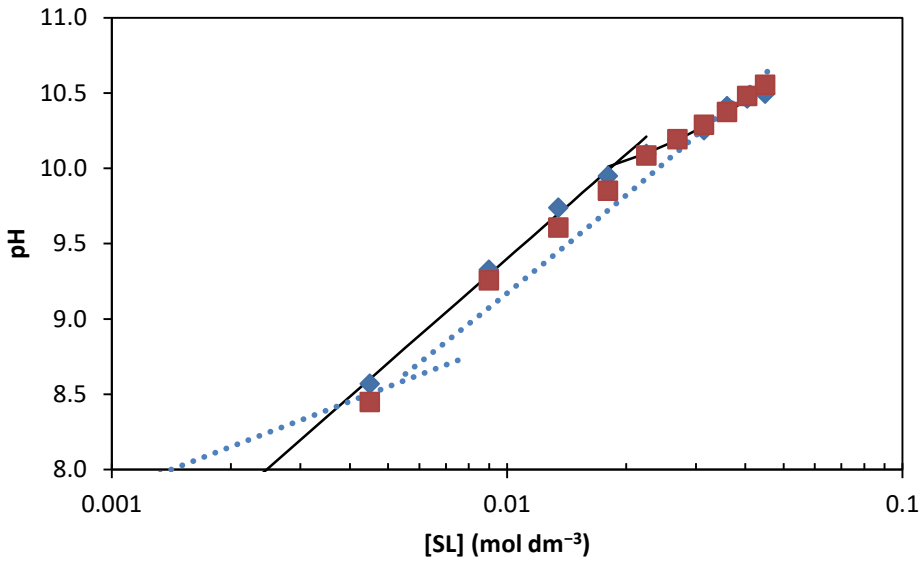


**Figure 2.28 The measured pH of solutions of different concentration of SL in 0.1 M KCl and 0.01 M NaOAc at 20°C. Two separate electrodes were used, a Malvern Ag/AgCl electrode (red squares) and a Cole-Palmer calomel electrode (blue diamonds). Between 22 mM and 45 mM, the data was fit to pH=20$m_{SL}$+9.65 and between 18 mM and 4.4 mM, the data was fit to pH=2.3log$m_{SL}$+14.0 (black lines). The blue dashed line shows the model used by Kralchevsky[132] for the pH of SL solutions.**

## 2.4 Conclusions

In this chapter of my thesis, I have used several separate techniques to characterise the system of TC in surfactant.

The effect of TC on the interfacial tension of surfactant solutions and their CMC has been investigated and the results are summarised in Table 2.10. The phenol form of TC had a strong effect on the observed interfacial tension of SDS above the CMC and the observed CMC. The phenolate does not have a strong effect on the interfacial tension of SDS and the CMC, although in water alone, the interfacial tension decreases significantly in saturated $TC^-$ solution. The differences between the partitioning of phenolate and phenol into micelles cannot be understood using interfacial tension measurements and other techniques need to be used to probe the bulk. The partitioning coefficient between bulk and the surface is 700 000. The partitioning of TC in SDS and SL is investigated by NMR in Chapter 3 to give partitioning coefficients of the phenol and the phenolate to understand what happens in bulk and not just at the surface. From the interfacial tension measurements, I have been able to determine the concentration of SDS in micelles, but not the concentration of TC in micelles or the size of the micelles. The effect of TC on the area per molecule of SDS, can be inferred from the change in gradient of the interfacial tension against concentration but not quantified. The ratio of TC: SDS at the surface cannot be found from these measurements.

Table 2.10 The critical micelle concentration surfactant systems (CMC) in mM and the interfacial tension above the CMC in mN $m^{-1}$.

| Sample | CMC/ mM | ST at 1% wt surfactant/ mN $m^{-1}$ |
|---|---|---|
| 1 to 10 TC: SDS in 0.1 M NaCl, 0.01 M NaOAc | 0.70 ±0.04 | 30.24 ±0.06 |
| 1 to 50 TC: SDS in 0.1 M NaCl, 0.01 M NaOAc | 0.80 ±0.04 | 31.05 ±0.07 |
| 1 to 100 TC: SDS in 0.1 M NaCl, 0.01 M NaOAc | 1.14 ±0.06 | 32.50 ±0.05 |
| SDS in 0.1 M NaCl, 0.01 M NaOAc | 1.36 ±0.07 | 33.7 ±0.05 |
| SDS in 0.05% TC, 0.1 M NaOH, 0.01 M NaOAc | 1.17 ±0.02 | 34.16 ±0.06 |
| SDS in 0.1 M NaOH, 0.01 M NaOAc | 1.31 ±0.02 | 34.05 ±0.06 |
| SL in 0.1 M KCl, 0.01 M NaOAc | 13 ±5 | 32.4 ±0.4 |

Using Small Angle neutron scattering, the effect of TC on micelle size and shape was investigated and the results are summarised in Table 2.11. When TC was in 1:9 ratio with SDS, the micelle size doubled and TC resided primarily in the shell region, when the concentration of TC was decreased so that there was a ratio of 1:19 with SDS, the scattering curve was very similar to the scattering curve with SDS only with a similar micelle size. The location of TC agrees with the work by Villalaín[34] where TC was found close to the headgroups of lipids when TC was dissolved in bilayers. This data is not able to quantify the number of TC molecules per micelle, but in combination with the CMC can be used to find the number of micelles.

Table 2.11 Summary of SANS data

| SDS/ % | TC/ % | Core Radius, $R_1$/ Å | Total Radius, $R_2$/ Å | $N_{agg}$ |
|---|---|---|---|---|
| 2 | 0 | 16.7 ±0.5 | 18.6 ±0.5 | 120 ±10 |
| 1.98 | 0.02 | 17.5 ±0.5 | 21.1 ±0.5 | 120 ±10 |
| 1.9 | 0.1 | 15.9 ±0.5 | 17.9 ±0.5 | 148 ±10 |
| 1.8 | 0.2 | 21.1 ±0.5 | 41.3 ±0.5 | 600 ±60 |

The results from UV-Vis experiments are summarised in Table 2.12. The molar extinction coefficient and $\lambda_{max}$ of TC can be used to provide information on the environment and form of TC. The TC absorbance peak is distinct from any surfactant absorbance peaks. The data did not give an indication of the proportion of TC inside and outside the micelles in the high pH solutions where SL was the surfactant of interest. The solubility of the phenolate in water was 0.68 ±0.08 mg/ mL which was considerably higher than the solubility of the phenol form of TC which was 0.004 ±0.002 mg/ mL. In the solutions of TC used with 1% surfactant, it appeared that all of the TC was dissolved and another method should be used to determine solubility of TC in 1% surfactant where the detection range is higher, such as NMR. In the concentrations used in personal care products, it is difficult to determine the partitioning and solubility of TC due to high absorbance.

Table 2.12 The molar extinction coefficient at 280 nm ($\varepsilon$) of TC in different systems

| System | ε at 280 nm/ $mol^{-1}dm^3cm^{-1}$ | $\lambda_{max}$/ nm |
|---|---|---|
| 1% SDS | 4 200 | 281 |
| 1% SL | 3 300 | 291 |
| 1% $C_{12}$TAB | 4 300 | 282 |
| 1% $C_{12}E_8$ | 4 800 | 283 |
| Methanol | 5 900 | 281 |
| Heptane | 4 200 | 278 |
| Chloroform | 3 700 | 279 |
| 0.1 M NaOH | 4 900 | 292 |

The solubility of TC in surfactant solutions is investigated further in Chapter 3 by NMR. In some of the experiments there was TC degradation caused by the light. In the stopped flow experiments, many different effects contributed to the changes in absorbance, especially photo-degradation and TC crystallising from solution. The change in absorbance with time has not been investigated further and other techniques have been used to get a broader understanding of the lifecycle of TC. The particle distribution of TC crystallised from solution was measured using Nanosight analysis. When soap solutions with TC and SDS are diluted, different size particles of TC form below the CMC of the surfactant. Some of these particles will settle on surface such as the skin and provide a source of TC between handwashing. Nanosight does not give a full characterisation of all the particles of TC that form upon dilution of TC and SDS solutions, only a subset of the particles are in the measurement range. Nanosight is only able to find the size of the particles and cannot be used to determine their shape.

The changing ratio of TC:$TC^-$ will most likely change the bacteriostatic properties, where $TC^-$ is likely to have different degree of interaction with FabI, which is partly mediated through the phenol group. If it follows the pattern observed by Chiappetta,[49] then the hydrogen-bonding will be reduced when the phenolate is used and it will be less effective against FabI. The bioavailability depends on the proportion of TC inside the micelles and the proportion in bulk. For example in non-ionic micelles, a solubilized organic is unavailable directly to microbes.[51]

# 3 Determination of the Partitioning of Triclosan in SDS and SL systems by NMR

## 3.1 Introduction

One of the principal advantages of solution NMR is that a simple data set that takes minutes to run can reveal a wide range of information. NMR has been used in the past in several different ways to investigate the partitioning of solutes between micelles and bulk. The peaks, chemical shift and relaxation times give information such as the orientation of the molecular complexes, inter-molecular interactions and the dynamics in solution.

There are many weak influences on chemical shift that can be quantified and analysed giving information on the aggregation and interactions specific to micellar systems. The observed chemical shift can be dependent on hydrogen bonding, ring current effects, conformational changes and the solvent environment, amongst other factors. The line-width of peaks is related to transverse relaxation times and can be used qualitatively to look at changes between phases and at aggregation.[240,241]

In some experiments, simply looking at the shape of the proton NMR peaks can reveal information about the strength of interaction between solute and surfactant. For example, Momot[242] observed broadening of the surfactant -$CH_2$- peak when a hydrophobic solute was dissolved in micelles. The peak shifted to a lower frequency upon inclusion of the solute and the degree of shift depended on the hydrophobicity of the surfactant chain. Duan[243] meanwhile looked at the broadening of Triclosan proton peaks in inclusion complexes with hydroxypropyl-β-cyclodextrin. The TC peaks split and broadened with inclusion to different degrees. The authors infer that the degree of broadening was related to the strength of interaction between specific Cd regions and the different regions of TC. The changes were used to infer orientation of TC in the Cd cavity.

A simple application of NMR techniques is to look at the observed shift ($\delta_{obs}$) to study partitioning. When there is fast exchange between two species (*i.e.* micelle and bulk) as compared to the NMR timescale, $k >> \delta_A - \delta_B$ (where $\delta$ is in Hz), only one peak is observed at a weighted average between the shift inside the micelle and in the bulk:[244]

$$\delta_{obs} = p_A\delta_A + p_B\delta_B \qquad \text{Equation 3.1}$$

where $p_A$ is the mole fraction of species A.

Line broadening for exchange that is intermediate on the NMR timescale can be described by[241,245]

$$\Delta\delta_{obs} = \frac{4\pi(p_A p_B)(p_A - p_B)^2}{k_A + k_B} \qquad \text{Equation 3.2}$$

where $k_A$ is the rate constant for the formation of B from A and $k_B$ is the rate constant for the reverse. When exchange between the two species is slow, two separate peaks are observed.

A simple expansion on this technique at fast exchange is to use a NMR shift reagent, for example $[Dy(ppp)_2]^{7-}$, to determine the micelle/ water partition coefficient based on the assumption that the agent does not affect the shift inside the micelle phase, as in the work of Fujiwara.[246] The partition coefficient was worked out thus:

$$\delta_{obs} = p_{mic}\delta_{mic} + (1 - p_{mic})\delta_{aq}$$ Equation 3.3

When the shift reagent was added the observed shift changed:

$$\delta_{obs(sr)} = p_{mic}\delta_{mic} + (1 - p_{mic})\delta_{aq(sr)}$$ Equation 3.4

The degree of binding can then be calculated based on the difference between the two aqueous shifts, without having to find the shift within the micelle.

Self-diffusion experiments have been commonly used to determine partitioning of a solute into micelles. The diffusion coefficient of a solute/ surfactant changes between micelles and bulk. In experiments where the exchange between bulk and micelles is faster than the delay in the DOESY pulse sequence, the observed diffusion coefficient is a weighted average of the two species. For example, Alonso, Harris and Kenwright[152] investigated the solubilisation of short chain (*n* = 3–6) alcohols and amines in CTAB micelles and found that these molecules reside preferentially in the palisade layer, i.e. towards the head groups and the surface. They used a model for calculating the degree of binding (*b*) based on the diffusion coefficients which gave the mole fractions of the solute inside the micelles and in the bulk:

$$b = \frac{(D_{obs} - D_{aq})}{(D_{mic} - D_{aq})}$$ Equation 3.5

$$p_{mic} = \frac{b[Solute]}{b[Solute] + [Surf]}$$ Equation 3.6

They then calculated the partition coefficient from the mole fractions of solute inside the micelles and in the bulk.

Lapenna[153] used 1D and 2D-DOESY NMR spectroscopy to find the solubilisation capacity of SDS micelles for the poorly water soluble molecules artemisinin and curcumin. The signals in the DOESY spectra were a mixture of the drug in micelles and free in solution: the exchange was faster than the pulse sequence. The solubilisation ratio ($r_{art}$) was calculated from the linear regression of solubility of drug against concentration of SDS and used to determine the predicted diffusion of artemisinin when the total concentration of artemisinin was above the aqueous saturation limit:

$$D_{Art} = \frac{D_{mic} + (D_{aq} - D_{mic})[Art]_{aq}}{[Art]_{aq} + r_{art}[SDS]_{mic}}$$ Equation 3.7

Dupont-Leclerq[155] used NMR to investigate the partitioning of carboxylic acids in micellar media and the effect partitioning had on the observed pKa through pHmetric and NMR diffusion experiments (Figure 3.1). They suggest that the pKa shift is mostly due to the modification of the dielectric constant and electrostatic effects in the micellar phase. The different forms of acid in the model they proposed are shown below. They found that for each non-ionic surfactant system (Brij-58 and Triton-X100) studied, the neutral acid was more easily incorporated into the micelles than the anionic form.

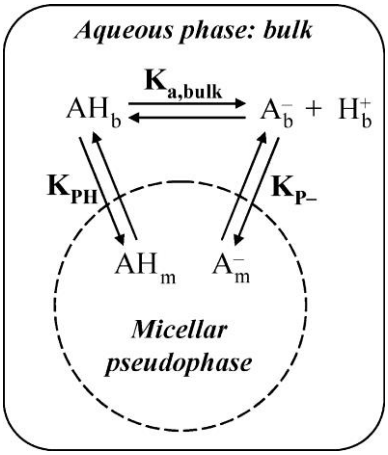


**Figure 3.1 Acid-base and partition equilibrium between the bulk phase and the micellar pseudophase.**

In their use of NMR to determine the pKa, a simple model was used where they just considered the difference in shift between the acid and the base, without considering the shift difference between the species inside the micelles and in the aqueous phase

$$pK_{a,obs} = pH - \log_{10}\left(\frac{\delta_{acid} - \delta_{obs}}{\delta_{obs} - \delta_{base}}\right)$$ **Equation 3.8**

The acid-base equilibrium is shifted if one of the forms of the solute is partitioned to a greater degree than the other. What is actually measured is the apparent acidity constant and from this, the partitioning coefficients can be calculated (Figure 3.1).

The pKa was determined using three different methods (NMR, IR and pH measurement) which gave similar values of $K_{a,obs}$ within error of each other. NMR diffusion experiments were also carried out to calculate the partitioning of the carboxylic acids into the micelles. The observed diffusion constant was a combination of the constants for the free solute and that in the micelle, where the same method was used as Alonso (Equation 3.6) to calculate the degree of binding and the partition coefficients.

One of the problems with this method of diffusion measurements to determine $K_p$ is that you need to work at pH where there is either only acid or only base and not somewhere in between.

The partitioning of bioactive agents affects their bioavailability. The bioavailability of TC will be different if the phenolate form is present as compared to the phenol form. When you consider that the interaction between TC and the enzyme FabI is partially through the OH group on TC, changes to that group with pH will affect the strength of the interaction and thus the bioactivity of TC. The two different forms of TC will have different partitioning into cells depending on the form available. For example, the more hydrophobic phenol will partition more strongly into the hydrophobic cell membranes than the more hydrophilic phenolate form of TC, which is investigated in Chapter 4 using TIR-Raman. It is important to understand the partitioning of TC in the formulations that are used in soaps to get a better picture of the bioavailability of TC, taking into account the form of TC present.

The peaks of TC have been assigned previously in literature,[82,243,247,248], assignments below, using splitting constants and a variety of 2D NMR techniques such as COSY (Correlation Spectroscopy, see

Section3.3.1.2), HSQC (Hetronuclear Single Quantum Coherence) and HMBC (Hetronuclear Multiple-Bond Correlation spectroscopy) (Figure 3.2 and Table 3.1).

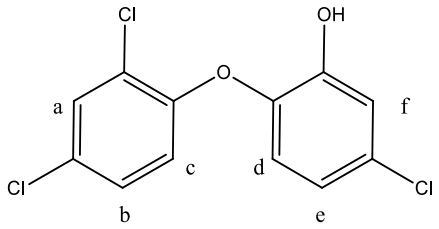


**Figure 3.2 The structure of TC with the different protons positions labelled.**

**Table 3.1 NMR assignments from Wilson[247] NMR was carried out in $CDCl_3$ at 400 MHz and referenced to $CHCl_3$ at 7.25 ppm.**

| Position | Shift/ ppm | Multiplicity | J/ Hz | Integral |
|---|---|---|---|---|
| a | 7.47 | d | 2.3 | 1H |
| b | 7.22 | dd | 2.3, 9.2 | 1H |
| c | 6.93 | d | 9.2 | 1H |
| d | 6.65 | d | 8.7 | 1H |
| e | 6.81 | dd | 2.6, 8.7 | 1H |
| f | 7.06 | d | 2.6 | 1H |

## 3.2 Materials and methods

### 3.2.1 Materials

TC (Igrasan ≥ 97%), sodium dodecyl sulphate (≥ 99%), sodium laurate (sodium dodecanoate 99-100%), sodium acetate, Trizma base, Trizma HCl and sodium carbonate (≥ 99.5%) were purchased from Sigma Aldrich (St Loius, MO, USA) and used as received. Potassium chloride, sodium chloride, sodium hydroxide and potassium hydroxide were purchased from Fisher Scientific (Loughborough, UK). Deuterium oxide (≥ 99.9%) was purchased from Cambridge Isotopes (Andover, MA, USA) and sodium hydrogen carbonate was purchased from BDH Laboratory supplies (Poole, UK).

### 3.2.2 NMR Analysis

NMR samples were prepared with constant concentrations of salt (0.11 M) of which 0.01 M was NaOAc (Table 3.2 and Table 3.3). The concentration of TC was also kept constant in all samples used to find $K_-$ and $K_+$ at 0.1 mg/mL. Buffers were used to maintain pH.

**Table 3.2 Buffers used to maintain pH in NMR samples for SDS solutions**

| pH | Buffer composition |
|---|---|
| 10.8 | 0.09 M $Na_2CO_3$, 0.01 M $NaHCO_3$, 0.01 M NaOAc |
| 10 | 0.06 M $Na_2CO_3$, 0.04 M $NaHCO_3$, 0.01 M NaOAc |

**Table 3.3 Buffers used to maintain pH in NMR samples for SL solutions**

| pH | Buffer composition |
|---|---|
| 10.8 | 0.009 M $Na_2CO_3$, 0.001 M $NaHCO_3$, 0.09 M KCl, 0.01 M NaOAc |
| 10 | 0.006 M $Na_2CO_3$, 0.004 M $NaHCO_3$, 0.09 M KCl, 0.01 M NaOAc |

SDS containing samples were sonicated using a sonicator bath to ensure TC dissolution and SL containing samples were heated in an oven and left to cool to room temperature. All samples were filtered through a 0.45-µm syringe filter before NMR experiments.

To determine the solubility of TC in solutions of different concentrations of surfactant, samples were prepared as above except that an excess of TC was used and samples were left over a weekend to equilibrate before samples were filtered through 0.45-µm nylon syringe filters and NMR experiments were run.

NMR experiments were carried out at 400 MHz. Data was analysed in MestreNova (Mestrelab Research S.L., Santiago de Compostela, Spain). Samples were analysed with the sodium acetate peak set to 1.9000 ppm (s, 3H) except for the sample with 0.1 M HCl where acetic acid was used (2.0850 ppm, s, 3H). All shifts quoted are relative to the acetate peak. The concentrations of surfactant and TC were found by comparing the averaged peak integrals to the sodium acetate peak. The concentration of $SDS_{mic}$ can be calculated by subtracting the CMC from the total concentration of SDS. For SL the CMC of 0.0099 mol $dm^{-3}$ was used to calculate $SL_{mic}$. Fitting was carried out using Origin 2015 to fit multiple proton sets together (global fit) and give error values. The samples in Table 3.4 were used as references for shift values. Fresh samples of the references were prepared weekly.

**Table 3.4 Sample compositions for NMR reference values**

| Sample | Composition | Acetate reference peak/ ppm |
|---|---|---|
| $TC^-_{aq}$ (SDS) | 0.1 mg/ mL TC, 0.1 M NaOH, 0.01 M NaOAc | 1.9000 |
| $TC^-_{aq}$ (SL) | 0.1 mg/ mL TC, 0.1 M KOH, 0.01 M NaOAc | 1.9000 |
| $TC^-_{mic}$ (SDS) | 0.1 mg/mL TC, 10% SDS, 0.1 M NaOH, 0.01 M NaOAc | 1.9000 |
| $TC^-_{mic}$ (SL) | 0.1 mg/mL TC, 8% SL, 0.1 M KOH, 0.01 M NaOAc | 1.9000 |
| $TC_{mic}$ (SDS) | 0.1 mg/mL TC, 1% SDS, 0.1 M HCl, 0.01 M NaOAc | 2.0850 |
| $TC_{mic}$ (SL) | 0.1 mg/mL TC, 1% SL, 0.05 M KCl, 2.21 mg/ mL Tris HCl, 4.36 g/ L Tris base, 0.01 M NaOAc | 1.9000 |

pH measurements were carried out on a Hanna Instruments (HI931410) pH meter in pH mode using a Cole-Parmer calomel electrode (5990-35) and a Malvern Ag/AgCl electrode (SEN0106). Calibrations were carried out on the same day as experiments. Measurements were either carried out at room temperature (20°C ±1°C) or in a water bath set to 25°C. . A technical report by ASTI[249] suggests that carbonates and bicarbonates may cause damage to the electrodes when they react with the oxides on the surface of the electrode and suggests that the time the electrode is in contact with these solutions should be limited.

## 3.3 Results and Discussion

### 3.3.1 Finding the Partition Coefficients

#### *3.3.1.1 The Model*

NMR can be used to understand the partitioning of TC between the bulk and the micelles, phenol and phenolate (Figure 3.3). If there is fast exchange on the NMR timescale and there is no solid TC in the system, the observed shift of TC is a weighted average of the different forms of TC in solution:

$$\delta_{obs} = p_{TC^-_{aq}}\delta_{TC^-_{aq}} + p_{TC^-_{mic}}\delta_{TC^-_{mic}} + p_{TC_{mic}}\delta_{TC_{mic}}$$ Equation 3.9

As the saturated concentration of the phenol form of TC in aqueous solution is so much lower than the saturation limits for the other forms of TC, it has been discounted from contributing significantly to the shift. The assumption is supported by NMR data taken of TC in $D_2O$ without salt, which showed no observable signal in the aromatic region.

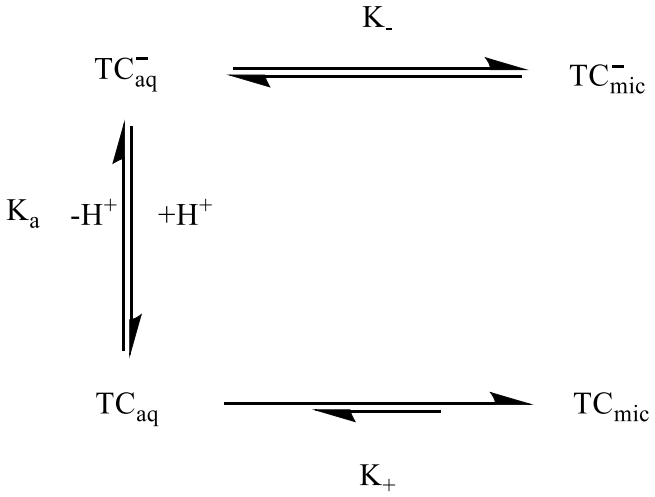


**Figure 3.3 The different phases of TC in the NMR system: the phenolate form in micelles ($TC^-_{mic}$) and the aqueous phase ($TC^-_{aq}$), and the phenol in the micellar phase ($TC_{mic}$) and bulk aqueous phase ($TC_{aq}$). The relevant equilibrium constants are shown.**

The observed shift can be used to find the partition coefficients of the phenol and phenolate between micelles and bulk. The partition coefficients depend on the standard states used and allow authors to compare partition coefficients when using different standard states. The standard states used in this work do not depend on knowledge of partial molar volumes, compared to the work by Dupont-Leclercq.[155]

At high pH, the contribution from $TC_{mic}$ toward the shift can be discounted, so an initial model was developed with just $TC^-_{aq}$ and $TC^-_{mic}$. At concentrations well below the saturation point of $TC^-$ in aqueous solution, TC will behave ideally hence the chemical potential of the aqueous phenolate is

$$\mu_{TC^-_{aq}} = \mu^{\ominus}_{TC^-_{aq}} + RT\ln\left(\frac{m_{TC^-_{aq}}}{m^{\ominus}}\right)$$ Equation 3.10

where $m_{TC^-_{aq}}$ is the concentration of $TC^-_{aq}$ and $m^{\ominus}$ is 1 mol $dm^{-3}$. In the ideal dilute solution, the standard state in expressed in molarities. The chemical potential of the phenolate in the micelles is

$$\mu_{TC^-_{mic}} = \mu^{\ominus}_{TC^-_{mic}} + RT\ln x_{TC^-_{mic}}$$ Equation 3.11

where $x_{TC^-_{mic}}$ is the mole fraction of $TC^-$ in the micelles. Since the volume of the micelles is not known *a priori,* the chosen standard state is in terms of mole fraction. When the system is at equilibrium the chemical potential of $TC^-_{aq}$ is equal to the chemical potential of $TC^-_{mic}$, $\mu_{TC^-_{aq}} = \mu_{TC^-_{mic}}$, so

$$x_{TC^-_{mic}} = \exp\left(\frac{-\Delta\mu^{\ominus}}{RT}\right)\frac{m_{TC^-_{aq}}}{m^{\ominus}} = K_{-}\frac{m_{TC^-_{aq}}}{m^{\ominus}}$$ Equation 3.12

In the situation where $m_{TC^-_{mic}} << m_{surf(mic)}$, the mole fraction of $TC^-_{mic}$ is inversely proportional to the concentration of surfactant in micelles ($m_{surf(mic)}$) :

$$x_{TC^-_{mic}} = \frac{m_{TC^-_{mic}}}{m_{TC^-_{mic}} + m_{surf\,(mic)}} \approx \frac{m_{TC^-_{mic}}}{m_{surf\,(mic)}}$$ Equation 3.13

Combining Equation 3.12 and 3.13 gives

$$\frac{m_{TC^-_{mic}}}{m_{TC^-_{aq}}} = K_{-}\frac{m_{surf\,(mic)}}{m^{\ominus}}$$ Equation 3.14

As the concentration of the phenol form of TC is effectively zero at very high pH,

$$\delta_{obs} = p_{TC^-_{aq}}\delta_{TC^-_{aq}} + p_{TC^-_{mic}}\delta_{TC^-_{mic}}$$ Equation 3.15

so

$$p_{TC^-_{mic}} = \frac{m_{TC^-_{mic}}}{m_{TC^-_{aq}} + m_{TC^-_{mic}}} = \frac{K_{-}\frac{m_{surf\,(mic)}}{m^{\ominus}}m_{TC^-_{aq}}}{m_{TC^-_{aq}} + K_{-}\frac{m_{surf\,(mic)}}{m^{\ominus}}m_{TC^-_{aq}}} = \frac{K_{-}\frac{m_{surf\,(mic)}}{m^{\ominus}}}{1 + K_{-}\frac{m_{surf\,(mic)}}{m^{\ominus}}}$$ Equation 3.16

and

$$p_{TC^-_{aq}} = \frac{m_{TC^-_{aq}}}{m_{TC^-_{aq}} + m_{TC^-_{mic}}} = \frac{1}{1 + K_{-}\frac{m_{surf\,(mic)}}{m^{\ominus}}}$$ Equation 3.17

Equation 3.15 then becomes

$$\delta_{obs} = \frac{\delta_{TC^-_{aq}} + \delta_{TC^-_{mic}}K_{-}\left(\frac{m_{surf\,(mic)}}{m^{\ominus}}\right)}{1 + K_{-}\left(\frac{m_{surf\,(mic)}}{m^{\ominus}}\right)}$$ Equation 3.18

If the concentration of TC is kept much lower than the saturation limit in the micelles and the solubility limit in bulk, the system is at equilibrium and $m_{TC^-_{mic}}$ is much smaller than $m_{surf\,(mic)}$, then the observed shifts can be fitted to Equation 3.18.

For samples/ systems where $TC_{mic}$ is also present, the model has been expanded. Starting from the above model (Equations 3.9 and 3.18)

$$\delta_{obs} = \frac{\delta_{TC^-_{aq}} + \delta_{TC^-_{mic}} K_- \left( \frac{m_{surf\,(mic)}}{m^\ominus} \right) + \delta_{TC_{mic}} \frac{m_{TC_{mic}}}{m_{TC^-_{aq}}}}{1 + K_- \left( \frac{m_{surf\,(mic)}}{m^\ominus} \right) + \frac{m_{TC_{mic}}}{m_{TC^-_{aq}}}}$$ Equation 3.19

As we know $K_a$, we can find $m_{TC_{aq}}$, even though it is too low to measure.

$$\frac{m_{TC^-_{aq}}}{m_{TC_{aq}}} = 10^{(pH - pKa)}$$ Equation 3.20

Equation 3.12 and 3.13 applied to the phenol form gives

$$\frac{m_{TC_{mic}}}{m_{TC_{aq}}} = K_+ \frac{m_{surf\,(mic)}}{m^\ominus}$$ Equation 3.21

Equation 3.20 and 3.21 combined give

$$\frac{m_{TC_{mic}}}{m_{TC^-_{aq}}} = K_+ \frac{m_{surf\,(mic)}}{m^\ominus} 10^{pKa - pH}$$ Equation 3.22

The proportion of $TC_{mic}$ is calculated

$$p_{TC_{mic}} = \frac{K_+ 10^{(pKa - pH)} \frac{m_{surf\,(mic)}}{m^\ominus}}{1 + K_- \frac{m_{surf\,(mic)}}{m^\ominus} + K_+ 10^{(pKa - pH)} \frac{m_{surf\,(mic)}}{m^\ominus}}$$ Equation 3.23

The chemical shift for the system where the three forms are present is therefore

$$\delta_{obs} = \frac{\delta_{TC^-_{aq}} + \delta_{TC^-_{mic}} K_- \frac{m_{surf\,(mic)}}{m^\ominus} + \delta_{TC_{mic}} K_+ \frac{m_{surf\,(mic)}}{m^\ominus} 10^{pKa - pH}}{1 + K_- \frac{m_{surf\,(mic)}}{m^\ominus} + K_+ \frac{m_{surf\,(mic)}}{m^\ominus} 10^{pKa - pH}}$$ Equation 3.24

The solubility of the phenol form of TC in aqueous solution is around 4 ng/mL,[10] and the phenolate form has a much higher solubility of 0.68 mg/mL in 0.1 M NaOH (Figure 2.9). In the experiments carried out in this thesis to find the partition coefficients, the concentration of TC was kept around 0.1 mg/mL, well below the solubility limit of $TC^-_{aq}$.

Experiments were run by changing the concentration of surfactant and with the concentration of TC, the pH and the salt concentration constant. The plots of $\delta_{obs}$ against the concentration of surfactant have been fitted to the above models to find $K_-$ and $K_+$, the phenolate and phenol partitioning coefficients. The effect of ring currents in micelles with one or more TC molecules is considered below in Section 3.3.2. A simple proton NMR spectrum takes less than five minutes to run making this technique quicker that NMR diffusion experiments. The diffusion experiments could be used to calculate $K_-$, but it would be difficult to calculate $K_+$ using NMR diffusion experiments as the concentration of $TC_{aq}$ at the solubility limit is below the limit of detection.

### 3.3.1.2 Assigning the shifts of $TC_{mic}$, $TC^-_{aq}$ and $TC^-_{mic}$

When fitting $\delta_{obs}$ to the model proposed above, first the shifts of $TC^-_{aq}$, $TC^-_{mic}$ and $TC_{mic}$ need to be found. Second, the concentration of surfactant in micelles in the sample measured needs to be calculated and, third, the pH of the solution needs to be maintained.

The reference shifts of $TC^-_{aq}$, $TC^-_{mic}$ and $TC_{mic}$ were calculated from standard samples measured on the same day that the rest of the samples were run (Figure 3.4). The assignments are shown in Figure 3.2 and Table 3.1. Assignments were carried out based on the J-coupling constants, COSY analysis of TC in chloroform (Figure 3.5) and previous assignments in literature.[247] Shifts in aqueous solutions are referenced relative to the sodium acetate peak at 1.900 ppm (3H, s, 0.01 M), apart from in 0.1 M HCl where the acetic acid peak at 2.085 ppm (3H, s, 0.01 M) was used. The $^{13}C$ spectra (Figure 3.6) is referenced relative to the $CDCl_3$ solvent peak at 77.16 ppm (triplet).[250]

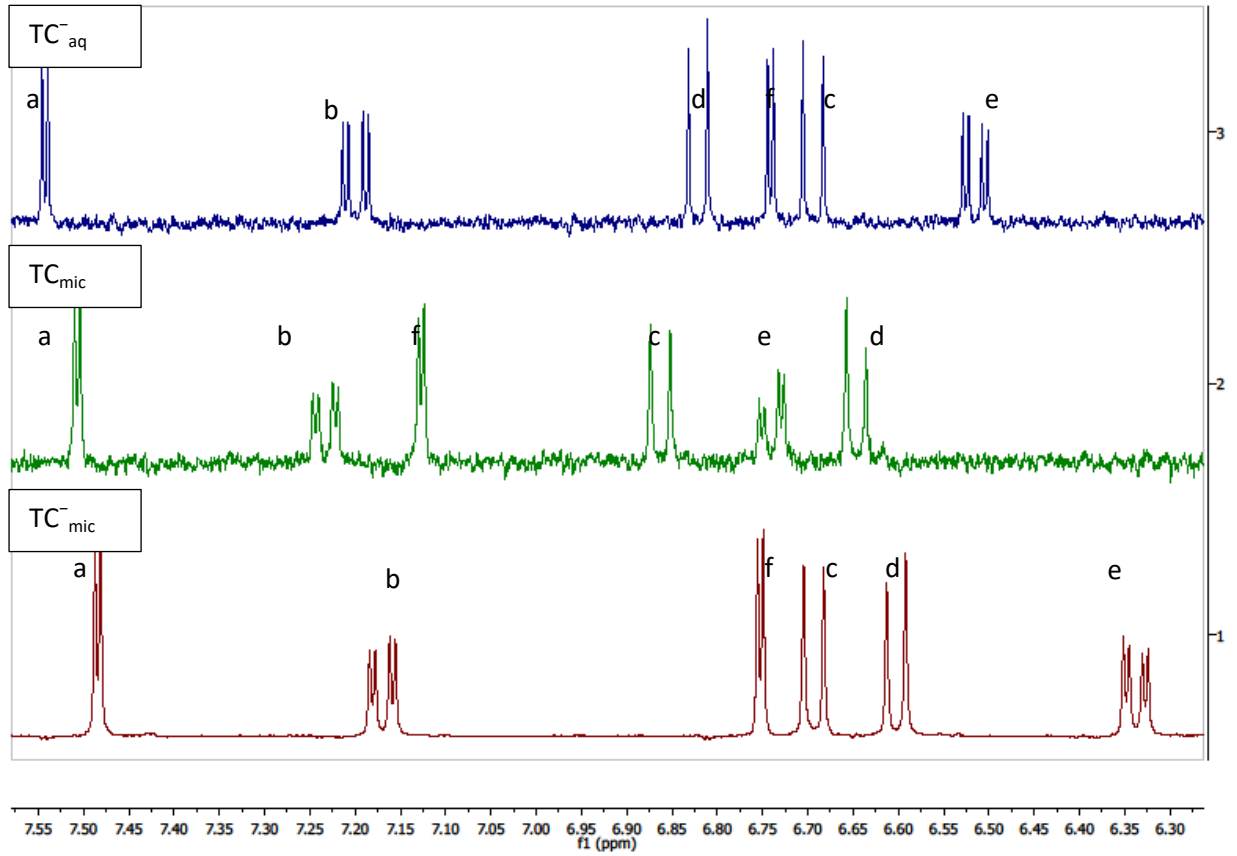


**Figure 3.4 NMR spectra of TC protons of $TC^-_{aq}$ (top, blue), $TC_{mic}$ (middle, green) and $TC^-_{mic}$ (bottom, red). The sample of $TC^-_{aq}$ was prepared with 0.1 M NaOH, 0.01 M NaOAc and 1 mM TC. The sample with $TC_{mic}$ was prepared with 0.1 M HCl, 0.01 M NaOAc, 1 mM TC and 1% SDS. The sample with $TC^-_{mic}$ was prepared with 0.1 M NaOH, 0.01 M NaOAc, 1 mM TC and 10% SDS and contained contributions from $TC^-_{aq}$.**

**$TC^-_{aq}$ $^1$H NMR (400 MHz, $D_2O$) δ 7.5426 (d, *J* = 2.5 Hz, 1H, a), 7.1995 (dd, *J* = 8.9, 2.6 Hz, 1H, b), 6.8213 (d, *J* = 8.4 Hz, 1H, d), 6.7412 (d, *J* = 2.6 Hz, 1H, f), 6.6942 (d, *J* = 8.9 Hz, 1H, c), 6.5151 (dd, *J* = 8.4, 2.6 Hz, 1H, e).**

**$TC_{mic}$ $^1$H NMR (400 MHz, $D_2O$) δ 7.5064 (d, *J* = 2.5 Hz, 1H, a), 7.2322 (dd, *J* = 8.8, 2.5 Hz, 1H, b), 7.1265 (d, *J* = 2.4 Hz, 1H, f), 6.8624 (d, *J* = 8.8 Hz, 1H, c), 6.7396 (dd, *J* = 8.6, 2.4 Hz, 1H, e), 6.6461 (d, *J* = 8.6 Hz, 1H, d).**

**$TC^-_{mic}$ (from the spectrum shown and not adjusted to take into account the contribution of $TC^-_{aq}$ to the observed shift) $^1$H NMR (400 MHz, $D_2O$) δ 7.4839 (d, *J* = 2.5 Hz, 1H, a), 7.1695 (dd, *J* = 8.9, 2.6 Hz, 1H, b), 6.7521 (d, *J* = 2.6 Hz, 1H, f), 6.6932 (d, *J* = 8.9 Hz, 1H, c), 6.6021 (d, *J* = 8.4 Hz, 1H, d), 6.3375 (dd, *J* = 8.4, 2.6 Hz, 1H, e).**

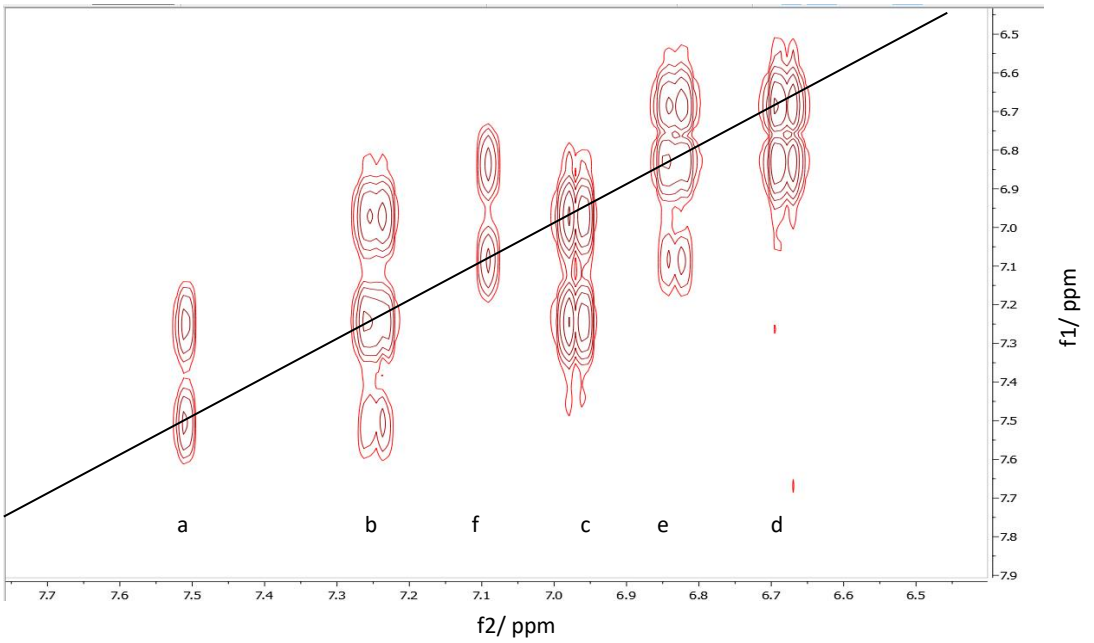


**Figure 3.5 400 mHz $^{1}$H COSY spectra of TC in $CDCl_3$: δ 7.4743 (d, *J* = 2.5 Hz, 1H, a), 7.2120 (dd, *J* = 8.8, 2.6 Hz, 1H, b), 7.0565 (d, *J* = 2.5 Hz, 1H, f), 6.9339 (d, *J* = 8.8 Hz, 1H, c), 6.7985 (dd, *J* = 8.7, 2.5 Hz, 1H, e), 6.6464 (d, *J* = 8.7 Hz, 1H, d).**

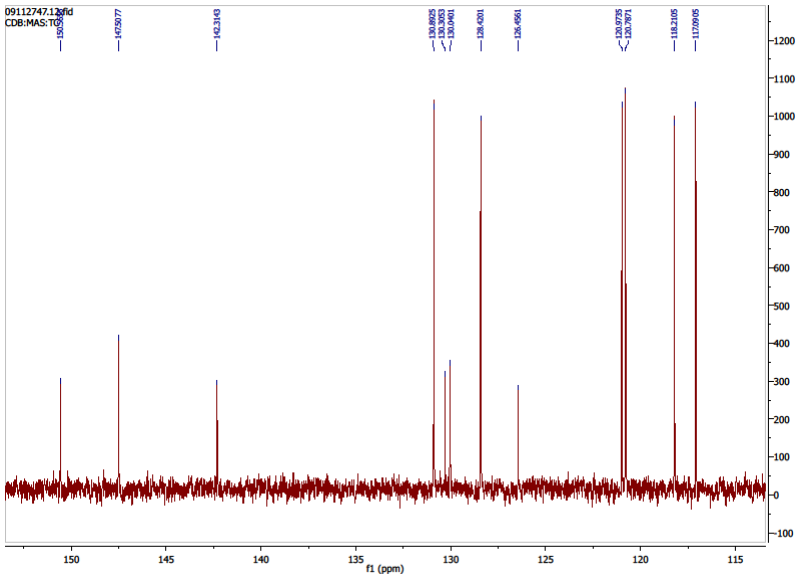


**Figure 3.6 400mHz $^{13}$C NMR spectra of TC in $CDCl_3$: δ 150.57 (i), 147.51 (g), 142.31 (h), 130.89 (a), 130.30 (k), 130.04 (l), 128.42 (b), 126.46 (j), 120.97 (c), 120.79 (e), 118.21 (d), 117.09 (f). Assignments are based on those by Wilson.[247]**

The samples prepared with 10% SDS in 0.1 M NaOH or 8% SL in 0.1 M KOH only provide approximate values of the chemical shifts for $TC^{-}_{mic}$ because they still contain a contribution from $TC^{-}_{aq}$. When 10% SDS is used as an approximate for $TC^{-}_{mic}$, if $K_{-}$ is 30, there is 12 times as much $TC^{-}_{mic}$ as $TC^{-}_{aq}$ in the measured sample, so that the difference between the $\delta_{obs}$ of $TC^{-}_{mic}$ and the actual value is significant. The values were adjusted during the fitting process to calculate the actual value of $\delta_{TC-mic}$. The values of $K_{-}$ and $\delta_{TC-mic}$ were determined iteratively until both values stopped changing with further interactions. $\delta_{TC-mic}$ was found from the $\delta_{obs}$, $K_{-}$ and $TC^{-}_{aq}$ according to

$$\delta_{TC^-_{mic}} = \frac{\delta_{obs}\left(1 + K_- \frac{m_{surf\,(mic)}}{m^\theta}\right) - \delta_{TC^-_{aq}}}{K_- \frac{m_{surf\,(mic)}}{m^\theta}}$$

Equation 3.25

Experiments were run at different pH to find $K_-$ and $K_+$. The total salt concentration was kept at 0.11 M, of which 0.01 M was NaOAc. At high pH, 0.1 M NaOH or KOH was used. At lower pH, carbonate buffers were used to maintain and control pH.

1% SL solutions form solid white gels in high concentrations of $Na^+$. These gels are formed by cylindrical nanofibres where the inside of the fibres are structurally similar to rod-like micelles and the $Na^+$ is free to move through the continuous water phase.[134,135] When 0.11 M $Na^+$ was used, the samples gelled before they could all be run (Figure 3.7). In a gelled sample, the SL peaks were broad and showed no splitting. The acetate peak was observed as a very clear sharp peak indicating that this species could move freely within the gel. The TC peaks could also be seen at slightly higher intensity than expected, they were broader than usual and did not show the usual splitting pattern (Figure 3.8).

Where possible $Na^+$ was substituted for $K^+$ in SL containing samples. The concentration of $Na^+$ was kept to 0.02 M or less. For experiments with SL, 0.01 M sodium carbonate buffer was used with 0.9 M KCl and 0.01 M NaOAc to avoid gelation. During the timescale of the experiment, and even overnight, no gelling was seen in samples at 0.02 M $Na^+$. The reference for $TC^-_{mic}$ with 0.1 M KOH showed gelling where the concentration of SL was 8%, so this sample was heated before any experiments.


**Figure 3.7 Solutions of 1% SL with different concentrations of NaCl and 0.01 M NaOAc. The concentrations of salt were 0.1 M (gel), 0.075 M (gel), 0.05 M (gel), 0.025 M (slight gel at top of vial) and 0.01 M (solution). All samples had been left overnight before a photo was taken.**

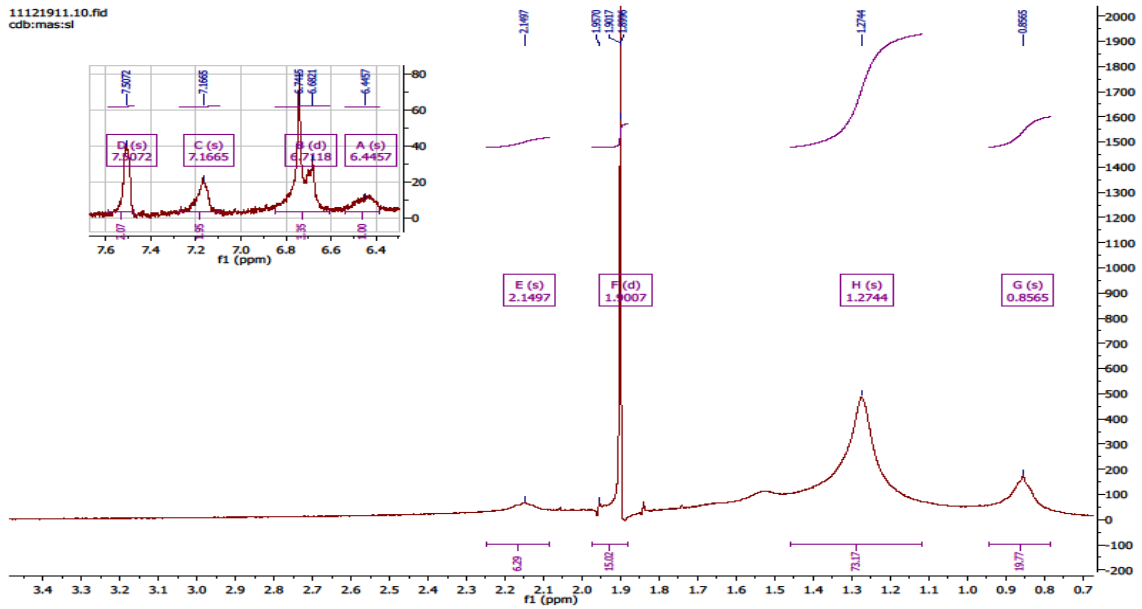


Figure 3.8 $^{1}$H NMR spectra at 400 mHz in $D_2O$ of 1% SL in 0.1 M NaOH and 0.01 M NaOAc with 0.1 mg/ mL TC.

The timescale of exchange in NMR spectroscopy can be measured by the broadening of peaks in solution NMR. Slow exchange on the NMR timescale leads to peaks from both forms being observed. In fast exchange, the observed peak is at a frequency that is the weighted average between the two peaks (Figure 3.9) and the exchange rate is faster than the frequency difference between the two peaks. When exchange is intermediate, the peak at the weighted average will be broadened.[251] In all of the following experiments carried out in this thesis, spectra show fast exchange, with single peaks for each of the TC proton peaks and the expected splitting patterns.

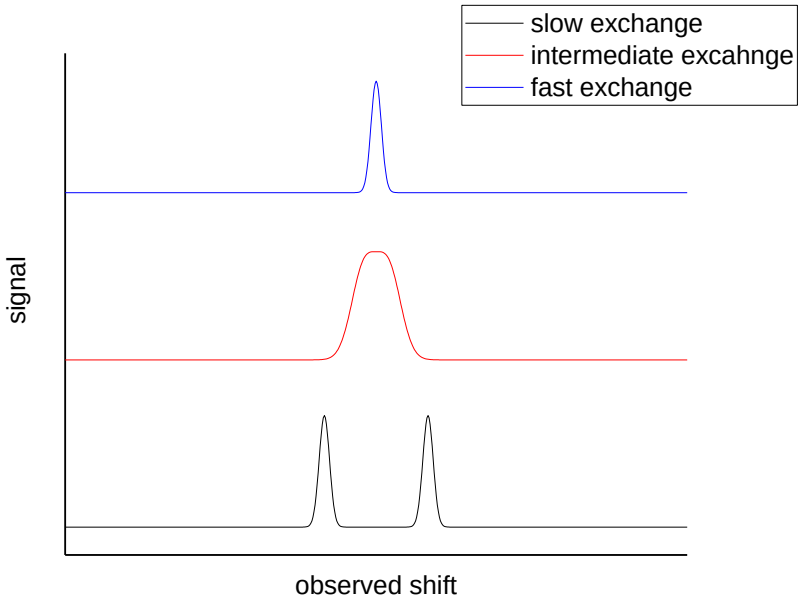


**Figure 3.9 A schematic showing the observed NMR peaks when there are two exchanging species undergoing fast exchange (top), intermediate exchange (middle) and slow exchange (bottom).**

Consider peak e and the resonances of $\delta_{TC-aq}$ at 6.5128 ppm and $\delta_{TC^-mic}$ at 6.3255 ppm with the respective frequencies of 2605 Hz and 2530 Hz relative to TMS. The exchange rate between free $TC^-$ and $TC^-$ in micelles has to be faster than 167 Hz for the spectra to appear as a single peak.

Where some peaks overlap, such as peaks d and e in SL with 0.1 M KCl there are second-order effects, which change $\delta_{obs}$ due to a small frequency difference between two or more coupled peaks causing the line intensities and positions change. In the extreme AB case, when the frequency difference becomes 0, the outermost lines of the two doublets have an intensity of zero and the two inner lines are equivalent (Figure 3.10). The peak positions are different from their first order values. At intermediate frequency separation the doublets show 'roofing', where the inner doublet resonance has a higher intensity than the outer doublet, and there is some deviation from the first order frequency. If the roofing effect is small then the line positions are not significantly changed.[244]

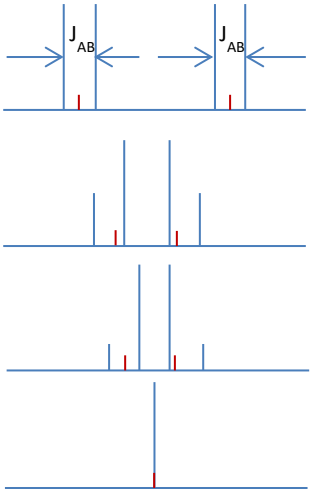


**Figure 3.10 The effect of second order effects on the observed peak position. Blue lines are the observed splitting pattern and red lines show the peak position.**

Care was taken over which peaks were included when fitting the data. Some peaks show a small total shift change during the course of an experiment and so they do not provide any information on the partition coefficients and add noise to the fitting procedure. For this reason, the shift of proton b was excluded from any fitting.

### *3.3.1.3 High pH Experiments to Calculate $K_-$*

Initial experiments with SDS were run at high pH in 0.1 M NaOH and fitted to the model where only $TC^-_{aq}$ and $TC^-_{mic}$ were present (Equation 3.18). $K_-$ was found by carrying out a global fit on peaks a and c to f. For the two different data sets with SDS as the surfactant, where experiments were run on different days, $K_-$ was found to consistently fit to 30 (Figure 3.11). Other sets of samples have been run using the same experimental set-up on the same and different 400 mHz machines over several years and fitted value of $K_-$ was within error of the values found from the data in Figure 3.11.

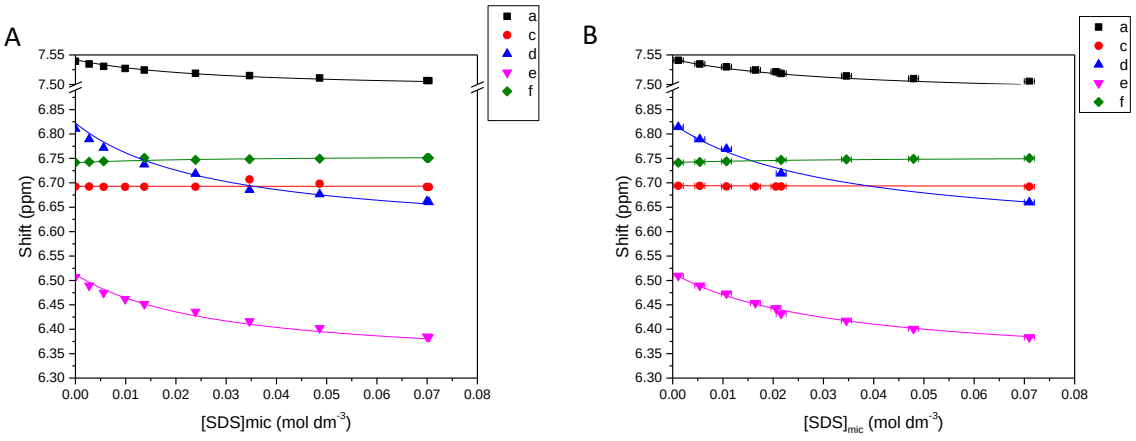


**Figure 3.11 (A) Shift in ppm of c (magenta), d (red), e (black) and f (green) against the concentration of SDS in micelles (mol $dm^{-3}$) in 0.1 M NaOH, 0.01 M NaOAc with fits shown by the solid lines. In all samples, the concentration of TC was 0.4 mM. $K_-$ was found to be 29.6 ± 0.6. (B) Shift in ppm of a (black), c (red), d (blue), e (magenta) and f (green) against the concentration of SDS in micelles (mol $dm^{-3}$) in 0.1 M NaOH, 0.01 M NaOAc with fits shown by the solid lines. In all samples, the concentration of TC was 0.8 mM. $K_-$ was found to be 30.5 ± 0.6. Fitting parameters are described in Table 3.5**

Table 3.5 Fitting parameters for TC in SDS, 0.1 M NaOH, 0.01 M NaOAc in Figure 3.11

| Figure | 3.11.A | 3.11.B |
|---|---|---|
| [TC]/ mM | 0.4 | 0.8 |
| $\delta_{TC^-_{aq}}$ of a | Not used for fit | 7.5427 |
| $\delta_{TC^-_{mic}}$ of a | Not used for fit | 7.4798 |
| $\delta_{TC^-_{aq}}$ of c | 6.6928 | 6.6942 |
| $\delta_{TC^-_{mic}}$ of c | 6.6931 | 6.6931 |
| $\delta_{TC^-_{aq}}$ of d | 6.8223 | 6.8214 |
| $\delta_{TC^-_{mic}}$ of d | 6.588 | 6.5862 |
| $\delta_{TC^-_{aq}}$ of e | 6.5128 | 6.5152 |
| $\delta_{TC^-_{mic}}$ of e | 6.3255 | 6.3247 |
| $\delta_{TC^-_{aq}}$ of f | 6.7412 | 6.7414 |
| $\delta_{TC^-_{mic}}$ of f | 6.7557 | 6.7529 |
| $K_-$ | 29.6 ±0.6 | 30.5 ±0.6 |

To calculate $K_-$ for TC in sodium Laurate solutions, two sets of experiments were run in 0.1 M KOH. The data was fitted to equation 1.18. When the concentration of TC was 0.5 mM, $K_-$ fitted to 11.9 ± 0.4 and when the concentration of TC was 0.7 mM, $K_-$ fitted to 12.8 ± 0.3 (Figure 3.12); these values are close but not within error. The values found for $K_-$ were found to be consistent on further runs where different NMR machines were used over several months.

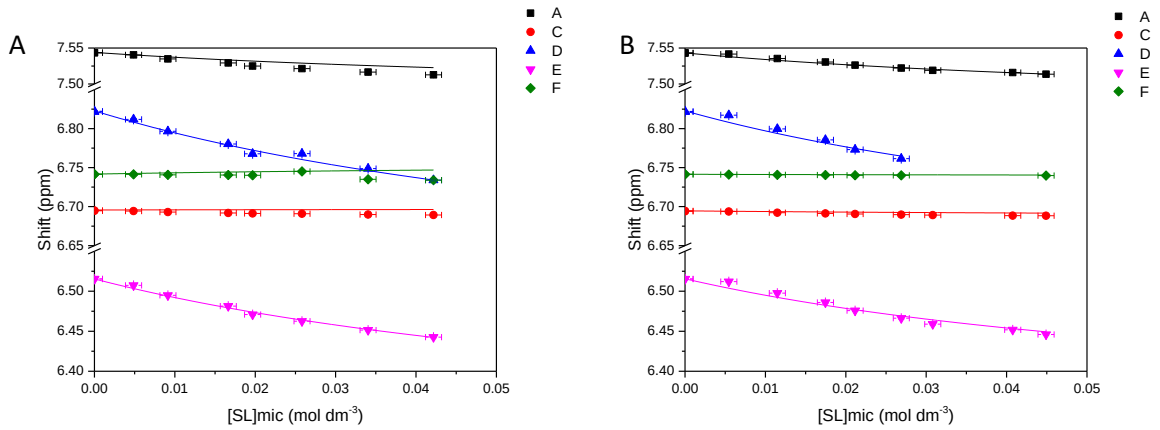


Figure 3.12 (A) Shift in ppm of a (black), c (red), d (blue), e (magenta) and f (green) against the concentration of SL in micelles (mol dm$^{-3}$) in 0.1 M KOH, 0.01 M NaOAc with fits shown by the solid lines. In all samples, the concentration of TC was 0.5 mM. $K_-$ was found to be 11.9 ± 0.4. (B) Shift in ppm of a (black), c (red), d (blue), e (magenta) and f (green) against the concentration of SL in micelles (mol dm$^{-3}$) in 0.1 M KOH, 0.01 M NaOAc with fits shown by the solid lines. In all samples, the concentration of TC was 0.7 mM. $K_-$ was found to be 12.8 ± 0.3. Fitting parameters are described in Table 3.6

Table 3.6 Fitting parameters for TC in SL, 0.1 M KOH, 0.01 M NaOAc in Figure 3.12

| [TC]/ mM | 0.5 | 0.7 |
|---|---|---|
| $\delta_{TC^-_{aq}}$ of a/ ppm | 7.5439 | 7.5432 |
| $\delta_{TC^-_{mic}}$ of a/ ppm | 7.4807 | 7.4627 |
| $\delta_{TC^-_{aq}}$ of c/ ppm | 6.6957 | 6.6946 |
| $\delta_{TC^-_{mic}}$ of c/ ppm | 6.6974 | 6.6877 |
| $\delta_{TC^-_{aq}}$ of d/ ppm | 6.8228 | 6.8228 |
| $\delta_{TC^-_{mic}}$ of d/ ppm | 6.5577 | 6.5960 |
| $\delta_{TC^-_{aq}}$ of e/ ppm | 6.5154 | 6.5156 |
| $\delta_{TC^-_{mic}}$ of e/ ppm | 6.2969 | 6.3338 |
| $\delta_{TC^-_{aq}}$ of f/ ppm | 6.7417 | 6.7415 |
| $\delta_{TC^-_{mic}}$ of f/ ppm | 6.7573 | 6.7392 |
| $K_-$ | 11.9 ±0.4 | 12.8 ±0.3 |

### 3.3.1.4 Lower pH Experiments to Calculate $K_+$

At lower pH, the contribution of $TC_{mic}$ towards the shift should be considered and an expanded model was used (Equation 3.24). Data in SDS solutions was collected with buffers formulated to remain at values of pH 10.8 and pH 10. The measured pH was 11.18 and pH 10.49 respectively. The pH was measured using a $H_2O$ calibrated pH meter. To convert into pD, a constant of around 0.4 can be added to the value displayed by the pH meter.[252] For consistency, throughout this study, the values quoted for the pH of the deuterated solutions is the value displayed by the pH meter, which is not adjusted to find pD using the conversion constant. Protonated buffer solutions were used as references for the measured pH values.

The NMR data collected fit well to the model (Figure 3.13). The data was fitted using $TC^-_{aq}$ and $TC^-_{mic}$ standards as above with $K_-$ set to 30. The reference for $TC_{mic}$ was 0.1 mg/mL TC, 1% SDS, 0.1 M HCl and 0.01 M NaOAc. The two data sets at pH 10.49 and 11.18 give values for $K_+$ of (1.85 ± 0.03) $\times 10^4$ and (2.38 ± 0.08) $\times 10^4$. The value used for the pKa of TC was 7.90 ±0.1.[236,253]

The largest experimental error in calculating $K_+$ is in the measurement of pH to 2 decimal places. For example, when the experiment at pH 10.49 was repeated with the same carbonate buffer formulation but fresh samples, the pH was measured as 10.55 and $K_+$ fitted to 2.09 ± 0.03 $\times 10^4$. The two data sets and fits appear to line up very well (Figure 3.14). If both sets of sample had the same pH, for example pH 10.5, the values of $K_+$ are 1.82 ±0.02 $\times 10^4$ and 1.89 ± 0.03 $\times 10^4$. Any error in the literature value for pKa leads to a systematic error in $K_+$. Other sets of samples have been run using the same experimental set-up on the same and different 400 mHz machines over several years and fitted change in shift has been consistent to within error of the values found from the data in Figure 3.13.

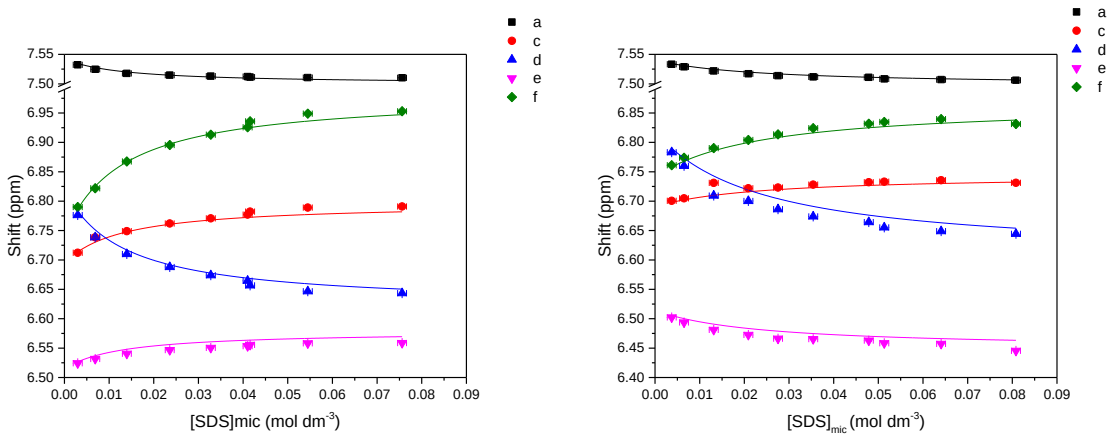


**Figure 3.13 (A) Shift in ppm of a (black), c (light blue), d (magenta), e (green) and f (dark blue) against the concentration of SDS in micelles (mol dm$^{-3}$) in 0.1 M carbonate buffer, 0.01 M NaOAc at pH 10.49 with fits shown by the solid lines. In all samples, the concentration of TC was 1.3 mM. $K_-$ was set to 30 and $K_+$ fitted to 18500 ± 300. (B) Shift in ppm of a (black), c (red), d (blue), e (magenta) and f (green) against the concentration of SDS in micelles (mol dm$^{-3}$) in 0.1 M carbonate buffer, 0.01 M NaOAc at pH 11.18 with fits shown by the solid lines. In all samples, the concentration of TC was 0.7 mM. $K_-$ was set to 30 and $K_+$ fitted to 23 800 ± 800. Fitting parameters are described in Table 3.7**

**Table 3.7 Fitting parameters for TC in SDS, 0.1 M carbonate buffer, 0.01 M NaOAc for the data in Figure 3.13**

| **[TC]/ mM** | **1.3** | **0.7** |
|---|---|---|
| **pH** | **10.49** | **11.18** |
| $\delta_{TC^-_{aq}}$ of a/ ppm | 7.5427 | 7.5403 |
| $\delta_{TC^-_{mic}}$ of a/ ppm | 7.4868 | 7.4889 |
| $\delta_{TC_{mic}}$ of a/ ppm | 7.5075 | 7.5165 |
| $\delta_{TC^-_{aq}}$ of c/ ppm | 6.6945 | 6.6905 |
| $\delta_{TC^-_{mic}}$ of c/ ppm | 6.6946 | 6.6936 |
| $\delta_{TC_{mic}}$ of c/ ppm | 6.8609 | 6.8672 |
| $\delta_{TC^-_{aq}}$ of d/ ppm | 6.8208 | 6.8193 |
| $\delta_{TC^-_{mic}}$ of d/ ppm | 6.5851 | 6.5879 |
| $\delta_{TC_{mic}}$ of d/ ppm | 6.6442 | 6.6492 |
| $\delta_{TC^-_{aq}}$ of e/ ppm | 6.5146 | 6.5145 |
| $\delta_{TC^-_{mic}}$ of e/ ppm | 6.3223 | 6.3249 |
| $\delta_{TC_{mic}}$ of e/ ppm | 6.7398 | 6.7451 |
| $\delta_{TC^-_{aq}}$ of f/ ppm | 6.7412 | 6.7408 |
| $\delta_{TC^-_{mic}}$ of f/ ppm | 6.7551 | 6.7560 |
| $\delta_{TC_{mic}}$ of f/ ppm | 7.1248 | 7.1311 |
| $K_-$ | 30 | 30 |
| $K_+$ | 18 500 ± 300 | 23 800 ± 800 |

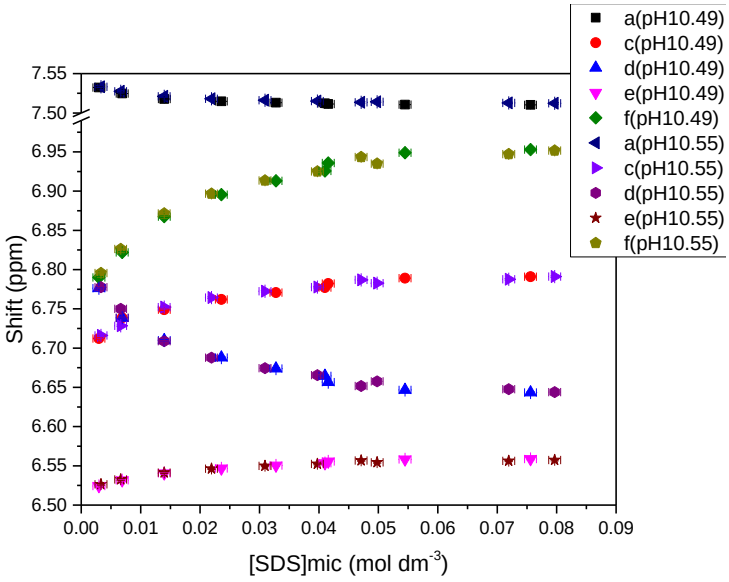


**Figure 3.14 Shift of proton peaks a and c-f from two different data sets at around the same pH. In the first set of samples the concentration of TC was 1.3 mM and the measured pH was 10.49. In the second data set the concentration of TC was 0.7 mM and the measured pH was 10.55.**

When lower pH data was used to find $K_+$ for SL in initial experiments, there were problems getting repeatable values of $K_+$ and good fits for all peaks. One of the possible causes was the pH of each sample changing with the concentration of SL. The samples prepared with SL contained 0.01 M carbonate buffer rather than 0.1 M buffer that was used in the experiments with SDS. Before carrying out measurements in the NMR machine, the pH of the solutions prepared in $D_2O$ was measured using the two separate pH meters (Figure 3.15). For the sample formulated with the pH 10 buffer (Figure 3.15.B), the pH of the solution hardly changed and the average pH was 10.38. The sample formulated with the pH 10.8 buffer showed very little pH variation with the Cole-Palmer electrode, and the Malvern electrode showed more variation. The average pH of the solutions was pH 10.65. The pH remains approximately constant with concentration of SL during the experiment. In any shown data collected with SL where a carbonate buffer was used, the pH of the 1% surfactant solution was measured with both electrodes and the average value was used as the value for the pH of the solutions.

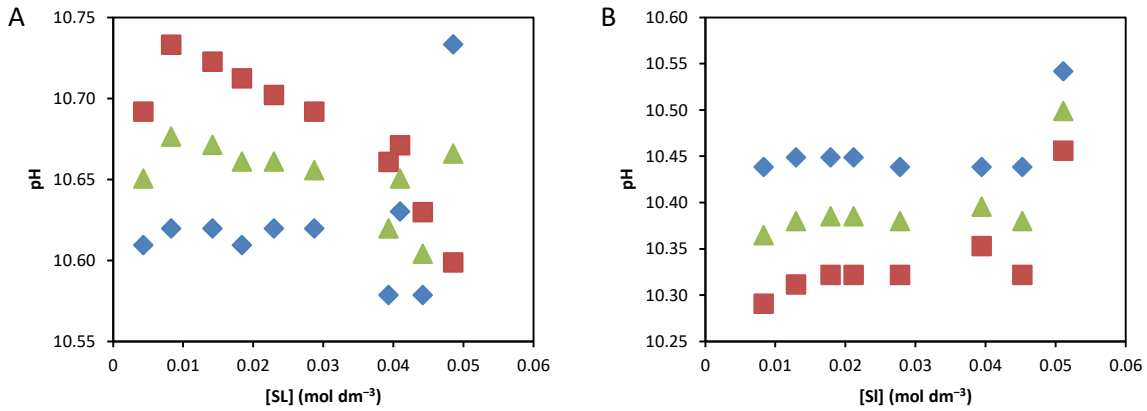


**Figure 3.15 Measured pH of the solutions of SL used in NMR analysis with $D_2O$ as the solvent (A) the average pH is 10.65 when the buffer was prepared to have a pH of 10.8 and (B) the average pH is 10.38 when the buffer was prepared to have a pH of 10.0. pH was measured using a Cole-Palmer electrode (blue) a Malvern electrode (blue) and an average was taken (green).**

If the pH of the samples remained largely constant at different concentrations of SL, then there must have been another reason why the data at lower pH did not fit very well to the model. During the previous experiments, at pH 10 and pH 10.8, the sample used to estimate $TC_{mic}$ was 1% SDS, 0.1 mg/mL TC in 0.1 M HCl. SDS was used instead of SL because SL is unstable in solution when the pH is less than 8.[132] An alternative sample was made to approximate $TC_{mic}$: 1% SL, 0.05 M Tris.HCl buffer, 0.05 M KCl and 0.01 M NaOAc. The Tris buffer was formulated to have a pH of 8.5 based on the calculations provided by Sigma-Aldrich: the buffer was formulated to a concentration of 0.05 M buffer using 4.36 mg/mL of Tris base and 2.21 mg/mL Tris-HCl.[254] At this pH, based on previous experiments with SDS, the dominant form of TC will be $TC_{mic}$, 99% of the TC present will be $TC_{mic}$ and the contribution of the other two forms of TC to $\delta_{obs}$ will be small to negligible.

The two data sets at pH 10.65 and pH 10.38 were fitted to the model equation 3.24 using values for the shifts of $TC^{-}_{aq}$, $TC^{-}_{mic}$ and $TC_{mic}$ collected on the same day as the experiments. To find $K_+$, the data for peak a, c–f fitted well when $K_-$ was set as 11.9 and $K_+$ was found to fit to $(1.8 \pm 0.3) \times 10^4$ at pH 10.65 and $(1.51 \pm 0.06) \times 10^4$ at pH 10.38 (Figure 3.16). The two values of $K_+$ are within error of one another and give reasonably good fits for peaks a, c-f.

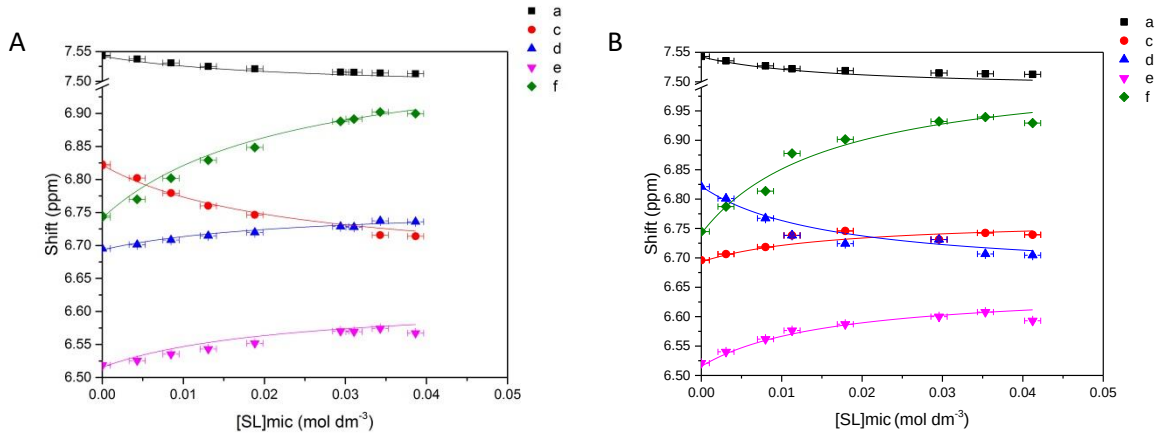


.

**Figure 3.16 (A) Shift in ppm of a (black), c (red), d (blue), e (magenta) and f (green) against the concentration of SL in micelles (mol dm$^{-3}$) in 0.09 M KCl, 0.01 M NaOAc, 0.01 M Carbonate buffer at pH 10.65 with fits shown by the solid lines. In all samples, the concentration of TC was 0.5 mM. $K_-$ was set to 11.9 and $K_+$ fitted to 18000 ± 3000. (B) Shift in ppm of a (black), c (red), d (blue), e (magenta) and f (green) against the concentration of SL in micelles (mol dm$^{-3}$) in 0.09 M KCl, 0.01 M NaOAc, 0.01 M Carbonate buffer at pH 10.38 with fits shown by the solid lines. In all samples, the concentration of TC was 0.5 mM. $K_-$ was set to 11.9 and $K_+$ fitted to 15100 ± 600. The fitting parameters are described in Table 3.8.**

**Table 3.8 Fitting parameters for TC in SL, 0.01 M carbonate buffer, 0.09 M KCl, 0.01 M NaOAc in Figure 3.16**

| **[TC]/ mM** | **0.5** | **0.5** |
|---|---|---|
| **pH** | **10.38** | **10.65** |
| $\delta_{TC_{aq}^-}$ of a/ ppm | 7.5424 | 7.5424 |
| $\delta_{TC_{mic}^-}$ of a/ ppm | 7.4583 | 7.4589 |
| $\delta_{TC_{mic}}$ of a/ ppm | 7.4941 | 7.4978 |
| $\delta_{TC_{aq}^-}$ of c/ ppm | 6.6932 | 6.6932 |
| $\delta_{TC_{mic}^-}$ of c/ ppm | 6.6869 | 6.6885 |
| $\delta_{TC_{mic}}$ of c/ ppm | 6.7854 | 6.7860 |
| $\delta_{TC_{aq}^-}$ of d/ ppm | 6.8220 | 6.8220 |
| $\delta_{TC_{mic}^-}$ of d/ ppm | 6.5887 | 6.5895 |
| $\delta_{TC_{mic}}$ of d/ ppm | 6.6885 | 6.6896 |
| $\delta_{TC_{aq}^-}$ of e/ ppm | 6.5153 | 6.5154 |
| $\delta_{TC_{mic}^-}$ of e/ ppm | 6.3275 | 6.3260 |
| $\delta_{TC_{mic}}$ of e/ ppm | 6.7258 | 6.7271 |
| $\delta_{TC_{aq}^-}$ of f/ ppm | 6.7413 | 6.7413 |
| $\delta_{TC_{mic}^-}$ of f/ ppm | 6.7369 | 6.7390 |
| $\delta_{TC_{mic}}$ of f/ ppm | 7.0973 | 7.1009 |
| $K_-$ | 11.9 | 11.9 |
| $K_+$ | 15 100 ± 600 | 18000 ± 3000 |

The observed shift is dominated by the shift of $TC_{mic}$ if the proportion of the phenol in micelles is greater than 99%. At 1% SDS, the pH of the solutions must be lower than pH 8.5 for $\delta_{obs}$ to be within 0.0005 ppm of the shift of the form $TC_{mic}$. The predicted shift at low pH has been plotted for both SDS and SL (Figure 3.17). As the pH of the solutions decreases, $\delta_{obs}$ varies less with concentration of surfactant. At low concentrations of surfactant, predicted shift deviates more strongly from the shift of $TC_{mic}$, as the proportion of $TC_{mic}$ is lower whereas at higher surfactant concentrations, $\delta_{obs}$ remains

stable as the proportion of $TC_{mic}$ remains fairly constant. For example, at pH 8.5 when there is 1% SL, the mole fraction of $TC_{mic}$ is 0.99, but when the concentration of SL is 0.25% (*i.e*. just above the CMC) the mole fraction of $TC_{mic}$ is 0.97 (Table 3.9). Solutions with pH lower than 9 should not be used to find $K_+$ as there is very little change in shift with concentration of surfactant so it is difficult to find $K_+$ with any precision.

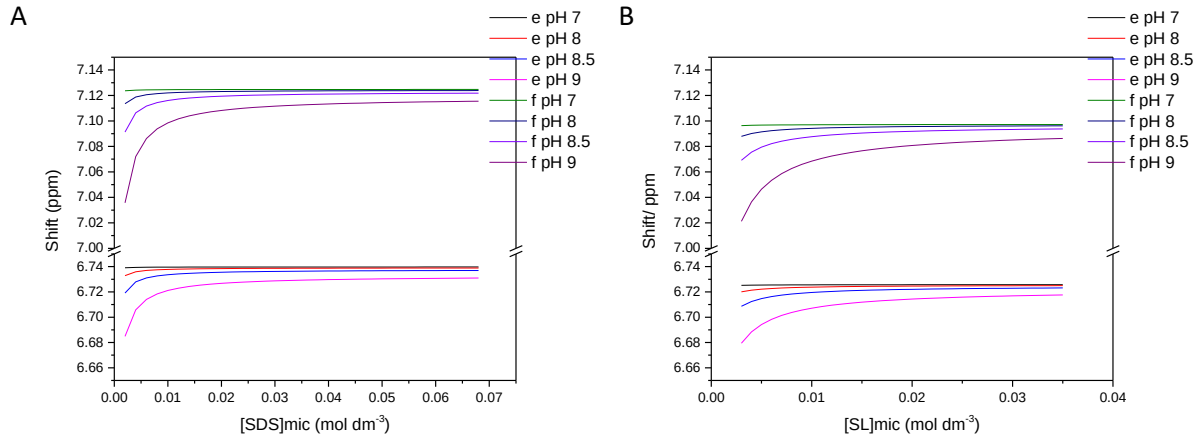


**Figure 3.17 Predicted shifts of TC peaks e and f against concentration of surfactant in micelles in different pH solutions of SDS (A) and SL (B) For SDS, peak e $\delta_{TC-aq}$ was 7.5146, $\delta_{TC-mic}$ was 6.3223 and $\delta_{TCmic}$ was 6.7398, and f $\delta_{TC-aq}$ was 6.7412, $\delta_{TC-mic}$ was 6.7551 and $\delta_{TCmic}$ was 7.1248. $K_-$ was set to 30 and $K_+$ was set to 22 000. For SL, e $\delta_{TC-aq}$ was 6.5153, $\delta_{TC-mic}$ was 6.3275 and $\delta_{TCmic}$ was 6.7258, and f $\delta_{TC-aq}$ was 6.7413, $\delta_{TC-mic}$ was 6.7369 and $\delta_{TCmic}$ was 7.0973. $K_-$ was set to 11.9 and $K_+$ was set to 16 000.**

**Table 3.9 The calculated mole fractions of $TC_{mic}$ at different pH and in different surfactant solutions.**

| | SDS | | SL | |
|---|---|---|---|---|
| **[Surfactant]** | 1% | 0.1% | 1% | 0.25% |
| **pH 7** | 0.9997 | 0.998 | 0.9997 | 0.9991 |
| **pH 8** | 0.997 | 0.98 | 0.997 | 0.991 |
| **pH 8.5** | 0.99 | 0.95 | 0.99 | 0.97 |
| **pH 9** | 0.97 | 0.85 | 0.97 | 0.92 |

The initial formulation space for surfactant and TC was 1% SDS and 0.1% TC as a model for hand soaps and body washes as that is approaching the formulation limits set by the European Union.[72,97] I prepared series of solutions starting at 1% surfactant with surfactant and TC in a 10:1 ratio with 0.1 M NaCl, 0.01 M NaOAc to observe how the shift and the proportions of the different forms of TC changed as the surfactant solution was diluted. $\delta_{obs}$ remained constant with concentration of surfactant (Figure 3.18). At the pH of these solutions, around pH 8.4, $TC_{mic}$ is the dominant form in solution and there was little contribution towards $\delta_{obs}$ from the phenolate forms of TC.

For the solutions with TC and SL in a 10:1 ratio in 0.1 M KCl, 0.01 M NaOAc, the pH was higher than the samples prepared in SDS. For example the pH of 1% SL in water was 10.5 (Figure 2.28) and as the concentration of SL approached the CMC the pH decreased to 8.5. In these samples, where there is more of a variation in the pH, there was more variation in $\delta_{obs}$ with concentration of SL than the SDS solutions (Figure 3.19). However, the shift remained constant with concentration of SL until the concentration of micellar SL decreased to 0.015 M. The shifts of peaks d and e showed second order effects and were observed as a single peak in all concentrations of SL except the lowest.

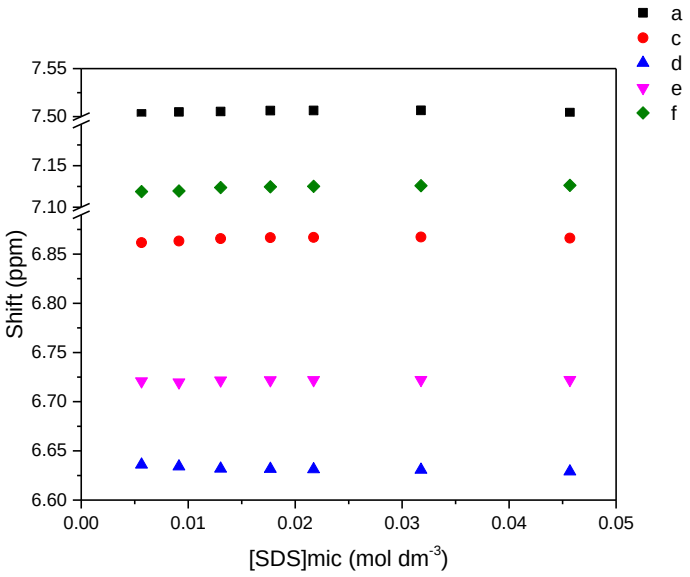


**Figure 3.18 The shift in ppm of TC peaks a (black), e (red), c (blue), d (magenta) and f (green) against concentration of SDS in micelles (mol dm$^{-3}$) in 0.1 M NaCl and 0.01 M NaOAc. SDS and TC are combined in a 1:10 ratio. The total shift change for a is 0.0038, for e is 0.0026, for c is 0.0058, for d is 0.0069 and for f is 0.0075.**

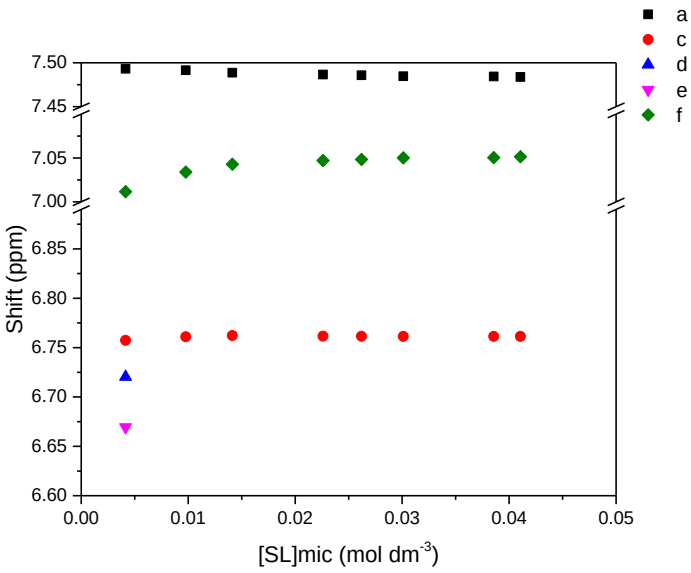


**Figure 3.19 The shift in ppm of TC peaks a (black), c (red), d (blue), e (magenta) and f (green) against concentration of SL in micelles (mol dm$^{-3}$) in 0.1 M KCl and 0.01 M NaOAc. SL and TC are combined in a 1:10 ratio. The total shift change for a is 0.093, for c is 0.0048, and for f is 0.0398.**

### 3.3.2 Ring Current Effects

Ring currents must be considered when fitting spectra of aromatic molecules. The magnetic field of the NMR spectrometer induces an electric current in the delocalised π-system of aromatic rings. The magnetic field of this ring current causes partial de-screening and screening of protons near the ring: protons in the plane of the face (*e.g.* the protons on benzene) are de-shielded and protons in or near the face are shielded.[244,255] There is some debate over the nature of ring current effects.[256–260] Wannere,[261] when reviewing a number of papers summarised that when the modern individual gauge for localised orbitals method is used to describe the aromaticity, the deshielding zone of

benzene begins further away from the centre of the ring and is weaker than traditionally expected and explained in organic textbooks (Figure 3.20). When using observed NMR shift to calculate the partitioning of aromatic molecules into micelles, the concentration of the aromatic within the micelles should be considered. For example, if there is more than one aromatic molecule per micelle, during the NMR timescale, the two molecules are likely to encounter one another and induce a change in the NMR shift of one another.

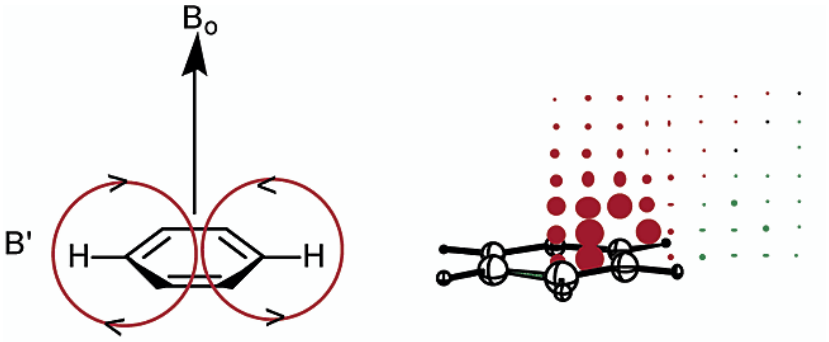


**Figure 3.20 Comparison of the conventional ring current model, $B_0$ and B' are the applied and induced magnetic fields, respectively, with the shielding environment computed by the individual gauge for localised orbitals (IGLO) method. Red and green colour dots represent magnetically shielded and deshielded points, respectively.**[261]

### *3.3.2.1 Ring Currents in SDS Solutions*

To assess the effect of ring currents, samples were prepared in 0.1 M NaCl, 0.01 M NaOAc and 1% SDS. In these samples, the only form of TC contributing towards the shift was $TC_{mic}$. $\delta_{obs}$ changed linearly with number of TC molecules per micelle (Figure 3.21 and Table 3.10). The pH of these solutions was pH 8.4, and the pH remained constant with the concentration of SDS. Based on the values of $K_-$ and $K_+$ found above of 30 and 22000, the fraction of TC in the micelle is 0.99 when the concentration of SDS is 1%. The change in shift with the concentration of TC per micelle is caused by ring current effects.

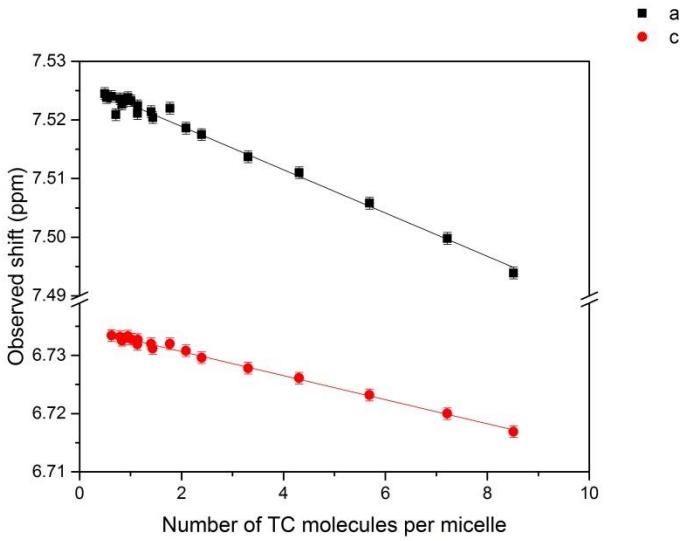


**Figure 3.21 Plot of shift of a (black) and c (red) against number of TC molecules per micelle in 1% SDS, 0.1 M NaCl and 0.01 M NaOAc. The number of TC molecules per micelle was calculated by dividing the concentration of TC by the concentration of micelles. The number of micelles was calculated by dividing the concentration of SDS in micelles by the aggregation number of SDS, which is 120 under these conditions.**

Table 3.10 The change in shift of TC peaks due to ring current effects in 1% SDS, 0.1 M NaCl and 0.01 M NaOAc.

| Peak | a | b | c | d | e | f |
|---|---|---|---|---|---|---|
| Gradient/ ppm per molecule of TC per micelle | -0.0037 | -0.0040 | -0.00286 | -0.00165 | -0.00207 | -0.00212 |
| Error in gradient | 1 x$10^{-4}$ | 1 x$10^{-4}$ | 5 x$10^{-5}$ | 4 x$10^{-5}$ | 4 x$10^{-5}$ | 7 x$10^{-5}$ |

A similar experiment was carried out in 0.1 M NaOH, where the concentration of SDS was kept constant at 0.08 mM and the concentration of TC was varied (Figure 3.22). In this system, there are two forms of TC: $TC^-_{mic}$ and $TC^-_{aq}$. To calculate the concentration of solute, TC, within micelles at high pH in 0.1 M NaOH, the value of $K_-$ and the concentration of surfactant in micelles can be used. At this pH, $TC^-_{aq}$ and $TC^-_{mic}$ are the only forms of TC in solution and the observed NMR shift is dependent on the mole fraction of each form:

$$m_{TC^-_{mic}} = \frac{K_-[TC]_{tot}\left(\frac{m_{surf\,(mic)}}{m^\circ}\right)}{1+K_-\left(\frac{m_{surf\,(mic)}}{m^\circ}\right)} \qquad \text{Equation 3.26}$$

The number of TC molecules per micelle can be calculated based on the proportion of $TC^-_{mic}$ and the total concentration of TC:

$$TC_{molec\,/\,micelle} = N_{agg}[TC]_{tot}\left(\frac{K_-}{1+K_-\left(\frac{m_{surf\,(mic)}}{m^\circ}\right)}\right) \qquad \text{Equation 3.27}$$

The effect of the number of $TC^-$ per micelle on the observed shift is lower than for the phenol form of TC. The number of TC molecules per micelle can then be calculated by dividing the concentration of TC in micelles by the concentration of micelles. The aggregation number of surfactants is used to calculate the number of micelles.

In the concentration range of SDS used, the aggregation number should be 120 (Table 2.9). For SL, the aggregation number was assumed to be 89, taken from the work of Rodríguez-Pulido.[233]

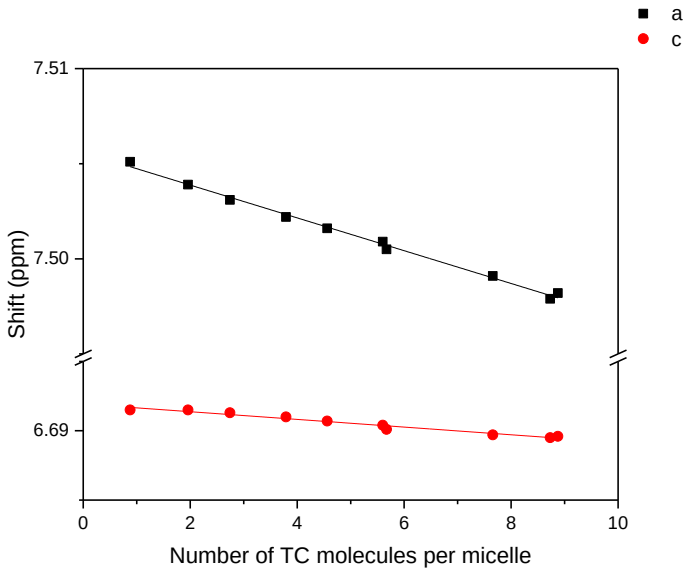


**Figure 3.22 Plot of shift of a (blue) and c (red) against number of $TC^-$ molecules per micelle in 1% SDS, 0.1 M NaOH and 0.01 M NaOAc. The number of TC molecules per micelle was calculated by dividing the concentration of TC by the concentration of micelles. The number of micelles was calculated by dividing the concentration of SDS in micelles by the aggregation number of SDS, which is 120 under these conditions.**

**Table 3.11 The change in shift of TC peaks due to ring current effects in 1% SDS, 0.1 M NaOH and 0.01 M NaOAc.**

| **Peak** | **a** | **b** | **c** | **d** | **e** | **f** |
|---|---|---|---|---|---|---|
| Gradient/ ppm per molecule of TC per micelle | -1.20 x$10^{-3}$ | -1.59 x$10^{-3}$ | -3.8 x$10^{-4}$ | 7.2 x$10^{-4}$ | 8.9 x$10^{-4}$ | -3.2 x$10^{-4}$ |
| Error in gradient | 3 x$10^{-5}$ | 3 x$10^{-5}$ | 2 x$10^{-5}$ | 2 x$10^{-5}$ | 4 x$10^{-5}$ | 2 x$10^{-5}$ |

In the experiment at high pH in 0.1 M NaOH (Figure 3.11), the number of TC molecules per micelle was between 0.36 (at 75 mM SDS) and 1.03 (at 3 mM SDS) when 0.4 mM TC was used. The effect of ring currents on $\delta_{obs}$ can be calculated from the gradient of shift against number of TC molecules per micelle: the ring current effects could be included in the model to improve the fit as an additional term.

The number of molecules of TC per micelle is combined with the change in shift due to the number of molecules per micelle (*e.g.* the gradient from Figure 3.22), $g_{TC^-_{mic}}$, $\delta_{obs}$ can be predicted taking into account ring current effects:

$$\delta_{obs} = \frac{\delta_{TC^-_{aq}} + \delta_{TC^-_{mic}} K_- \left(\frac{m_{surf\,(mic)}}{m^\Theta}\right) + g_{TC^-_{mic}} N_{agg}\, m_{TC(tot)} K_-}{1 + K_- \left(\frac{m_{surf\,(mic)}}{m^\Theta}\right)}$$

**Equation 3.28**

At lower pH, the calculation for the number of TC molecules per micelle should incorporate $K_+$ to take into account the proportion of the phenol as well as the phenolate form of TC within the micelles:

$$TC_{molec/micelle} = N_{agg}\frac{m_{TC(tot)}}{m^{\circ}}\left(\frac{K_{-}+K_{+}10^{(pKa-pH)}}{1+K_{-}\left(\frac{m_{surf(mic)}}{m^{\circ}}\right)+K_{+}10^{(pKa-pH)}\left(\frac{m_{surf(mic)}}{m^{\circ}}\right)}\right)$$

Equation 3.29

So the observed shift is

$$\delta_{obs} = \frac{\delta_{TC^{-}_{aq}}+\delta_{TC^{-}_{mic}}K_{-}\frac{m_{surf(mic)}}{m^{\ominus}}+\delta_{TC_{mic}}K_{+}\frac{m_{surf(mic)}}{m^{\ominus}}10^{pKa-pH}+g_{TC^{-}_{mic}}\frac{m_{TC(tot)}}{m^{\ominus}}N_{agg}K_{-}+g_{TC_{mic}}\frac{m_{TC(tot)}}{m^{\ominus}}N_{agg}K_{+}10^{pKa-pH}}{1+K_{-}\frac{m_{surf(mic)}}{m^{\ominus}}+K_{+}\frac{m_{surf(mic)}}{m^{\ominus}}10^{pKa-pH}}$$

Equation 3.30

where $g_{TC_{mic}}$ is the gradient of the plot of shift against the concentration of the phenol in micelles.

If model data is used, the effect of ring currents on the individual peaks is readily observable in 0.1 M NaOH. In the data shown in Figure 3.23, the model $\delta_{obs}$ is calculated using the equation including ring currents (Equation 3.31). The effect of ring currents on $\delta_{obs}$ is more distinct at low surfactant concentrations. As the concentration of surfactant decreases, the number of TC molecules per micelle increases and the change in $\delta_{obs}$ is larger, as more TC molecules encounter one another within the time of the experiment.

However, when the fitting of $K_{-}$ is carried out on model data for peaks a and c-f, where ring currents are included in the model data using a global fit, the effect on the total fitting is less significant than just observing the change in fit for individual peaks. For example, when the concentration of TC was set to 1.5 mM with $K_{-}$ set to 30, the value of $K_{-}$ from simple fitting of the model data was 28.7 ± 0.2 (Figure 3.24). As the concentration of TC increases, the fit of the data from the simple model becomes poorer and the fitted value of $K_{-}$ varies from the real value. The simple model also does not fit the model data so well at low concentrations of SDS, as the ratio of TC to SDS increases. The concentration of TC in the solutions used for the simple model should remain below 2 mM and constant with concentration of surfactant to remain valid, otherwise to fit the data, the ring currents model should be used instead when the only contributors to shift are $TC^{-}_{aq}$ and $TC^{-}_{mic}$.

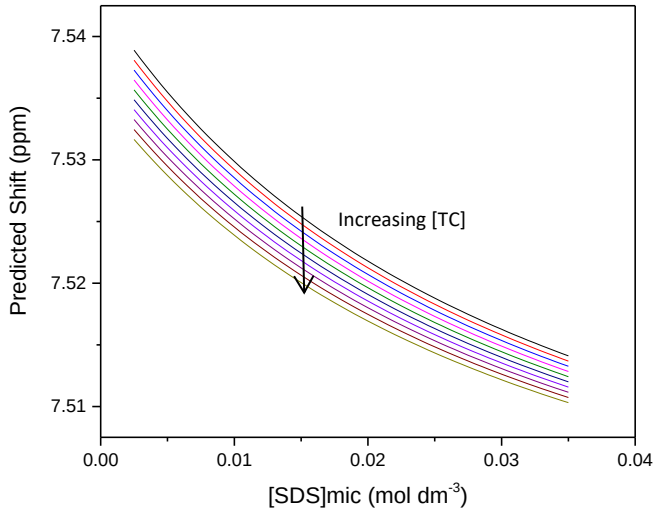


**Figure 3.23 Predicted shift of peak a with concentration of SDS when just $TC^-_{aq}$ and $TC^-_{mic}$ are present with ring current effects included. $K_-$ set to 30 and the concentration of TC was between 0 and 1.8 mM.**

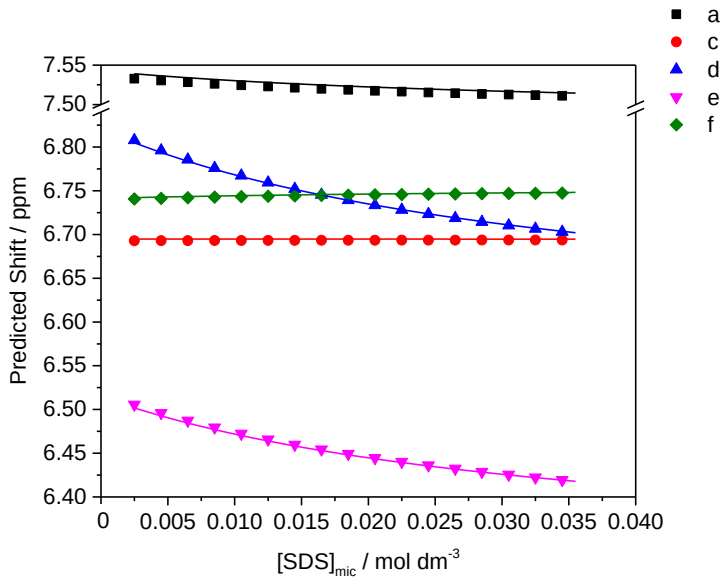


**Figure 3.24 Fitting model NMR data including the effect of ring currents to the simple model excluding effects of ring currents. Data was created with $K_-$ set to 30 and the concentration of TC was set to 1.5 mM and with just $TC^-_{aq}$ and $TC^-_{mic}$, ring currents were included in the model data calculations. $K_-$ was found to be 28.7 ± 0.2 after fitting without ring currents included.**

If this model is used to refit the data collected in 0.1 M NaOH, $K_-$ fitted to 31.1 ± 0.7, when $K_-$ found using the simplified model was 30.5 ±0.6. The value found with ring currents is the same as the value found without ring currents (Figure 3.25 and Table 3.12) to within the experimental error in the measurement.

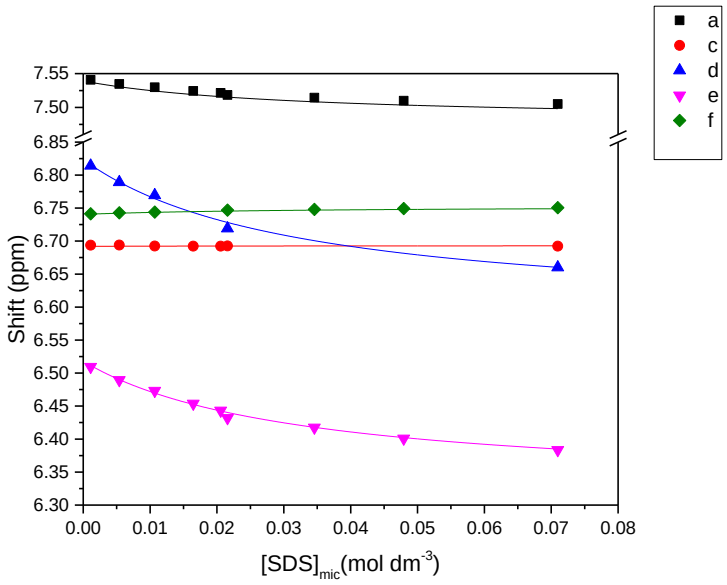


**Figure 3.25 Shift in ppm of a (red), c (magenta), d (olive), e (black) and f (turquoise) against the concentration of SDS in micelles (mol dm$^{-3}$) in 0.1 M NaOH, 0.01 M NaOAc with fits shown by the solid lines Fitting was carried out using the ring currents model. In all samples, the concentration of TC was 0.8 mM. $K_-$ was found to be 31.1 ± 0.7. Fitting parameters are described in Table 3.12.**

**Table 3.12 Fitting parameters for the data shown in Figure 3.25 with and without ring currents included in the model.**

| Fitting model | Without Ring Currents | With Ring Currents |
|---|---|---|
| **[TC]/ mM** | **0.8** | **0.8** |
| $\delta_{TC^-_{aq}}$ of a/ ppm | 7.5427 | 7.5427 |
| $\delta_{TC^-_{mic}}$ of a/ ppm | 7.4798 | 7.4798 |
| $g_{TC_{mic}}$ / ppm$^{-1}$ | - | -0.0012 |
| $\delta_{TC^-_{aq}}$ of c/ ppm | 6.6942 | 6.6942 |
| $\delta_{TC^-_{mic}}$ of c/ ppm | 6.6931 | 6.6931 |
| $g_{TC_{mic}}$ / ppm$^{-1}$ | - | -0.00038 |
| $\delta_{TC^-_{aq}}$ of d/ ppm | 6.8214 | 6.8214 |
| $\delta_{TC^-_{mic}}$ of d/ ppm | 6.5862 | 6.5862 |
| $g_{TC_{mic}}$ / ppm$^{-1}$ | - | 0.00072 |
| $\delta_{TC^-_{aq}}$ of e/ ppm | 6.5152 | 6.5152 |
| $\delta_{TC^-_{mic}}$ of e/ ppm | 6.3247 | 6.3247 |
| $g_{TC_{mic}}$ / ppm$^{-1}$ | - | 0.00089 |
| $\delta_{TC^-_{aq}}$ of f | 6.7414 | 6.7414 |
| $\delta_{TC^-_{mic}}$ of f | 6.7529 | 6.7529 |
| $g_{TC_{mic}}$ / ppm$^{-1}$ | - | -0.00032 |
| $K_-$ | 30.5 ±0.6 | 31.1 ±0.7 |

When the ring currents model was used to fit data collected at lower pH, pH 11.18 and pH 10.55, the fitted values of $K_+$ were sufficiently close to the value found when fitting was carried out using the simplified model. For the data at pH 11.18, $K_+$ calculated with ring currents, 2.46 ±0.08 x10$^4$, was within error of the value for $K_+$ found from simplified fitting, 2.4 ±0.1 x10$^4$ (Table 3.13). For the data

at pH 10.55, $K_+$ from fitting with ring currents was 2.14 ±0.04 x$10^4$ was within error of the value found using the simplified model, 2.08 ±0.04 x$10^4$.

**Table 3.13 Summary of partition coefficients for TC in SDS found through fitting with and without ring currents**

| pH | Ring Currents | | No Ring Currents | |
|---|---|---|---|---|
| | $K_-$ | $K_+$ (x$10^4$) | $K_-$ | $K_+$ (x$10^4$) |
| 13 | 27.9 ± 0.6 | - | 29.6 ±0.6 | - |
| 11.18 | 30 | 2.4 ±0.1 | 30 | 2.4 ± 0.1 |
| 10.55 | 30 | 2.14 ± 0.04 | 30 | 2.08 ± 0.04 |
| 9.6 | 30 | 2.8 ± 0.3 | 30 | 2.3 ± 0.1 |

The predicted $\delta_{obs}$ for peaks a and c-f at different pH was plotted using the simple model and the ring currents model with a concentration of TC of 0.5 mM from pH 11 (Figure 3.26.A) to pH 8 (Figure 3.26.D). The model with ring currents included deviates from the simple model at low concentrations of SDS and low pH. For pH 10 and higher, both calculated shifts show reasonable agreement. At lower pH, there is more disagreement between the two models: the number of TC molecules per micelle increases as the pH decreases and the phenol has a stronger ring current effect.

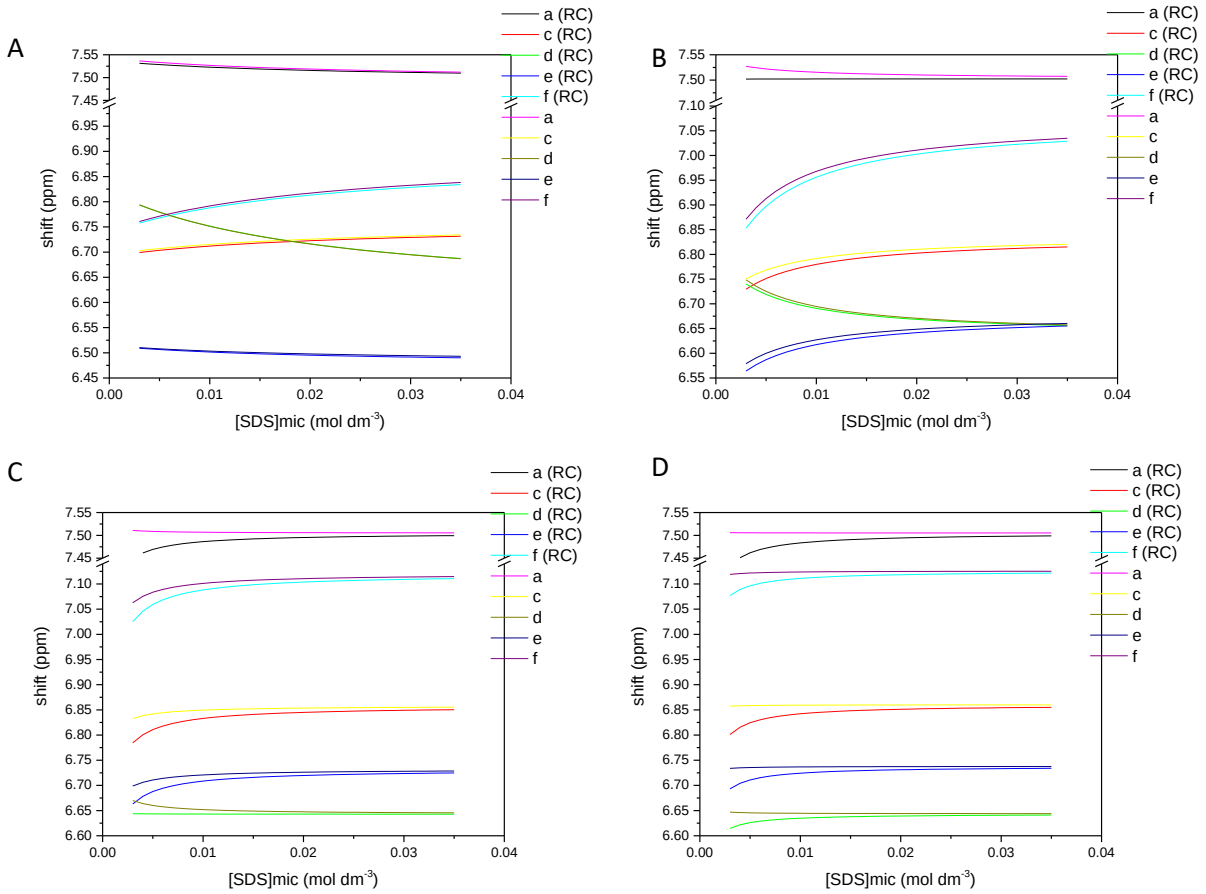


**Figure 3.26 The difference between the predicted shifts of peak a, c-f for TC with and without ring current effects at pH 11 (A), pH 10 (B), pH 9 (C) and pH 8 (D) for SDS in 0.11 M salt. $K_-$ was set to 30, $K_+$ was set to 2.2 x$10^4$ and the concentration of TC was 0.5 mM.**

In experimental data collected at pH 9.6, the number of TC molecules per micelle varied between 0.7 molecules of TC per micelle with 0.085 M $SDS_{mic}$ and up to 9 molecules of TC per micelle as the concentration of $SDS_{mic}$ decreased to 0.005 M. When ring currents were included in the model (Figure 3.27), the fitting of some peaks was better and the fitting of other peaks appeared to be poorer than when the simple model was used (black lines). $K_+$ fitted to 2.8 ±0.1 x$10^4$ with ring currents and 2.30 ±0.08 x$10^4$ for the simple model. Ring currents should be included when fitting data collected below pH 10 rather than fitting with the simple model.

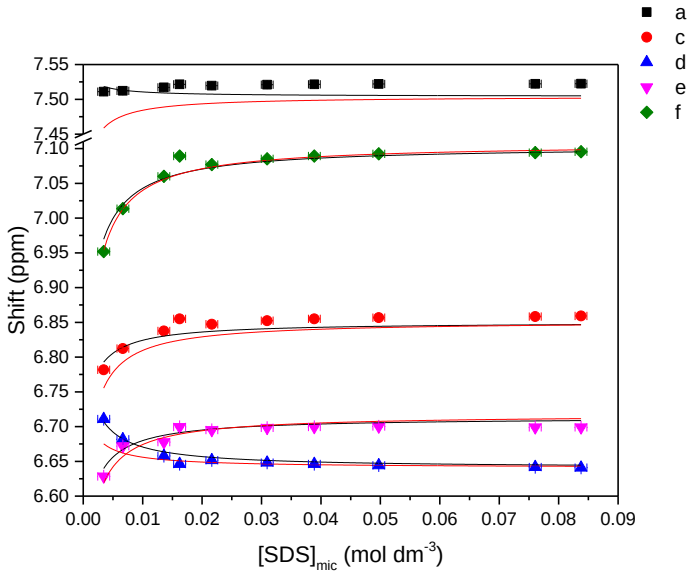


**Figure 3.27 Shift in ppm of a (black), c (red), d (blue), e (magenta) and f (green) against the concentration of SDS in micelles (mol $dm^{-3}$) in 0.05 M Tris buffer, 0.05 M NaCl, 0.01 M NaOAc at pH 9.60 with fits shown by the solid lines. The fitting using the model with ring currents are shown by the red lines and the fitting without ring currents are shown by the black lines. In all samples, the concentration of TC was 0.7 mM. $K_-$ was set to 30 and $K_+$ fitted to 28 000 ± 3000 with ring currents and 23 000 ± 800 without ring currents. Fitting parameters are described in Table 3.14**

Table 3.14 Fitting parameters for data in Figure 3.27 with SDS in 0.7 mM TC at pH 9.6

| [TC]/ mM | 0.7 |
|---|---|
| **pH** | **9.60** |
| $\delta_{TC^-_{aq}}$ of a/ ppm | 7.5428 |
| $\delta_{TC^-_{mic}}$ of a/ ppm | 7.4868 |
| $\delta_{TC_{mic}}$ of a/ ppm | 7.5053 |
| $\delta_{TC^-_{aq}}$ of c/ ppm | 6.6948 |
| $\delta_{TC^-_{mic}}$ of c/ ppm | 6.6947 |
| $\delta_{TC_{mic}}$ of c/ ppm | 6.8605 |
| $\delta_{TC^-_{aq}}$ of d/ ppm | 6.8207 |
| $\delta_{TC^-_{mic}}$ of d/ ppm | 6.5856 |
| $\delta_{TC_{mic}}$ of d/ ppm | 6.6438 |
| $\delta_{TC^-_{aq}}$ of e/ ppm | 6.5146 |
| $\delta_{TC^-_{mic}}$ of e/ ppm | 6.3229 |
| $\delta_{TC_{mic}}$ of e/ ppm | 6.7386 |
| $\delta_{TC^-_{aq}}$ of f/ ppm | 6.7413 |
| $\delta_{TC^-_{mic}}$ of f/ ppm | 6.7549 |
| $\delta_{TC_{mic}}$ of f/ ppm | 7.1265 |
| $K_-$ | 30 |
| $K_+$ without ring currents | 23 000 ± 800 |
| $K_+$ with ring currents | 28 000 ± 3 000 |

### *3.3.2.2 Ring Currents in SL Solutions*

The ring current effect in SL solutions was studied at high pH in 0.1 M KOH with a constant concentration of SL and changing concentration of TC (Figure 3.28). In the absence of buffer or base, the pH varies with concentration of SL (Figure 2.31) and each will have different proportions of TC in the phenol and phenolate forms leading to difficulty in calculating the concentration of TC in micelles. At low pH, SL protonates to lauric acid, which has a lower solubility,[132] so data has not been collected to describe the effect of phenol per micelle on the observed shift.

Plots of shift against molecules of $TC^-$ per micelle were linear with negative gradients (Figure 3.28 and Table 3.15). The concentration of $TC^-_{mic}$ was calculated using Equation 3.26.

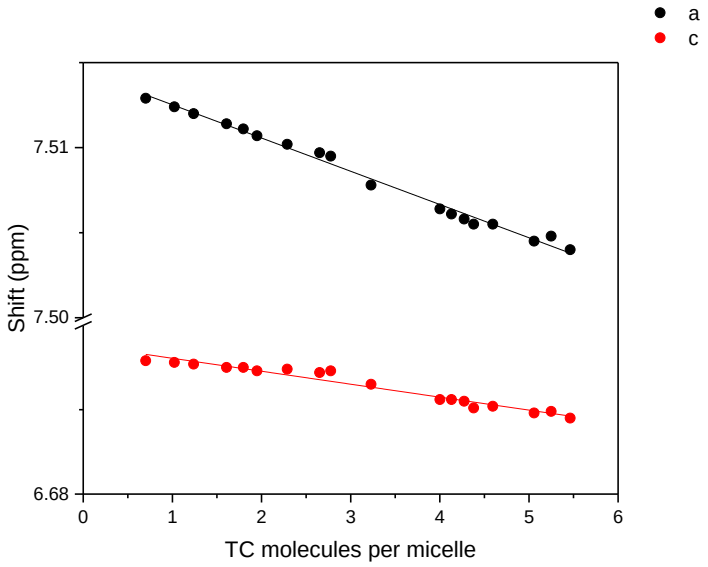


**Figure 3.28 Shift of peaks a (red) and c (black) against number of TC molecules per micelle in 1% SL, 0.1 M KOH and 0.01 M NaOAc. The number of TC molecules per micelle was calculated by dividing the concentration of TC in micelles by the concentration of micelles. The number of micelles was calculated by dividing the concentration of SL in micelles by the aggregation number of SL, which is 89 under these conditions.[233]**

**Table 3.15 The change in shift of TC peaks due to ring current effects in 1% SL, 0.1 M KOH and 0.01 M NaOAc.**

| Peak | a | b | c | d | e | f |
|---|---|---|---|---|---|---|
| Gradient (ppm) | -0.00195 | -0.00203 | -0.00077 | -0.00048 | -0.00018 | -0.00090 |
| Error in gradient x$10^{-5}$ (ppm) | 5 | 5 | 4 | 4 | 5 | 6 |

The NMR data collected at high pH to calculate $K_-$ was refitted to take into account the ring current effects (using Equation 3.28) and the value found for $K_-$ (12.6 ±0.3) was within error of the value found using the simple fitting method, which was 12.8 ±0.3 (Figure 3.29).

When data collected at pH 10.65 and pH 10.38 were refitted using ring currents, the values for $K_+$ from both models were the same within error. The model they were fitted to is

$$\delta_{obs} = \frac{\delta_{TC^-_{aq}} + \delta_{TC^-_{mic}} K_- \frac{m_{surf(mic)}}{m^\ominus} + \delta_{TC_{mic}} K_+ \frac{m_{surf(mic)}}{m^\ominus} 10^{pKa-pH} + g_{TC^-_{mic}} \frac{m_{TC(tot)}}{m^\ominus} N_{agg} \left(K_- + K_+ 10^{pKa-pH}\right)}{1 + K_- \frac{m_{surf(mic)}}{m^\ominus} + K_+ \frac{m_{surf(mic)}}{m^\ominus} 10^{pKa-pH}}$$

**Equation 3.31**

The model contains an approximation that the change in shift caused by more than one phenol per micelle is the same as for the phenolate, which in the case of SDS is not true. At pH 10.65, $K_+$ fitted to 1.8 ±0.3 x$10^4$ and at pH 10.38, $K_+$ fitted to 1.51 ±0.06 x$10^4$ (Table 3.17). Only when the concentration of TC begins to approach saturation does the effect of ring currents need to be considered.

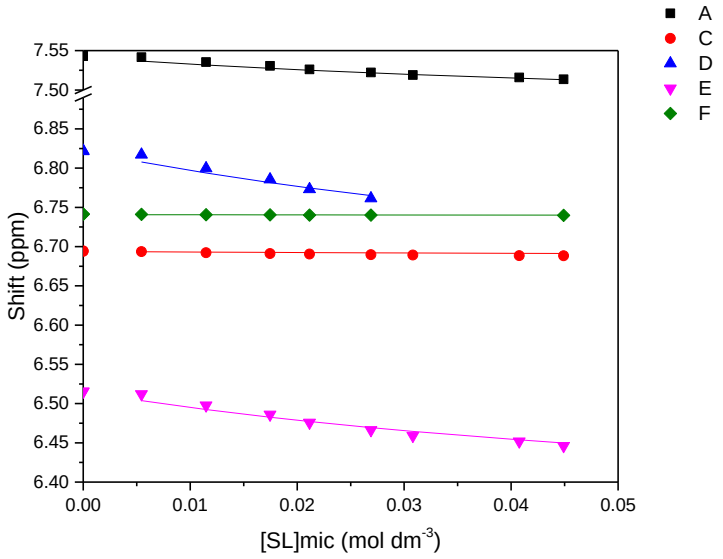


**Figure 3.29 Shift in ppm of a (black), c (red), d (blue), e (magenta) and f (green) against the concentration of SL in micelles (mol dm$^{-3}$) in 0.1 M KOH, 0.01 M NaOAc with fits shown by the solid lines. Fitting was carried out using the expanded model taking into account ring current effects. In all samples, the concentration of TC was 0.7 mM. $K_-$ was found to be 12.6 ± 0.3. Fitting parameters are described in Table 3.16.**

**Table 3.16 Fitting parameters for 0.7 mM TC in SL with 0.1 M KOH, 0.01 M NaOAc in Figure 3.29 with and without ring current effects included.**

| Fitting model | Without Ring Currents | With Ring Currents |
|---|---|---|
| **[TC]/ mM** | **0.7** | **0.7** |
| $\delta_{TC^-_{aq}}$ of a/ ppm | 7.5432 | 7.5432 |
| $\delta_{TC^-_{mic}}$ of a/ ppm | 7.4627 | 7.4625 |
| $g_{TC_{mic}}$ / ppm$^{-1}$ | - | -0.00195 |
| $\delta_{TC^-_{aq}}$ of c/ ppm | 6.6946 | 6.6946 |
| $\delta_{TC^-_{mic}}$ of c/ ppm | 6.6877 | 6.6866 |
| $g_{TC_{mic}}$ / ppm$^{-1}$ | - | -0.00077 |
| $\delta_{TC^-_{aq}}$ of d/ ppm | 6.8228 | 6.8228 |
| $\delta_{TC^-_{mic}}$ of d/ ppm | 6.5960 | 6.5954 |
| $g_{TC_{mic}}$ / ppm$^{-1}$ | - | 0.00048 |
| $\delta_{TC^-_{aq}}$ of e/ ppm | 6.5156 | 6.5156 |
| $\delta_{TC^-_{mic}}$ of e/ ppm | 6.3338 | 6.3333 |
| $g_{TC_{mic}}$ / ppm$^{-1}$ | - | 0.00018 |
| $\delta_{TC^-_{aq}}$ of f/ ppm | 6.7415 | 6.7415 |
| $\delta_{TC^-_{mic}}$ of f/ ppm | 6.7392 | 6.7388 |
| $g_{TC_{mic}}$ / ppm$^{-1}$ | - | -0.00090 |
| $K_-$ | 12.8 ±0.3 | 12.6 ±0.3 |

Table 3.17 Summary of partition coefficients for TC in SL found through fitting with and without ring currents

| pH | Ring Currents | | No Ring Currents | |
|---|---|---|---|---|
| | $K_-$ | $K_+$/ x10$^4$ | $K_-$ | $K_+$/ x10$^4$ |
| 12.5 | 12.6 ±0.3 | - | 12.8 ±0.3 | - |
| 10.65 | 11.9 | 1.8 ± 0.3 | 11.9 | 1.8 ± 0.3 |
| 10.38 | 11.9 | 1.51 ± 0.06 | 11.9 | 1.51 ± 0.06 |

The effect of ring currents on the observed NMR shift is pH dependent. For data collected where $TC_{mic}$ is the dominant form in solution, the effect of ring currents on the fitting is stronger. For the systems used above to calculate $K_-$ and $K_+$, when the concentration of TC remains low and there is a wide range of surfactant concentrations, the effect of ring currents on the fitted values of $K_-$ and $K_+$ is limited. When the concentration of TC is closer to saturation and the number of micelles is small, ring currents will begin to cause significant changes to $\delta_{obs}$ and cause changes to the fitted values of $K_-$ and $K_+$ when the simple model is used. The data collected at low concentrations of surfactant gives more information about the partition coefficients than the data at high concentrations when the shift changes less in concentration.

At points it is reasonable to assume the simple model fits the data sufficiently well, for example, at high pH, concentrations of SDS more than double the CMC and low concentrations of TC. However, as the pH decreases and the concentration of TC increases, ring currents become more significant and should be included in the model to fit the data precisely. Below pH 10 and above 2 mM TC the model with ring currents should be used to fit data. For SL, a similar approach should be taken.

### 3.3.3 Solubility of TC in SDS and SL solutions

The solubility of TC in aqueous solutions of surfactant with salt was measured by NMR to determine the solubilizing ability of the two surfactants for TC. Samples were prepared by saturating solutions of surfactant with excess TC over three days. They were prepared with a total salt concentration of 0.11 M. The TC concentration in each solution was calculated from comparing the integrals of TC to the sodium acetate integral. The plots of TC concentration against surfactant concentration (Figure 3.30) were linear with gradients (*i.e.* solubility ratios) of 0.159 ± 0.005 for SDS and 0.156± 0.009 for SL; as can be seen, the solubilizing power of both surfactants is similar. Both solubility plots have an intercept below zero, and give CMC values of 0.0046 ± 0.0006 mol dm$^{-3}$ for SDS and 0.013 ±0.001 mol dm$^{-3}$ for SL. The aggregation numbers of SDS and SL, 120 and 89 respectively, were used to calculate the number of TC molecules per micelle of SDS (Table 2.9) and SL.[233] There were 15 molecules of TC per micelle of SDS and 14 molecules per micelle of SL at saturation.

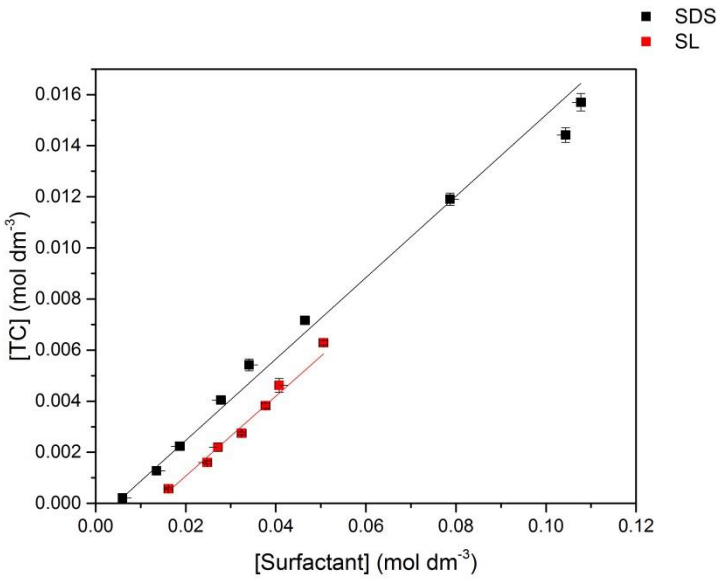


**Figure 3.30 The saturated concentration of TC in mol dm$^{-3}$ against the concentration of surfactant in micelles in mol dm$^{-3}$ for SDS (black) and SL (red). Both systems contained 0.01 M NaOAc as a reference and 0.1 M salt (NaCl with SDS and KCl with SL). The solutions were left over a weekend to allow equilibrium to be reached. Both plots have been fitted linearly. For SDS, the gradient is 0.159 ±0.005 and the x intercept is 4.6 ± 0.6 x10$^{-3}$ mol dm$^{-3}$. For SL, the gradient is 0.156 ± 0.008 and the x intercept is 0.013 ± 0.001 mol dm$^{-3}$.**

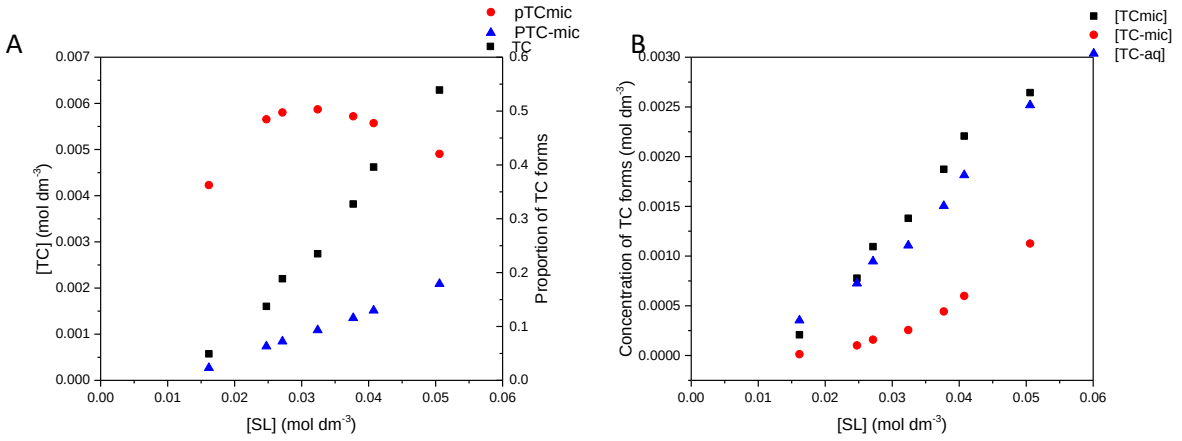


**Figure 3.31 Solubility curve of TC in SL with 0.1 M KCl and 0.01 M NaOAc with calculations of $p_{TCmic}$ and $p_{TC-mic}$ overlaid taken from the predicted pH (A) and the calculated concentration of different forms of TC in different concentrations of SL with 0.1 M KCl and 0.01 M NaOAc (B).**

The form of TC in the solutions of SDS was $TC_{mic}$ so the solubility curve describes the solubility of phenol TC in SDS whereas in the solutions of SL, because the pH changes with concentration of SL, there were different proportions of the phenol and phenolate in solution. The solubility curve of TC in SL includes contributions from both the phenol and phenolate, so it is unexpected that the gradient is the same as the data collected with SDS. The pH of the solutions varies between 10.7 at 0.05 M SL and 9.8 at 0.016 M SL, based on the data collected in Figure 2.31. The proportions of $TC_{mic}$ and $TC^{-}_{mic}$ were predicted based on the pH and the values of $K_+$ and $K_-$ found above. The proportion of $TC^{-}_{mic}$ increased with pH and concentration of SL whereas the proportion of $TC_{mic}$ was more varied with concentration of SL (Figure 3.31.A). The observed solubility plot of TC in SL included contributions from all three forms of TC (Figure 3.31.B), the proportions of $TC_{mic}$ and $TC^{-}_{aq}$ were similar in all samples and the proportion of $TC^{-}_{mic}$ increased with concentration.

The CMC value for SDS calculated by NMR is higher than the value found by interfacial tension measurements, even though the ratio of TC to SDS is 50% higher than the highest ratio measured by interfacial tension measurement and the CMC decreases with concentration of TC. The CMC value depends on the method of determination: the weighted contribution of free surfactant and surfactant micelles to the observed property changes with measurement method.[262] Also, the SDS used in the solubility study was taken from the bottle and used without purification, whereas the samples used for IFT measurements where recrystallized 3 times. The SDS used in the NMR experiments will be further contaminated by dodecanol from hydrolysis of SDS in the three days solubilisation time.[263] The CMC value for SL is within error of the value found through pendant drop measurements, 0.099 M (Table 2.8).

## 3.4 Conclusions

$K_-$ and $K_+$ have been found for both SDS and SL: $K_-$ is 30 ±2 for SDS and 11.9 ±0.6 for SL and and $K_+$ is 1.6 ± 0.2 $\times 10^4$ for SL and 2.2 ± 0.2 $\times 10^4$ for SDS. The molar solubility ratios of SDS and SL as calculated by NMR are 0.159 ±0.005 for SDS and 0.156 ±0.009 for SL. The value calculated for $K_+$ is much larger than $K_-$ showing that the phenol form of TC partitions much more strongly into micelles than the phenolate. In 1% SDS, there is 700 times more of the phenol in the micelles than in the aqueous solution, whereas the proportion of phenolate in the micelles and aqueous solution is nearly the same. In 1% SL, there is half the amount of the phenolate in bulk as the phenolate in micelles and there is 600 times the phenol in micelles than in aqueous solution. The ratio of phenol to phenolate of course depends on the pH of the solution.

The partition coefficients found in Chapter 3 by NMR for TC between the micelles and bulk cannot be directly compared to the partition coefficient between the surface and the bulk found in Section 2.3.1 due differences in the standard states. The surface-bulk partition coefficient, $K_{+,sur}$, was calculated from the surface concentration (that is, the surface excess divided by the monolayer thickness), over the bulk concentration of TC. $K_{+,sur}$ was 700 000, calculated at low coverage of SDS as a rough estimate. There is 700 times more phenol in micelles than bulk at 1% SDS calculated from $K_+$, this is effectively the excess concentration of phenol in micelles as compared to bulk. At 1% SDS, there is 0.034 M SDS in micelles, which is 9.8 g $dm^{-3}$ of SDS, so SDS in micelles is approximately 1/100$^{th}$ of the total volume of the solution. In this case, there is 700 times more SDS in 1/100$^{th}$ of the volume of the solution, so the partition coefficient of the phenol between bulk and micelles, taking into account the differences in volume is 70 000, which is a factor of 10 less than the surface-bulk partition coefficient found in Section 2.3.1.

As shown in the SANS work (Table 2.9), TC resides in the core region of the micelles close to the headgroup. SDS and SL have similar length chains, so if TC resided in the core, the partition coefficients would be very similar, whereas the SDS and SL headgroups are different functional groups and will interact differently from one another.

The effect of ring currents on the fitting of the NMR data has been accounted for and fitted. The new values found for $K_-$ and $K_+$ from fitting with ring currents are either within error or within 7% of the values found using the standard fitting when the used is at a pH higher than 10 and the concentration of TC is less than 2 mM. In future work, only the simple fitting should be carried out rather than calculating the ring current contribution as will.

# 4 TIR-Raman Analysis of Triclosan Insertion into Supported Lipid Bilayers

## 4.1 Introduction

Supported phospholipid bilayers can be useful models for cell membranes. TIR-Raman is a suitable technique to study the effect of changes to the environment on the bilayer structure. TIR- Raman has previously been used to study the silica-water interface. The depth studied depends on the angle of incidence, for example if the angle of incidence is 73°, the evanescent wave penetrates around 100 nm.[182,185] The CH stretches can give information about the conformational order of the bilayer, with the surface providing an external reference to understand the orientation of the lipid molecules.[182,264] Churchwell[179] and Lee[184,265] have collected spectra of POPC as a supported membrane on silica using TIR-Raman (Figure 4.1).

In this thesis, TIR-Raman has been used to study the effect of Triclosan (TC) on supported phospholipid bilayers. The advantage of TIR-Raman over other techniques is the surface selectivity, so that the properties of a single bilayer can be probed. TC has Raman signals in different locations to the lipid signal at 1600 $cm^{-1}$ and 3075 $cm^{-1}$. TC can be observed in the membrane and the effect of TC on the bilayer can be probed through changes in the lipid signal.

A TIR-Raman spectrum of the phospholipid POPC in the C-H stretching region between 2800 and 3000 $cm^{-1}$ is shown in Figure 4.1. The assignments of POPC are a. overtone of the $CH_2$ bending mode, b. symmetric CH stretch ($d_+$), c. anti-symmetric CH stretch ($d_-$), d. overtone of the CH scissoring mode with its Fermi resonance, e. anti-symmetric terminal methyl stretch, f. symmetric head-group methyl stretch, g. vinylic CH vibrations, h. anti-symmetric stretch of choline head-groups. In the fingerprint region the following assignments have been made: 1. In plane $CH_2$ twist, 2. Fermi doublet of $CH_2$ scissoring mode, 3. C=C stretch, 4. Ester C=O stretch.[179]

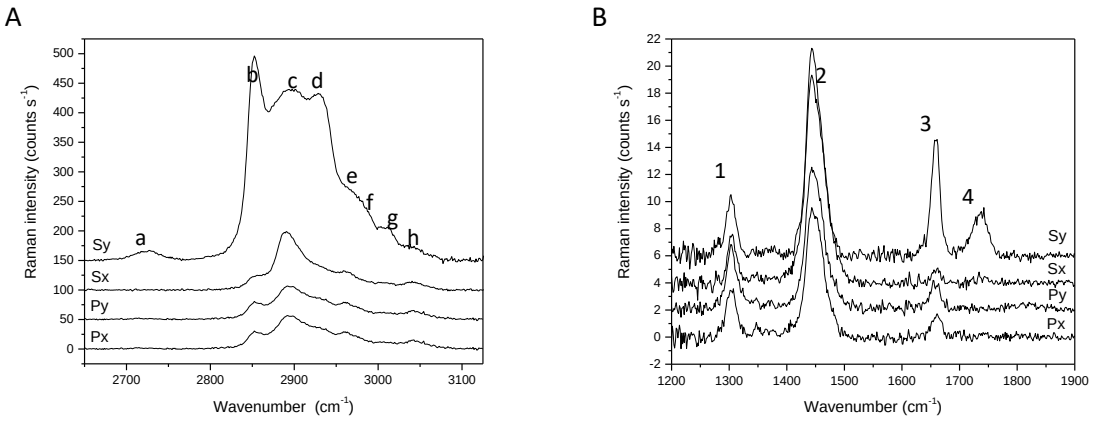


**Figure 4.1 Raman spectra of POPC at the silica–water interface: (A) sy, sx, py, px spectra of POPC in the 2900 $cm^{-1}$ region; and (B) sy, sx, py, px spectra of POPC in the fingerprint region. Adapted from Lee (2005).[184]**

A number of Raman experiments on solid TC have been reported in literature. Iconomopoulou and Voyiatzis[266] carried out Raman spectroscopy on uniaxially drawn polymer films of high density polyethene with grafted TC, focussing on the TC peaks at 3073 $cm^{-1}$ and 710 $cm^{-1}$. Chen *et al*.[267] used confocal Raman microscopy to investigate TC-functionalised polysiloxanes. The ratio of the aromatics peaks in TC (1585 and 1645 $cm^{-1}$) with the carbonyl bands in the coating (1726 $cm^{-1}$) was

used to determine the relative concentration of TC. TC resided primarily at the air interface rather than towards the centre of the coating. The TC peaks at 3075 $cm^{-1}$ and 1600 $cm^{-1}$, C-H stretching and the C-C stretching mode of the phenyl rings respectively, are at different frequencies to the lipid peaks.

Many authors[16,20,26–29] have shown that TC is membrane-active in cell membrane models, such as liposomes, and in living cells. The activity of TC against bacteria is at least in part due to the damage it causes to cell membranes, although the major mode of action in gram-positive bacteria is against the enzyme FabI.[18,21]

One example of the membrane activity of TC is the work of Villalaín.[30] The gel-to-fluid phase transition temperature ($T_m$) for DMPC, DMPG and DEPE was lowered in the presence of TC with the main transition being almost eliminated at 30 mol% TC. Jones and colleagues[31–33] prepared liposomes and noticed that the transition was affected by the presence of TC, when at above 60 mol%, no transition was observed in DPPC. There was improved permeability towards glucose at lower temperatures, due to the increased fluidity of the membranes in the presence of TC.

Villalaín followed up his earlier work with a magic angle NMR study[34] looking at the orientation of TC in a model membrane. He found that TC was parallel to the plane of the bilayer, close to the head-group. A molecular dynamics study by Orsi, Noro and Essex[35] agreed with the findings of Villalaín. Paloncýová[268] estimated there was a free energy minimum 1.5 nm from the centre of the bilayer for TC and calculated the partition coefficient of TC into DOPC membranes from water as 5.3 using COSMOmic modelling methods.

Lee[265] studied the transition temperature of DMPC bilayers by TIR-Raman. He found that the phase transition was much broader than found with LUVs of DMPC. Under S polarised light, the intensities of the C-H stretches increased as temperature decreased, and the ratio of antisymmetric and symmetric vibrations, $I(d_-)/I(d_+)$, increased with temperature (Figure 4.2 and Figure 4.3). The onset of the ratio increase was 26°C for DMPC. POPC shows no variation in peak ratio with temperature. As the temperature decreases in DMPC, the acyl chains become more ordered and stand more upright against the surface. As the chains become more ordered, the volume per chain decreases and dense islands of lipid form.[269,270] There was also a peak frequency increase with temperature for DMPC bilayers which was more pronounced in the anti-symmetric CH stretch. The wavenumber with the maximum intensity decreased with temperature.

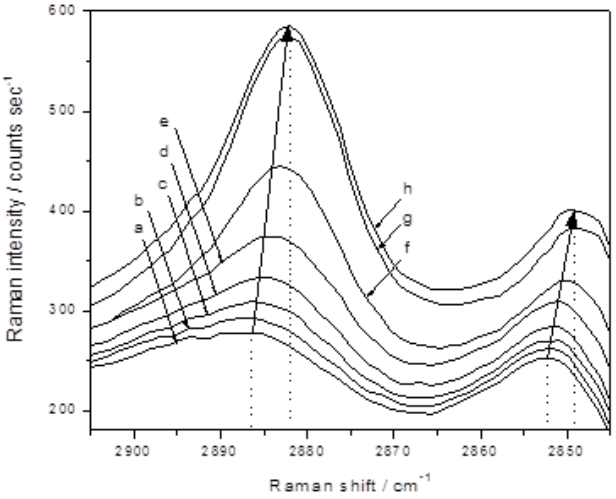


**Figure 4.2 Temperature-dependence of the Raman spectra of *DMPC* in the methylene vibration modes of C-H stretching region, 1.2 *W*, *s*-polarised excitation, unpolarised detection: (a) 42.0°*C*, (b) 38.1°*C*, (c) 32.0°*C*, (d) 26.6°*C*, (e) 23.3°*C*, (f) 20.8°*C*, (g) 16.8°*C*, and (h) 13.2 °*C*. The arrows direct a decrease of temperature.**[265]

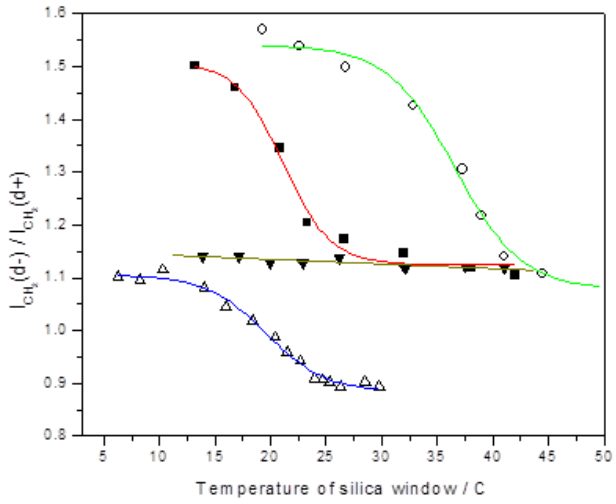


**Figure 4.3 Variation in *I*(d-)/*I*(d+) with the temperature for *slb*'s of (■) *DMPC*, (○) *DPPC*, and (▼) *POPC* and for (Δ) *DMPC* vesicle in a bulk suspension. Laser power was 1.2*W*, *s*-polarised excitation, unpolarised detection.**[265]

Feng[269] proposed a model for the behaviour of supported DMPC bilayers on mica around the $T_m$ based on AFM images (Figure 4.4). Well below the $T_m$, there is a well ordered gel phase with defects showing the mica surface. As the temperature increases, the defects blur and cracks appear due to the partial melting of the upper leaflet of the bilayer. At two degrees above the transition temperature, the entire outer leaflet is in the fluid phase and the bilayer appears flat and featureless. As the temperature increases, the bottom leaflet begins to melt, causing further defects in the appearance of the bilayer. Around eight degrees above $T_m$, the bottom layer completely converts to the fluid phase.

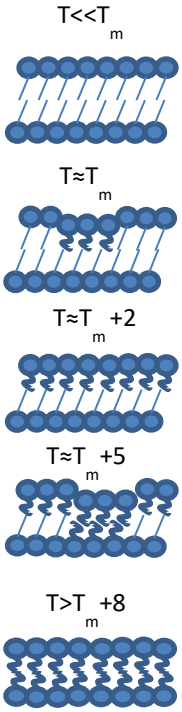


**Figure 4.4 Schematics of supported bilayers of pure PCs during phase transition. Adapted from Feng[269]**

Klumpp *et al.*[271] observed the phase transition behaviour of DPPC in the presence of 2,4-dichlorophenol (2,4-DCP) using FT-Raman spectroscopy on liposomes. 2,4-DCP (Figure 4.5) is a molecule with a similar structure to TC and is thought to be one of the decomposition products of TC.[82] Klumpp[271] found that the C-H scissoring vibration at 1440 $cm^{-1}$ revealed the pre-transition $L_{\beta}$-$P_{\beta'}$ of DPPC at around 31-32°C, below the main transition $P_{\beta'}$-$L_{\alpha}$ at around 40-41°C which was observed in the C-H stretching region at 2900 and 2850 $cm^{-1}$. With 2,4-DCP/DPPC at 44 mol%, the main transition occurred at the lower temperature of 22-25°C.

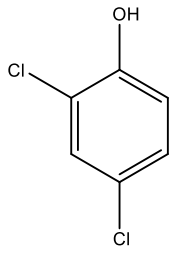


**Figure 4.5 The structure of 2,4-dichlorophenol**

Different mixtures of phospholipids can be used to alter the properties of the bilayer and mimic different cell membrane structures. In the study described in this thesis, experiments were initially carried out using bilayers of POPC. POPC has a transition temperature below 0°C and forms reliable bilayers.[179] Experiments were carried out to investigate the effect of TC on the bilayer, looking at the effect of the TC concentration and the pH. Experiments were also carried out to investigate the removal of TC from the bilayer. In the standard experiments carried out, a bilayer was formed in pH 7.4 buffer and a spectrum was taken. The bilayer was treated with a solution containing TC at approximately 0.1 mg/ mL in pH 10.8 carbonate buffer. The bilayer was left for about fifteen minutes before taking a measurement. The bilayer was then rinsed with 20 mL of pH 7.4 buffer and then with

a further 100 mL of buffer. Using experiments based around this design, the effect of TC on bilayers of POPC has been investigated.

The study was expanded to include the effect of TC on the transition of DMPC bilayers. Other researchers[26,30] have shown that TC decreased the transition temperature of DMPC.

POPE/POPG bilayers are good models for *E. coli.*[168] as bacterial membranes contain higher amounts of phosphatidylglycerol (PG) than mammalian membranes.[272,273] POPG is a negatively charged lipid and changes the charge of the bilayer. POPE is known to increase the curvature of a bilayer when compared to a POPC and is less likely to form bilayers in a calcium-free buffer.[168] Models for bacterial membranes were used in this study: mixtures of POPC/ POPG in a 1:1 ratio and POPE/POPG in 1:1 and 3:1 ratios.

Detergent Resistant Membranes (DRM) have poor solubility in non-ionic surfactants such as Triton, and have high concentrations of cholesterol causing the lipid ordered phase $L_o$ to form, an intermediate phase between the gel and fluid phases.[274,275] DRM bilayers were also prepared to study the effect of TC on lipid mixtures in the liquid ordered phase.

Cholesterol and sphingolipids can be used to alter the fluidity of the bilayer. For example, more complex lipid mixtures have to be used to model the stratum corneum, the skin surface, which contains cholesterol, fatty acids and ceramides instead of phospholipids.[276,277] Models have been developed for the outer skin surface: Downing[278] used 40% epidermal ceramide, 25% cholesterol, 25% palmitic acid and 10% cholesteryl sulphate. These models were not used in my study as they varied significantly from the other phospholipids used in this thesis and can have more complex phase behaviour.[279]

The structures of the lipids used in this thesis are shown in Table 4.1 and a summary of the properties of the lipids used is in Table 4.2.

Table 4.1 Structures of lipids

| Lipid | Structure of major component |
|---|---|
| POPC | 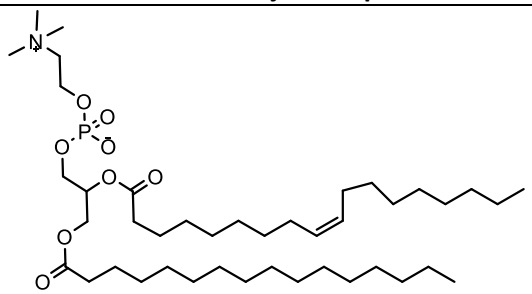 |
| POPG | 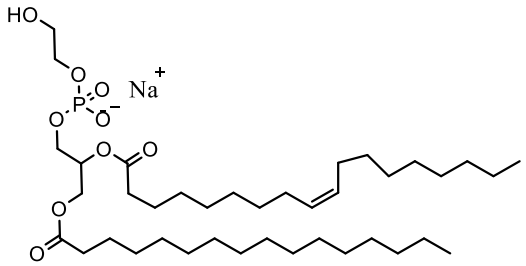 |
| POPE | 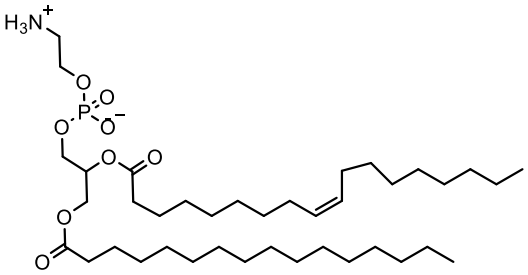 |
| Sphingomyelin | 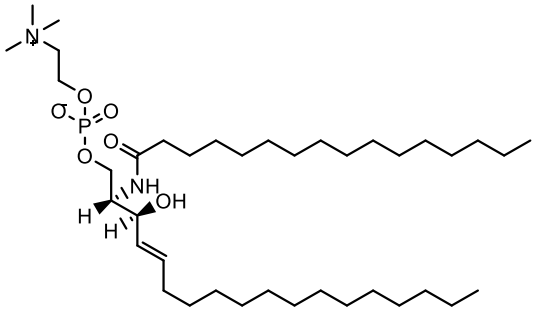 |
| Cholesterol | 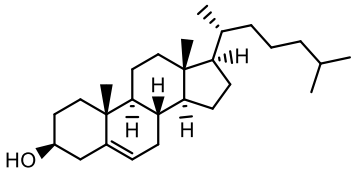 |
| DMPC | 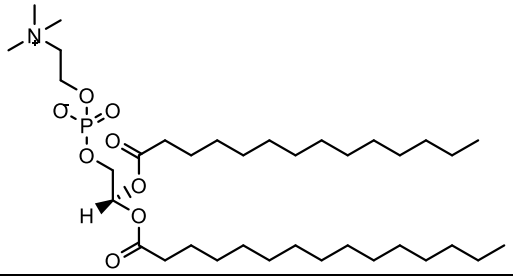 |

Table 4.2 Selected properties of lipids studied in this thesis.[280]

| Lipid abbreviation | Full name | $T_m$/ °C | Charge | $M_w$/ g $mol^{-1}$ |
|---|---|---|---|---|
| POPC | 1-palmitoyl-2-oleoyl-*sn*-glycero-3-phosphocholine | -2 | Zwitterionic | 760.09 |
| POPG | 1-hexadecanoyl-2-(9Z-octadecenoyl)-*sn*-glycero-3-phospho-(1'-*rac*-glycerol) | -2 | −1 | 770.989 |
| POPE | 1-hexadecanoyl-2-(9Z-octadecenoyl)-*sn*-glycero-3-phosphoethanolamine | 25 | Zwitterionic | 717.996 |
| Sphingomylein (SM) | Hexadecanoyl Sphingomyelin (egg) | ≈40 | Zwitterionic | 656.505 |
| Cholesterol (Chol) | Cholesterol | - | Uncharged | 400.637 |
| DMPC | 1,2-dimyristoyl-*sn*-glycero-3-phosphocholine | 24 | Zwitterionic | 677.933 |

## 4.2 Materials and Methods

### 4.2.1 Materials

TC (Igrasan ≥ 97%), sodium acetate, Tris base, Tris.HCl, HEPES, calcium chloride, hydrochloric acid and sodium carbonate (≥ 99.5%) were purchased from Sigma Aldrich (St Loius, MO, USA) and used as received. Sodium chloride and sodium hydroxide were purchased from Fisher Scientific (Loughborough, UK). Deuterium oxide (≥ 99.9%) was purchased from Cambridge Isotopes (Andover, MA, USA) and sodium hydrogen carbonate was purchased from BDH Laboratory supplies (Poole, UK). Lipids were purchased from Avanti polar lipids (Alabaster, AL, USA).

### 4.2.2 Methods

#### *4.2.2.1 TIR-Raman Spectroscopy*

All glassware and equipment used in this experiment was sonicated in dilute Decon solution for 15 minutes and then rinsed 20 times in MilliQ water before use. All items were left soaking in MilliQ water up until use. The silica hemispheres were left in chromic acid (chromium trioxide in sulphuric acid) for 45 minutes and rinsed with MilliQ water before use. The Raman cell was assembled and left filled with water. A background spectrum was collected with buffer in the cell.

To prepare the bilayer, lipid was first dissolved in chloroform. The chloroform was removed by rotary evaporation to leave a thin lipid film and then left to dry for 2 hours under vacuum at room temperature. The lipid film was hydrated to 0.3 mg/ mL and sonicated for 1.5 hrs in a sonicator bath at between 20 and 30°C (or at least 10°C above $T_m$). The buffer used was 20 mM Tris.HCl at pH 7.4 with 2 mM $CaCl_2$ unless otherwise stated. The pH of the buffer was adjusted with HCl and NaOH and measured using a Hanna Instruments (HI931410) pH meter in pH mode using a Cole-Parmer calomel electrode (5990-35). Calibrations were carried out on the same day as experiments with Hanna Instruments pH calibration solutions pH 4.010, pH 7.010 and pH 10.010.

The lipid solution was inserted into the cell (Figure 4.6) and left for 45 minutes at room temperature, or at 30°C for lipid compositions containing DMPC or POPE. The temperature of the laser lab is controlled by air conditioning to 21 ±1°C. 50 mL of buffer was passed through the cell and a spectrum taken of the lipid signal from the bilayer supported on the hemisphere. The cell used has a

wall-jet geometry so that delivery of the solute is diffusion controlled. The glass injection capillary is a few millimetres below the centre of the hemisphere so that there is stagnation point flow and the local velocity of the fluid at the bottom of the hemisphere is zero.[187] The total volume of the cell is 6 mL.

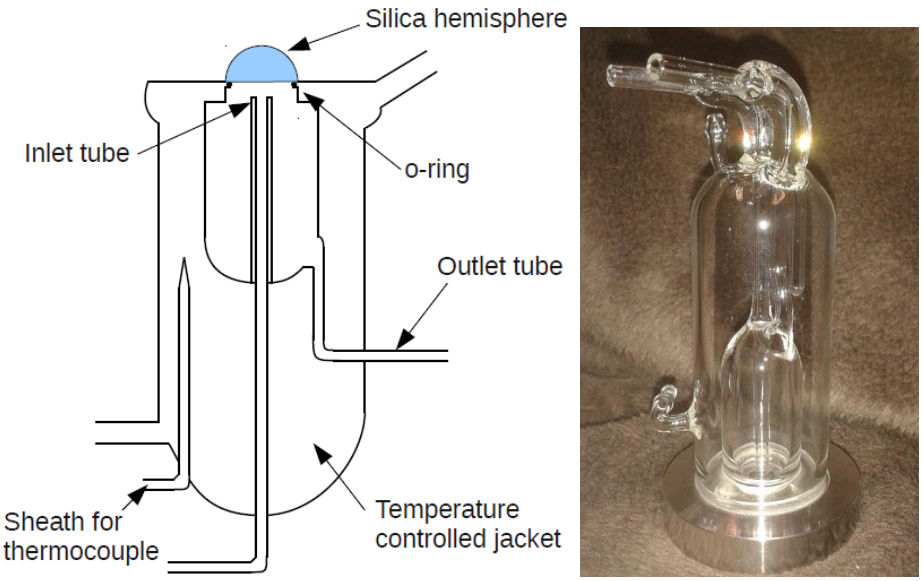


**Figure 4.6 Raman cell used for experiments. In the photo, the cell is upside down.[178]**

After the bilayer was formed, TC was inserted into the cell in 20 mM carbonate buffer at pH 10.8 and left for at least ten minutes. A spectrum was taken and then the cell was washed with pH 7.4 buffer before taking further measurements. Often, the cell was washed with 20 mL of buffer and a measurement taken before being washed with 100 mL of buffer and left for up to an hour before a final measurement.

Experiments were run at 300 mW laser power using a 532 nm laser and taking 6 acquisitions of 20 s (at 2900 $cm^{-1}$) or 5 acquisitions of 60 s (at 1600 $cm^{-1}$). If experiments were run at 1000 mW laser power, they were 5 acquisitions of 10 s (at 2900 $cm^{-1}$) or 5 acquisitions of 60 s (at 1600 $cm^{-1}$). The angle of incidence was 73°. All data was collected with S polarised light going to the sample and the light coming away from the sample unpolarised unless otherwise stated; the notation $S_x$ means the light going to the sample from the laser was S polarised and the light collected was x polarised. The data shown in this document has the background buffer signal at the same polarisation subtracted using MatLab (for code see Section 8.3.1), unless otherwise stated.

In experiments where the temperature of the cell was monitored, the temperature was changed using a regulated water bath. The temperature of the cell was measured and recorded. Otherwise experiments were carried out at room temperature of around 21 ±1°C, without the temperature controlled jacket being used.

The Renishaw Raman spectrometer used for experiments was originally designed for confocal Raman experiments. It has been modified so that the laser light is delivered to the spectrometer separately. The laser emits light at 532 nm (Opus 532, Laser Quantum, Manchester UK) which is delivered to the sample through an optical set-up (Figure 4.7). Firstly, the beam passes through a polarising beam splitter and then a half wave plate, allowing either S or P polarised light to reach the

sample. The beam then passes through a telescope that expands and collimates the beam using a −25 and a +125 mm lens. The beam is then reflected from a 90° mirror to a periscope and to the final mirror. The beam is focussed to an ellipse on the hemisphere using a gradient index lens (f=120 mm).

The scattered light is collected and sent to the spectrometer through an ultra-long distance 50 x microscope objective with a numerical aperture of 0.55 and a Leica DM-SM microscope (Figure 4.8). The collection apparatus is from the original Raman microscope. An edge filter removes the 532 nm Rayleigh line. The collected light passes through an optional half-wave plate and polariser, allowing control over the polarisation of the collected light. The light is focussed through a 200 µm slit, collimated, reflected through a prism onto a 1200-lines per mm diffraction grating and focussed into the CCD with a lens. The grating is kept fixed in position during collection and the spectra window width is 663 $cm^{-1}$ when centred at 2900 $cm^{-1}$ and 791 $cm^{-1}$ when centred at 1600 $cm^{-1}$. Good quality spectra can be taken at 1000 mW laser power in 50 s.

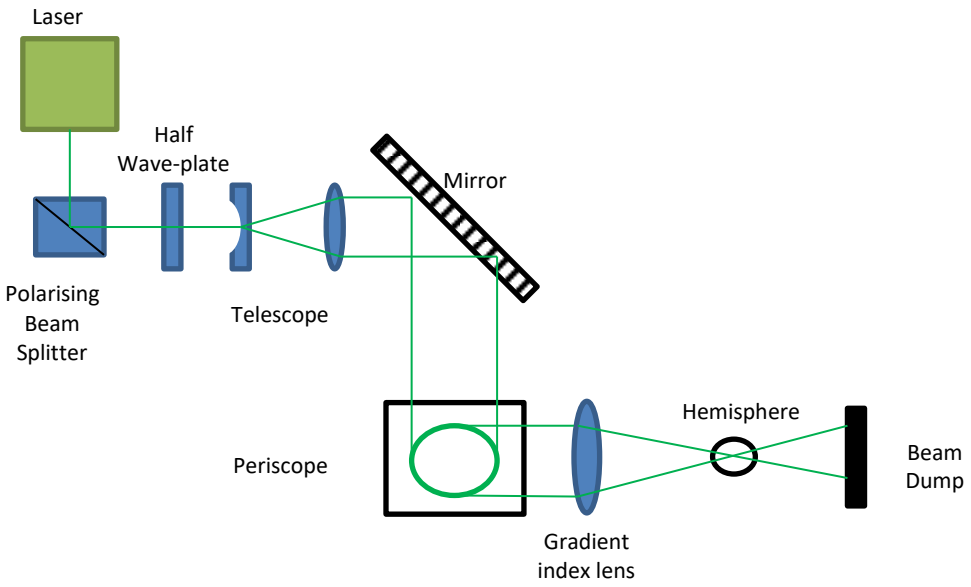


**Figure 4.7 The delivery optics of the Renishaw TIR-Raman Spectrometer.**

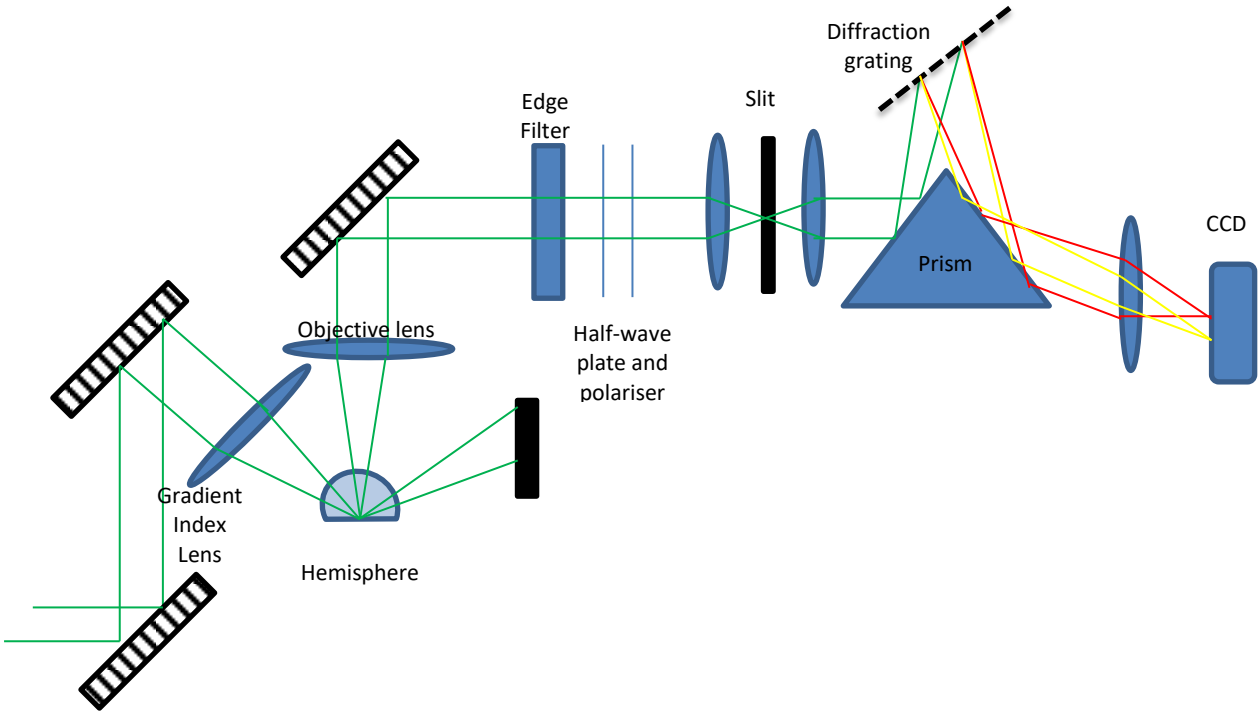


Figure 4.8 The collection optics of the Renishaw TIR-Raman Spectrometer

### 4.2.2.2 *Raman Imaging*

A Raman imaging system with global imaging total internal reflection illumination was used under the direction of M. Possiwan. The cell used is the same as normal TIR-Raman experiments. A schematic of the collection optics are shown below (Figure 4.9). The thin-film tuneable bandpass filter (Semrock, centre wavelength 628 nm, 14 nm bandwidth) is on a motorized stage so that the angle can be computer controlled. The input optics differed from the spectroscopy set-up so that the beam passes through the polarizer and is delivered by the mirrors and through the lens (f= 120 mm) to give a spot size of 80×40 µm. The telescope apparatus is not used.[281]

The spectral images can be used to construct maps of component distribution using an in-house MatLab fitting function which was not used in the experiments described in this thesis.

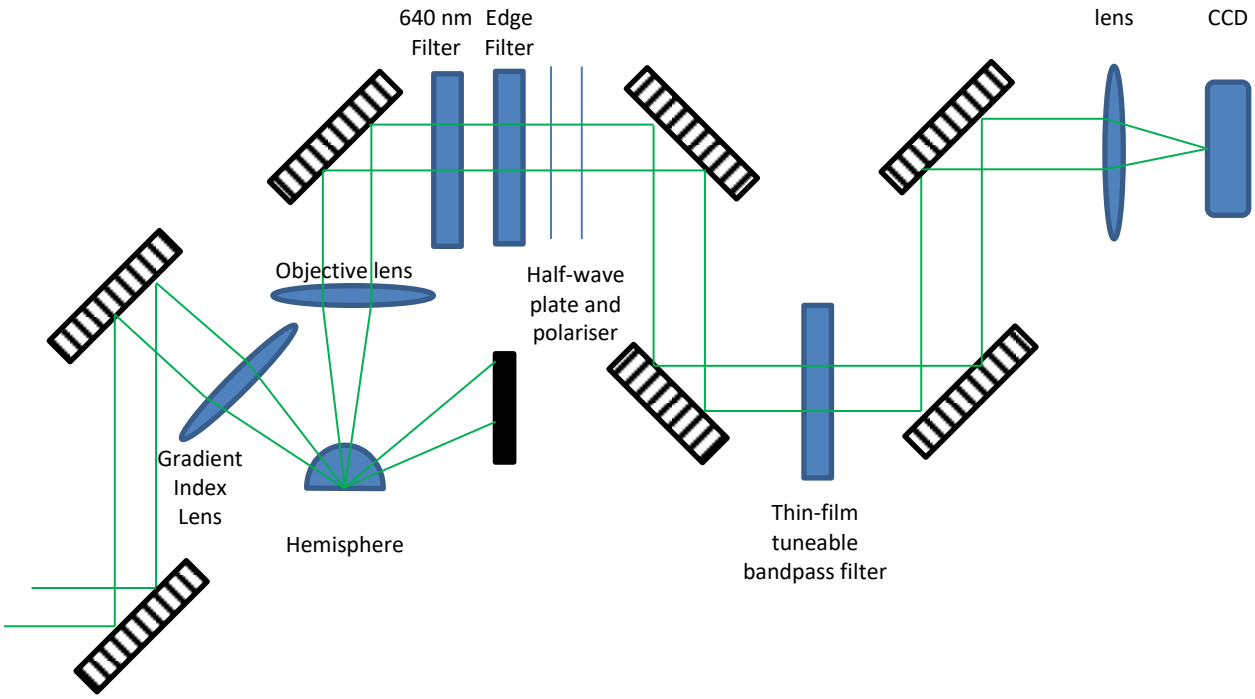


**Figure 4.9 The set-up for Total Internal Reflection Raman Imaging.**[281]

### *4.2.2.3 Refractive Index*

The refractive index of 10% SDS, 1% TC in water was measured using an automatic refractometer (RFM970 Bellingham and Stanley) with water and butanol as calibrations at 20°C. The refractive index used for water was 1.33299 at 589 nm and the refractive index used for butanol was 1.39939 at 632.8 nm.[282]

### *4.2.2.4 Fluorescence Microscopy*

Fluorescence microscopy of supported lipid bilayers[283–285] was carried out under the direction of Margarita Staykova and Liam Stubbington. Lipid vesicles were prepared by dissolving 1 mg of lipid in chloroform and removing the chloroform with a stream of argon to leave a thin film. The lipid of choice was mixed with the fluorescent probe 1 mol % rhodamine 1,2-dihexadecanoyl-sn-glycero-3-phosphoethanolamine (Rh-DPPE) at 1 mol %. The lipid film was kept under vacuum for 2 hours to remove any remaining chloroform. The lipid was mixed with buffer to give a concentration of 0.5 mg/ mL lipid. The lipid solution was placed into ice and sonicated using a sonicator horn at 30% amplitude for 5 minutes. The sample was centrifuged for 40 minutes at 4 400 rpm to remove the large titanium particles produced by the sonicator tip. The solution was then diluted to 0.05 mg/ mL lipid.

A cell was prepared using PDMS and a glass cover slip or glass slide (Figure 4.10). The PDMS and glass were plasma cleaned before assembly at 15 mbar for 15 s. The PDMS and glass were connected by heating at 70°C for 3 minutes. The 0.05 mg/ mL lipid solution was passed through the cell and left to incubate for an hour. The cell was then rinsed through with buffer to remove excess lipid.

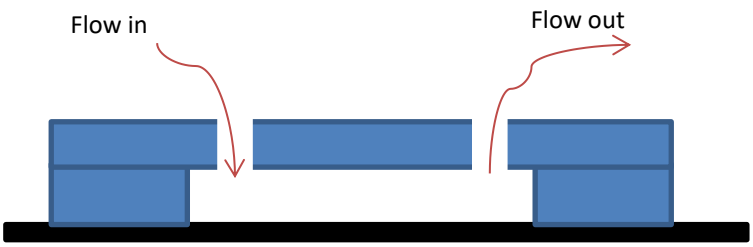


**Figure 4.10 Structure of PDMS cell for fluorescence microscopy. The black shows a glass cover slip and the blue shows PDMS**

Experiments were typically run by imaging the bilayer and taking a video as a TC containing solution was rinsed through the cell. Then a video was taken with buffer rinsing through the cell. Typical measurement conditions were to take an image per second. Imaging was carried out on a Nikon Eclipse Ti-E inverted microscope. Images were analysed in ImageJ (National Institutes of Health) with the Bio-Formats plugin (Open Microscopy Environment) to calculate average pixel intensity across the image.

#### *4.2.2.5 Nanosight Analysis*

Nanosight tracks the Brownian motion of individual particles based on the scattering of the particles in a laser beam. With a 20 x objective connected to a CCD camera, the scattering from the particles can be seen and tracked.[222] The distance travelled by each particle allows the hydrodynamic radius to be calculated based on the Stokes-Einstein equation:

$$\frac{\overline{(x,y)}^2}{4} = Dt = \frac{Tk_B}{3\pi\eta d}$$ **Equation 4.1**

This gives high resolution particle distribution. Sample concentrations should be $10^7$-$10^9$ particles per mL.[223] Vesicles solutions were prepared using appropriate ratios of liposome, buffer and TC.

## 4.3 Results and Discussion

### 4.3.1 Solid TC

The Raman peaks of TC used in this study are the aromatic C-H stretching peak at 3075 $cm^{-1}$ and the C-C stretching mode of the phenyl rings which in the solid state spectra is a doublet at 1600 $cm^{-1}$. The peaks in the solid state Raman spectra (Figure 4.11 and Table 4.3) have been assigned based on the IR assignments by Özişik.[286] The peaks in the region 1000 to 1300 $cm^{-1}$ correspond to in-plane bending of the aromatic ring C-H bonds and the peaks in the region 750 to 900 $cm^{-1}$ correspond to out-of-plane bending of the aromatic ring C-H bonds.[287] Özişik assigns most peaks in these two regions as combination bands.

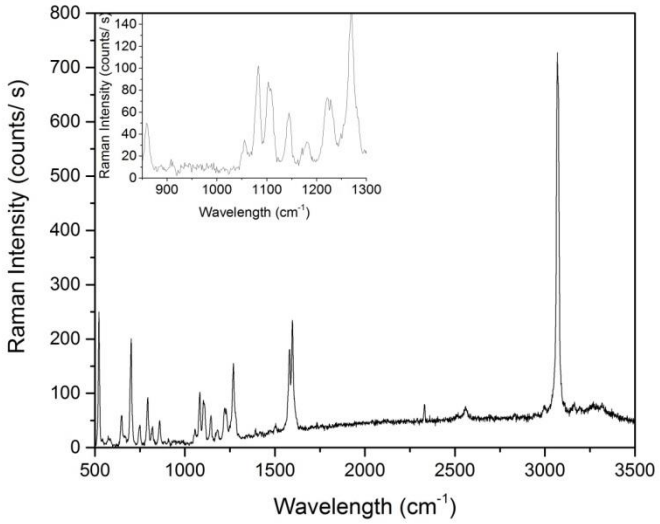


**Figure 4.11 Raman spectra of TC powder collected with 30 mW laser power. The insert shows the fine detail of the spectrum between 800 and 1300 $cm^{-1}$. Data was collected under the direction of C. Mercier.**

**Table 4.3 Peaks in the Raman spectra of Solid TC with their relative intensities and assignments.**

| Peak location | Relative intensity | Assignment |
|---|---|---|
| 3390 | 0.10 | ν(O-H) |
| 3068 | 1 | ν(C-H) |
| 1597 | 0.33 | ν(C-C) |
| 1269 | 0.22 | δ(CH) + ν(C-O) + ν(C-C) |
| 1221 | 0.11 | ν(C-O) + ν(C-C) + δ(CH) |
| 1181 | 0.05 | δ(OH) + ν(C-O) |
| 1144 | 0.09 | δ(CCH) + ν(C-C) |
| 1102 | 0.13 | δ(CCH) + ν(C-C) |
| 1083 | 0.15 | ν(C-C) + ν(C-Cl) + δ(CCH) |
| 1055 | 0.06 | ν((C-C) + δ(CCH) + ν(C(𝕝)-Cl) |

### 4.3.2 TC in POPC bilayers

I have collected data to show TC insertion into supported single lipid bilayers on silica. The supported lipid bilayer is used as a model for the cell membrane. I have investigated the effect of TC on the membrane and what happens to the membrane after treatment with TC when the Raman cell was rinsed through with buffer.

Spectra have been collected in two regions: around 2900 $cm^{-1}$ and around 1600 $cm^{-1}$. Spectra collected at 2900 $cm^{-1}$ show strong lipid peaks at 2800-3050 $cm^{-1}$ (for example Figure 4.12). All data shown has had the water background removed using a background subtract function in MatLab (R2014a, The MathWorks, Inc. Natick, Ma) (see Section 8.3.1 for the code). In the background subtract function; the baselines of the background and the spectrum of interest are subtracted, using the lowest point in the data set. The spectrum of interest is scaled to the intensity of water band in the background using a correction factor. The altered background is subtracted from the re-scaled data. Unless otherwise stated, data was collected using S polarised light and unpolarised detection. The data collected with the centre at 2900 $cm^{-1}$ ranged from 2573-3264 $cm^{-1}$ with an

average bin size of 1.15 $cm^{-1}$ and the data collected with the centre at 1600 $cm^{-1}$ ranged from 1200-2000 $cm^{-1}$ with an average bin size of 1.38 $cm^{-1}$.

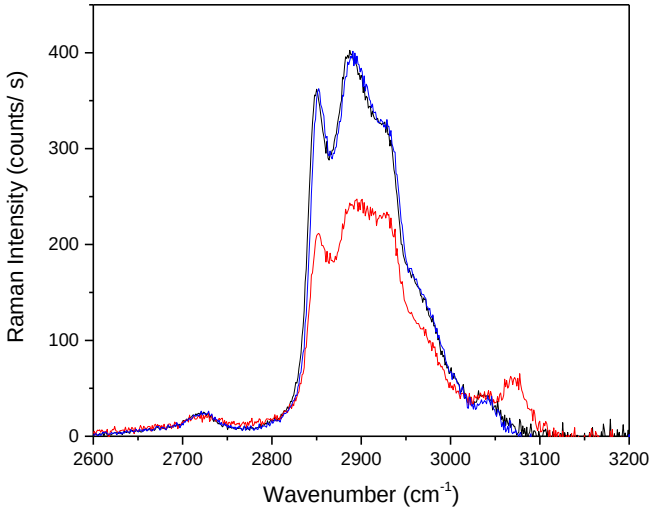


**Figure 4.12 TIR-Raman spectra of POPC bilayer in pH 7.4 buffer with 2 mM $CaCl_2$ (black), POPC bilayer with 0.1 mg/ mL TC in pH 10.8 buffer (red) and POPC bilayer rinsed with Tris buffer after treatment with TC (blue). The background was subtracted from the data. Laser power was 1000 mW.**

A TC peak can be seen at 3075 $cm^{-1}$ when at high concentrations within the bilayer, although at lower concentrations, it is harder to see it separated from the baseline and noise. The band between 1550 and 1700 $cm^{-1}$ from the hemisphere and the water background makes it more difficult to subtract the background from spectra collected at 1600 $cm^{-1}$ (Figure 4.13) because the intensity of the band does not always scale linearly with the water band at 1200 $cm^{-1}$, occasionally leading to negative intensities after background subtraction (Figure 4.14). However, the TC peak at 1600 $cm^{-1}$ tends to be clearer than the peak at 3075 $cm^{-1}$. The TC peak at 1600$cm^{-1}$ has similar intensity to the lipid C=C stretch at 1650 $cm^{-1}$ and there is little overlap between the two peaks so the TC peak is easy to distinguish. In some of the data collected at 1600 $cm^{-1}$, there was strong fluorescence which was removed using a homemade function written as fluorescent remove (Section 8.3.3), an example of the effect is shown in Figure 4.14. The function fits a straight line to data between 1800 $cm^{-1}$ and 2000 $cm^{-1}$ and uses that as the background from fluorescence across the spectrum. The fluorescence background is subtracted from the data. The TC peak at 1600 $cm^{-1}$ is observed as a single peak in solution and in the bilayer, not as the doublet, which is observed in solid TC.

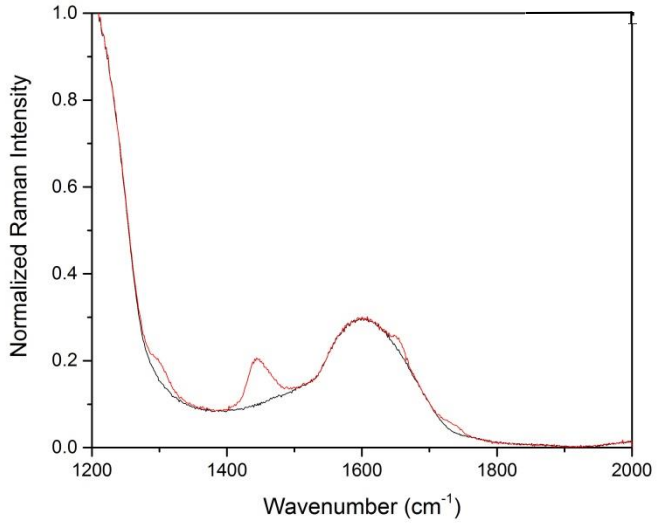


**Figure 4.13 Normalized Raman intensity of pH 7.4 Tris buffer with 2 mM $CaCl_2$ and the hemisphere (black) and POPC bilayer in pH 7.4 Tris buffer with 2 mM $CaCl_2$ before background subtraction has been applied (red)**

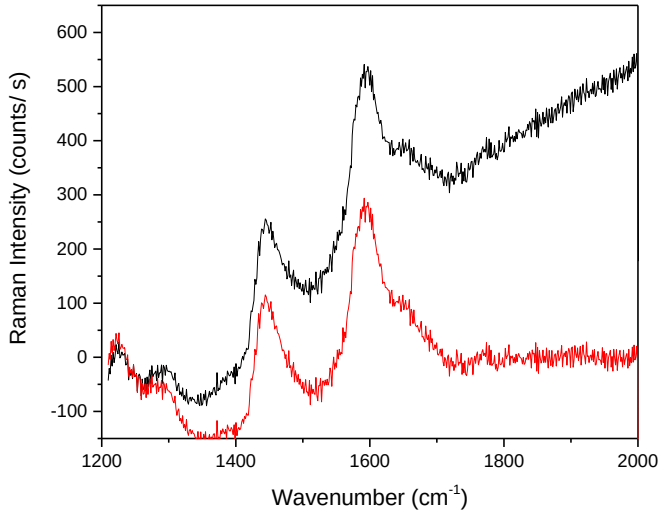


**Figure 4.14 Spectra collected at 1600 $cm^{-1}$ with the water background subtracted containing fluorescence (black) and with the fluorescence removal function used (red).**

Initial experiments were on 1-palmitoyl-2-oleoyl-sn-glycero-3-phosphocholine (POPC) bilayers supported on a silica hemisphere in 20 mM Tris buffer at pH 7.4 with 20 mM $CaCl_2$. Experiments were carried out at around 21°C, where a POPC bilayer is in the fluid disordered state ($L_\alpha$) and insensitive to small temperature fluctuations. The peak ratio, $I(d_-)/I(d_+)$, remains constant with temperature somewhere between 1.12-1.15. An initial experiment was carried out where Raman data was collected between 2600-3200 $cm^{-1}$ using S light. When 20 mL of 0.1 mg/ mL TC solution at pH 10.8 in 20 mM carbonate buffer was added, the lipid signal decreased and a clear signal was seen of TC around 3075 $cm^{-1}$ (Figure 4.12). The bilayer was rinsed with around 150 mL of pH 7.4 Tris. HCl buffer, and the lipid signal was restored and the TC signal disappeared.

The pH of biological systems is around pH 7.4 so I kept the bilayer at that pH as much as possible. However, the solubility of TC at pH 7.4 is 4 ng/mL, which is well below the MIC. To deliver a biologically effective concentration of TC, the pH was increased to pH 10.8. At pH 10.8 the phenolate form of TC is the dominant form; the phenolate form has a higher solubility of around 0.7 mg/ mL (See section 2.3.3). Another method to deliver TC would be to include it in micelles; however concentrations of surfactant sufficient to form micelles solubilize the bilayer. The experimental design also mimics the pH change that occurs when TC is applied to the body in an SL soap system, when the pH of 1% SL is 10.55 (Figure 2.30) and then rinsed with tap water, which is at a much lower pH.

Experiments showed that care should be taken over the amount to TC added to the membrane: too little and no signal is observed from the TC and there is no change in the lipid signal, too much and the bilayer is destroyed. In a number of experiments where a higher concentration of TC was added, the bilayer was removed (for example Figure 4.15). Even when the cell was washed through with buffer, the lipid signal did not return to the original intensity. However, if too little TC was used, no signal was observed at 3075 $cm^{-1}$, there was very little signal at 1600 $cm^{-1}$ and there was very little change in the lipid peak. The reduction of lipid signal after TC treatment is caused by the presence of TC in the bilayer rather than the change in buffer. When the bilayer was treated with a TC–free carbonate buffer, the lipid peak signal did not change (Figure 4.16).

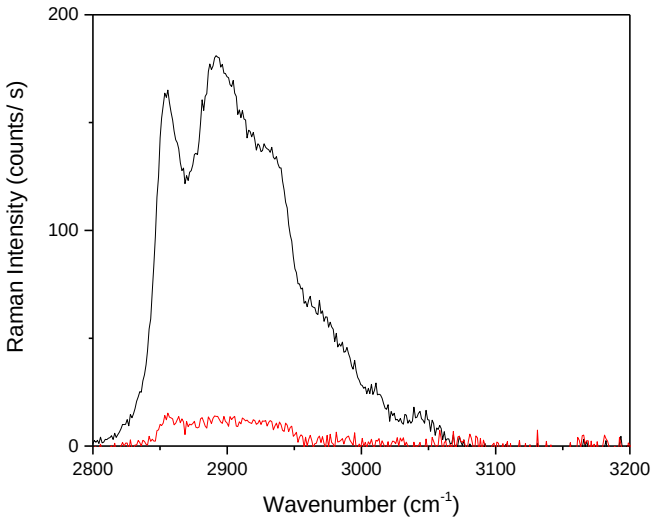


**Figure 4.15 TIR-Raman spectra of POPC bilayer in pH 7.4 buffer with 2 mM $CaCl_2$ (black), POPC bilayer with 0.5 mg/ mL TC in pH 10.8 buffer (red). The background was subtracted from the data. Laser power was 1000 mW.**

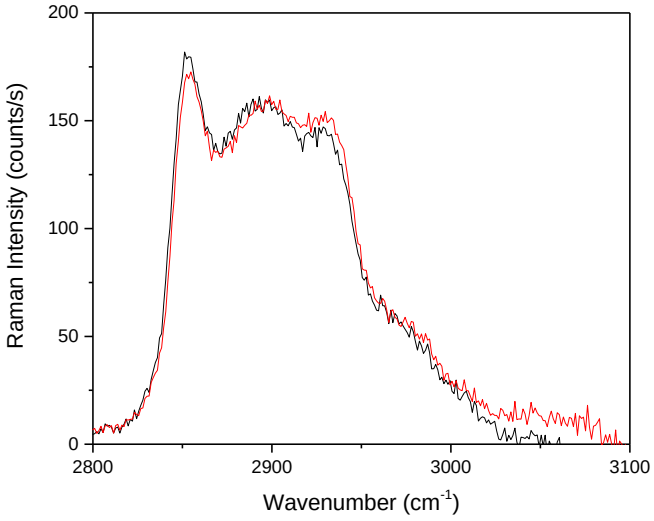


**Figure 4.16 TIR-Raman spectra using $S_y$ light of POPC bilayer in pH 7.4 tris buffer with 2 mM $CaCl_2$ (black) and POPC bilayer in pH 10.8 carbonate buffer (red). Laser power was 1000 mW.**

In some experiments, no TC peak was seen at 3075 $cm^{-1}$ when there was TC in bulk at pH 10.8, but when the cell was rinsed with 20 mL of neutral buffer, the TC peak increased as did the lipid peak (Figure 4.17). When the cell was rinsed with more buffer, the bilayer signal was restored to its original value and the TC peak decreased. It is likely that there was some TC in the bilayer at pH 10.8, which affected the bilayer and caused the bilayer signal to decrease but not enough TC for a peak to be detected at 3075 $cm^{-1}$. When the pH in the cell decreases, the phenol form of TC dominates rather than the phenolate form. The phenol partitions much more strongly into the bilayer than the phenolate, see Chapter 3 for partitioning into surfactant, leading to a higher concentration of TC in the bilayer.

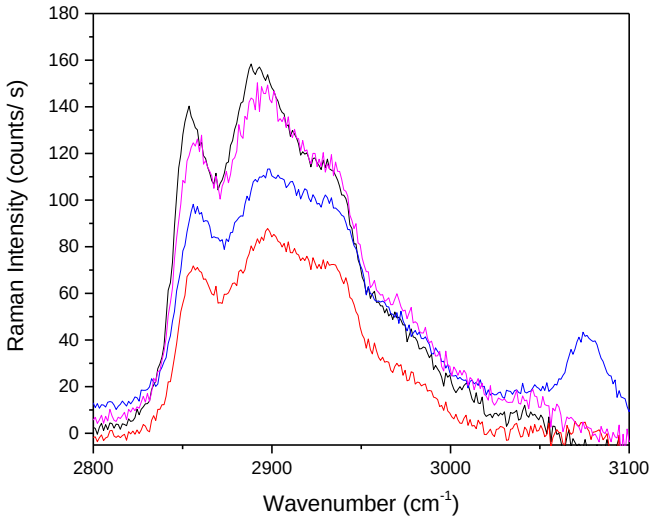


**Figure 4.17 TIR-Raman of POPC bilayer in pH 7.4 buffer with 2 mM $CaCl_2$ (Black), POPC bilayer and 0.1 mg/ mL TC in pH 10.8 buffer (red) and bilayer rinsed with 20 mL of pH 7.4 buffer with 2 mM $CaCl_2$ made with $D_2O$ after TC treatment (blue) and rinsed with 50 mL of pH 7.4 buffer with 2 mM $CaCl_2$ (pink). Laser power was 1000 mW.**

The lipid peak intensity tends to increase when the buffer changes from pH 10.8 to pH 7.4. The phenolate from of TC is negatively charged and may cause the bilayer to come away from the surface, as the silica surface is also negatively charged. As the pH decreases, the charge of the bilayer will decrease and the bilayer will be less repelled from the surface. The pH 7.4 buffer contained 2mM $Ca^{2+}$ and that may have contributed to the increase in the lipid signal as $Ca^{2+}$ is known to promote bilayer formation,[288] whereas the pH 10.8 buffer does not contain any $Ca^{2+}$. However, there is no lipid in the solution after the cell is rinsed to form fresh bilayer. In samples where just pH 10.8 buffer has been added, but no TC, the lipid signal has stayed the same so it is likely that the reduction in the bilayer signal is caused by TC rather than the pH.

Raman measurements were also taken at a range of polarisations and wavelengths to investigate which polarisations gave the clearest signal for TC. In Figure 4.18 the TC signal at 3075 $cm^{-1}$ can be seen most clearly in $S_y$ light (B) and least clearly in $S_x$ light (A). In all polarisations, the lipid signal decreased when TC was in the cell and increased when the bilayer was rinsed with large volumes of buffer. If TC were to cause a change in tilt, usually, a decrease would be expected in one polarisation and an increase in signal at the other polarisation.[179,289] For example, in the gel-to-fluid phase transition, as the temperature decreases, the intensity of the S polarised spectrum increases but the P polarised spectrum decreases in intensity.[265] The results in Figure 4.18 suggest that some of the lipid is lost from the evanescent wave when TC is inserted into the cell and returns as the bilayer is rinsed. The temporary loss may be due to protrusions that form from the bilayer upon the insertion of TC and are drawn back into the bilayer upon rinsing. If the bilayer lifts from the surface as a whole, it would still be in the evanescent wave, but the electric field would be weaker. In an ionic strength of 0.02 M, the Debye length is approximately 2 nm so the electrostatic interaction between the bilayer and the surface would decay to zero within 10 nm, which is not enough to account for the drop in signal observed.

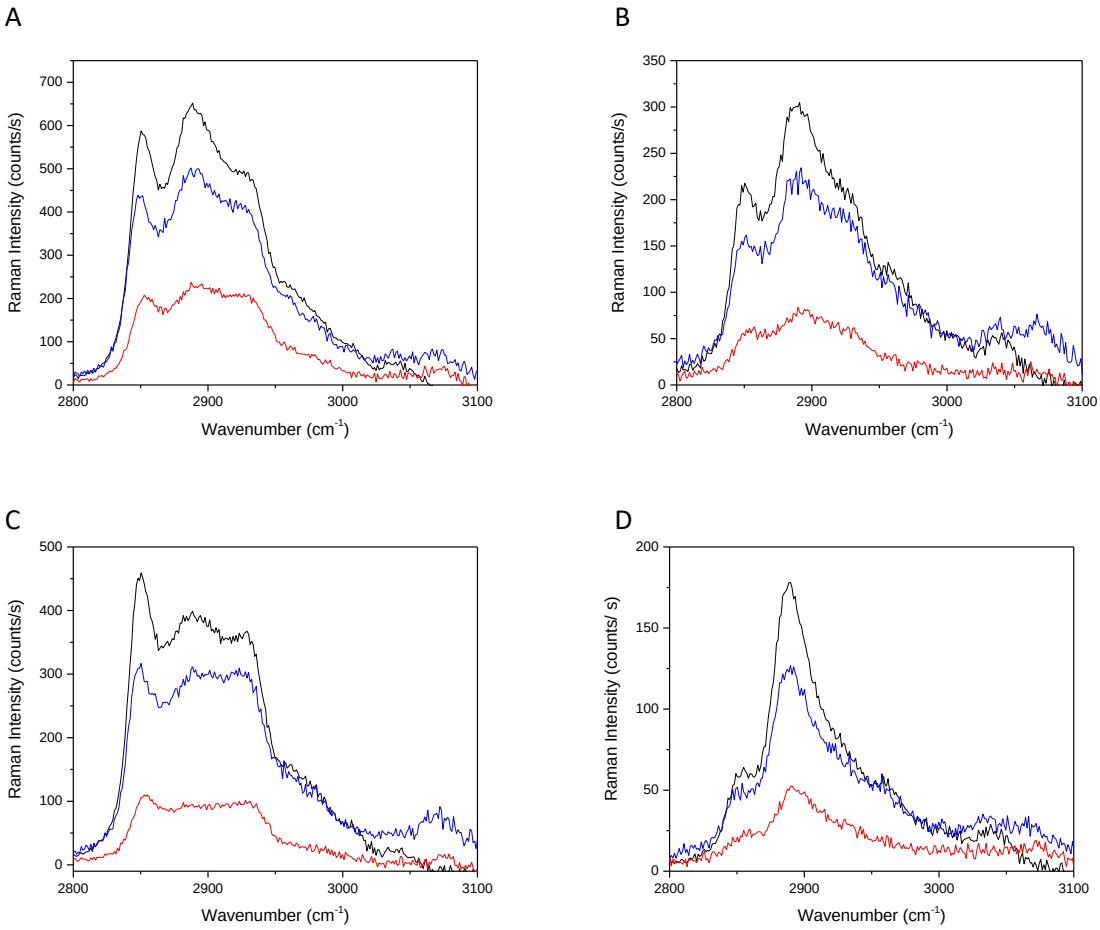


**Figure 4.18 TIR-Raman of POPC bilayer in pH 7.4 buffer with 2 mM $CaCl_2$ (Black), POPC bilayer and TC in pH 10.8 buffer (red) and bilayer rinsed with 50 mL of pH 7.4 buffer with 2 mM $CaCl_2$ after TC treatment (blue) using different light polarisations S light (A), P light (B), $S_y$ light (C) and $S_x$ light (D). Laser power was 1000 mW.**

In data collected at 1600 $cm^{-1}$, a similar effect was seen. The TC peak at 1600 $cm^{-1}$ increased after TC treatment of the bulk when the cell was rinsed with 50 mL of pH 7.4 buffer. The lipid peak at 1450 $cm^{-1}$ decreased significantly when TC was inserted into the cell at pH 10.8 and increased when the cell was rinsed with pH 7.4 buffer. The change in the intensity of lipid peak at 1450 $cm^{-1}$ was larger than the peak at 2900 $cm^{-1}$: when TC was in the cell the peak at 1450 $cm^{-1}$ was 14% of the original peak whereas at 2900 $cm^{-1}$, the peak decreased to 35% of the original in S polarised light. When the cell was rinsed, both lipid peaks increased in intensity, at 1450 $cm^{-1}$ the peak was 38% of the original and at 2900 $cm^{-1}$ it was 75% of the original. The peak at 1450 $cm^{-1}$ is the Fermi doublet of the $CH_2$ scissoring mode whereas the peak at 2900 $cm^{-1}$ contains contributions from several modes including the symmetric and antisymmetric stretches, and the overtone of the scissoring mode. The peaks in the 2900 $cm^{-1}$ region have been used to describe the effect of TC on the lipid bilayer, especially the peaks at 2850 and 2880 $cm^{-1}$, rather than the peak at 1450 $cm^{-1}$ because they include contributions from several modes and are more intense peaks. The change in the $I(d_-)/I(d_+)$ ratio has also been used to infer the ordering of the lipid in the bilayer.

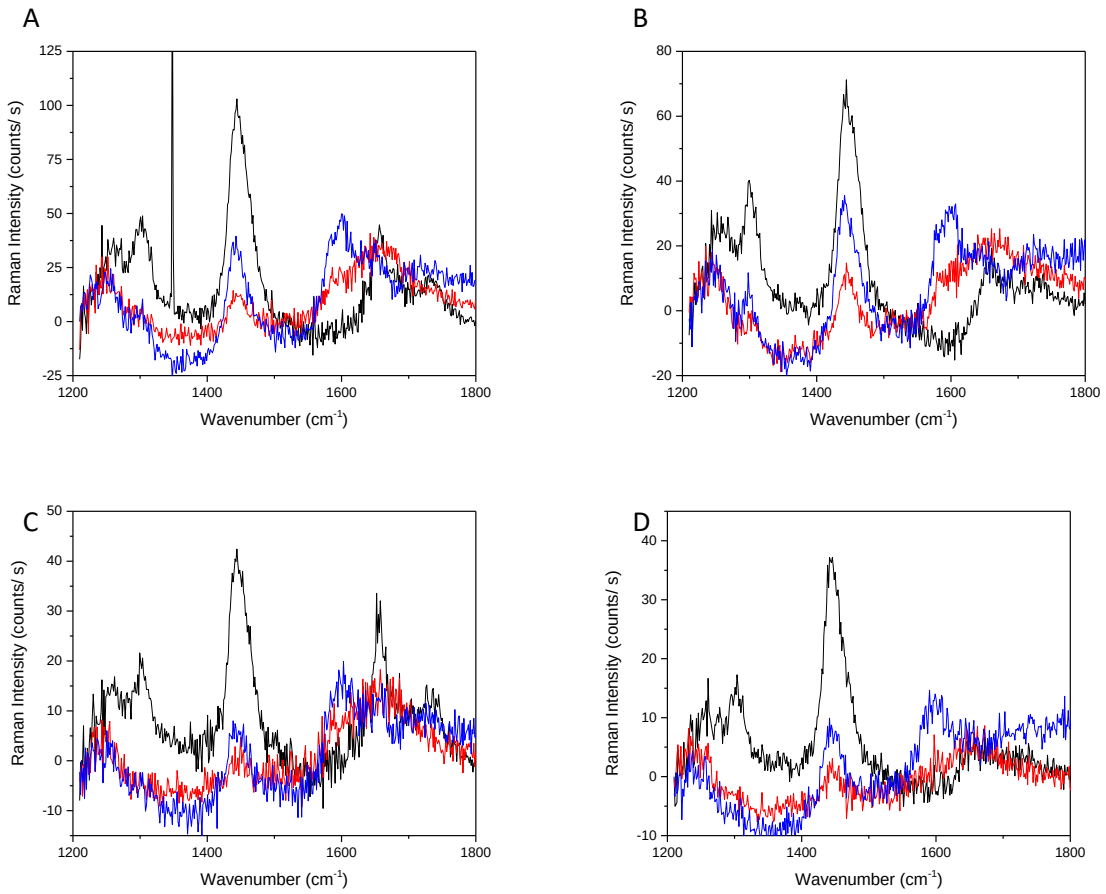


**Figure 4.19 TIR-Raman of POPC bilayer in pH 7.4 buffer with 2 mM $CaCl_2$ (Black), POPC bilayer and TC in pH 10.8 buffer (red) and bilayer rinsed with 50 mL of pH 7.4 buffer with 2 mM $CaCl_2$ after TC treatment (blue) using different light polarisations S light (A), P light (B), $S_y$ light (C) and $S_x$ light (D). Laser power was 1000 mW.**

The peaks at 1600 and 3075 $cm^{-1}$ are not sensitive to the difference between the phenol and phenolate forms and therefore TIR-Raman is not a suitable technique for calculating the partition coefficient of the phenol and phenolate forms between micelles and bulk solution.

### *4.3.2.1 Calculating the Concentration of TC within the Bilayer*

The concentration of TC within the bilayer can be calculated from the intensity of the TC peak if the intensity can be compared to spectra where the concentration of TC is known. To calculate the concentration of TC within the membrane, spectra were taken with a known concentration of TC without a bilayer and the intensity compared to TC peaks in bilayers. When a saturated solution of TC at pH 10.8 was used, there were slight TC peaks at 1600 $cm^{-1}$ (Figure 4.20). At 1000 mW, the signal to noise was too low to get accurate peak intensities. A 10% SDS solution was used to increase the concentration of TC in solution and improve the peak intensity and resolution. The anionic surfactant SDS does not absorb to the negatively charged silica surface, so any signal seen is from the bulk, rather than a surface excess.

With the high concentration of SDS, the Debye length is negligible compared to the penetration depth. If there is 0.1 M 1:1 electrolyte, the Debye length is approximately 1 nm.[290] When TC was included with SDS, peaks were easily seen at 1600 $cm^{-1}$ (Figure 4.21). The electric field decays exponentially with distance *z*.

$$\frac{E}{E_0} = \exp(-\frac{1}{l}z)$$ Equation 4.2

where $E_0$ is the electric field at the interface and $l$ is the penetration depth,

$$l = \frac{\lambda_o}{2\pi n_2}\left(\left(\frac{n_1}{n_2}\right)^2 \sin^2\theta - 1\right)^{-\frac{1}{2}}$$ Equation 4.3

where $n_1$ is the refractive index of the medium with the lower refractive index, $n_2$ is the refractive index of the medium with the higher refractive index, $\lambda_o$ is the wavelength of the input light and $\theta$ is the angle of incidence. The refractive index of 10% SDS was determined experimentally as 1.35.The penetration depth in 10% SDS is 220 nm and the TIR-Raman scattering signal decays exponentially from the interface at $½l$. The average distance from the surface for Raman signal in a solution of 10% SDS is 110 nm. For solutions made with water, the penetration depth is 200 nm and Raman-scattering is collected from 100 nm from the interface.

For S light, the TC peak at 1600 $cm^{-1}$ had an intensity of 38 counts per second when the concentration of TC in bulk was 0.035 M. The intensity of the signal is proportional to the polarizability derivative, $\alpha'$, and the integral of the square of the electric field with distance and concentration with distance from the interface, $z$,

$$I_{TC,r} \propto \alpha' \int_0^\infty E^2(z) m(z) dz$$ Equation 4.4

$$I_{TC,r} \propto m_{TC}\alpha' \int_0^\infty \left[E_0 \exp^{-z/l}\right]^2 dz$$ Equation 4.5

The intensity of the TC peak is proportional to the concentration of TC in bulk and the penetration depth.

$$I_{TC,r} \propto 2m_{TC}\alpha' {E_0}^2 l$$ Equation 4.6

In the experiments detailed in this thesis, the concentrations of TC used to treat bilayers are 100 times lower than that used as the reference: for these concentrations, the expected TC peak from the bulk solution is lower than the limit of detection: I attempted to collect spectra of 0.1 mg/ mL TC without the bilayer, but saw no signal from TC. In most of the experiments shown below, the laser power was 300 mW but in the experiments to collect the reference data, the laser power was 1000 mW.

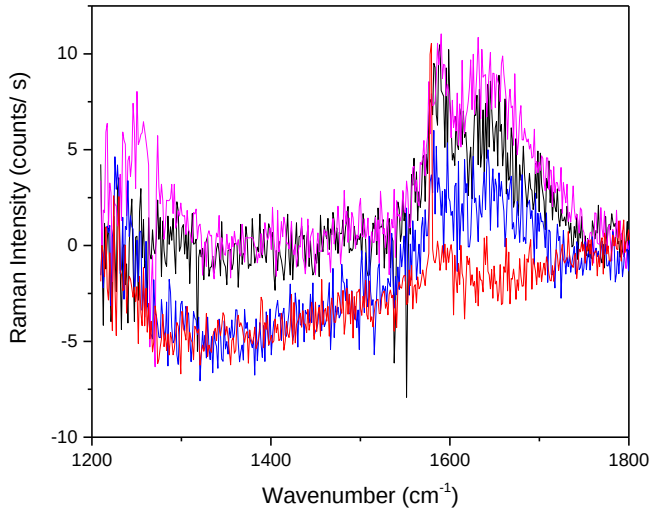


**Figure 4.20 TIR-Raman spectra collected at 1600 cm–1 using S polarised light (black), $S_y$ polarised light (blue), $S_x$ polarised light (red) and P polarised light (pink) of a saturated TC solution in pH 10.8 carbonate buffer. Laser power was 1000 mW.**

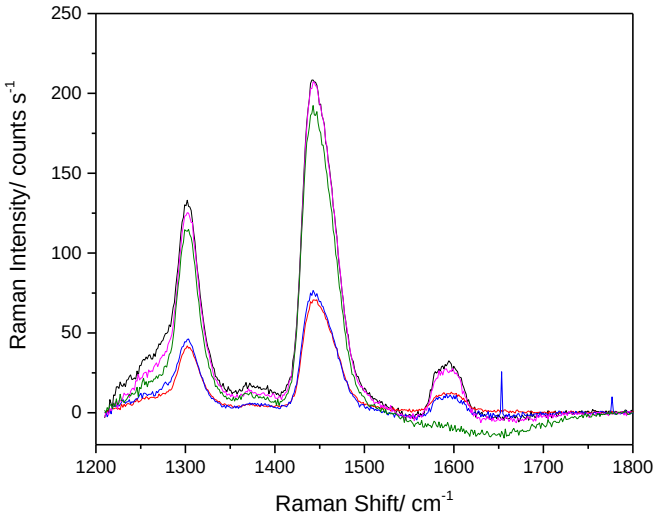


**Figure 4.21 TIR-Raman spectra collected at 1600 $cm^{-1}$ using S polarised light (black), $S_y$ polarised light (blue), $S_x$ polarised light (red) and p polarised light (pink) of 0.035 M TC solution and 0.35 M SDS in pH 7.4 Tris buffer with 2mM $CaCl_2$. S polarised light was used to collect a spectrum of 0.35 M SDS in pH 7.4 buffer with 2 mM $CaCl_2$ (green). Laser power was 1000 mW.**

The concentration of TC in the bilayer can be measured from the intensity of the TC peak at 1600 $cm^{-1}$. For example, in the data shown in Figure 4.22, the TC peak at 1600 $cm^{-1}$ had an intensity of 9.7 counts/ s when the laser power was 300 mW and the light was S polarised. For samples where there is a surface excess of TC, the intensity of the TC peak is proportional to the polarizability derivative, the square of the electric field at the interface and the surface excess of TC, $\Gamma_{TC,s}$:

$$I_{TC,s} \propto \alpha' {E_0}^2 \Gamma_{TC,s} \qquad \text{Equation 4.7}$$

The surface concentration of TC can be worked out thus:

$$\Gamma_{TC,s} = \frac{2I_{TC,s}m_{TC,r}l}{I_{TC,r}\left(\frac{P_s}{P_r}\right)}$$ Equation 4.8

where $I_{TC,s}$ is the intensity of the TC peak in the sample, $I_{TC,r}$ is the intensity of the TC peak in the reference, $P_s$ is the laser power in the sample, $P_r$ is the laser power used in the reference and $m_{TC,r}$ is the concentration of TC in the reference. The surface excess concentration of TC is calculated as 3.2 x$10^{-6}$ mol $m^{-2}$ in the experiment in Figure 4.22. The ratio of TC to molecules of lipid can be estimated by comparing the surface concentration of TC to the surface concentration of the lipid. The area per molecule of POPC is 60 $Å^2$ in a complete bilayer[291] and I assumed that there is full coverage in the initial bilayer and took into account both leaflets. The lipid peak in the C-H stretching region decreases with TC in the cell, and I assume the lipid peak decrease is due to lipid lost from the bilayer or a lifting of the bilayer from the substrate rather than a change in lipid tilt. Through comparing the intensity of the lipid peak at 2900 $cm^{-1}$ of the initial bilayer and the bilayer with TC (Figure 4.22.B), the interface concentration of lipid when TC is in the cell can be calculated:

$$\Gamma_{lipid} = \frac{2}{N_a A_{lipid}} \frac{I_{l,s}}{I_{l,b}}$$ Equation 4.9

where $A_{lipid}$ is the area per molecule of the lipid, $N_a$ is Avogadro's number, $I_{lipid,s}$ is the intensity of the lipid peak in the sample and $I_{lipid,b}$ is the intensity of the lipid peak in the original bilayer. If lipid bilayer lifts from the substrate surface, both the TC and lipid peaks decrease in intensity by the same amount, so the calculation of the mole fraction of TC in the bilayer is still correct.

In the example below, the lipid peak with TC had half the intensity of the original lipid peak. From these calculations, the ratio of POPC molecules to TC molecules is calculated

$$\frac{\Gamma_{lipid,b}}{\Gamma_{TC,s}} = \frac{2.77\times10^{-6}\,molm^{-2}}{3.2\times10^{-6}\,molm^{-2}} = 0.86$$ Equation 4.10

The ratio of lipid to TC is large: from the calculated concentrations there is more TC in the bilayer than lipid. The solubility of TC in SDS and SL is 1:6 molecules of TC to surfactant. POPC has two tails per head group so the solubility could double to 1:3 assuming similar interactions. It therefore seems likely that some of the TC detected in the Raman spectrum is not dissolved in the bilayer. The reasons why this conclusion might arise are discussed in Section 4.3.2.3.

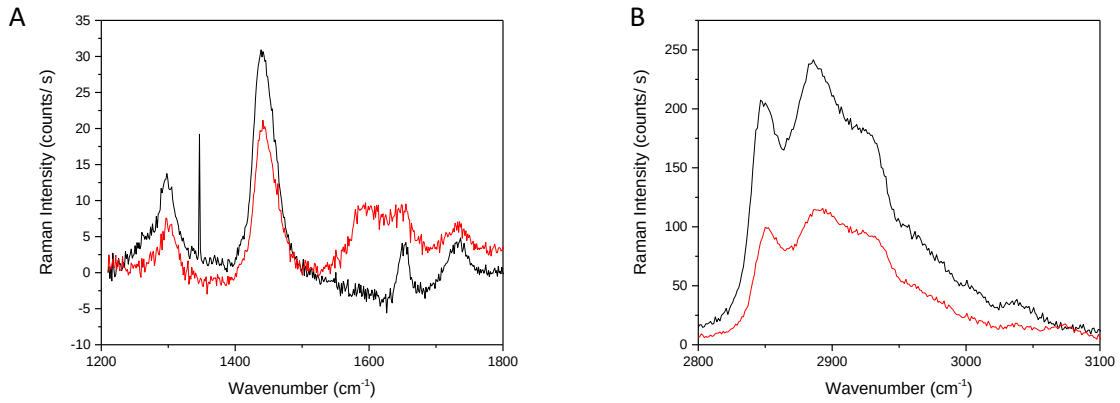


**Figure 4.22 TIR-Raman spectra collected at 1600 $cm^{-1}$ (A) and 2900 $cm^{-1}$ (B) using S polarised light of a POPC bilayer in pH 7.4 Tris buffer with 2 mM $CaCl_2$ (black) and the POPC bilayer treated with 0.3 mg/ mL TC in pH 10.8 buffer and rinsed with 15 ml of pH 7.4 buffer with 2 mM $CaCl_2$ (red). Laser power was 300 mW. The narrow peak at ~1350 $cm^{-1}$ for the POPC bilayer is caused by cosmic rays.**

### *4.3.2.2 Effect of TC Concentration on POPC bilayers*

A POPC bilayer was prepared in pH 7.4 buffer and then treated with a solution of TC at pH 10.8. The bilayer was rinsed with around 120 mL of pH 7.4 buffer and left for an hour then treated with a different concentration of TC. However, once the membrane has been treated a number of times, the concentration of TC built up within the membrane and the bilayer was permanently damaged. The area of bilayer underneath the laser spot may have been destroyed but the rest of the bilayer was likely to still be intact. The effect of varying the concentration of TC used to treat POPC bilayers has been investigated.

The lipid peak intensity changed very little when 0.01 mg/ mL TC was used to treat the bilayer (Figure 4.23). When the concentration of TC was increased to 0.05 mg/ mL, the lipid peak intensity decreased by 20%, and increased again as the cell was rinsed. The change in the lipid peak intensity with TC treatment of different concentrations has been plotted in Figure 4.24. When the bilayer was treated with both 0.2 mg/ mL TC and 0.4 mg/ mL TC, there was some strong fluorescence, making it difficult to compare the results directly. The fluorescence suggests that the TC was damaged by the laser and it appears that this permanently damaged the membrane as the lipid bilayer did not return to the original intensity upon rinsing. The high TC peak observed when the bilayer in Figure 4.23.C was rinsed with buffer is most likely caused by a crystal of TC in the beam, so this point is omitted from Figure 4.25.

From the data collected at 1600 $cm^{-1}$, there is a clear increase in the concentration of TC within the evanescent wave as the concentration of TC to which the bilayer was exposed increased (Figure 4.25). The data collected is noisy: each bilayer was slightly different and had different imperfections meaning that TC absorbed to different amounts in each bilayer.

The calculated ratio of TC to lipid within the membrane when the treated with 0.01 mg/ mL TC, was approximately a 1:18 mol ratio of TC to lipid. At this concentration, TC did not appear to damage or alter the bilayer signal. When 0.2 mg/ mL TC and 0.3 mg/ mL TC were used to treat the bilayer, the ratio of lipid to TC was around 0.85 lipid molecules for every TC molecule.

The change in intensity of the TC peak upon rinsing is not predictable, with 0.15 mg/ mL TC, the TC peak increased on rinsing but with 0.1 mg/ mL, the TC peak decreased on rinsing (Figure 4.25). The highest peak height was with the bilayer rinsed with 20 mL of pH 7.4 buffer after being treated with 0.4 mg/ mL TC. This corresponds to a lipid to TC ratio of 0.45:1. Data was not collected when 0.4 mg/ mL TC was in the cell due to fluorescence. The variability of the TC peak upon rinsing probably arises from the presence or absence of TC crystals in the laser spot.

For all samples, when the cell was rinsed with 100 mL of buffer, the TC peak reduced significantly (Figure 4.25), but in a number of samples a significant amount of TC remained in the bilayer even after rinsing. If TC forms crystals at the interface upon rinsing, TC will be very resistant to rinsing as the solubility of TC is very low.

This experiment has been carried out a number of times with different concentrations of TC. In the repeats, the intensity changes of the lipid peaks and the concentration of TC within the bilayer has not been consistent. However, the general trends have been consistent. To summarise the trends observed, treating with the lowest concentrations of TC, less than 0.02 mg/ mL, did not change the intensity of the lipid peak, and only a small TC peak was observed at 1650 $cm^{-1}$. For the intermediate concentrations of TC treatment, between 0.02 mg/mL and 0.15 mg/mL, the lipid peak decreased when TC was in the cell and returned to the original intensity after rinsing and resting. For the higher concentration TC treatments, more than 0.15 mg/mL, permanent damage to the bilayer was observed, in combination with high TC peaks.

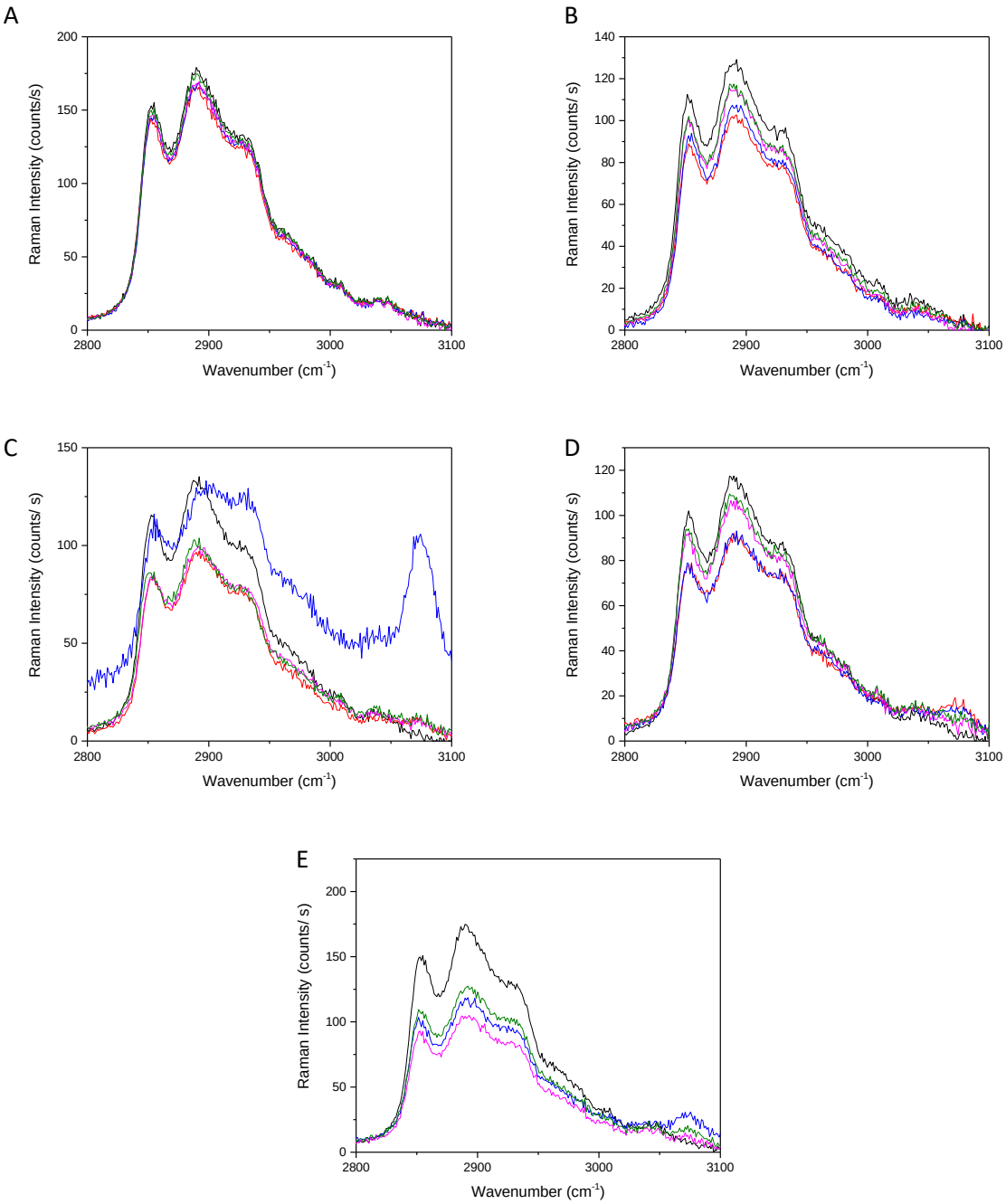


**Figure 4.23 TIR-Raman spectra collected at 2900 $cm^{-1}$ using S polarised light of a POPC bilayer (black) in pH 7.4 Tris buffer with 2mM $CaCl_2$. The bilayer was treated with different concentrations of TC in pH 10.8 buffer and left for 15 minutes (red). The bilayer was rinsed with 20 mL of pH 7.4 Tris buffer with 2 mM $CaCl_2$ (blue) and with a further 100 mL of pH 7.4 buffer (pink) and left for an hour (green). The bilayers was treated with the following concentrations of TC: 0.01 mg/ mL (A), 0.05 mg/ mL (B), 0.2 mg/ mL TC (C), 0.3 mg/ mL TC (D) and 0.4 mg/ mL TC (E). Laser power was 300 mW.**

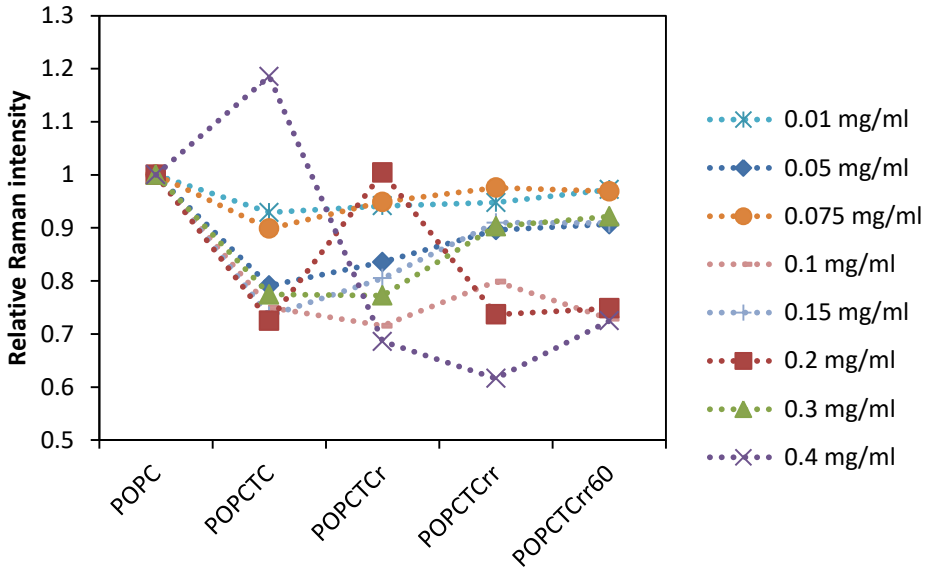


**Figure 4.24 Raman intensity at 2850 $cm^{-1}$ relative to the original bilayer plotted against experimental progress: The bilayer was treated with different concentrations of TC in pH 10.8 buffer and left for 15 minutes POPCTC. The bilayer was rinsed with 20 mL of pH 7.4 Tris buffer with 2 mM $CaCl_2$ POPCTCr and with a further 100 mL of pH 7.4 buffer POPCTCrr and left for an hour POPCTCrr60. The bilayers was treated with the following concentrations of TC: 0.01 mg/ mL (light blue), 0.05 mg/ mL (dark blue), 0.2 mg/ mL TC (red), 0.3 mg/ mL TC (green) and 0.4 mg/ mL TC (purple). Lines are to guide the eye.**

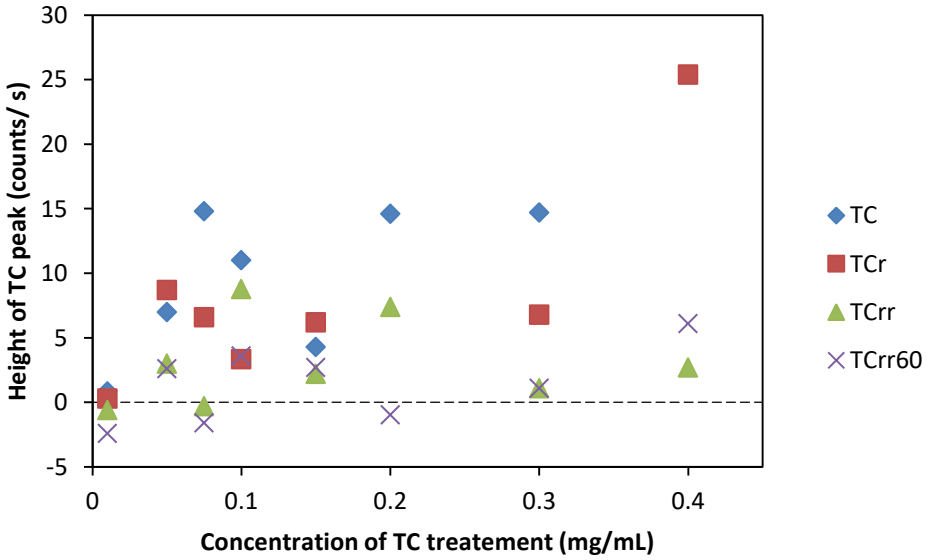


**Figure 4.25 Height of the TC peak at 1600 $cm^{-1}$ against the concentration of the TC treatment when the TC solution is in the cell (blue), when the bilayer was rinsed with 20 mL of pH 7.4 buffer with 2 mM $CaCl_2$ (red) and when the bilayer was rinsed with 100 mL of buffer (green) and left for an hour (purple).**

### *4.3.2.3 TC Crystallisation on the Bottom of the Hemisphere*

In some experiments, the concentration of TC in the rinsed sample was high enough that crystals or deposits could be seen on the bottom of the hemisphere. For example, in the experiment in Figure 4.26 a POPC bilayer was treated with 0.1 mg/ mL TC at pH 10.8. There was a small reduction in the lipid peak and a slight TC peak at 3075 $cm^{-1}$. When the bilayer was rinsed with around 20 mL of pH 7.4 buffer, the bottom of the hemisphere appeared to be covered with crystals and when a

spectrum was taken (POPCTCr), there was an intense TC peak (Figure 4.26.B). The $I(d_-)/I(d_+)$ peak ratio when there was TC on the bottom of the hemisphere was considerably higher than the peak ratio of lipid alone, 1.20 compared to 1.12. If the peak ratio increases, it implies that the bilayer becomes more ordered or the phase changes. It is not surprising that there was be solid TC in the cell: when the pH switched from pH 10.8 to pH 7.4, the solubility of TC dropped and the excess TC crystallised out of solution. The diffusivity of $H^+$>>TC, so the pH drops before TC diffuses into the buffer. The rinsing occurred when the cell was upside down, so TC crystals may have settled onto the hemisphere. However, the hemisphere is located at the top of the cell during measurements and TC crystals are denser than water, at 1.54 $gcm^{-3}$ so the crystals must be attached to the hemisphere otherwise they should settle towards the bottom of the cell.[7] Some of the crystallisation appears to be around the laser spot.

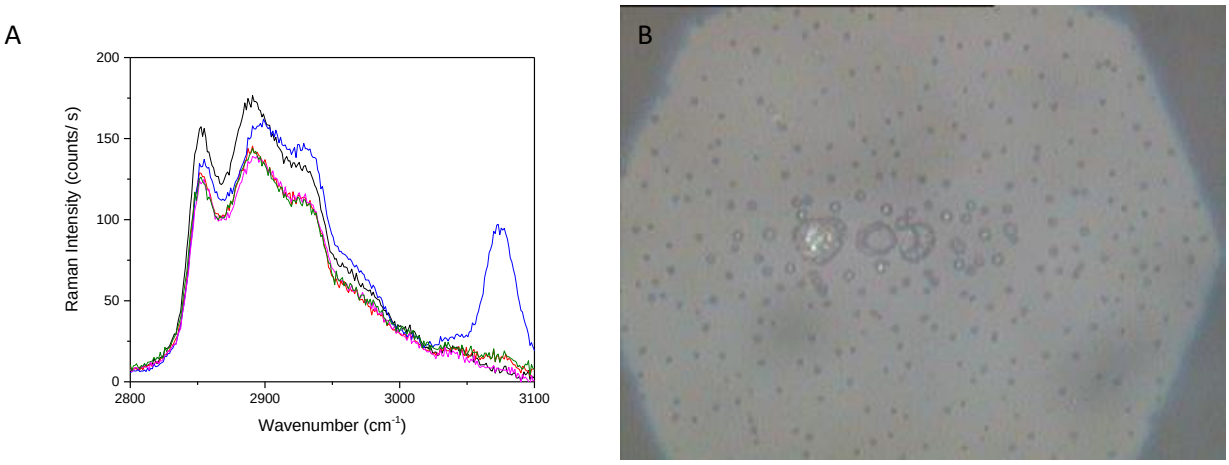


**Figure 4.26 TIR-Raman of POPC bilayer in pH 7.4 buffer with 2 mM $CaCl_2$ (Black), POPC bilayer and 0.1 mg/ mL TC in pH 10.8 buffer (red) and bilayer rinsed with 20 mL of pH 7.4 buffer with 2 mM $CaCl_2$ after TC treatment (blue) and rinsed with 120 mL of pH 7.4 buffer with 2 mM $CaCl_2$ (pink) and left for one hour (green) using S light. Laser power was 300 mW. (B) image of the bottom of the hemisphere of POPCTCr after a measurement was taken.**

In other experiments, TC has crystallised around the laser spot and burned. When the cell was treated with a solution of 0.3 mg/ mL TC and then rinsed I was unable to acquire a spectrum for the lipid and the only signal was from TC (Figure 4.27.A). After the laser was turned off, a blemish was seen where the laser had been (Figure 4.27.B). There was strong fluorescence caused by bilayer damage.

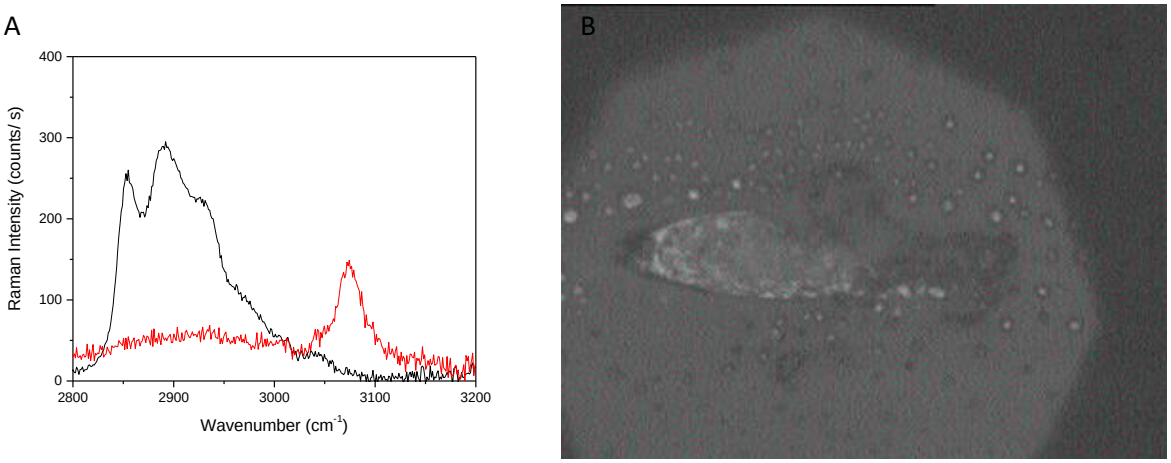


**Figure 4.27 (A) TIR-Raman of POPC bilayer in pH 7.4 buffer with 2 mM $CaCl_2$ (Black), POPC bilayer and bilayer rinsed with 20 mL of pH 7.4 buffer with 2 mM $CaCl_2$ after TC treatment (0.3 mg/ mL) (red) using S light. Laser power was 1000 mW. (B) Image of the bottom of the silica hemisphere showing marks after the laser has been turned on. The hemisphere appeared clean and flat before the laser was turned on.**

A further experiment was carried out where a suspension of TC was pumped through the cell. I used 0.023 mg/ mL TC in a saturated suspension at pH 8 (Figure 4.28). The solubility of TC at this pH is 4 ng/mL, so most of the TC was delivered in the solid form. The TC suspension was pumped through at a rate of 50 mL/hr for half an hour and then was left for half an hour before washing through 20 mL of buffer and 100 mL of buffer. The saturated solution was pumped through to ensure that the solution remained agitated so that the solid TC did not settle to the bottom of the cell. In the measurements, with the TC suspension flowing through the cell, the TC peak was very intense but there was very little decrease in the bilayer signal with during treatment.

There was a significant TC peak in the Raman spectrum after TC was inserted into the cell, which increased as TC was flowed through. Upon rinsing with pH 7.4 buffer, the TC peak decreased. An image of the bottom of the hemisphere showed lots of small crystals of TC had formed and/or settled at the laser focus (Figure 4.29). Most likely, the large TC peak is caused by this crystal of TC. The lipid peaks retained similar intensities throughout the experiment until the final rinse but the shape of the lipid peaks changed during the experiment indicating that the bilayer was damaged.

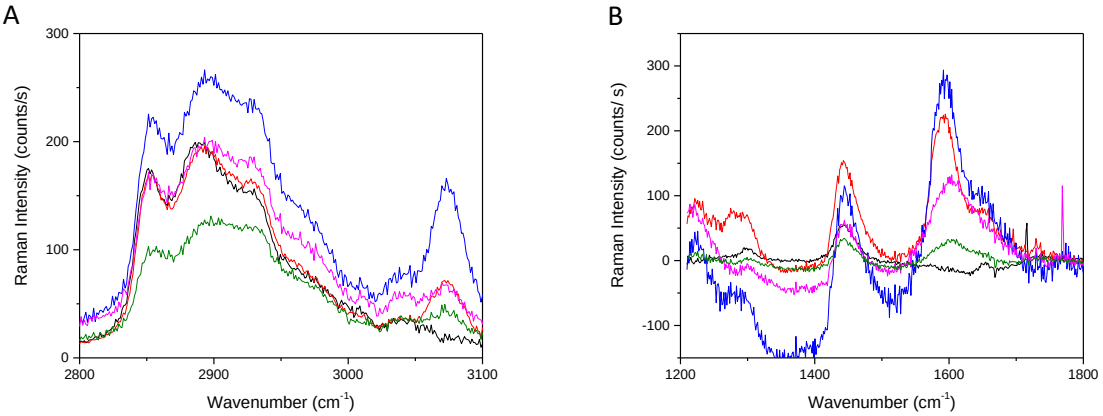


**Figure 4.28 TIR-Raman spectra collected at 2900 $cm^{-1}$ (A) and 1600 $cm^{-1}$ (B) using S polarised light. Laser power was 300 mW. POPC bilayer in pH 7.4 tris buffer with 2 mM $CaCl_2$ (black), POPC in 0.023 mg/ mL TC suspension at pH 8 measured straight away (red) and after 30 minutes (blue), POPC after being treated with TC and rinsed with 20 mL of pH 7.4 tris buffer with 2 mM $CaCl_2$ (pink) and rinsed with 120 mL of pH 7.4 tris buffer with 2 mM $CaCl_2$ (green).**

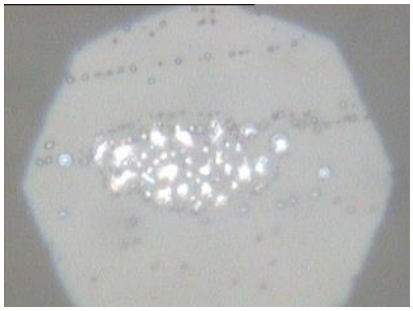

**Figure 4.29 Images of the bottom of the hemisphere with a POPC bilayer when a saturated suspension of 0.023 mg/ mL TC at pH 8 is pumped through the cell. The solubility of TC is around 4 ng/ml at pH 8.**

In these experiments and a number of others, TC crystallised around the laser spot or on the bottom of the hemisphere when the cell was rinsed with 20 mL of low pH buffer after treatment at pH 10.8. The TC crystals cause high TC peaks to be observed. It is not surprising that TC crystallises out on the pH switch, from high pH to neutral pH, the solubility of TC drops and the excess TC will crystallise.

The crystals that form around the laser spot may be from laser-induced crystallisation where the optical trapping force of the laser induces crystallisation from a supersaturated solution. Other workers[292] have directly exploited this mechanism to control crystallisation of organic molecules.

When there has been a high TC peak, the lipid intensity did not return to the original intensity, indicating permanent damage to the bilayer. The solid TC was difficult to rinse away and TC remained in the treated area after the bilayer was rinsed with buffer.

#### *4.3.2.4 Imaging Experiment*

A TIR-Raman imaging experiment was carried out to investigate the cause of the high TC peaks that occur on rinsing and the crystallisation of TC on the hemisphere. The imaging experiments are designed to show whether there is separation of different components within the bilayer. Raman images are taken of separate regions of the spectrum using different filter angles and combined to determine the composition of lipid and TC across the bilayer. Spectra can also be collected in the same experiment with a few mirror flips.

In experiments with TC, five different filter settings were used. A 628 nm Semrock filter (14 nm bandwidth, part number: TBP01-628/14-25x36) was used at 0°, 5°, 14° and 25° and a separate 640 nm Edmund Optics (620 IL 25) filter was used to image the TC region, around 3075 $cm^{-1}$, in combination with the 0° filter. $D_2O$ was chosen so that the image with the extra filter did not contain any water bands. The transmission curves for the different filter angles are shown below with the spectra of POPC in $D_2O$ (without the $D_2O$ background subtracted), and TC overlaid (Figure 4.30). When the filter is set to 25° the only bands that should be observed are from the buffer and when the filter is set to 14°C the only bands contributing to the image should be the lipid peak and the water peak. When the filter is at 0° and 5°, all three species contribute to the image. When the extra filter is used, the TC peak should be the strongest signal, although there is still some overlap from the edge of the lipid peak.

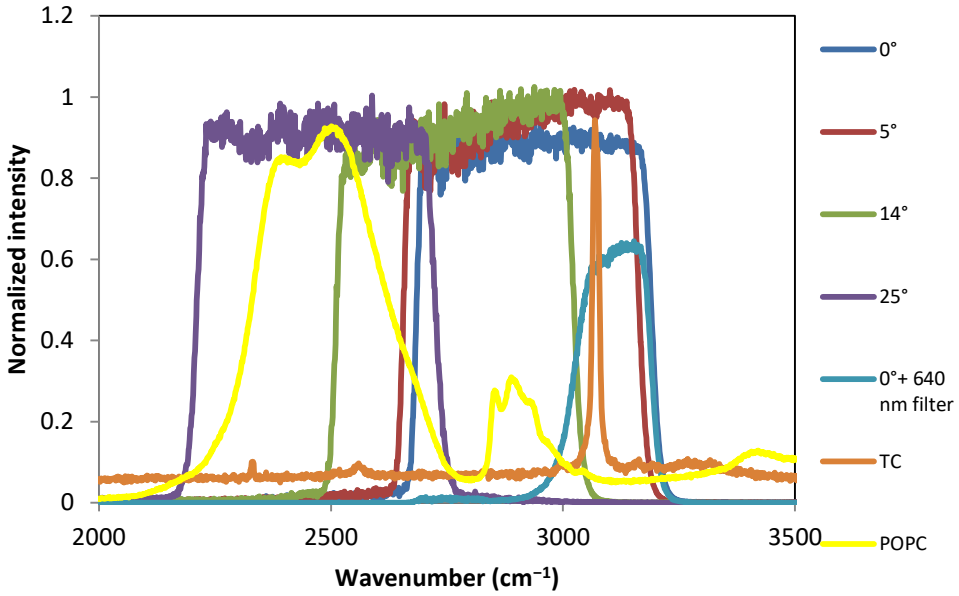


**Figure 4.30 An overlay of the normalised spectra of POPC in pH 7.4 in $D_2O$ buffer (without the background subtracted) and solid TC with the transmission curves for the filter angles used in the imaging experiment.**

Raman images were taken of the pure POPC bilayer at pH 7.4, during treatment with 0.3 mg/ mL TC at pH 10.8 and after the cell was rinsed with 20 mL of pH 7.4 buffer. A significant TC peak was seen when TC was in the cell. When the cell was rinsed, the TC peak increased dramatically and there was some fluorescence (Figure 4.31.A). An optical image of the bottom of the hemisphere showed TC crystals (Figure 4.31.B).

The Raman images of the pure bilayer indicated a reasonably uniform bilayer, with a few spots which may be attached vesicles (Figure 4.32). There is a bright spot on the edge of all the images apart from the image with the extra filter. The spot remained throughout the experiment at the same intensity, which suggests it is an artefact of the experiment and the alignment. If the bright spot was from a thicker patch of lipid, it would not be observed in the image at 25°. The buffer signal should be uniform across the image.

In the images with TC in the bulk, the bilayer was uniform (Figure 4.33). The images collected with the extra filter, which should include mostly TC, showed a slight increase in intensity, of approximately 12 counts, compared to the pure bilayer and one small bright spot.

When the cell was rinsed with 20 mL of low pH buffer after being treated with TC, the Raman images appeared spotty (Figure 4.34). These spots are seen in the same locations at all filter angles, although with different intensities and can be seen in the optical image of the bottom of the hemisphere. If the bright spots were simply the Raman spectra of TC crystals or lipid crystals, they would not be observed in the image collected at 25°, which should only contain contributions from the buffer. In some previous experiments where the concentration of TC was high and the laser was on the sample for too long, the sample started to fluoresce leading to poor spectra. It may be that the spots are caused by TC which has been burnt by the laser and fluoresces over a wide range of wavenumbers.

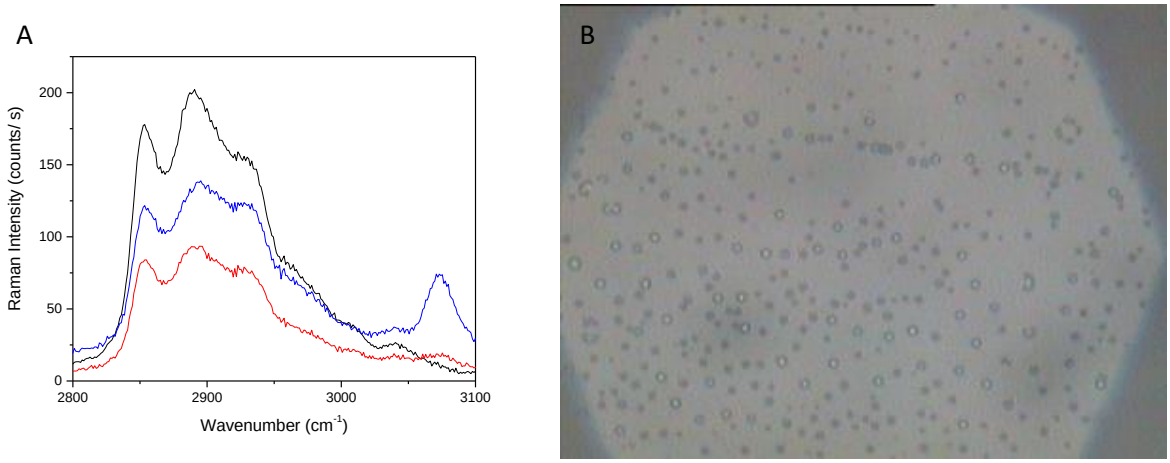


**Figure 4.31 TIR-Raman of POPC bilayer in pH 7.4 buffer with 2 mM $CaCl_2$ (Black), POPC bilayer and 0.3 mg/ mL TC in pH 10.8 buffer (red) and bilayer rinsed with 20 mL of pH 7.4 buffer with 2 mM $CaCl_2$ after TC treatment (blue) using S light. Laser power was 300 mW. (B) Image of the bottom of the hemisphere in pH 7.4 buffer after the cell was treated with 0.3 mg/ mL TC**

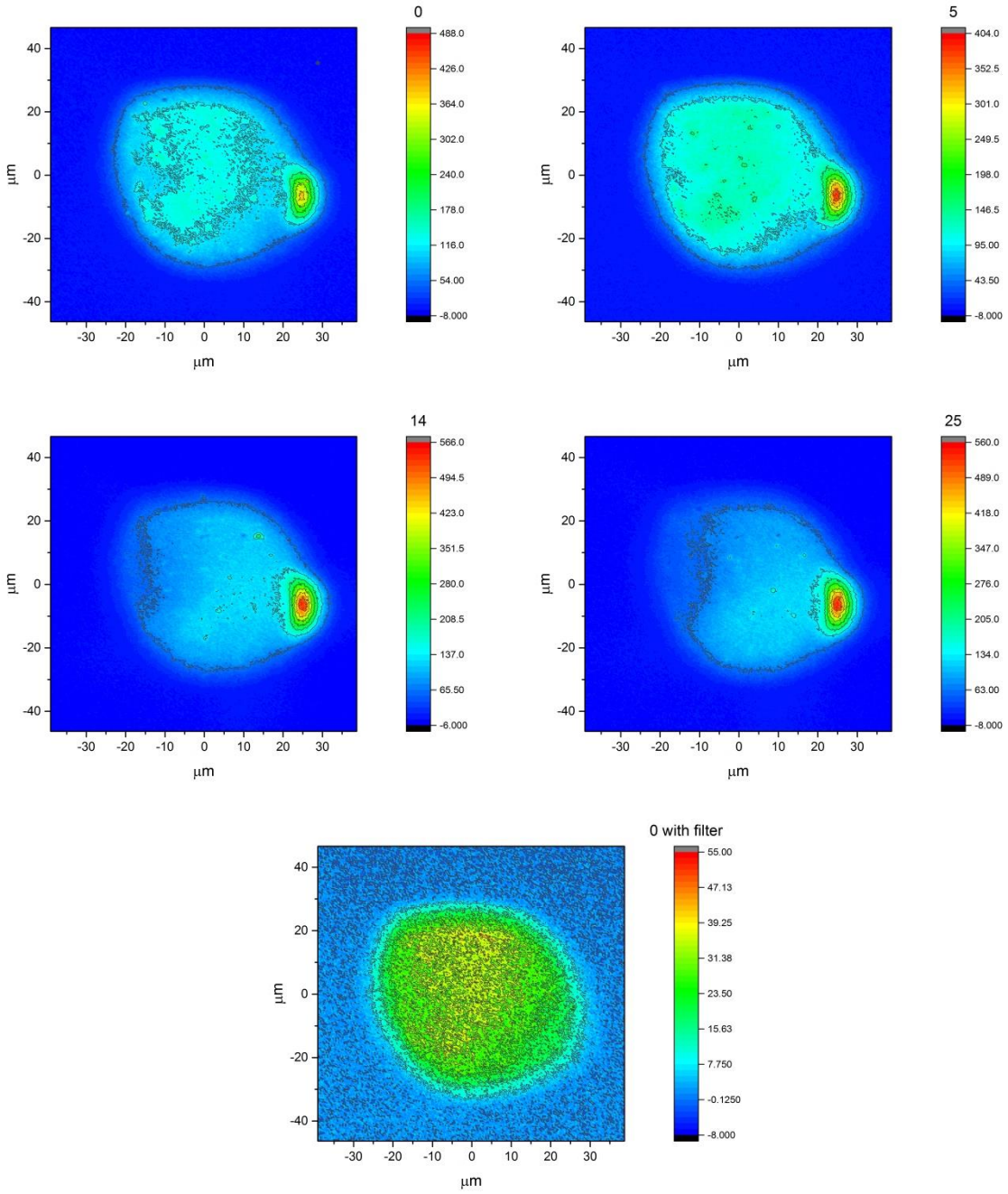


**Figure 4.32 Images from different filter angles of the POPC bilayer in pH 7.4 buffer with 2 mM $CaCl_2$ (A) 0°C, (B) 5°, (C) 14°, (D) 25° and (E) 0° with the 640 nm filter**

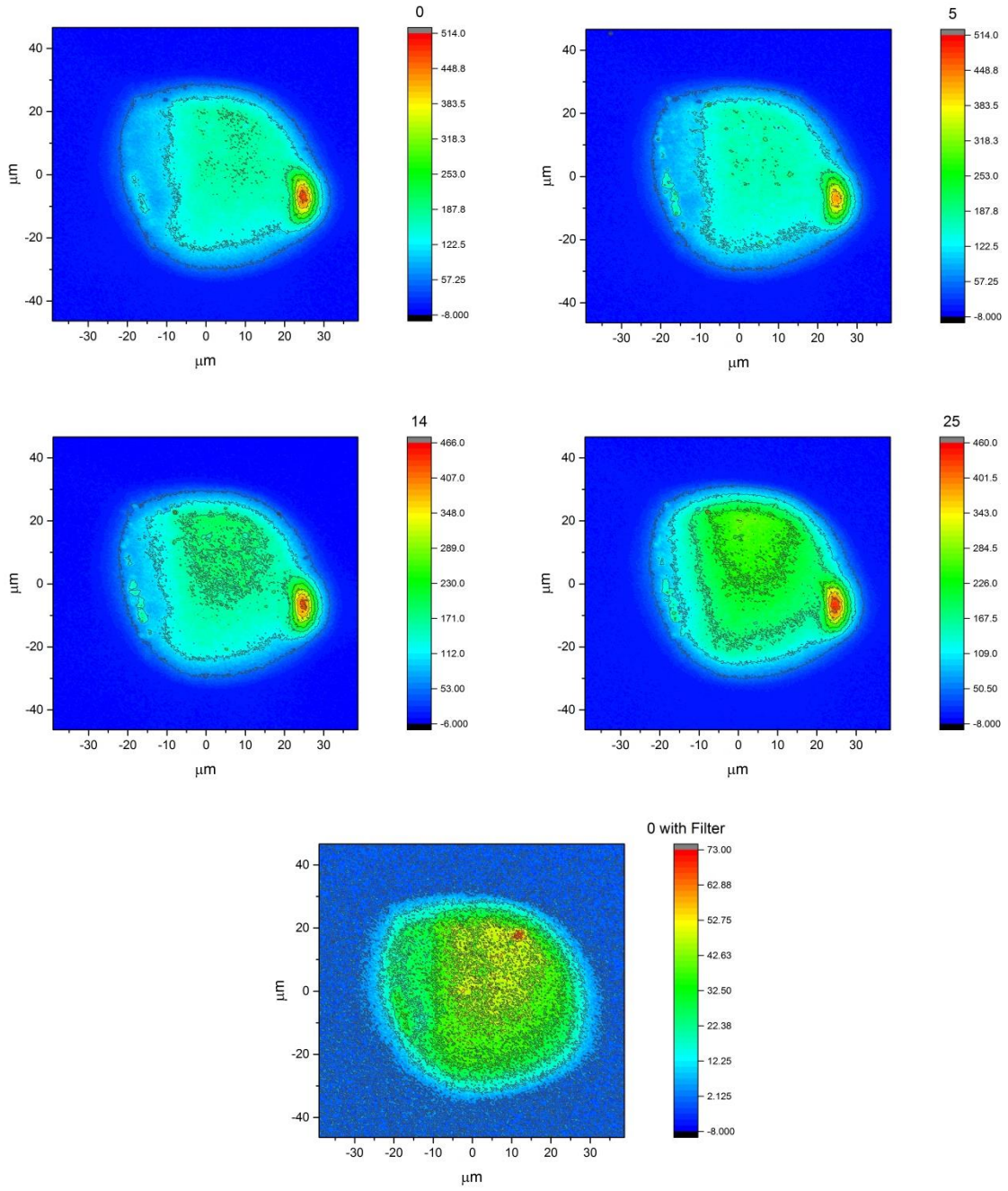


**Figure 4.33 Images from different filter angles of POPC bilayer in pH 10.8 buffer with 0.3 mg/ mL TC (A) 0°C, (B) 5°, (C) 14°, (D) 25° and (E) 0° with the 640 nm filter**

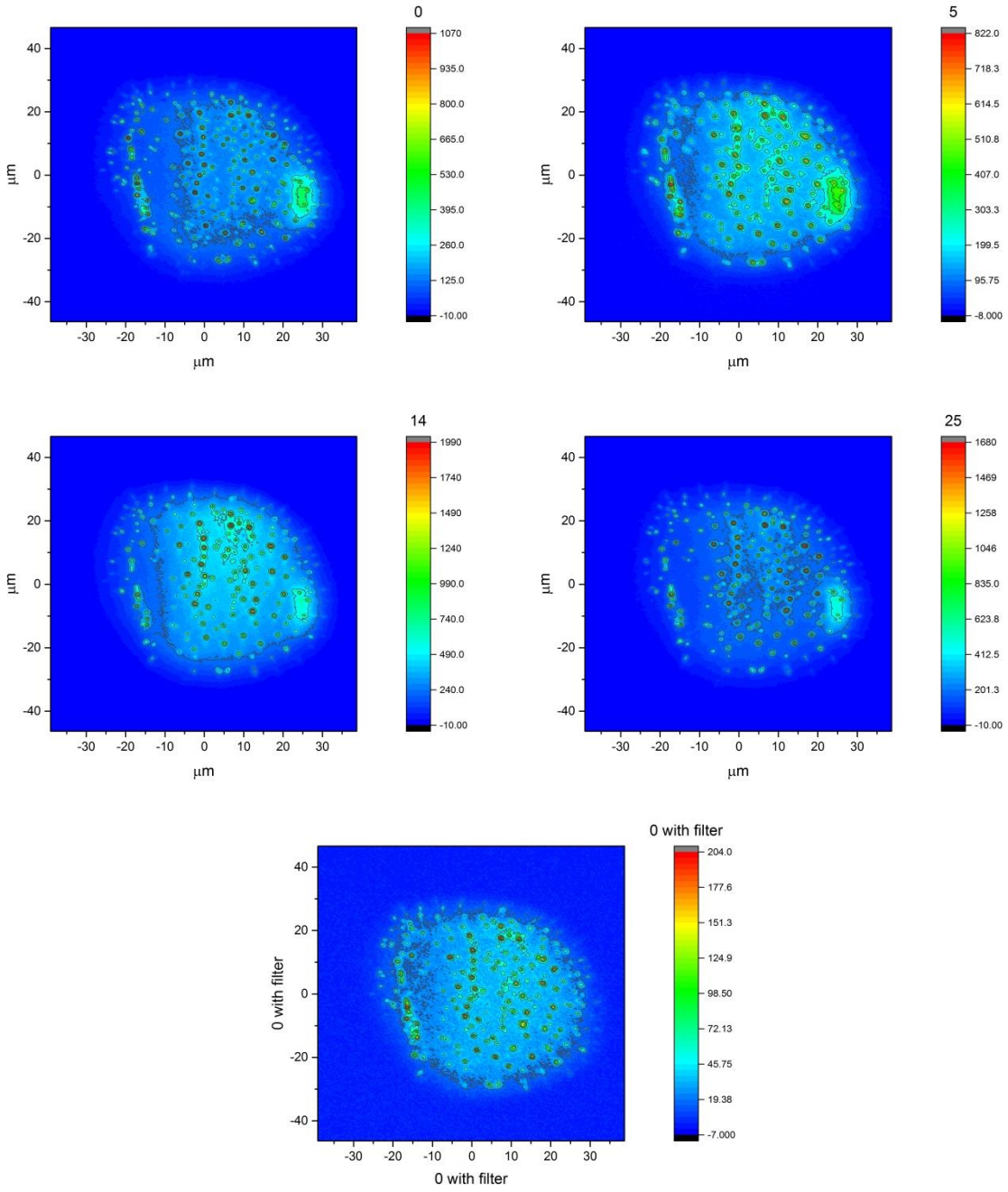


**Figure 4.34 Images from different filter angles of POPC bilayer in pH 7.4 buffer with 2 mM $CaCl_2$ after being treated with 0.3 mg/ mL TC (A) 0°C, (B) 5°, (C) 14°, (D) 25° and (E) 0° with the 640 nm filter**

### *4.3.2.5 Changing the Rinsing Conditions*

In the experiments described in Section 4.3.2.2, above, TC was inserted into the cell at pH 10.8. The bilayer was then rinsed with pH 7.4 buffer. Sometimes, rinsing increased the intensity of the TC peak. I carried out an experiment where the speed of rinsing was changed to explore the rinsing process further and the persistency of TC within the bilayer.

Buffer was pumped through the cell slowly, so that the pH change in the cell was more gradual than the fast rinse carried out with 20 ml buffer in one go. The intensity of peaks of TC and the lipid were observed as rinsing progressed. In the experiment shown in Figure 4.35, a solution of 0.09 mg/ mL

TC at pH 10.8 was inserted into the cell and then pH 7.4 buffer was washed through the cell at a rate of 4.3 mL/ hr. Measurements were taken every 15 minutes, and spectra are shown with 30 minutes gaps to guide the eye. As the buffer was washed through the cell, the intensity of the TC peak at 1600 $cm^{-1}$ decreased (Figure 4.36.A). As the TC peak decreased at 1600 $cm^{-1}$, the lipid peak at 2850 and 2880 $cm^{-1}$ increased (Figure 4.36.B). The pH of biological systems is around pH 7.4 so I kept the bilayer at that pH as much as possible in previous experiments rather than rinsing with pH 10.8 buffer.

In my prior experiments, the TC peak sometimes increased with rinsing with 20 mL of buffer (for example see Figure 4.25). During the rapid rinse, when the pH inside the cell switched, the protons diffused towards the region of the bilayer and the pH decreased faster than the TC diffused away from the surface. At lower pH, the phenolate TC becomes phenol leading to a high concentration of the phenol near the surface, which partitions more strongly into the bilayer than the phenolate. A high concentration of TC entered the bilayer. The phenol has a lower solubility than the phenolate, so as the phenol formed, it crystallised out of solution. When the rate at which the pH was changed with rinsing was decreased, there was a less rapid switch between phenol and phenolate.

There was an increase in the lipid peak at 2900 $cm^{-1}$ as the TC peak decreased in intensity, although the lipid signal was not restored to the intensity of the original bilayer. In this experiment, the pH change after the treatment of the bilayer with TC was gradual, allowing $TC^-_{aq}$ to diffuse away from the surface before it became the phenol form, so that there was less TC at the surface to partition into the membrane and to crystallise.

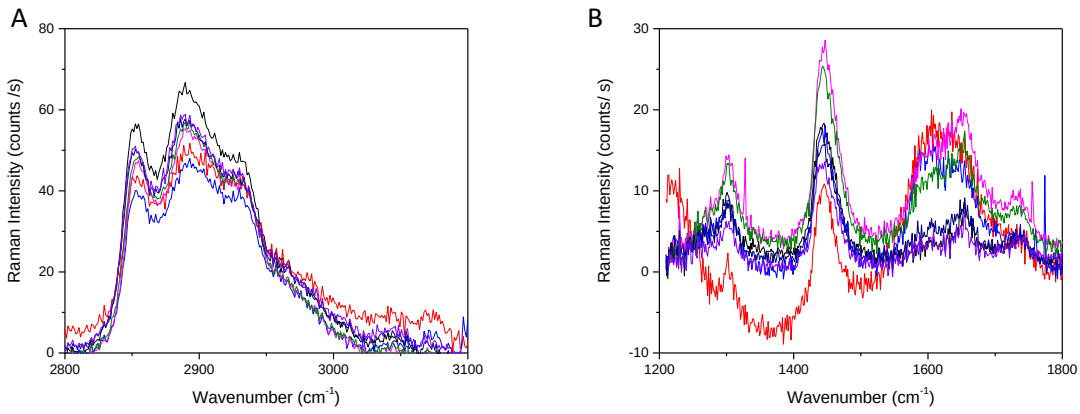


**Figure 4.35 TIR-Raman spectra collected at 2900 $cm^{-1}$ (A) and 1600 $cm^{-1}$ (B) using S polarised light. Laser power was 300 mW. POPC bilayer in pH 7.4 tris buffer with 2 mM $CaCl_2$ (black), POPC in 0.09 mg/ mL TC solution at pH 10.8 after 30 minutes (red) and rinsed with pH 7.4 buffer with 2 mM $CaCl_2$ pumping through at 4.3 ml/ hr for 30 minutes (blue), 60 minutes (pink) and 90 minutes (green), and rinsed with 100 mL of pH 7.4 tris buffer with 2 mM $CaCl_2$ (navy) and left for an hour (purple).**

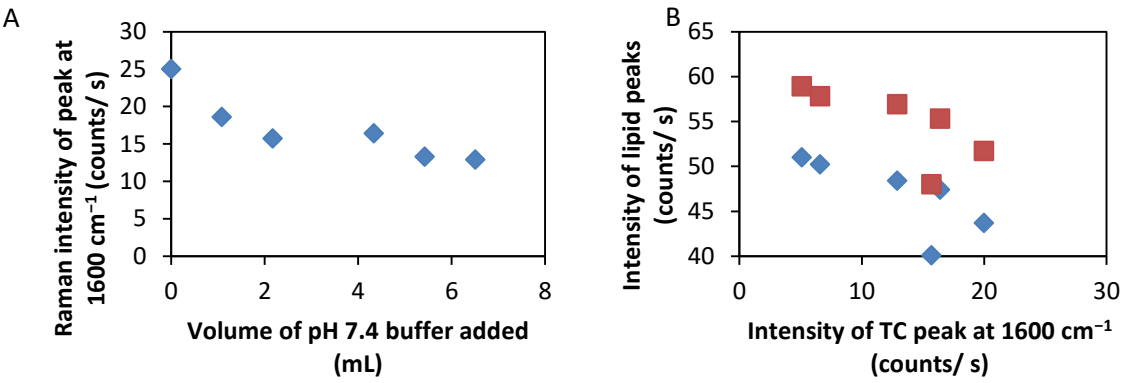


**Figure 4.36 (A) The change in the intensity of the TC peak at 1600 $cm^{-1}$ against volume of pH 7.4 buffer with 2 mM $CaCl_2$ used and (B) the change in the intensity of the lipid peaks at 2850 (blue diamonds) and 2880 $cm^{-1}$ (red squares) against the intensity of the TC peak at 1600 $cm^{-1}$.**

The volume of pH 7.4 buffer required to remove TC from the bilayer was studied. A POPC bilayer was treated with 0.3 mg/ mL TC and then rinsed with buffer at a rate of 30 mL per hour. Measurements were taken every 15 minutes (Figure 4.37). The spectra collected with TC in bulk in the cell show high fluorescence.

The lipid peak intensity in the $CH_2$ stretching region increased with rinsing (Figure 4.38) until the rinsing was stopped and did not increase further when the cell was rinsed with an extra 100 mL of buffer. The TC peak at 1600 $cm^{-1}$ decreased to zero after 60 mL of buffer was rinsed through the cell, (Figure 4.39).

The concentration of TC within the bilayer decreased with rinsing and the lipid intensity increased. The lipid peak intensity takes time to recover after TC treatment, even when TC has been removed from the cell. The time taken to rinse the bilayer may be as important as the volume of buffer used to rinse the bilayer. Previous experiments, when the bilayer has been rinsed with 100 mL of pH 7.4 buffer very quickly, have sometimes shown residual TC peaks at 1600 $cm^{-1}$. When the rate of buffer washing through the cell was slowed down, the TC peak decreased with time. Time is more important than volume in this system because at the point on the hemisphere where measurements were taken was directly above the centre of the inlet tube. At this point, due to the geometry of the tube, the point at the surface is a stagnation point where the fluid velocity is zero and the transport is by diffusion alone. In these circumstances, the rate of removal of TC from the surface is dependant on the rate of diffusion across the stagnent boundary layer. Woods[178] used a model system to calculate the thickness of the diffusion layer in the wall jet geometry and found it to be in the order of tens of microns.

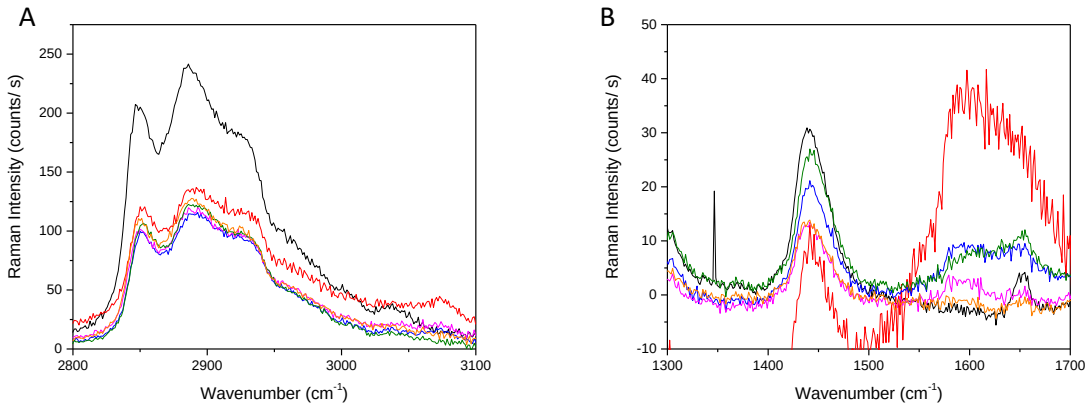


**Figure 4.37 TIR-Raman spectra collected at 2900 $cm^{-1}$ (A) and 1600 $cm^{-1}$ (B) using S polarised light. Laser power was 300 mW. POPC bilayer in pH 7.4 tris buffer with 2 mM $CaCl_2$ (black), POPC in 0.3 mg/ mL TC solution at pH 10.8 after 15 minutes (red) and rinsed with pH 7.4 buffer with 2 mM $CaCl_2$ pumping through at 30.4 ml/ hr for 30 minutes (blue), 60 minutes (pink), 90 minutes (green) and 120 minutes (orange).**

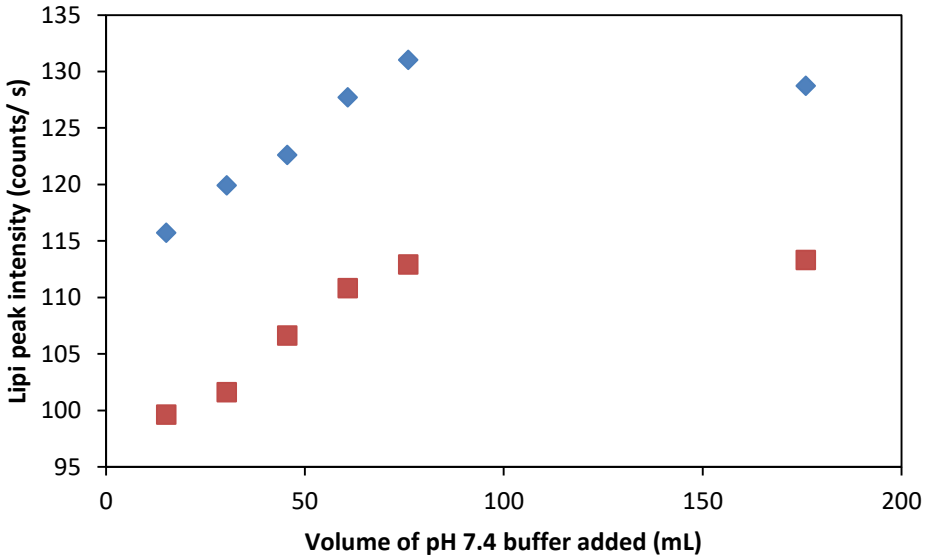


**Figure 4.38 The intensity of the lipid peaks at 2850 $cm^{-1}$ (red) and 2885 $cm^{-1}$ (blue) of a POPC bilayer against volume of pH 7.4 buffer with 2 mM $CaCl_2$ rinsed through the cell after being treated with 0.3 mg/ mL TC at pH 10.8.**

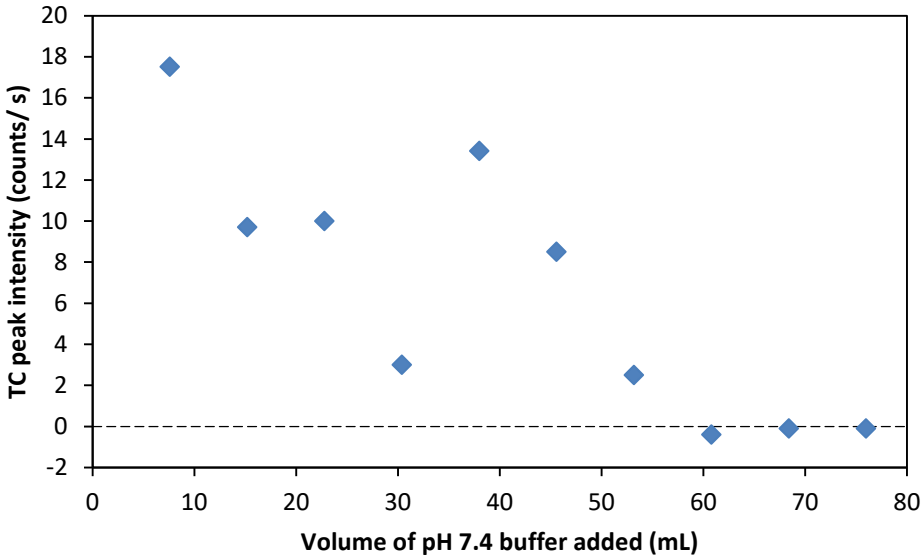


**Figure 4.39 The intensity of the TC peak at 1600 $cm^{-1}$ in a POPC bilayer against volume of pH 7.4 buffer with 2 mM $CaCl_2$ rinsed through the cell after being treated with 0.3 mg/ mL TC at pH 10.8.**

When the bilayer was rinsed with buffer at pH 9.5, above the pKa of TC (7.9),[8] TC was rinsed from the cell without the switch from the phenolate form to the phenol form. In the experiment in Figure 4.40, a POPC bilayer was treated with 0.3 mg/ mL TC at pH 10.8 and then rinsed with pH 9.5 carbonate buffer. The concentration of TC was high enough to permanently damage the bilayer: the lipid intensity did not return to its original value and there was some fluorescence when TC was in the bulk. The TC peak at 1600 $cm^{-1}$ did not increase upon rinsing, and the data collected during the rinsing steps suggested that TC was removed from the bilayer in the first rinse, as no TC peak was observed above the baseline. 20 mL of buffer rinsed the TC from the bilayer. No crystallisation of TC around the laser spot was observed. The data collected at 2900 $cm^{-1}$ for the rinsed sample appears to show a very small TC peak at 3075 $cm^{-1}$ only just above the noise level. This peak is likely caused by fluorescence. When the raw data, without the background subtraction is compared to the original bilayer, the curve of the water peak is a different shape to the curve of the water peak for the original bilayer of POPC: there is extra light from fluorescence, not TC (Figure 4.41). The data collected at 1600 $cm^{-1}$ for the rinsed sample has a low intensity, however, there is no fluorescence in the sample and the data does not suggest that there is large concentration of TC in the rinsed sample.

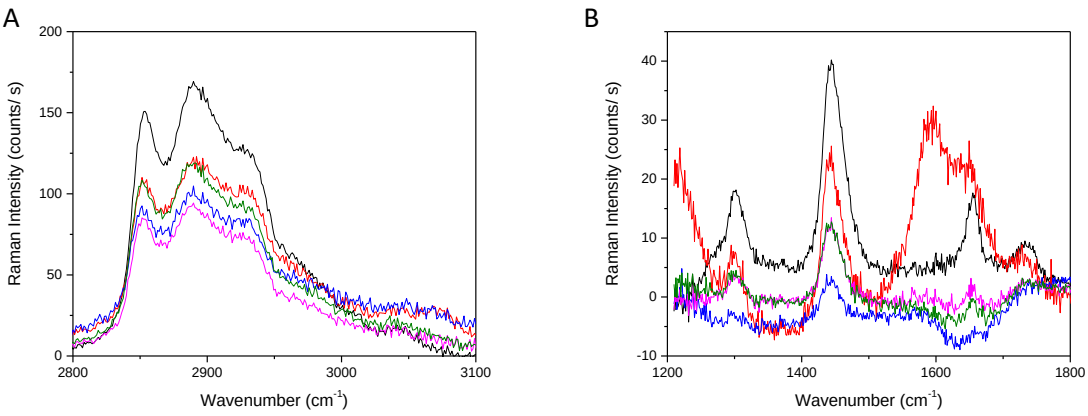


**Figure 4.40 TIR-Raman spectra collected at 2900 $cm^{-1}$ (A) and 1600 $cm^{-1}$ (B) using S polarised light. Laser power was 300 mW. POPC bilayer in pH 7.4 tris buffer with 2 mM $CaCl_2$ (black), POPC in 0.3 mg/ mL TC solution at pH 10.8 after 15 minutes (red) and rinsed with 20 mL of pH 9.5 carbonate buffer (blue) and 80 ml of pH 9.5 buffer (pink) and left for an hour (green).**

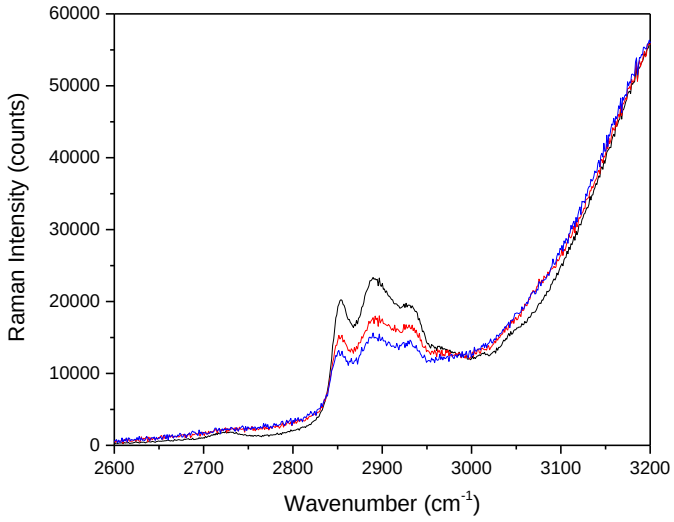


**Figure 4.41 TIR-Raman spectra collected at 2900 $cm^{-1}$ using S polarised light without the water background subtracted. Spectra were normalized so that the water peak had the same intensity. Laser power was 300 mW. POPC bilayer in pH 7.4 tris buffer with 2 mM $CaCl_2$ (black), POPC in 0.3 mg/ mL TC solution at pH 10.8 after 15 minutes (red) and rinsed with 20 mL of pH 9.5 carbonate buffer (blue).**

In the experiments described in Section 4.3.2.2, it took up to an hour for the bilayer signal to return to the original intensity after rinsing with 120 mL of buffer. An example is shown below from the experiment where a POPC bilayer was treated with the TC suspension at pH 8 (see Figure 4.28) and rinsed with 120 mL of buffer. The lipid peak increased with time after rinsing, even though there was still a significant amount of TC within the bilayer (Figure 4.42).

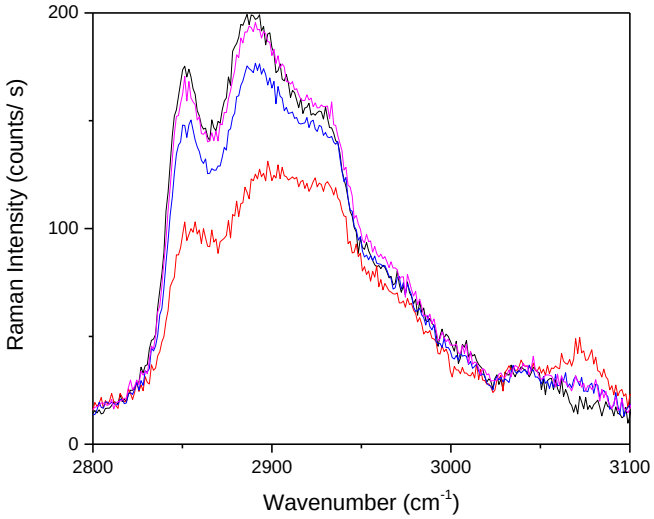


**Figure 4.42 POPC bilayer in pH 7.4 buffer with 2 mM $CaCl_2$ (black), after being treated with TC and rinsed with 120 mL of low pH buffer straight after rinsing (red), 15 minutes after rinsing (blue) and 30 minutes after rinsing (pink). Laser power was 300 mW.**

The persistence of TC within the bilayer after treatment is very dependent on rinsing conditions. If the buffer used to rinse the bilayer is pH 7.4, the TC concentration in the bilayer region decreases gradually with volume of buffer added if the rinsing process is slow. If the rinsing process is fast, the phenol crystallises and can take longer to rinse from the bilayer. If the bilayer is rinsed with buffer above the pKa of TC, the phenolate TC rinses very quickly from the bilayer.

If TC were applied to skin in a hand washing process at high pH, for example from a sodium laurate solution and if the hands were only rinsed quickly with plain water, the TC would go from the phenolate to the crystals of TC, which would require a lot of rinsing to remove. In this handwashing regime, the antibacterial TC would remain on the hands for a long time, ensuring antibacterial protection between hand washes.

#### *4.3.2.6 Investigations into the Cause of the Changes in the Lipid Intensity with TC*

In the TIR-Raman experiments shown above, the lipid peak decreased with TC in the cell and increased when the cell was rinsed with buffer. Other group members have observed similar results when the bilayer was treated with SDS.[179,281] When Churchwell[179] used low concentrations of per-deuterated−SDS, well below the CMC, to treat a phospholipid bilayer, the SDS inserted into the bilayer and the bilayer signal decreased (Figure 4.43). When the treated bilayer was rinsed with buffer, the SDS signal decreased and the lipid signal returned to around the original intensity.[179,281] When a higher concentration of SDS was used, the bilayer did not recover.

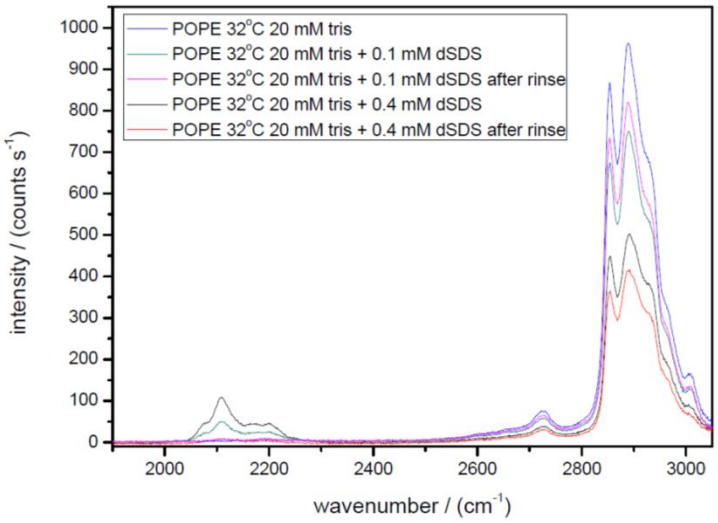


**Figure 4.43 TIR-Raman Spectra collected by Churchwell[179] showing the interaction of 0.1 and 0.4 mM dSDS with a POPE bilayer in 20 mM pH 7.4 Tris buffer at 32°C. The laser power was 800 mW, the angle of incidence was 73° and spectra were acquired at 18 x10 s.**

When Eis[293] used fluorescence microscopy to observe the effect of SDS on the lipid bilayer directly, tubules were seen coming out of the bilayer when there was SDS within the cell (Figure 4.44). When the cell was rinsed with buffer, the tubules were drawn back into the bilayer on the surface. The tubules form to regulate the stress within the bilayer.[283] The tubules grow to lengths well outside of the range of the evanescent wave, so that their contents would not be observed by TIR-Raman. During the rinsing, the lipid that was in tubules was drawn back to the surface, demonstrating why the lipid peak decreases when there is SDS in the cell and why the peak increases again upon rinsing. Cho *et al*.[294] also observed tubules forming from a bilayer treated with 2 mM SDS.

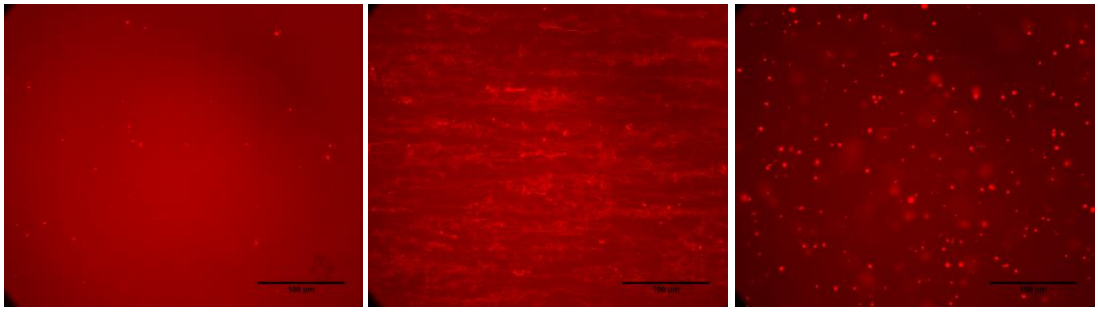

**Figure 4.44 A POPC bilayer with 1 mol % Rh-DPPE in buffer (A), treated with 0.33 mM dSDS at a flow rate of 25 µlmin$^{-1}$ (B) and rinsed with buffer at a flow rate of 25 µlmin$^{-1}$ after treatment with dSDS (C). Taken from the work of E. Eis.[293]**

Fluorescence microscopy has been used on bilayers treated with TC to observe whether the decrease in Raman intensity of the lipid peaks is caused by tubules forming or another mechanism is at work. Experiments were carried out on a POPC bilayer treated with different concentrations of TC. Rh-DPPE was used at 1 mol% as the fluorescence probe. When the bilayer was treated with 0.1 mg/ mL TC, images were taken every second. No tubules were observed coming out from the bilayer (Figure 4.45). The bilayer was not damaged either and there did not appear to be areas where the bilayer was removed from the surface. Many of the bilayer features, such as brighter spots remained throughout the experiment. It was observed that the intensity of the fluorescence decreased with time. When the average pixel intensity of the image was plotted against time, a sudden drop in

fluorescence was observed in the first few seconds of treatment and then the intensity remained stable with time (Figure 4.46).

When the bilayer was rinsed with buffer to remove the TC, the fluorescence intensity increased. The intensity did not return to the original value, but to a much lower intensity. When the bilayer was rinsed with more buffer, the intensity remained the same.

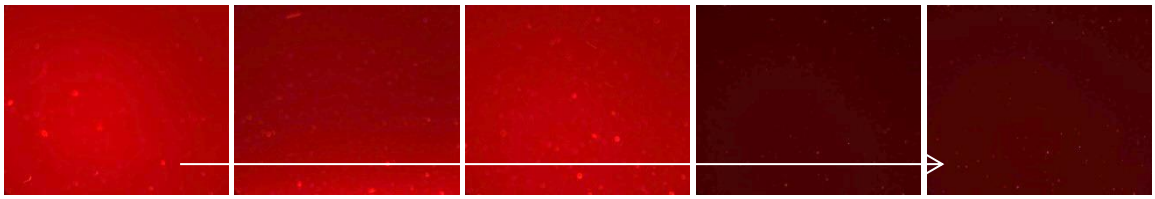

**Figure 4.45 Fluorescence Microscopy images of a POPC lipid bilayer with 1 mol % Rh-DPPE treated with 0.1 mg/ mL TC. Images shown are around 10 s apart**

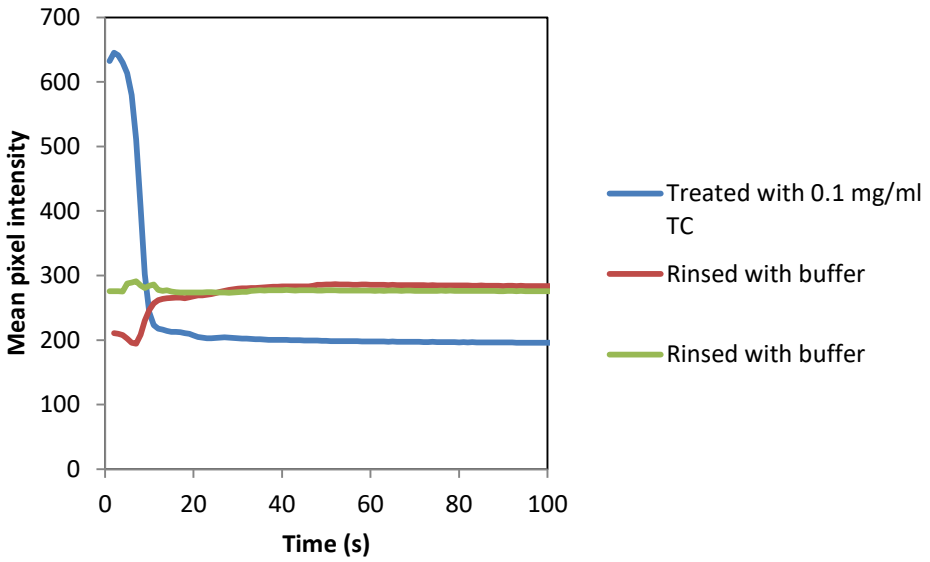


**Figure 4.46 Intensity of fluorescence (mean pixel intensity across the image) against time in s of a POPC Lipid bilayer with 1 mol % Rh-DPPE treated with 0.1 mg/ mL TC (blue), and rinsed with pH 7.4 buffer with 2 mM $CaCl_2$ after being treated (red). The bilayer was rinsed with a further half ml of buffer (green).**

A fresh bilayer was prepared and treated with a higher concentration of TC, 0.4 mg/ mL. In experiments carried out using TIR-Raman, this high concentration of TC has often led to the TC burning and to strong fluorescence from the sample. In the fluorescence microscopy experiment, the bilayer was treated several times with this concentration of TC and the bilayer did show pore development. Each time the bilayer was treated with TC, the fluorescence intensity decreased (Figure 8.16), the bilayer did not appear to form pores or be removed from the surface. When the bilayer was rinsed with buffer after treatment with TC, the fluorescence intensity increased again, but not to the intensity of the bilayer before it was treated with TC.

There are several possible reasons for the loss of fluorescence intensity. It is possible that TC quenched the rhodamine dye (Rh) and when TC was removed from the bilayer, the dye was no longer quenched. If the only effect TC had on the bilayer was quenching the dye, the fluorescence should have increased back to the original intensity, which it did not. Some of the changes in

fluorescence intensity may have been caused by photobleaching of the Rh by the laser, however the change in intensity caused by photobleaching is small compared to the total change in intensity (see Section 8.4)

Experiments were carried out using the Nanosight to understand further the effect of TC on a POPC bilayer. Vesicles were prepared using the sonicator horn to give a size of around 39 nm (Figure 4.47, Figure 4.48 and Table 4.4). The solutions were prepared so that the concentration of lipid was 0.08 mg/ mL, which gave a particle concentration within the range required for Nanosight experiments. When the lipid vesicle solution was treated with TC, the concentration and size of the vesicles decreased. The samples treated with TC were filtered before Nanosight measurements were taken using a 0.45-µm filter to remove any TC particles. The original vesicle solution was not filtered before measurement. The vesicles treated with 0.02 mg/ mL TC were around the same mode size as the original vesicles, but the concentration and the mean size were lower. The vesicles treated with a higher concentration of TC, 0.08 mg/ mL were smaller than either of the other vesicle solutions.

Vesicles were also prepared with TC and POPC combined together before the lipid mixture was hydrated, these had a size of 32 nm, smaller than the vesicles prepared with just POPC. The prepared ratio of lipid to TC was 3:1. The experiments by Jones[31–33] have previously shown that TC can be combined with phospholipids before vesicle formation and that vesicles still form. Whilst there are differences between the size and shape of the liposomes produced with and without TC in the lipid mixture, the difference may be from the preparation method. It is widely known that in sonication, there is a large batch-to-batch variation in sizes.[295]

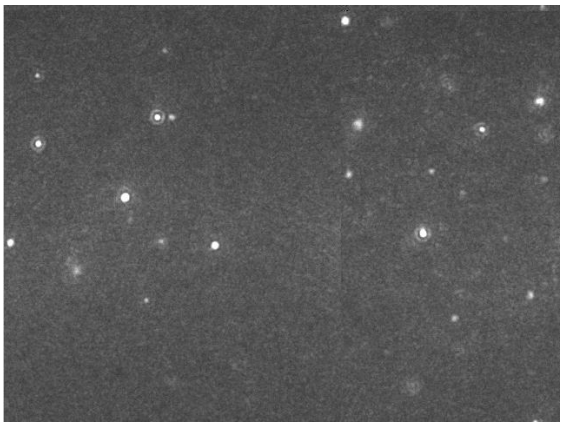

**Figure 4.47 Nanosight image of solution of POPC vesicle (0.083 mg/ mL) using 20x magnification. The light observed is light scattered by the vesicles.**

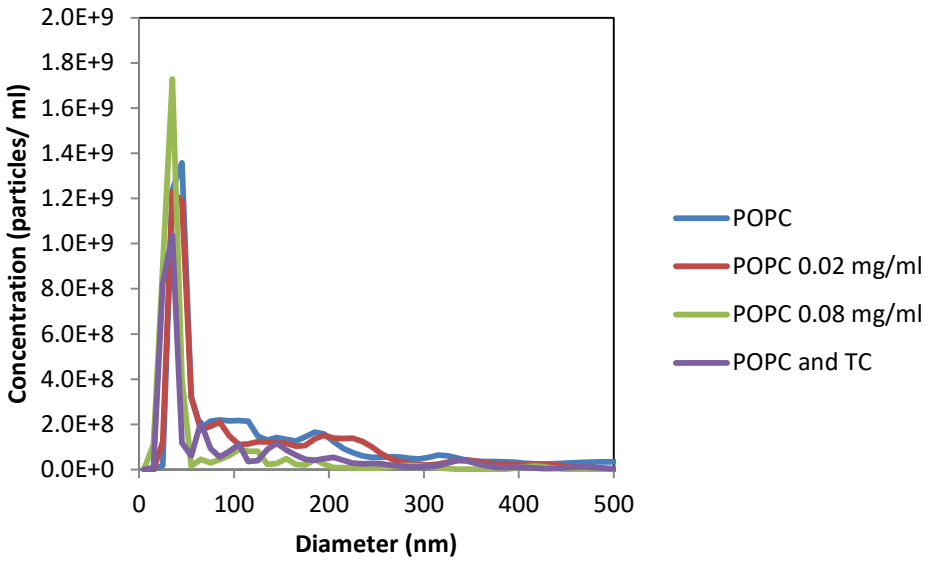


Figure 4.48 The size profile of POPC vesicles mixed with different concentrations of TC

Table 4.4 The data collected from the Nanosight for POPC vesicles mixed with different concentrations of TC and vesicles prepared with TC.

| | POPC (0.08 mg/mL lipid) | POPC mixed with 0.02 mg/ mL TC | POPC mixed with 0.08 mg/ mL TC | POPC and TC liposomes (3:1 molar ratio) |
|---|---|---|---|---|
| **mean size (nm)** | 151 ± 6 | 116 ± 5 | 54 ± 5 | 100 ± 9 |
| **mode size (nm)** | 39 ± 2 | 39 ± 2 | 31 ± 3 | 29 ± 2 |
| **SD** | 154 ± 6 | 107 ± 6 | 66 ± 6 | 110 ± 20 |
| **Concentration (particles /ml)** | 7.1 ± 0.5 x$10^9$ | 6.1 ± 0.5 x$10^9$ | 4.0 ± 0.9 x$10^9$ | 4 ± 1 x$10^9$ |

The size of the vesicles decreased with TC treatment and more of the large vesicles were removed or decreased in size and the total concentration of particles decreased. It is possible that some of the lipid that is removed from the bilayer forms micelles with TC, which are below the limit of detection of the Nanosight.

### 4.3.3 The Effect of TC on Different Membrane Types

The study was expanded to include bilayers with different properties. A bilayer with an accessible transition temperature, DMPC, was used to study the effect of TC on the transition temperature and the fluidity of the bilayer. Phospholipid mixtures that mimicked bacterial membranes were used to understand the effect of TC on bilayers with the same properties as bacterial membranes. The effect of TC on the fluidity of the bilayer was also studied by using a detergent-resistant membrane, which is in an ordered liquid phase ($L_o$) rather than the disordered phase ($L_\alpha$).

#### *4.3.3.1 The Transition Temperature of DMPC Bilayers*

In this experiment 1,2-dimyristoyl-sn-glycero-3-phosphocholine (DMPC) was used to study the effect TC has on the $T_m$ of the bilayer. TC has been shown by other workers[26,30] to fluidize the bilayer and depress the transition temperature of phospholipid bilayers. The effect of TC on DMPC bilayers

above and below the $L_\alpha$ to $L_\beta$ transition temperature, $T_m$, was investigated further. For DMPC, $T_m$= 24°C.[296]

Spectra were taken at different temperatures around $T_m$ and the ratio of the intensity of the methylene stretching peaks was compared. The effect of temperature on the DMPC spectra can be seen: the lipid peak intensity in S polarised light increased as the temperature decreased (Figure 4.49.A). The peak ratio, $I(d_-)/I(d_+)$, of DMPC remained constant between 30°C and 26°C and then increased as the temperature decreased (Figure 4.50), which is in agreement with the data collected by Lee.[265] DMPC became more ordered as the temperature decreased, going from the fluid phase to the gel phase. When there was TC in the cell (DMPC TC), the peak ratio remained the same with temperature. When the cell was rinsed with 20 mL of buffer after TC treatment the spectra did not change with temperature (Figure 4.49.B and Figure 4.50). There was no $L_\alpha$ to $L_\beta$ phase transition in the temperature range studied when TC was within the bilayer. In these experiments, no spectra were taken at 1600 $cm^{-1}$, so the concentration of TC cannot be calculated, but TC peaks were observed at 3075 $cm^{-1}$ when TC was in bulk at pH 10.8 and in the sample rinsed with 20 mL of pH 7.4 buffer (Table 4.5).

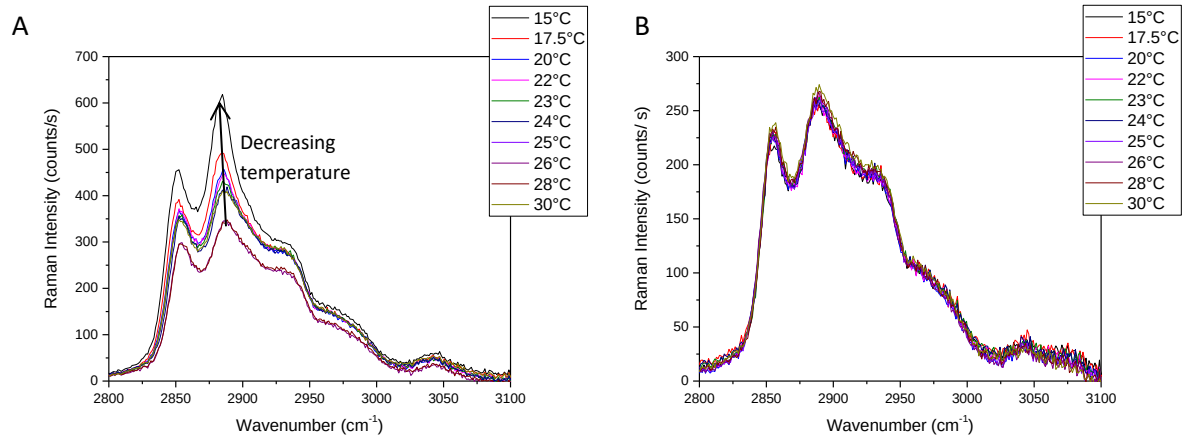


**Figure 4.49 TIR- Raman spectra collected at 2900 $cm^{-1}$ using S polarised light. (A) Spectra of DMPC supported lipid bilayer (SLB) taken at different temperatures in pH 7.4 tris buffer (20 mM). (B) Spectra of DMPC SLB after being treated with 0.1 mg/ mL TC at pH 10.8 and rinsed using 20 mL of pH 7.4 buffer taken at different temperatures. The buffer solutions used were $CaCl_2$ free. Laser power was 1000 mW**

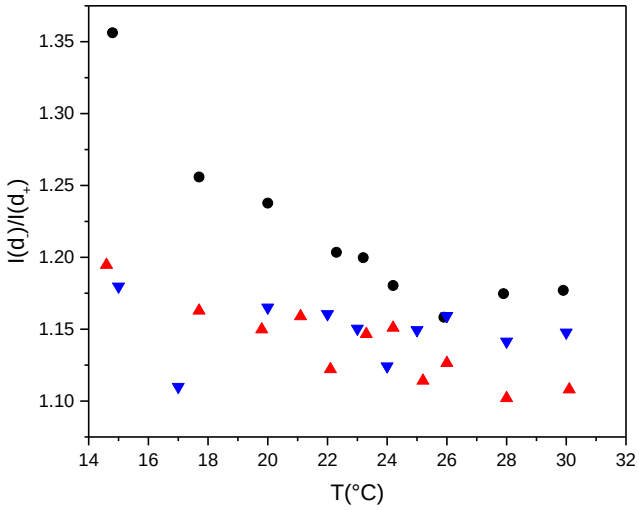


**Figure 4.50 $I(d_-)/I(d_+)$ with temperature for DMPC at pH 7.4 (●black), DMPC in a 0.1 mg/ mL TC solution at pH 10.8 (▲) and DMPC in pH 7.4 buffer after being treated with TC (▼).**

**Table 4.5 Intensity of the peak at 3075 $cm^{-1}$ at 30°C for a DMPC bilayer in pH 7.4 buffer (DMPC), treated with 0.1 mg/ mL TC at pH 10.8 (DMPC TC) and rinsed with 20 mL of pH 7.4 buffer (DMPC TCr)**

| Sample | Intensity at 3075 $cm^{-1}$/ counts/ s |
|---|---|
| DMPC | 16.7 |
| DMPC TC | 45.9 |
| DMPC TCr | 20.4 |

The experiment was then repeated with one tenth the concentration of TC, 0.01 mg/ mL TC (Figure 4.51 and Figure 4.52.A). The intensity ratio of $d_-/d_+$ when TC solution was in the cell was similar to DMPC before treatment (Figure 4.53). The gradual transition from the fluid phase to the gel phase was observed. When the cell was rinsed with 20 mL of buffer, the concentration of TC within the bilayer increased (Figure 4.52.B). The background at 1600 $cm^{-1}$ was subtracted by comparing the Raman intensity at 1650 $cm^{-1}$ (Section 8.3.2) rather than using the highest intensity peak to scale the data as in the standard background subtract function (Section 8.3.1). When the intensity of the highest point was used to scale the data before background subtraction, the intensity at 1600 $cm^{-1}$ was negative for some of the spectra after the background was subtracted. When a temperature scan was taken of the rinsed sample, the transition temperature of DMPC was reduced and the bilayer remained in the fluid state at lower temperatures than DMPC before treatment. The bilayer was rinsed with a further 50 mL of buffer and the intensity ratio did not change as strongly with temperature as for the original bilayer. A significant TC peak was observed when TC was in the bulk and which decreased upon rinsing. There was very little change in the intensity of the lipid peak at 2900 $cm^{-1}$ during the experiment although the bilayer was not restored to the original intensity after rinsing.

The area per molecule of DMPC is 60 $Å^2$.[297] When TC was in bulk at 0.01 mg/ mL, based on the intensity of the TC peak at 1600 $cm^{-1}$, the ratio of TC to lipid was 1:3 calculated from the data

collected at 30°C (Figure 4.52) and using equations 4.6-4.10. When the cell was rinsed with 20 mL of pH 7.4 buffer, the ratio of TC to lipid was 1:15.

TC suppresses the transition of DMPC from fluid phase to gel phase even when there is insufficient concentration of TC to be observed at 1600 $cm^{-1}$ and the change in lipid peak intensity at 2900 $cm^{-1}$ is small.

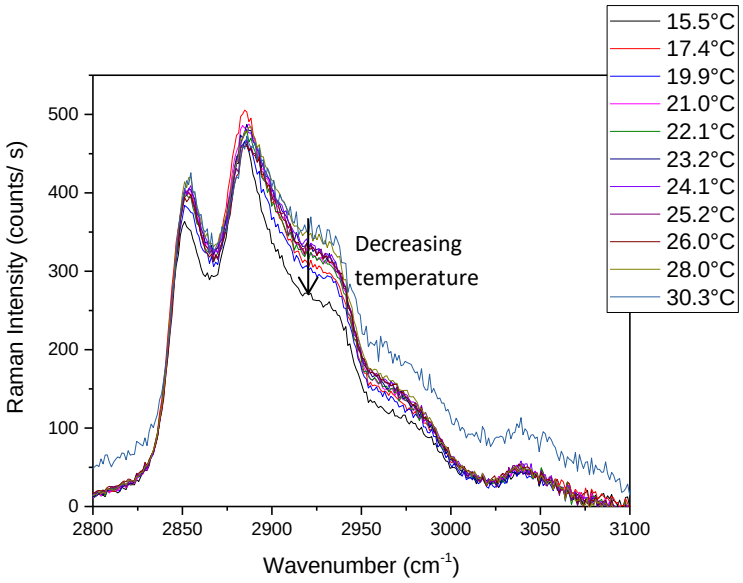


**Figure 4.51 TIR- Raman spectra collected at using S polarised light of DMPC SLB after being treated with 0.01 mg/ mL TC at pH 10.8 and rinsed using 20 mL of pH 7.4 Tris buffer taken at different temperatures. Buffer solutions were $CaCl_2$ free. Laser power was 1000 mW.**

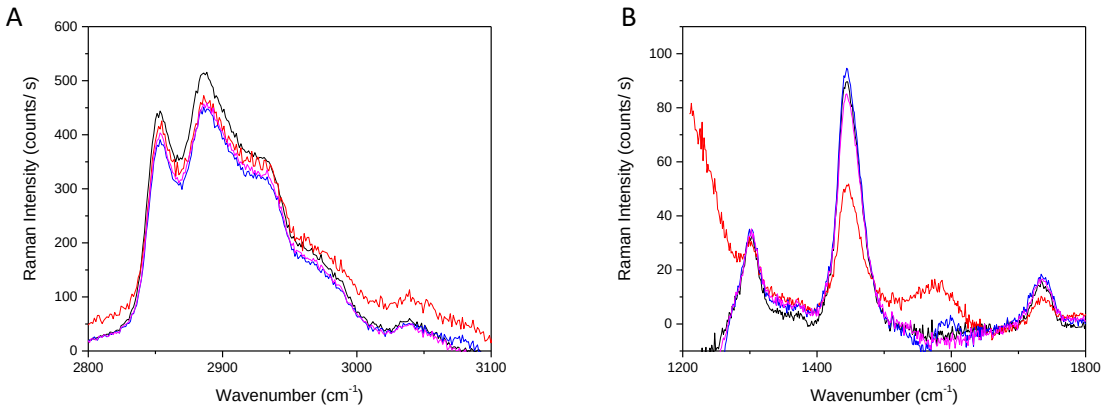


**Figure 4.52 TIR- Raman spectra collected at using S polarised light of DMPC SLB in pH 7.4 Tris buffer (black), DMPC treated with 0.01 mg/ mL TC in pH 10.8 carbonate buffer (red), DMPC after TC treatment rinsed with 20ml of pH 7.4 buffer (blue) and after TC treatment rinsed with 100ml of pH 7.4 buffer (pink) all collected at 30°C at 2900 $cm^{-1}$ (A) and 1600 $cm^{-1}$ (B). Buffer solutions were $CaCl_2$ free. Laser power was 1000 mW.**

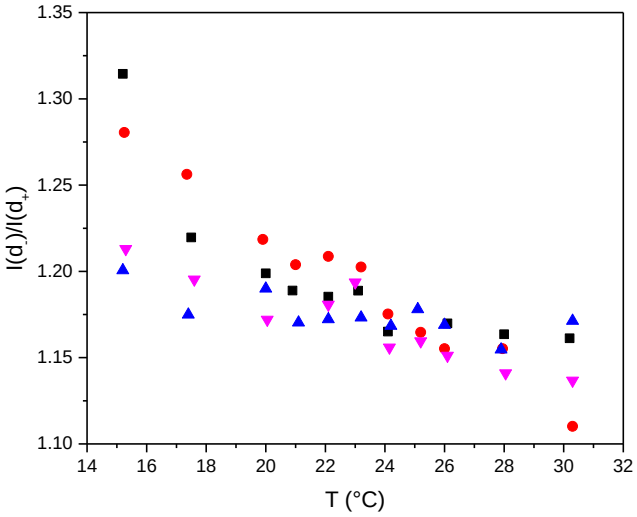


**Figure 4.53 $I(d_-)/I(d_+)$ with temperature for DMPC in pH 7.4 Tris buffer (■), DMPC in a 0.1 mg/ mL TC in pH 10.8 carbonate buffer (●), DMPC in pH 7.4 buffer after being treated with TC (▲) and DMPC after being rinsed in 100 mL of buffer (▼).**

### *4.3.3.2 Bacterial Membrane Models*

I expanded the study to include the effect of TC on phospholipid membranes that were closer to the membranes found in bacterial cells. Bacterial membranes are known to contain higher amounts of phosphatidylgylcerol (PG) than mammalian membranes. *Staphylococcus* and *Bacillus* bacteria are both well studied gram-positive bacteria. *Staphylococcus* are commonly found bacteria carried on the skin that can cause a wide range of infections from skin and soft tissue infections to invasive infections if they enter wounds or the gut.[298] *Bacillus subtilus* is commonly used as a model for gram positive bacteria and is often found in the gut.[299] *Bacillus cereus* is one of the bacteria responsible for food poisoning.[300] *Escherichia coli* is a gram negative bacteria that has been linked to diarrhea and food poisoning and is often used as a prokaryotic model organism.[301,302]

For *Staphylococcus aureus*, PG is the dominant lipid in the cell membrane at around 57%, *S. epidermis* is up to 90% PG and *Bacillus subtilus* membranes contain 29% PG.[272,273] *S. Mutans*, a bacteria commonly associated with dental plaque, has two main components of the cell membrane PG and cardolipin both of which are anionic.[303,304] Cheng[305] suggested that 1:1 PC:PG was a good model for *S. aureus* and 1:1 ratio of PE/PG was considered to be a good model for the gram positive bacteria *B. cereus*. Cheng investigated the structure and interaction of the peptide aurein 2.2 and its variants in model lipid liposomes and live bacteria to find appropriate lipid mixtures to use as models for bacterial cells.

*E. coli* membranes contain on average 74% PE and 19% PG.[168,306] Suárez-Germà[306,307] used a 3:1 ratio of POPE:POPG as a model for *E.coli* in AFM experiments on mica. From surface area-pressure isotherms on a Langmuir monolayer, the transition temperature of the mixture was 23.3°C. When Seeger[308] measured the transition temperature of the 3:1 POPE/POPG mixture using AFM, the transition temperatures of the two bilayer leaflets were observed separately, with the proximal leaflet showing a transition at around 30°C and the distal leaflet transition around the transition temperature of POPE, which is 25°C. Picas[309] found that the concentration of calcium is important for

bilayer formation of PE/PG mixtures on mica, and concentrations of calcium below 20mM lead to less than full coverage of the surface. PG head groups are negatively charged and phosphatidylethanolamine headgroups are zwitterions. Calcium ions are thought to both neutralize the negative charge of the surface and interact with the phospholipids by forming bridges. When a PE/PG bilayer forms, there may be natural separation of the lipids into PE and PG rich domains. Picas[309] suggests that the leaflet in contact with the mica becomes enriched with PG, but after mixing with a calcium-free buffer, the two leaflets mix.

Initial experiments were run with 1:1 POPE/POPG in pH 7.4 tris buffer with 2 mM $CaCl_2$; however, these experiments seemed to lead to incomplete coverage of the bilayer, with the lipid intensity being substantially lower than a POPC bilayer (Figure 4.54). When the concentration of $Ca^{2+}$ was doubled to 4 mM, the lipid intensity rose to well above the intensity of the POPC bilayer before the water background was removed and suggested a different orientation on the surface. Since there was difficulty forming a reliable bilayer in the 1:1 ratio of POPE/ POPG, the proportion of the negatively charged POPG was reduced to 25% and the buffer changed to 20 mM HEPES at pH 7.4 with 150 mM NaCl and 2 mM $CaCl_2$.

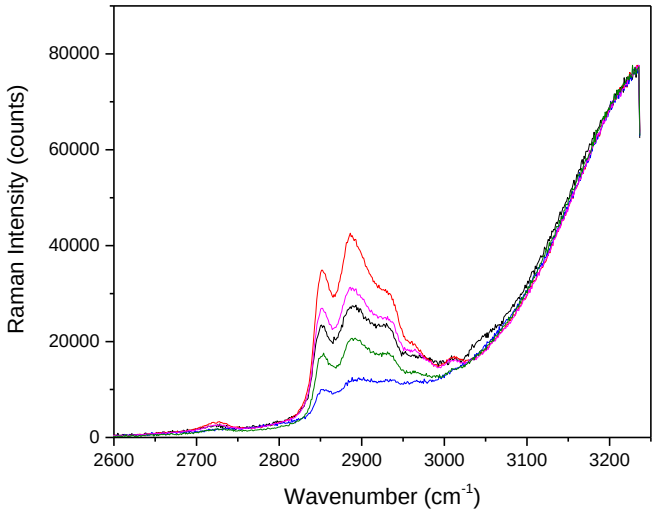


**Figure 4.54 TIR-Raman spectra collected at 2900 $cm^{-1}$ using S polarised light without the background subtracted of a POPC bilayer (black) and a 1.5:1 POPE/ POPG bilayer (red) in pH 7.4 Tris buffer with 4mM $CaCl_2$, a 1:1 POPE/POPG bilayer (blue) in pH 7.4 Tris buffer with 2mM $CaCl_2$, a 3.6:1 POPE/POPG bilayer in pH 7.4 Hepes buffer with 150 mM NaCl, 2 mM $CaCl_2$ (pink) and a 1.2: 1 POPC/POPG bilayer in pH 7.4 Tris buffer with 2 mM $CaCl_2$ (green). Laser power was 300 mW.**

When the ratio of POPE within the bilayer was increased, the bilayer had a similar intensity to the POPC bilayer suggesting near complete coverage of the silica surface. The bilayer did not appear to degrade after being prepared, a spectrum was collected an hour after the bilayer formed and showed no difference from the original peak. When treated with 0.1 mg/ mL TC, the bilayer signal reduced significantly and after rinsing, the bilayer signal decreased and did not recover with further rinsing (Figure 4.55), unlike the previous experiments with POPC. There is a clear TC peak at 3075 $cm^{-1}$ in the samples with TC in the cell and after rinsing with 20 mL of the lower pH buffer. The TC peak at 1600 $cm^{-1}$ was difficult to observe due to the shape of the lipid peak at 1650 $cm^{-1}$ (Figure 4.55.B). The $I(d_-)/I(d_+)$ peak ratio did not change significantly during the treatment with TC and

rinsing. The lipid bilayer was permanently damaged by TC treatment and the damage was made worse upon rinsing.

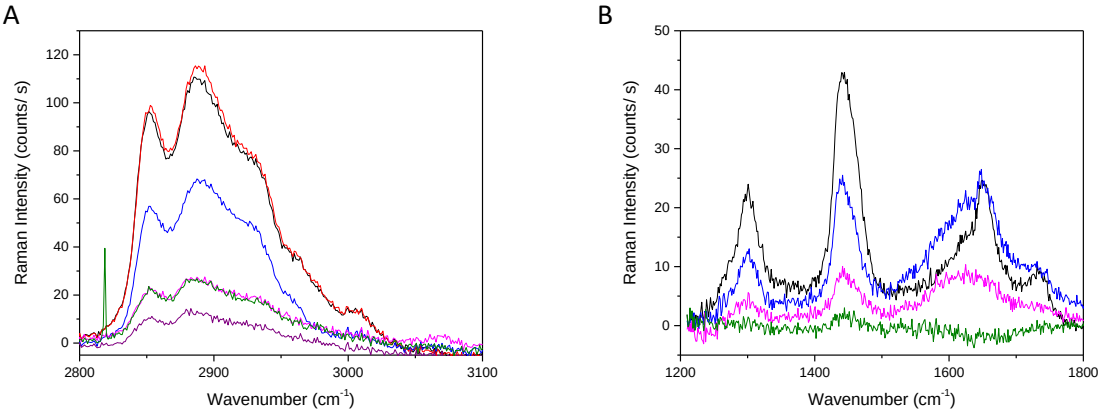


**Figure 4.55 TIR-Raman spectra collected at 2900 $cm^{-1}$ (A) and 1600 $cm^{-1}$ (B) using S polarised light a 3.6:1 POPE/ POPG bilayer (black) in pH 7.4 HEPES buffer with 2mM $CaCl_2$ and 150 mM NaCl. The bilayer was left for an hour and a further spectrum taken (red). The bilayer was treated with 0.1 mg/ mL TC at pH 10.8 for half an hour (blue) and rinsed with 20 mL of pH 7.4 buffer with 2 mM $CaCl_2$ (pink) followed by 100 mL of pH 7.4 buffer with 2 mM $CaCl_2$ (green) and left for an hour (purple). Laser power was 300 mW.**

In the experiment where a PE/PG membrane was treated with a solution of TC at pH 10.8, there was no $Ca^{2+}$ in the carbonate buffer. Picas[309] states that the concentration of $Ca^{2+}$ is important for bilayer formation and stability therefore it is important to test the stability of the bilayer in a $Ca^{2+}$-free buffer. A 2.7:1 POPE/POPG bilayer was treated with a $Ca^{2+}$ free buffer (pH 7.4 HEPES, 150 mM NaCl) and the bilayer showed no damage and did not show any further damage when the bilayer was washed with further calcium containing buffer (Figure 4.56). Whilst there was some change in lipid intensity in the different buffer, the membrane is not destroyed. The destruction of the membrane is caused by the TC rather than being treated with a $Ca^{2+}$ free buffer.

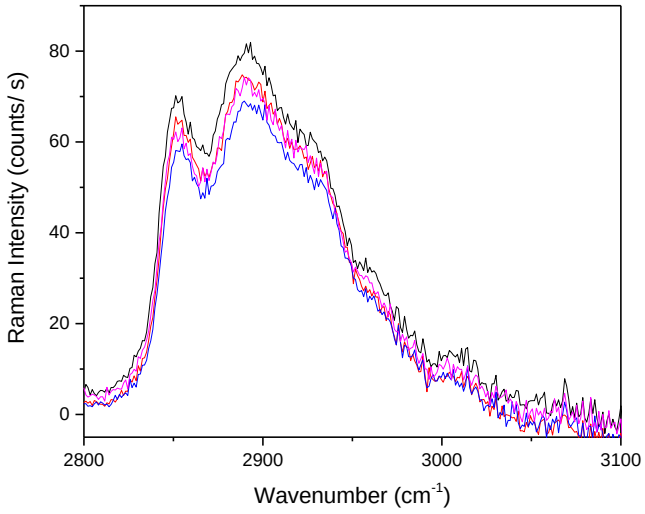


**Figure 4.56 TIR-Raman spectra collected at 2900 $cm^{-1}$ using S polarised light of a 2.7:1 POPE/ POPG bilayer (black) in pH 7.4 HEPES buffer with 2mM $CaCl_2$ and 150 mM NaCl. The bilayer was left half an hour and a further spectrum taken (red). The bilayer was treated with pH 7.4 HEPES buffer with 150 mM NaCl for half an hour (blue) and rinsed with 20 mL of pH 7.4 buffer with 2 mM $CaCl_2$ (pink). Laser power was 300 mW.**

A temperature study was carried out on the 3:1 POPE/POPG membrane in HEPES buffer, to study the effect TC has on the membrane, in a similar way to the experiments carried out with DMPC. The POPE/POPG bilayer was formed with the cell at 30°C, above the $T_m$ of POPE. As the temperature of the cell decreased, the lipid peaks in the 2900 $cm^{-1}$ region increased in intensity and shifted to lower wavenumbers (Figure 4.57.A).

The lipid peak ratio, $I(d_-)/I(d_+)$, increased with decreasing temperature between 30°C and 15°C, indicative of the change from the disordered fluid state at 30°C to the ordered gel phase at 15°C (Figure 4.58).The temperature of the bilayer was increased to 30°C and treated with 0.05 mg/ mL TC in 20 mM carbonate buffer. Spectra were taken as the temperature decreased (Figure 4.57.B). The bilayer signal decreases significantly with temperature and time in the cell. The loss of bilayer is likely to be caused by TC damaging the bilayer rather than a phase transition. The peak ratio varies randomly with temperature due to the increase in noise from the decrease in intensity (Figure 4.58). The experiment was repeated with a lower concentration of TC, 0.008 mg/ mL TC, and the bilayer signal decreased when TC was inserted into the cell and the bilayer was almost completely removed.

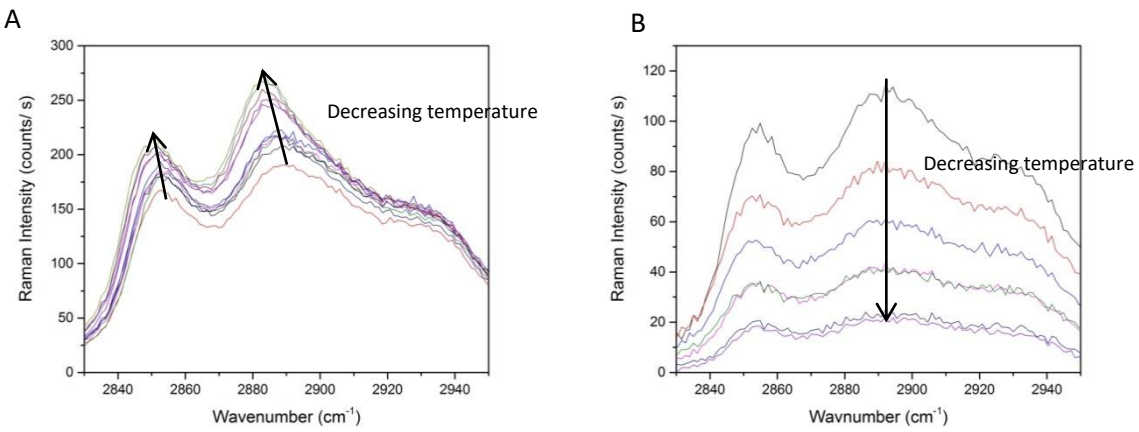


**Figure 4.57 TIR-Raman spectra collected at 2900 $cm^{-1}$ using S polarised light. Laser power was 300 mW. (A) A 3:1 POPE/POPG bilayer in pH 7.4 20 mM HEPES buffer, 2 mM $CaCl_2$ and 150 mM NaCl at different temperatures between 30°C (black) and 15°C (light blue). (B) A 3:1 POPE/POPG bilayer in pH 10.8 20 mM carbonate buffer with 0.05 mg/ mL TC at different temperatures between 30°C (black) and 21°C (purple).**

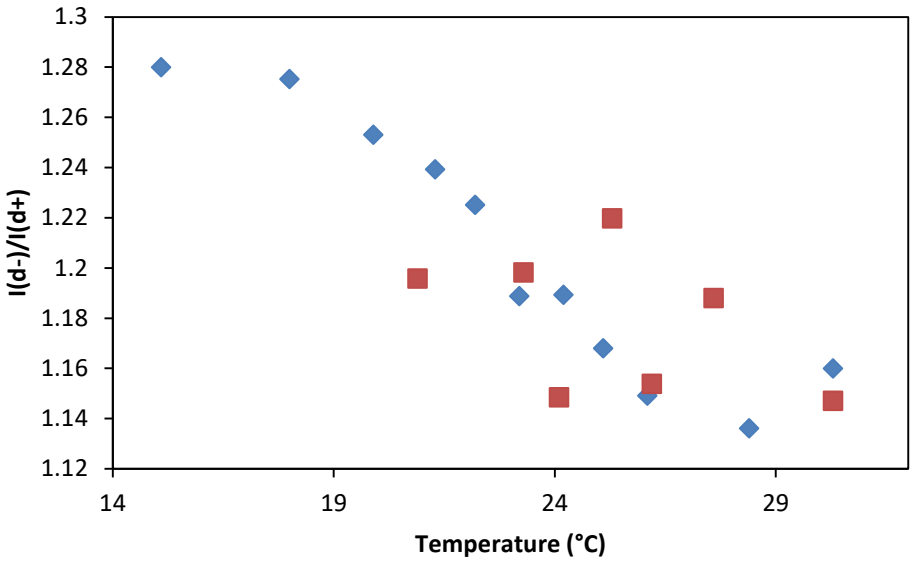


**Figure 4.58 Lipid peak intensity ratio ($I(d_-)/I(d_+)$) of 3:1 POPE/POPG at different temperatures in pH 7.4 HEPES buffer with 2 mM $CaCl_2$ and 150 mM NaCl (blue), and in pH 10.8 carbonate buffer with 0.05 mg/ mL TC (red).**

A bilayer was prepared with 3:1 ratio POPE to POPG with 0.01 molar ratio of Rh-DPPE in 20 mM HEPES with 2 mM $CaCl_2$ and 150 mM NaCl and examined by fluorescence microscopy. When the bilayer was treated with TC, at both 0.1 mg/ mL and 0.4 mg/ mL, the fluorescence intensity dropped significantly in the first 30 seconds after TC was inserted into cell the and did not recover upon rinsing (see Figure 8.17 and Figure 8.18 in the Appendix) in a manner very similar to the experiments carried out with POPC described in Section 4.3.2.6. In the images, some fluorescence remained after treatment and there was neither pore formation, nor tubule formation. The bilayer did not appear to be completely removed. The fluorescence intensity in the images after treatment was higher than a region where there was a bubble in the cell with no bilayer.

Mixtures of POPC and POPG in a 1:1 ratio were studied as an alternative model for bacterial cell membranes such as *S. aureus*. A model was used with 1.2:1 POPC/POPG in to 20 mM Tris at pH 7.4

with 2 mM $CaCl_2$. The lipid bilayer signal at 2900 $cm^{-1}$ was not as high as a POPC bilayer, but the two peaks at 2850 and 2880 $cm^{-1}$ were clear so further experiments were carried out with this bilayer (Figure 4.54). When treated with 0.01 mg/ mL TC, the bilayer signal showed no change (Figure 4.59), but when treated with 0.1 mg/ mL TC, the bilayer was strongly damaged and was not restored with rinsing (Figure 4.60).

The decrease in peak intensity was not caused by TC burning the bilayer, as there was no strong fluorescence in any of the measurements. The destruction of the membrane was also not caused by the $Ca^{2+}$-free buffer, otherwise, the destruction would be seen when the lower concentration of TC was used. The bilayer was removed from the hemisphere permanently when it was treated with 0.1 mg/ mL TC.

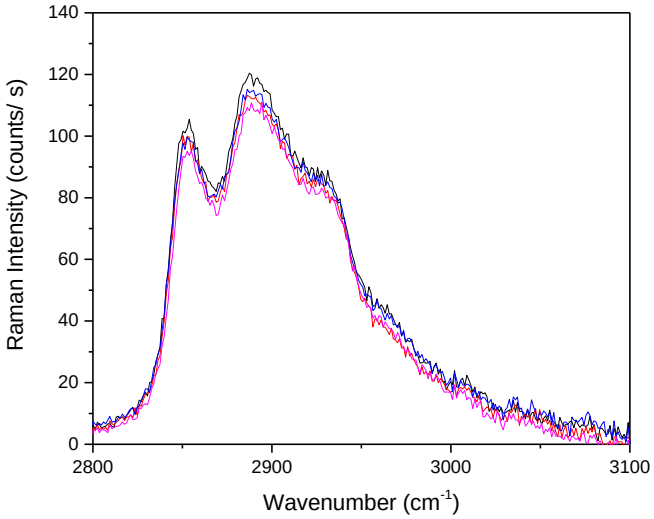


**Figure 4.59 TIR-Raman spectra collected at 2900 $cm^{-1}$ using S polarised light of a 1.2:1 POPC/ POPG bilayer (black) in pH 7.4 Tris buffer with 2mM $CaCl_2$. The bilayer was treated with 0.012 mg/ mL TC at pH 10.8 for half an hour (red) and rinsed with 20 mL of pH 7.4 buffer with 2 mM $CaCl_2$ (blue) and an extra 100 mL of buffer (pink). Laser power was 300 mW.**

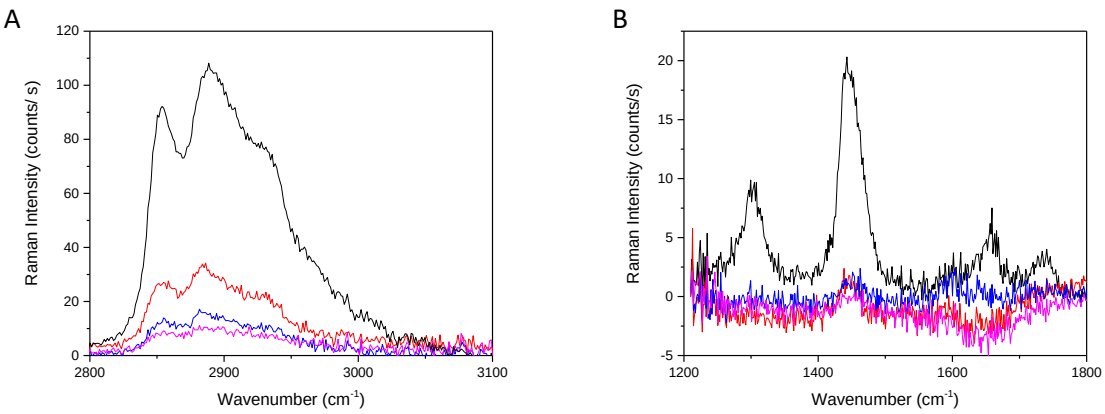


**Figure 4.60 TIR-Raman spectra collected at 2900 $cm^{-1}$ (A) and 1600 $cm^{-1}$ (B) using S polarised light of a 1.2:1 POPC/ POPG bilayer (black) in pH 7.4 Tris buffer with 2mM $CaCl_2$. The bilayer was treated with 0.12 mg/ mL TC at pH 10.8 for half an hour (red) and rinsed with 20 mL of pH 7.4 buffer with 2 mM $CaCl_2$ (blue) and an extra 100 mL of buffer (pink). Laser power was 300 mW.**

Both bilayer compositions with POPG appear to be more sensitive to TC than POPC and DMPC bilayers. In both systems, when TC damages the membrane, the damage was permanent, in contrast to POPC treated with TC, where the bilayer tended to be restored when it was rinsed with low pH buffer. Both of the bacterial membrane compositions contain high concentrations of POPG, a negatively charged lipid. Inter-molecular interactions between the lipids and $Ca^{2+}$ are essential for formation of a stable bilayer.[309] It is highly likely, that when TC becomes inserted into the membrane, it disrupts the interaction between the POPG and $Ca^{2+}$ and causes the bilayer to become more unstable. The negatively charged phenolate will also increase the charge of an already negatively charged bilayer leading to repulsion between the bilayer and the silica surface. However, it is difficult to say with certainty that the effects of TC on the supported lipid bilayers are representative of the effects in bacterial cells.

A model closest to the composition of *S. mutans* is the 1:1 POPC/POPG. A model was not developed for *S. Mutans* because both of the principal lipids are anionic[303,304] so it would be difficult to fuse a bilayer to the negatively charged hemisphere. An alternative hemisphere could be used to study these lipid mixtures as supported bilayers; for example, sapphire has a positive charge at pH 7.4.[310]

#### *4.3.3.3 Detergent Resistant Membranes*

Another phospholipid model membrane used in this study was a detergent-resistant membrane model. Detergent-resistant membranes (DRM) are so named because of their poor solubility in non-ionic surfactants such as Triton. They tend to be rich in sphingolipids and cholesterol (Chol) and a common model for DRMs is 1:1:1 POPC: Sphingomyelin: Chol.[274,275] Sphingolipids contain a backbone of sphingoid bases which are long saturated acyls chains (Table 4.1). As a consequence, they have high transition temperatures. For example, sphingomyelin (SM) has a transition temperature between 37 and 41°C.[311] The high concentrations of cholesterol in the membrane allows the formation of the liquid ordered phase ($L_o$), a phase with more chain ordering than the $L_\alpha$ phase.

I carried out experiments with a mixture of POPC: Chol: SM at room temperature (21 ±1°C) in a roughly 1:1:1 ratio, below the transition temperature of SM, but above the $T_m$ of POPC. The bilayer was in the liquid ordered phase. When a DRM was treated with 0.12 mg/ mL TC for half an hour, there was a decrease in the lipid signal at 2900 $cm^{-1}$ and a peak at 3075 $cm^{-1}$ indicating TC partitioning into the bilayer. After rinsing with 20 mL of buffer, there was a strong TC peak at 1600 $cm^{-1}$ indicating a high concentration of TC within the bilayer (Figure 4.62). The background of data at 1600 $cm^{-1}$ was subtracted by comparing the Raman intensity of the spectrum of interest and the background at 1550 $cm^{-1}$ (Section 8.3.2) rather than using the highest intensity peak to scale the data. When the highest peak was used to scale the data, the intensity at 1600 $cm^{-1}$ for some of the spectra was negative after the background was subtracted. After rinsing with 120 mL of buffer, the majority of the TC had been removed from the membrane and the lipid peak intensity increased. By the following day the lipid peak at 2900 $cm^{-1}$ was around the original intensity (Figure 4.61). The change in intensity of the lipid peak with treatment is comparable to the data collected using the single lipid POPC bilayer.

The ratio of TC to lipid was calculated using Equations 4.6-4.10, assuming the area per molecule in the bilayer is the same as POPC, 60 $Å^2$. When TC was first inserted into the cell the ratio of TC to lipid was 1:1.6, which increased after half an hour treatment with TC in pH 10.8 buffer to 1:1. When the bilayer was rinsed with 20 mL of pH 7.4 buffer, the concentration of TC in the bilayer decreased and

the ratio of TC to lipid was 1:2.2. The condensing effect of cholesterol on the area per molecule and the area per molecule of sphingomyelin were not taken into account.[275,312] If they were, the lipid molecules per TC would be higher.

When the lipid peak ratio, $I(d_-)/I(d_+)$, was investigated, there was a decrease when TC was inserted into the cell, indicating that the membrane chains had become more disordered (Figure 4.62). As the amount of TC in the bilayer decreased during rinsing, the peak ratio increased, suggesting that the bilayer became more ordered when there was less TC to disrupt the membrane. When the membrane was rinsed with 100 mL of buffer and left for an hour, the $I(d_-)/I(d_+)$ peak ratio returned to the original value. The following day for the lipid peak intensity returned to the original intensity.

The results are very similar to the results with POPC bilayers, except for the change in the bilayer ordering. POPC is in the liquid disordered phase before treatment with TC. The lipid peak intensity for the DRM follows the same pattern as the experiments with POPC, where the bilayer intensity decreases with TC in the cell and is restored upon rinsing, sometimes taking an hour or more to return to original peak intensity. It takes time for the bilayer to recover after being treated with TC, but it does return to the original order.

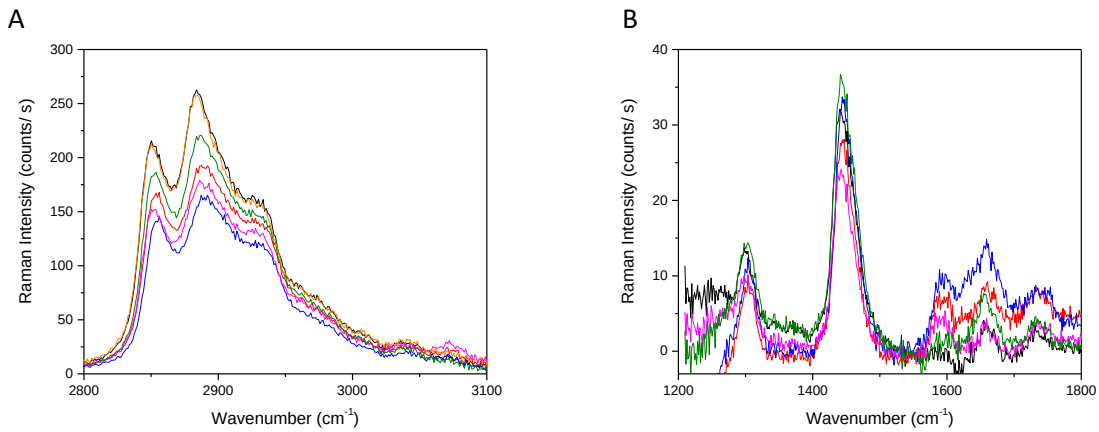


**Figure 4.61 TIR-Raman spectra collected at 2900 $cm^{-1}$ (A) and 1600 $cm^{-1}$ (B) using S polarised light at 21 ±1°C. Laser power was 300 mW. DRM with 1.1: 1.7: 1 POPC: Chol: SM in pH 7.4 tris buffer with 2 mM $CaCl_2$ (black), DRM in 0.12 mg/ mL TC solution at pH 10.8 measured straight away (red) and after 30 minutes (blue), DRM after being treated with TC and rinsed with 20 mL of pH 7.4 tris buffer with 2 mM $CaCl_2$ (pink) and rinsed with 120 mL of pH 7.4 tris buffer with 2 mM $CaCl_2$ (green) and left overnight (orange).**

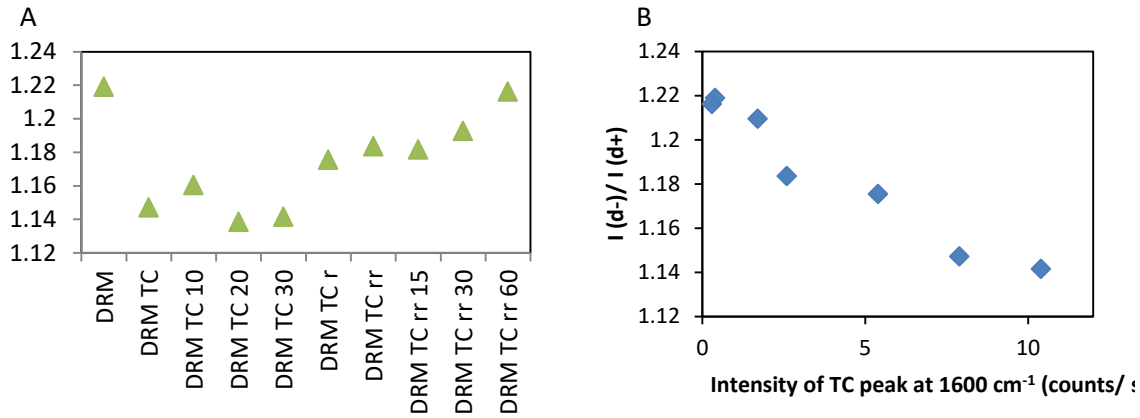


**Figure 4.62 The peak ratio of DRM under treatment with TC against sample (A) and against intensity of the TC peak at 1600 cm−1. The samples are DRM with 1.1: 1.7: 1 POPC: Chol: SM in pH 7.4 tris buffer with 2 mM CaCl2 (DRM), DRM in 0.12 mg/ mL TC solution at pH 10.8 measured straight away (DRM TC) and measured every 10 minutes for 30 minutes (blue), DRM after being treated with TC and rinsed with 20 mL of pH 7.4 tris buffer (DRM TC r) and rinsed with 120 mL of pH 7.4 tris buffer (DRM TC rr).**

## 4.4 Conclusions

TC inserts into POPC bilayers when the bilayer is treated with TC at pH 10.8. When TC inserted into the bilayer, the intensity of lipid bilayer signal decreased. In some experiments, the loss of bilayer signal is permanent. The temporary loss may be due to protrusions that form from the bilayer upon the insertion of TC and are drawn back into the bilayer upon rinsing. If the bilayer lifts from the surface as a whole, it would still be in the evanescent wave, but the electric field would be weaker. In an ionic strength of 0.02 M, the Debye length is approximately 2 nm so the electrostatic interaction between the bilayer and the surface would decay to zero within 10 nm, which is not enough to account for the drop in signal observed. In other experiments, when the bilayer was extensively rinsed with pH 7.4 buffer, the lipid signal intensity increased, suggesting that the material removed from the bilayer was drawn back in. The change was not due to the change in buffer, but was caused by TC. This reversible change in intensity was not due to tubule formation, which is what occurs when a POPC bilayer is treated with SDS, as in the experiments by Eis[293] and Churchwell.[179]

In most experiments when the bilayer was rinsed with pH 7.4 buffer after being treated with TC, the concentration of TC within the bilayer increased. As the pH decreased, the phenol form of TC dominated rather than the phenolate form because the diffusivity of $H^+$>>TC, so the pH drops before TC diffuses into the buffer. The phenol partitions much more strongly into the bilayer, due in part to the much lower aqueous solubility of TC compared to $TC^-$. This led to a higher concentration of TC in the bilayer than when the phenolate was in solution. In some experiments, TC crystallised on the bottom of the hemisphere, which led to very high TC peaks. I developed a method to estimate the concentration of TC within the POPC membrane, and lipid-to-TC ratios of between 18:1 and 0.8:1 molecules of lipid to TC when there was TC in the bulk solution.

When TC crystallised on the bottom of the hemisphere, rinsing the cell quickly with a lot of buffer did not remove all the TC. In some experiments, when the cell was rinsed with 120 mL of buffer, there were still TC peaks at 1600 $cm^{-1}$. When the rinse process was slowed down, TC was removed from the bilayer after around 65 mL of buffer was used. However, in the experiment where the

buffer used to rinse the cell was above the pKa of TC, after the first 20 mL of buffer, TC was removed from the bilayer.

I explored the rinsing of the POPC bilayers after they were treated with TC by slowing down the rinsing step. For example when adding 7 mL of buffer over an hour and a half, the TC peak decreased upon rinsing and the lipid peak increased as the TC peak decreased. When the buffer is pumped through slowly, the pH change in the cell is sufficiently slow that the phenolate can diffuse away from the membrane before it is converted into the phenol form. This suggests that to remove TC from the bilayers, the time taken to rinse the bilayer is as important as the volume of buffer used.

If TC were applied to skin in a hand-washing process at high pH, for example from a sodium laurate solution, and the hands were only rinsed quickly with plain water, the TC would go from phenolate to crystals of TC, which would require a lot of rinsing to remove. In this handwashing regime, the antibacterial TC would remain on the hands for a long time, ensuring antibacterial protection between hand washes.

I have used DMPC SLBs to observe the change in gel-to-fluid phase transition in the presence of TC. TC fluidizes the bilayer and suppresses the transition temperature as shown by other authors.[26,30] When the bilayer was treated with 0.01 mg/ mL TC, the transition temperature did not change when there was TC in the bulk. However, when the bilayer was rinsed with 20 mL of pH 7.4 buffer, the transition was suppressed.

Bilayers that are models of bacterial membranes are not as stable as POPC alone and do not appear to give full bilayer coverage. Forming membranes with 50/50 POPE and POPG was difficult so the ratio of POPG was decrease to 25 mol%. In these membranes, TC damaged the bilayer, with the lipid signal decreasing upon rinsing. The bilayer signal was not restored in the way that it is with the POPC system. I saw similar effects when I treated a POPC/POPG 50/50 membrane, although the damage depended more on the concentration of TC used in the treatment. When 0.01 mg/ mL TC was used, there was no damage, but when 0.1 mg/ mL TC was used, the bilayer was removed. For these two membrane types, there is some doubt over whether the effects seen under TC treatment are representative of the effect in *vivo,* or whether they are just representative of a negatively charged bilayer fused onto a silica hemisphere. When $TC^-$ inserts into an already negatively charged bilayer, there will be an increase in the repulsion between the bilayer and the negatively charged silica surface. Both of the bacterial membrane compositions with high concentrations of POPG, inter-molecular interactions between the lipids and $Ca^{2+}$ are essential for formation of a stable bilayer.[309] It is highly likely, that when TC becomes inserted into the membrane, it disrupts the interaction between the POPG and $Ca^{2+}$ and causes the bilayer to become more unstable.

In DRMs, which are more rigid membranes than a POPC bilayer, the effect of TC was similar to that observed with POPC, in that the lipid signal decreased with TC in the cell and was restored with rinsing. One distinct effect that was observed was an increase in the disorder, when TC was inserted the $I(d_-)/I(d_+)$ peak ratio decreased. During rinsing, the order in the bilayer increased and returned to the original peak ratio an hour after the cell was rinsed with 120 mL of buffer.

TC has been shown to insert into bilayers and in some cases TC destroys the bilayer. When rinsing is rapid, TC crystallises at the interface and remains even when the cell is rinsed with up to 10 times the volume of the cell. It takes time for the bilayer to recover after treatment with TC.

# 5 Conclusions

In this thesis, I have used a range of techniques to study the lifecycle of the active ingredient Triclosan. Each technique provides information on the different stages of the lifecycle or focuses on different parts of the system at the same lifecycle stage. All of the methods were chosen to complement one another and each part of this thesis builds towards a more complete picture of TC in personal care products. The parts can be taken and applied to other active ingredients in similar formulations. The limitations of each of the techniques used are described in each of the chapters and discussed more generally here.

An example of the way different techniques supplement one another is that the results from Chapter 2 were essential for the calculations carried out in Chapter 3. In Chapter 2, I found the CMC of the surfactants with TC from IFT measurements, which allowed the concentration of surfactant in micelles to be calculated. From SANS analysis, the aggregation number of the surfactant was found so that the number of micelles could be calculated. In Chapter 3, partition coefficients were found by fitting data in plots of $\delta_{obs}$ and the concentration of surfactant in micelles. The concentration of phenol and phenolate in micelles could be found from the partition coefficients, $K_-$ and $K_+$ which allowed the number of molecules of phenol and phenolate per micelle to be calculated, using the aggregation number. The concentration range studied included the 1% surfactant, the concentration used in personal care products[97] and lower concentrations to just above the CMC.

In the NMR experiments, the shifts of the active ingredient peaks have to change between micelles and bulk to be able to calculate partitioning and the peaks cannot overlap with one another or the surfactant peaks. For active ingredients with aromatic groups, ring currents should be considered when fitting $\delta_{obs}$, especially when there is a high concentration of solute per micelle. In the systems studied with TC, the effect of ring currents was not significant in terms of the fitted values of $K_+$ and $K_-$.

For TC, NMR was used to determine the partitioning between bulk and micelles in preference to UV-Vis absorbance techniques. In the UV-Vis experiments, there was a decrease in the extinction coefficient for TC in surfactant as compared to the phenolate in bulk and the phenol in methanol. $\lambda_{max}$ varied with the presence of the phenol and the phenolate. There was difficulty in determining the proportion of phenol to phenolate in the system using $\lambda_{max}$ alone when the error in $\lambda_{max}$ and the bandwidth of the spectrometer were taken into account, for example see Figure 2.20.

In solution state NMR, solid TC does not contribute to the narrow NMR peaks in the proton spectrum because it does not undergo rapid tumbling. Particles that develop in the solution, as seen in the experiments in Section 2.3.5 by Nanosight, are not observed by NMR. The information provided by the NMR experiments in Chapter 3 does not provide information about the equilibration time after the solution was diluted from a stock solution. I briefly used stopped flow with UV-Vis as described in Section 2.3.4 to attempt to understand the equilibration process after dilution but the observed changes to spectra were caused by many different factors including photo-reactivity and particles crystallising so that repeatability and interpretation were problematic.

The effect of TC at one of the sites of action was investigated using TIR-Raman on lipid bilayers. TIR-Raman was used as the main technique for studying TC insertion into lipid bilayers because TC can be spectroscopically observed separate from the lipid region.

In the TIR-Raman experiments, during TC insertion the lipid peak intensity decreased and then increased after the bilayer was rinsed with buffer. For the lipid bilayers containing POPG, the bilayer was completely removed after TC treatment. Some of this effect is likely to be a consequence of studying a supported lipid bilayer on silica and the negatively charged phenolate causing the bilayer to be repelled from the surface. The effects of TC on the lipid bilayer may not be representative of the interaction *in vivo.*

Once TC crystallised on the surface of the hemisphere, it was resistant to rinsing. To remove TC from the bilayers, the time taken to rinse the bilayer is as important as the volume of buffer used and the pH.

If TC were applied to skin in a hand-washing process at high pH, for example from a sodium laurate solution, and the hands were only rinsed quickly with plain water, the dissolved phenolate TC would crystallise and require significant rinsing to remove from the cell membranes. In this handwashing regime, the antibacterial TC would remain on the hands for a long time, ensuring antibacterial protection between hand washes. This is in agreement with the work described by other workers above which showed significant TC retention several hours after application in human volunteers even after rinsing.[11,41–43]

If AFM or fluorescence microscopy had been instead of TIR-Raman, the effect of TC on the lipid would be observed but it would not be possible to calculate the ratio of lipid to TC in the bilayer. TIR-Raman has been used to study the insertion of other small molecules into the bilayer, such as SDS,[179,293] when the lipid peaks overlap with the peaks of the small molecule. Often, the small molecule is deuterated to deconvolute the insertion of the small molecule into the bilayer separately from the effect of the molecule on the bilayer. This technique can be used for other bilayer active molecules in personal care products if the peaks overlap with the lipid peaks.

The methods discussed and described in this thesis should be applied to novel antimicrobials for personal care products as part of the product development procedure. The ratio of acid to base can have an effect on the activity of the ingredient, as discussed in the TIR-Raman experiments on lipid bilayers in Chapter 4. For a pH sensitive molecule, it is important to understand the partitioning and how it is affected by surfactants and the pH of the formulation. For antibacterial ingredients with a lower pKa than TC, the ratio of acid to base in personal care products may be very sensitive to concentration of the surfactant. For TC, in SDS with no buffer, the predominant form of TC is the phenol in the micelles, whereas in SL with no added buffer, the proportion of phenol to phenolate changes with the concentration of SL. The specific action of TC on FabI is also sensitive to pH because the interaction is partly through the phenol group (see Figure 1.4).[25] To interpret the NMR data to find the partitioning coefficients, a number of the experiments detailed in Chapter 2 have to be carried out, such as finding the CMC of the surfactant at the appropriate active ingredient concentration.

The mode of action of the AI must be known to understand the effect of the acid and base in micelles and bulk on the bacteriostatic effect and the bioavailability of the active ingredient. The membrane activity of the active ingredient can be investigated by TIR-Raman as shown in Chapter 4. The techniques used and developed here can be used in future to investigate the lifecycle of other similar active ingredients. It is of vital importance to understand the lifecycle before a novel

antimicrobial is released to market and to continue research after release to develop understanding of the negative consequences of the antimicrobial and mitigate against them.

# 6 Bibliography


(1) FDA. Safety and Effectiveness of Consumer Antiseptics; Topical Antimicrobial Drug Products for Over-the-Counter Human Use; Proposed Amendment of the Tentative Final Monograph; Reopening of Administrative Record https://www.federalregister.gov/articles/2013/12/17/2013-29814/safety-and-effectiveness-of-consumer-antiseptics-topical-antimicrobial-drug-products-for (accessed Dec 17, 2013).

(2) *Unilever Sustainability Plan*; 2012.

(3) Shaw, C. House Passes Triclosan Retail Ban http://www.house.leg.state.mn.us/SessionDaily/SDView.aspx?StoryID=5284 (accessed Sep 15, 2014).

(4) Fiss, E. M.; Rule, K. L.; Vikesland, P. J. Formation of Chloroform and Other Chlorinated Byproducts by Chlorination of Triclosan-Containing Antibacterial Products. *Environ. Sci. Technol.* **2007**, *41*, 2387–2394.

(5) Bedoux, G.; Roig, B.; Thomas, O.; Dupont, V.; Le Bot, B. Occurrence and Toxicity of Antimicrobial Triclosan and By-Products in the Environment. *Environ. Sci. Pollut. Res. Int.* **2012**, *19* (4), 1044–1065.

(6) Lindström, A.; Buerge, I. J.; Poiger, T.; Bergqvist, P.-A.; Müller, M. D.; Buser, H. R. Occurrence and Environmental Behavior of the Bactericide Triclosan and Its Methyl Derivative in Surface Waters and in Wastewater. *Environ. Sci. Technol.* **2002**, *36* (11), 2322–2329.

(7) Latosińska, J. N.; Latosińska, M.; Tomczak, M. a; Seliger, J.; Zagar, V.; Maurin, J. K. Conformations and Intermolecular Interactions Pattern in Solid Chloroxylenol and Triclosan (API of Anti-Infective Agents and Drugs). A 35 Cl NQR, 1 H-14 N NQDR, X-Ray and DFT/QTAIM Study. *Magn. Reson. Chem.* **2012**, No. February, 89–105.

(8) Loftsson, T.; Ossurardóttir, I. B.; Thorsteinsson, T.; Duan, M. S.; Masson, M. Cyclodextrin Solubilization of the Antibacterial Agents Triclosan and Triclocarban: Effect of Ionization and Polymers. *J. Incl. Phenom. Macrocycl. Chem.* **2005**, *52* (1), 109–117.

(9) Moran, J.; Addy, M.; Jackson, R.; Newcombe, R. G. Comparative Effects of Quaternary Ammonium Mouthrinses on 4-Day Plaque Regrowth. *J. Clin. Periodontol.* **2000**, *27* (1), 37–40.

(10) du Preez, J. L.; Yang, W.; Grove, C.; de Villiers, M. M. Improving the Aqueous Solubility of Triclosan by Solubilization, Complexation, and in Situ Salt Formation. *J. Cosmet. Sci.* **2003**, *54* (December), 537–550.

(11) Hagedorn-Leweke, U.; Lippold, B. Absorption of Sunscreens and Other Compounds Through Human Skin inVivo: Derivation of a Method to Predict Maximum Fluxes. *Pharm. Res.* **1995**, *12* (9), 1354–1360.

(12) Ramos, A. I.; Braga, S. S.; Almeida Paz, F. a. Triclosan. *Acta Crystallogr. C.* **2009**, *65* (Pt 8), 404–405.

(13) Latosińska, J. N.; Tomczak, M. A.; Kasprzak, J. Thermal Stability and Molecular Dynamics of Triclosan in Solid State Studied by 35Cl–NQR Spectroscopy and DFT Calculations. *Chem. Phys. Lett.* **2008**, *462* (4–6), 284–288.

(14) Latosińska, J. N.; Latosińska, M.; Tomczak, M. A.; Medycki, W. Conformational Stability and Thermal Pathways of Relaxation in Triclosan (Antibacterial/Excipient/Contaminant) in Solid-

State. Combined Spectroscopic (1H NMR) and Computational (Periodic DFT) Study. *J. Phys. Chem. A* **2015**, *119* (20), 4864–4874.

(15) McDonnell, G.; Russell, A. D. Antiseptics and Disinfectants: Activity, Action, and Resistance. *Clin. Microbiol. Rev.* **1999**, *12* (1), 147–179.

(16) Bhargava, H. N.; Leonard, P. A. Triclosan : Applications and Safety. *Am. J. Infect. Control* **1996**, *24* (3), 209–218.

(17) Todar, K. Structure and Function of Bacterial Cells. In *Todar's Online Textbook of Bacteriology*; Madison, Wisconsin, 2012; p 5.

(18) Heath, R. J.; Rubin, J. R.; Holland, D. R.; Zhang, E.; Snow, M. E.; Rock, C. O. Mechanism of Triclosan Inhibition of Bacterial Fatty Acid Synthesis. *J. Biol. Chem.* **1999**, *274* (16), 11110–11114.

(19) Slater-Radosti, C.; Van Aller, G.; Greenwood, R.; Nicholas, R.; Keller, P. M.; DeWolf, W. E.; Fan, F.; Payne, D. J.; Jaworski, D. D. Biochemical and Genetic Characterization of the Action of Triclosan on Staphylococcus Aureus. *J. Antimicrob. Chemother.* **2001**, *48* (1), 1–6.

(20) Saleh, S.; Haddadin, R. N. S.; Baillie, S.; Collier, P. J. Triclosan – an Update. *Lett. Appl. Microbiol.* **2011**, *52* (2), 87–95.

(21) Levy, C. W.; Roujeinikova, A.; Sedelnikova, S.; Baker, P. J.; Stuitje, A. R.; Slabas, A. R.; Rice, D. W.; Rafferty, J. B. Molecular Basis of Triclosan Activity. *Nature* **1999**, *398*, 383–384.

(22) McMurry, L. M.; Oethinger, M.; Levy, S. B. Triclosan Targets Lipid Synthesis. *Nature* **1998**, *394* (6693), 531–532.

(23) Web of Science apps.webofknowledge.com (accessed Mar 16, 2016).

(24) Bergler, H.; Fuchsbichler, S.; Högenauer, G.; Turnowsky, F. The Enoyl-[Acyl-Carrier-Protein] Reductase (FabI) of Escherichia Coli, Which Catalyzes a Key Regulatory Step in Fatty Acid Biosynthesis, Accepts NADH and NADPH as Cofactors and Is Inhibited by Palmitoyl-CoA. *Eur. J. Biochem.* **1996**, *242* (3), 689–694.

(25) Maity, K.; Bhargav, S. P.; Sankaran, B.; Surolia, N.; Surolia, A.; Suguna, K. X-Ray Crystallographic Analysis of the Complexes of Enoyl Acyl Carrier Protein Reductase of Plasmodium Falciparum with Triclosan Variants to Elucidate the Importance of Different Functional Groups in Enzyme Inhibition. *IUBMB Life* **2010**, *62* (6), 467–476.

(26) Lygre, H.; Moe, G.; Skalevik, R.; Holmsen, H. Interaction of Triclosan with Eukaryotic Membrane Lipids. *Eur. J. Oral Sci.* **2003**, *111*, 216–222.

(27) Corbin, A.; Pitts, B.; Parker, A.; Stewart, P. S. Antimicrobial Penetration and Efficacy in an in Vitro Oral Biofilm Model. *Antimicrob. Agents Chemother.* **2011**, *55* (7), 3338–3344.

(28) Singh, M. P. Rapid Test for Distinguishing Membrane-Active Antibacterial Agents. *J. Microbiol. Methods* **2006**, *67* (1), 125–130.

(29) Zuckerbraun, H. L.; Babich, H.; May, R. J.; Sinensky, M. C. Triclosan : Cytotoxicity, Mode of Action, and Induction of Apoptosis in Human Gingival Cells in Vitro. *Eur. J. Oral Sci.* **1998**, *106* (16), 628–636.

(30) Villalaín, J.; Mateo, C. R.; Aranda, F. J.; Shapiro, S.; Micol, V. Membranotropic Effects of the Antibacterial Agent Triclosan. *Arch. Biochem. Biophys.* **2001**, *390* (1), 128–136.

(31) Jones, M. N.; Francis, S. E.; Hutchinson, F. J.; Handley, P. S.; Lyle, I. G. Targeting and Delivery of Bactericide to Adsorbed Oral Bacteria by Use of Proteoliposomes. *Biochim. Biophys. Acta - Biomembr.* **1993**, *1147* (2), 251–261.

(32) Kaszuba, M.; Robinson, A. M.; Song, Y. H.; Creeth, J. E.; Jones, M. N. The Visualisation of the Targeting of Phospholipid Liposomes to Bacteria. *Colloids Surfaces B Biointerfaces* **1997**, *8* (6), 321–332.

(33) Jones, M. N.; Kaszuba, M.; Reboiras, M. D.; Lyle, I. G.; Hill, K. J.; Song, Y.-H.; Wilmot, S. W.; Creeth, J. E. The Targeting of Phospholipid Liposomes to Bacteria. *Biochim. Biophys. Acta - Biomembr.* **1994**, *1196* (1), 57–64.

(34) Guillén, J.; Bernabeu, A.; Shapiro, S.; Villalaín, J. Location and Orientation of Triclosan in Phospholipid Model Membranes. *Eur. Biophys. J.* **2004**, *33* (5), 448–453.

(35) Orsi, M.; Noro, M. G.; Essex, J. W. Dual-Resolution Molecular Dynamics Simulation of Antimicrobials in Biomembranes. *J. R. Soc. Interface* **2011**, *8* (59), 826–841.

(36) Lubarsky, H. V; Gerbersdorf, S. U.; Hubas, C.; Behrens, S.; Ricciardi, F.; Paterson, D. M. Impairment of the Bacterial Biofilm Stability by Triclosan. *PLoS One* **2012**, *7* (4), 1–16.

(37) Barboza-Silva, E.; Castro, A. C. D.; Marquis, R. E. Fluoride, Triclosan and Organic Weak Acids as Modulators of the Arginine Deiminase System in Biofilms and Suspension Cells of Oral Streptococci. *Oral Microbiol. Immunol.* **2009**, *24* (4), 265–271.

(38) Marsh, P. D. Plaque as a Biofilm: Pharmacological Principles of Drug Delivery and Action in the Sub- and Supragingival Environment. *Oral Dis.* **2003**, *9*, 16–22.

(39) Vroom, J. M.; Grauw, K. J. De; Gerritsen, H. C.; Bradshaw, D. J.; Marsh, P. D.; Watson, G. K.; Birmingham, J. J.; Allison, C. Depth Penetration and Detection of pH Gradients in Biofilms by Two-Photon Excitation Microscopy Depth Penetration and Detection of pH Gradients in Biofilms by Two-Photon Excitation Microscopy. *Appl. Environ. Microbiol.* **1999**, *65*, 3502–3511.

(40) Loftsson, T.; Leeves, N.; Bjornsdottir, B.; Duffy, L.; Masson, M. Effect of Cyclodextrins and Polymers on Triclosan Availability and Substantivity in Toothpastes in Vivo. *J. Pharm. Sci.* **1999**, *88* (12), 1254–1258.

(41) Cummins, D.; Creeth, J. E. Delivery of Antiplaque Agents from Dentifrices, Gels, and Mouthwashes. *J. Dent. Res.* **1992**, *71* (7), 1439–1449.

(42) Gilbert, R. J.; Williams, P. E. The Oral Retention and Antiplaque Efficacy of Triclosan in Human Volunteers. *Br. J. Clin. Pharmacol.* **1987**, *23* (5), 579–583.

(43) Nole, G.; Johnson, A.; Znaiden, A.; Resch, C. Antibacterial Lotion Testing: A Practical Approach to Demonstrate the Antibacterial Efficacy of a Triclosan-Containing Leave-on Moisturizer. *Int. J. Cosmet. Sci.* **2000**, *22* (5), 341–347.

(44) Veiga, M. D.; Merino, M.; Cirri, M.; Maestrelli, F.; Mura, P. Comparative Study on Triclosan Interactions in Solution and in the Solid State with Natural and Chemically Modified Cyclodextrins. *J. Incl. Phenom. Macrocycl. Chem.* **2005**, *53* (1-2), 77–83.

(45) Aragon, D. M.; Ruidiaz, M. A.; Vargas, E. F.; Bregni, C.; Chiappetta, D. A.; Sosnik, A.; Martınez, F. Solubility of the Antimicrobial Agent Triclosan in Organic Solvents of Different Hydrogen Bonding Capabilities at Several Temperatures. *J. Chem. Eng. Data* **2008**, *53*, 2576–2580.

(46) Zhang, H.; Wang, D.; Butler, R.; Campbell, N. L.; Long, J.; Tan, B.; Duncalf, D. J.; Foster, A. J.; Hopkinson, A.; Taylor, D.; et al. Formation and Enhanced Biocidal Activity of Water-Dispersable Organic Nanoparticles. *Nat. Nanotechnol.* **2008**, *3* (8), 506–511.

(47) Kim, J.-C.; Lee, H. Y.; Kim, M. H.; Lee, H.-J.; Kang, H.-Y.; Kim, S. M. Preparation and Characterization of Chitosan/gelatin Microcapsules Containing Triclosan. *Colloids Surfaces B Biointerfaces* **2006**, *52* (1), 52–56.

(48) Huang, H.-Y.; Lai, Y.-C.; Chiu, C.-W.; Yeh, J.-M. Comparing Micellar Electrokinetic Chromatography and Microemulsion Electrokinetic Chromatography for the Analysis of Preservatives in Pharmaceutical and Cosmetic Products. *J. Chromatogr. A* **2003**, *993* (1-2), 153–164.

(49) Chiappetta, D. A.; Degrossi, J.; Teves, S.; D'Aquino, M.; Bregni, C.; Sosnik, A. Triclosan-Loaded Poloxamine Micelles for Enhanced Topical Antibacterial Activity against Biofilm. *Eur. J. Pharm. Biopharm.* **2008**, *69* (2), 535–545.

(50) Mahugo Santana, C.; Sosa Ferrera, Z.; Santana Rodriguez, J. J. Use of Non-Ionic Surfactant Solutions for the Extraction and Preconcentration of Phenolic Compounds in Water prior to Their HPLC-UV Detection. *Analyst* **2002**, *127* (8), 1031–1037.

(51) Wang, Z. Bioavailability of Organic Compounds Solubilized in Nonionic Surfactant Micelles. *Appl. Microbiol. Biotechnol.* **2011**, *89* (3), 523–534.

(52) Volkering, F.; Breure, A. M.; van Andel, J. G.; Rulkens, W. H. Influence of Nonionic Surfactants on Bioavailability and Biodegradation of Polycyclic Aromatic Hydrocarbons. *Appl. Environ. Microbiol.* **1995**, *61* (5), 1699–1705.

(53) Grimberg, S. J.; Miller, C. T.; Aitkin, M. D. Surfactant-Enhanced Dissolution of Phenanthrene into Water for Laminar Flow Conditions. *Environ. Sci. Technol.* **1996**, *30* (10), 2967–2974.

(54) Jahan, K.; Ahmed, T.; Maier, W. J. Modeling the Influence of Nonionic Surfactants on Biodegradation of Phenanthrene. *Water Res.* **1999**, *33* (9), 2181–2193.

(55) Guha, S.; Jaffé, P. R. Bioavailability of Hydrophobic Compounds Partitioned into the Micellar Phase of Nonionic Surfactants. *Environ. Sci. Technol.* **1996**, *30* (4), 1382–1391.

(56) Aufiero, M.; Butler, C.; Jaser, J. An Analysis of Methods for Detecting Triclosan and Removal of Triclosan from Water Using Activated Carbon and Zeolites, Worcester Polytechnic Institute, Worcester, MA, 2012.

(57) Wong-Wah-Chung, P.; Rafqah, S.; Voyard, G.; Sarakha, M. Photochemical Behaviour of Triclosan in Aqueous Solutions: Kinetic and Analytical Studies. *J. Photochem. Photobiol. A Chem.* **2007**, *191* (2-3), 201–208.

(58) Cabaleiro, N.; Pena-Pereira, F.; de la Calle, I.; Bendicho, C.; Lavilla, I. Determination of Triclosan by Cuvetteless UV–vis Micro-Spectrophotometry Following Simultaneous Ultrasound Assisted Emulsification–microextraction with Derivatization: Use of a Micellar-Ionic Liquid as Extractant. *Microchem. J.* **2011**, *99* (2), 246–251.

(59) Lu, H.; Ma, H.; Tao, G. Spectrophotometric Determination of Triclosan in Personal Care Products. *Spectrochim. Acta Part A Mol. Biomol. Spectrosc.* **2009**, *73* (5), 854–857.

(60) Loftsson, T.; Hreinsdóttir, D.; Másson, M. Evaluation of Cyclodextrin Solubilization of Drugs. *Int. J. Pharm.* **2005**, *302* (1–2), 18–28.

(61) Liu, T.; Wu, D. High-Performance Liquid Chromatographic Determination of Triclosan and Triclocarban in Cosmetic Products. *Int. J. Cosmet. Sci.* **2012**, *34* (5), 489–494.

(62) Kysliak, O.; Smyk, N. Visual Spectroscopy Detection of Triclosan. *Chem. Pap.* **2010**, *64* (4), 523–527.

(63) Silva, A. R. M.; Nogueira, J. M. F. New Approach on Trace Analysis of Triclosan in Personal Care Products, Biological and Environmental Matrices. *Talanta* **2008**, *74* (5), 1498–1504.

(64) Lourens, G. J. Process for Producing Diphenylethers and Esters. WO 99/10310, 1999.

(65) Schreiber, W.; Marky, M. Process for the Preparation of a Very Pure Commercial Form of 4,2',4'-trichloro-2-Hydroxydiphenyl Ether. EP0086745 (A1), 1983.

(66) Grant, P. A. Optimization and Scale-up for Commercialization of a Novel Synthesis of Triclosan, University of Pretoria, 2000.

(67) Vanden Heuvel, J. P.; Lucier, G. Environmental Toxicology of Polychlorinated Dibenzo-P-Dioxins and Polychlorinated Dibenzofurans. *Environ. Health Perspect.* **1993**, *100*, 189–200.

(68) Anti-bacterial ingredients https://www.unilever.com/about/safety-and-enviroment/product-and-ingredient-safety/about-ingredients/anti-bacterials/index.html (accessed Jan 7, 2015).

(69) Petroski, W. Iowa Senate Panel OKs Ban on Antibacterial Chemical. *The Des Moines Register*. Des Moines February 2, 2015.

(70) Biocides approvals withdrawn https://www.gov.uk/government/news/biocides-approvals-withdrawn (accessed Mar 22, 2016).

(71) Spolarich, A. E. *Triclosan Safety Exposed*; 2014.

(72) Scientific Committee on Consumer Safety. *Opinion on Triclosan (Antimicrobial Resistance)*; 2010.

(73) Dann, A. B.; Hontela, A. Triclosan: Environmental Exposure, Toxicity and Mechanisms of Action. *J. Appl. Toxicol.* **2011**, *31* (4), 285–311.

(74) Yueh, M.-F.; Taniguchi, K.; Chen, S.; Evans, R. M.; Hammock, B. D.; Karin, M.; Tukey, R. H. The Commonly Used Antimicrobial Additive Triclosan Is a Liver Tumor Promoter. *Proc. Natl. Acad. Sci.* **2014**, *111* (48), 17200–17205.

(75) Connor, S. Triclosan: Soap Ingredient Can Trigger Liver Cancer in Mice, Warn Scientists. *The Independent*. London November 17, 2014.

(76) Knapton, S. Toothpaste Chemical May Increase Risk of Cancer, Warn Scientists. *The Telegraph*. London November 18, 2014.

(77) Bazian. Triclosan soap linked to mouse liver cancers http://www.nhs.uk/news/2014/11November/Pages/triclosan-soap-link-with-mouse-liver-cancers.aspx (accessed Mar 22, 2016).

(78) Cullinan, M. P.; Bird, P. S.; Heng, N. C. K.; West, M. J.; Seymour, G. J. No Evidence of Triclosan-Resistant Bacteria Following Long-Term Use of Triclosan-Containing Toothpaste. *J. Periodontal Res.* **2014**, *49* (2), 220–225.

(79) Russell, A. D. Whither Triclosan? *J. Antimicrob. Chemother.* **2004**, *53* (5), 693–695.

(80) McBain, A. J.; Ledder, R. G.; Sreenivasan, P.; Gilbert, P. Selection for High-Level Resistance by Chronic Triclosan Exposure Is Not Universal. *J. Antimicrob. Chemother.* **2004**, *53* (5 ), 772–777.

(81) Tixier, C.; Singer, H. P.; Silvio, C.; Muller, S. R. Phototransformation of Triclosan in Surface Waters: A Relevant Elimination Process for This Widely Used Biocide- Laboratory Studies , Field Measurements, and Modeling. *Environ. Sci. Technol.* **2002**, *36* (16), 3482–3489.

(82) Latch, D. E.; Packer, J. L.; Stender, B. L.; VanOverbeke, J.; Arnold, W. A.; McNeill, K. Aqueous Photocehmistry of Triclosan: Formation of 2,4-Dichlorophenol, 2,8-Dichlorodibenzo-P-Dioxin, and Oligomerization Products. *Environ. Toxicol. Chem.* **2005**, *24* (3), 517–525.

(83) Martínez-Zapata, M.; Aristizábal, C.; Peñuela, G. Photodegradation of the Endocrine-Disrupting Chemicals 4n-Nonylphenol and Triclosan by Simulated Solar UV Irradiation in Aqueous Solutions with Fe(III) and in the Absence/presence of Humic Acids. *J. Photochem. Photobiol. A Chem.* **2013**, *251* (2013), 41–49.

(84) Singer, H.; Stephan Müller; Céline Tixier; and Laurent Pillonel. Triclosan: Occurrence and Fate of a Widely Used Biocide in the Aquatic Environment: Field Measurements in Wastewater Treatment Plants, Surface Waters, and Lake Sediments. *Environ. Sci. Technol.* **2002**, *36* (23), 4998–5004.

(85) Sijm, D. T. H. M.; Opperhuizen, A. Biotransformation, Bioaccumulation and Lethality of 2,8-Dichlorodibenzo-P-Dioxin: A Proposal to Explain the Biotic Fate and Toxicity of PCDD's and PCDF's. *Chemosphere* **1988**, *17* (1), 83–99.

(86) DeLorenzo, M. E.; Keller, J. M.; Arthur, C. D.; Finnegan, M. C.; Harper, H. E.; Winder, V. L.; Zdankiewicz, D. L. Toxicity of the Antimicrobial Compound Triclosan and Formation of the Metabolite Methyl-Triclosan in Estuarine Systems. *Environ. Toxicol.* **2008**, *23* (2), 224–232.

(87) Hay, A. G.; Dees, P. M.; Sayler, G. S. Growth of a Bacterial Consortium on Triclosan. *FEMS Microbiol. Ecol.* **2001**, *36* (2-3), 105–112.

(88) Kim, S. A.; Moon, H.; Lee, K.; Rhee, M. S. Bactericidal Effects of Triclosan in Soap Both in Vitro and in Vivo. *J. Antimicrob. Chemother.* **2015**, *70* (12), 3345–3352.

(89) AFP. Antibacterial Soap with Triclosan "No Better at Killing Germs" – Study. *The Guardian*. Paris September 16, 2015.

(90) Urquhart, J. Antibacterial Soap Has Poor Killing Power. *Chemistry World*. Cambridge September 2015.

(91) Luby, S. P.; Agboatwalla, M.; Feikin, D. R.; Painter, J.; Billhimer, W.; Altaf, A.; Hoekstra, R. M. Effect of Handwashing on Child Health: A Randomised Controlled Trial. *Lancet* **2005**, *366* (9481), 225–233.

(92) Aycliffe, G. A. J.; Babb, J. R.; Davies, J. G.; Lilly, H. A. Hand Disinfection - A Comparison of Various Agents in Laboratory and Ward Studies. *J. Hosp. Infect.* **1988**, *11* (3), 226–243.

(93) Kampf, G.; Kramer, A. Epidemiologic Background of Hand Hygiene and Evaluation of the Most Important Agents for Scrubs and Rubs. *Clin. Microbiol. Rev.* **2004**, *17* (4), 863–893.

(94) Aiello, A. E.; Larson, E. L.; Levy, S. B. Consumer Antibacterial Soaps: Effective or Just Risky? *Clin. Infect. Dis.* **2007**, *45*, S137–S147.

(95) Jones, R. D.; Jampani, H. B.; Newman, J. L.; Lee, A. S. Triclosan: A Review of Effectiveness and Safety in Health Care Settings. *Am. J. Infect. Control* **2000**, *28* (2), 184–196.

(96) Fewtrell, L.; Kaufmann, R. B.; Kay, D.; Enanoria, W.; Haller, L.; Jr, J. M. C. Water, Sanitation, and Hygiene Interventions to Reduce Diarrhoea in Less Developed Countries: A Systematic Review and Meta-Analysis. *Lancet Infect. Dis.* **2005**, *5* (1), 42–52.

(97) Moore, A. F. Final Report on the Safety Assessment of Sodium Lauryl Sulfate and Ammonium Lauryl Sulfate. *J. Am. Coll. Toxicol.* **1983**, *2* (7), 127–181.

(98) Madelmont, C.; Perron, R. Study of the Influence of the Chain Length on Some Aspects of Soap/water Diagrams. *Colloid Polym. Sci.* **1976**, *254*, 581–595.

(99) Marques, E.; Khan, A.; Miguel, M. da G.; Lindman, B. Self-Assembly in Mixtures of a Cationic and an Anionic Surfactant : The Sodium Dodecyl Sulfate-Didodecy Ldimethylammonium Bromide- Water System. *J. Phys. Chem.* **1993**, *97*, 4729.

(100) Lochhead, R. Y. Shampoo and Conditioner Science. In *Practical Modern Hair Science*; Evans, T., Wickett, R. R., Eds.; Allured Pub Corp: Carol Stream, IL, 2012; pp 75–116.

(101) Jang, J.-H.; Park, Y.-D.; Ahn, H.-K.; Kim, S.-J.; Lee, J.-Y.; Kim, E.-C.; Chang, Y.-S.; Song, Y.-J.; Kwon, H.-J. Analysis of Green Tea Compounds and Their Stability in Dentifrices of Different pH Levels. *Chem. Pharm. Bull.* **2014**, *62* (4), 328–335.

(102) Price, R. B. T.; Sedearous, M.; Hiltz, G. S. The pH of Tooth-Whitening Products. *J. Can. Dent. Assoc. (Tor).* **2000**, *66*, 421–426.

(103) Toothpaste Properties http://www.colgateprofessional.com.au/LeadershipAU/Roles/Student/Sidebar/Resources/Toothpaste_Properties.pdf (accessed Aug 4, 2015).

(104) Household Products Database: Chemical Information for Sodium Lauryl Sulfate http://householdproducts.nlm.nih.gov/cgi-bin/household/brands?tbl=chem&id=78 (accessed Jan 9, 2016).

(105) Household Products Database: Chemical information for Sodium Laurate http://householdproducts.nlm.nih.gov/cgi-bin/household/brands?tbl=chem&id=715&query=sodium+laurate&searchas=TblChemicals (accessed Jan 9, 2016).

(106) Moroi, Y. *Micelles: Theortical and Applied Aspects*; Plenum Press: New York, N.Y., 1992.

(107) Williams, R. J.; Phillips, J. N.; Mysels, K. J. The Critical Micelle Concentration of Sodium Lauryl Sulphate at 25°C. *Trans. Faraday Soc.* **1955**, *51*, 728–737.

(108) Corrin, M. L.; Klevens, H. B.; Harkins, W. D. The Determination of Critical Concentrations for the Formation of Soap Micelles by the Spectral Behavior of Pinacyanol Chloride. *J. Chem. Phys.* **1946**, *14* (8).

(109) Israelachvili, J. N.; Mitchell, D. J.; Ninham, B. W. Theory of Self-Assembly of Hydrocarbon Amphiphiles into Micelles and Bilayers. *J. Chem. Soc. Faraday Trans. 2* **1976**, *72*, 1525–1568.

(110) Moosavi-Movahedi, A. A.; Gharanfoli, M.; Nazari, K.; Shamsipur, M.; Chamani, J.; Hemmateenejad, B.; Alavi, M.; Shokrollahi, A.; Habibi-Rezaei, M.; Sorenson, C.; et al. A Distinct Intermediate of {RNase} A Is Induced by Sodium Dodecyl Sulfate at Its pKa. *Colloids*

*Surfaces B Biointerfaces* **2005**, *43* (3–4), 150–157.

(111) Hines, J. D. The Preparation of Surface Chemically Pure Sodiumn-Dodecyl Sulfate by Foam Fractionation. *J. Colloid Interface Sci.* **1996**, *180* (2), 488–492.

(112) Quina, F. H.; Preto, R.; Bales, B. L. Growth of Sodium Dodecyl Sulfate Micelles with Detergent Concentration. *J. Phys. Chem.* **1995**, *99*, 17028–17031.

(113) Woolfrey, S. G.; Banzon, G. M.; Groves, M. J. The Effect of Sodium Chloride on the Dynamic Surface Tension of Sodium Dodecyl Sulfate Solutions. *J. Colloid Interface Sci.* **1986**, *112* (2), 583–587.

(114) Kronberg, B.; Holmberg, K.; Lindman, B. *Surface Chemistry of Surfactants and Polymers*; John Wiley & Sons, Ltd.: Chichester, 2014.

(115) Fung, B. M.; Zhao, J. NMR Study of the Transformation of Sodium Dodecyl Sulfate Micelles. *Langmuir* **1993**, *9* (16), 1228–1231.

(116) Mazer, N. A.; Benedek, G. B.; Carey, M. C. An Investigation of the Micellar Phase of Sodium Dodecyl Sulfate in Aqueous Sodium Chloride Solutions Using Quasielastic Light Scattering Spectroscopy. *J. Phys. Chem.* **1976**, *80* (10), 1075–1085.

(117) Princen, L. H.; Mysels, K. J. Some Effects of Lauryl Alcohol on Light Scattering by Sodium Lauryl Sulfate. *J. Phys. Chem.* **1959**, *63* (10), 1781–1782.

(118) Lunkenheimer, K.; Czichocki, G. On the Stability of Aqueous Sodium Dodecyl Sulfate Solutions. *J. Colloid Interface Sci.* **1993**, *160* (2), 509–510.

(119) Mysels, K. J. Surface Tension of Solutions of Pure Sodium Dodecyl Sulfate. *Langmuir* **1986**, *2* (4), 423–428.

(120) Tajima, K. Radiotracer Studies on Adsorption of Surface Active Substance at Aqueous Surface. II. The Effect of Excess Salt on the Adsorption of Sodium Dodecylsulfate. *Bull. Chem. Soc. Jpn.* **1970**, *43* (10), 3063–3066.

(121) *Active Ingredients Eligible for Minimum Risk Pesticide Products*; Washington D.C., 2015.

(122) *Food Additives Permitted for Direct Addition to Food for Human Consumption: Sodium Lauryl Sulfate*; Food and Drug Administration: United States of America, 2015; p 1.

(123) Noweck, K.; Grafahrend, W. Fatty Alcohols. In *Ullmann's Encyclopedia of Industrial Chemistry*; Wiley-VCH Verlag GmbH & Co. KGaA, 2000.

(124) Bethell, D.; Fessey, R. E.; Namwindwa, E.; Roberts, D. W. The Hydrolysis of C12 Primary Alkyl Sulfates in Concentrated Aqueous Solutions. Part 1. General Features, Kinetic Form and Mode of Catalysis in Sodium Dodecyl Sulfate Hydrolysis. *J. Chem. Soc., Perkin Trans. 2* **2001**, No. 9, 1489–1495.

(125) Kretschmann, J.; Carduck, F.-J.; Wuest, W.; Harth, H.; Springer, D. Process for the Sulfonation And/or Sulfatization of Organic Components with SO3 in an Organic Reaction Medium. US4973686 (A), 1990.

(126) Kékicheff, P.; Grabielle-Madelmont, C.; Ollivon, M. Phase Diagram of Sodium Dodecyl Sulfate-Water System: 1. A Calorimetric Study. *J. Colloid Interface Sci.* **1989**, *131* (1), 112–132.

(127) Basappa, G.; Belmar, M. T.; Telford, J. H. Concentrated Surfacatnt Compositions.

US200/8139434, 2008.

(128) Yuji, Y.; Masaki, T.; Makoto, H.; Yuki, O. Skin Disinfectant. US2008/103203, 2008.

(129) Reicherz, H.; Heydt, S. Bar Soap. US2007/203040, 2007.

(130) Jackson, L. P.; Andrade, R.; Pleasent, I.; Grady, B. P. Effects of pH and Surfactant Precipitation on Surface Tension and CMC Determination of Aqueous Sodium N-Alkyl Carboxylate Solutions. *J. Surfactants Deterg.* **2014**, *17* (5), 911–917.

(131) Rodríguez-Pulido, A.; Casado, A.; Muñoz-Úbeda, M.; Junquera, E.; Aicart, E. Experimental and Theoretical Approach to the Sodium Decanoate−Dodecanoate Mixed Surfactant System in Aqueous Solution. *Langmuir* **2010**, *26* (12), 9378–9385.

(132) Kralchevsky, P. A.; Danov, K. D.; Pishmanova, C. I.; Kralchevska, S. D.; Christov, N. C.; Ananthapadmanabhan, K. P.; Lips, A. Effect of the Precipitation of Neutral-Soap, Acid-Soap, and Alkanoic Acid Crystallites on the Bulk pH and Surface Tension of Soap Solutions. *Langmuir* **2007**, *23* (7), 3538–3553.

(133) Kanicky, J. R.; Poniatowski, A. F.; Mehta, N. R.; Shah, D. O. Cooperativity among Molecules at Interfaces in Relation to Various Technological Processes: Effect of Chain Length on the pKa of Fatty Acid Salt Solutions†. *Langmuir* **2000**, *16* (1), 172–177.

(134) Yuan, Z.; Lu, W.; Liu, W.; Hao, J. Gel Phase Originating from Molecular Quasi-Crystallization and Nanofiber Growth of Sodium Laurate-Water System. *Soft Matter* **2008**, *4* (8), 1639–1644.

(135) McBain, J.; Brock, G. Phase Rule Studies of Soap. II. The System Sodium Laurate—Sodium Chloride—Water. *J. Am. Chem. Soc.* **1938**, *60*, 1870–1876.

(136) Zacharie, B.; Ezzitouni, A.; Duceppe, J.-S.; Penney, C. A Simple and Efficient Large-Scale Synthesis of Metal Salts of Medium-Chain Fatty Acids. *Org. Process Res. Dev.* **2009**, *13* (3), 581–583.

(137) Borzelli, R. D.; Cunder, J. Continuous Process for Preparing Dry Metallic Salts of Higher Fatty Acids. 4,307,027, 1981.

(138) Duceppe, J.; Ezzitouni, A.; Penney, C.; Zacharie, B. Preparation of Metal Salts of Medium-Chain Fatty Acids. WO2005012217 (A2), 2005.

(139) Aniansson, E. A. G.; Wall, S. N. On the Kinetics of Step-Wise Micelle Association. *J. Phys. Chem.* **1974**, *78* (10), 1024–1030.

(140) Aniansson, E. A. G.; Wall, S. A Correction and Improvement of “On the Kinetics of Step-Wise Micelle Association” by E. A. G. Aniansson and S. N. Wal. *J. Phys. Chem.* **1975**, *79* (8), 857–858.

(141) von Gottberg, F. K.; Smith, K. a.; Hatton, T. A. Dynamics of Self-Assembled Surfactant Systems. *J. Chem. Phys.* **1998**, *108* (5), 2232–2244.

(142) MacMorland, M. MChem Project Report, Durham University, 2010.

(143) Lang, J.; Tondre, C.; Zana, R.; Bauer, R.; Hoffmann, H.; Ulbricht, W. Chemical Relaxation Studies of Micellar Equilibriums. *J. Phys. Chem.* **1975**, *79* (3), 276–283.

(144) Zana, R. Aqueous Surfactant-Alcohol Systems: A Review. *Adv. Colloid Interface Sci.* **1995**, *57* (1), 1–64.

(145) Aniansson, E. A. G.; Wall, S. Theory of the Kinetics of Micellar Equilibria and Quantitative Interpretation of Chemical Relaxation Studies of Micellar Solutions of Ionic Surfactants. *J. Phys. Chem.* **1976**, *80* (9), 905–922.

(146) Dushkin, C. D. Model of the Quasi-Monodisperse Micelles with Application to the Kinetics of Micellization, Adsorption and Diffusion in Surfactant Solutions and Thin Liquid Films. *Colloids Surfaces A Physicochem. Eng. Asp.* **1998**, *143* (2–3), 283–299.

(147) Griffiths, I. M.; Breward, C. J. W.; Colegate, D. M.; Dellar, P. J.; Howell, P. D.; Bain, C. D. A New Pathway for the Re-Equilibration of Micellar Surfactant Solutions. *Soft Matter* **2013**, *9* (3), 853–863.

(148) Zhu, Z.; Reed, W. F. Enhanced Surfactant Supra-Micellar Assembly by Hydrophobic Dopants. *Langmuir* **2013**, *29* (33), 10376–10382.

(149) Zhu, Z.; Reed, W. F. Polymeric Suppression of Dopant-Enhanced Surfactant Supramicellar Assemblies. *Macromol. Chem. Phys.* **2015**, *216* (2), 205–210.

(150) Shah, S. S.; Naeem, K.; Shah, S. W. H.; Laghari, G. M. Differential Absorbance Measurements of Amphiphilic Hemicyanine Dyes, Solubilization Study in Anionic Surfactant. *Colloids Surfaces A Physicochem. Eng. Asp.* **2000**, *168* (1), 77–85.

(151) Kawamura, H.; Manabe, M.; Miyamoto, Y.; Fujita, Y.; Tokunaga, S. Partition Coefficients of Homologous .omega.-Phenylalkanols between Water and Sodium Dodecyl Sulfate Micelles. *J. Phys. Chem.* **1989**, *93* (14), 5536–5540.

(152) Alonso, B.; Harris, R. K.; Kenwright, A. M. Micellar Solubilization: Structural and Conformational Changes Investigated by 1H and 13C Liquid-State NMR. *J. Colloid Interface Sci.* **2002**, *251* (2), 366–375.

(153) Lapenna, S.; Bilia, A. R.; Morris, G. A.; Nilsson, M. Novel Artemisinin and Curcumin Micellar Formulations: Drug Solubility Studies by NMR Spectroscopy. *J. Pharm. Sci.* **2009**, *98* (10), 3666–3675.

(154) Jaiswal, P. V; Ijeri, V. S.; Srivastava, A. K. Effect of Surfactants on the Dissociation Constants of Ascorbic and Maleic Acids. *Colloids Surfaces B Biointerfaces* **2005**, *46* (1), 45–51.

(155) Dupont-Leclercq, L.; Giroux, S.; Henry, B.; Rubini, P. Solubilization of Amphiphilic Carboxylic Acids in Nonionic Micelles: Determination of Partition Coefficients from pKa Measurements and NMR Experiments. *Langmuir* **2007**, *23* (21), 10463–10470.

(156) Crans, D. C.; Trujillo, A. M.; Bonetti, S.; Rithner, C. D.; Baruah, B.; Levinger, N. E. Penetration of Negatively Charged Lipid Interfaces by the Doubly Deprotonated Dipicolinate†. *J. Org. Chem.* **2008**, *73* (24), 9633–9640.

(157) Tamm, L. K.; McConnell, H. M. Supported Phospholipid Bilayers. *Biophys. J.* **1985**, *47* (1), 105–113.

(158) Castellana, E. T.; Cremer, P. S. Solid Supported Lipid Bilayers: From Biophysical Studies to Sensor Design. *Surf. Sci. Rep.* **2006**, *61* (10), 429–444.

(159) Johnson, S. J.; Bayerl, T. M.; McDermott, D. C.; Adam, G. W.; Rennie, A. R.; Thomas, R. K.; Sackmann, E. Structure of an Adsorbed Dimyristoylphosphatidylcholine Bilayer Measured with Specular Reflection of Neutrons. *Biophys. J.* **1991**, *59* (2), 289–294.

(160) Han, C.-T.; Chao, L. Creating Air-Stable Supported Lipid Bilayers by Physical Confinement Induced by Phospholipase A2. *ACS Appl. Mater. Interfaces* **2014**, *6* (9), 6378–6383.

(161) Reimhult, E.; Fredrik Höök; Bengt Kasemo. Intact Vesicle Adsorption and Supported Biomembrane Formation from Vesicles in Solution: Influence of Surface Chemistry, Vesicle Size, Temperature, and Osmotic Pressure. *Langmuir* **2003**, *19* (5), 1681–1691.

(162) Cremer, P. S.; Steven G. Boxer. Formation and Spreading of Lipid Bilayers on Planar Glass Supports. *J. Phys. Chem. B* **1999**, *103* (13), 2554–2559.

(163) Kaasgaard, T.; Leidy, C.; Crowe, J. H.; Mouritsen, O. G.; Jørgensen, K. Temperature-Controlled Structure and Kinetics of Ripple Phases in One- and Two-Component Supported Lipid Bilayers. *Biophys. J.* **2003**, *85* (1), 350–360.

(164) Richter, R. P.; Rémi Bérat; Alain R. Brisson. Formation of Solid-Supported Lipid Bilayers: An Integrated View. *Langmuir* **2006**, *22* (8), 3497–3505.

(165) Kam, L.; Steven G. Boxer. Formation of Supported Lipid Bilayer Composition Arrays by Controlled Mixing and Surface Capture. *J. Am. Chem. Soc.* **2000**, *122* (51), 12901–12902.

(166) Johnson, J. M.; Ha, T.; Chu, S.; Boxer, S. G. Early Steps of Supported Bilayer Formation Probed by Single Vesicle Fluorescence Assays. *Biophys. J.* **2002**, *83* (6), 3371–3379.

(167) Csúcs, G.; Ramsden, J. J. Interaction of Phospholipid Vesicles with Smooth Metal-Oxide Surfaces. *Biochim. Biophys. Acta - Biomembr.* **1998**, *1369* (1), 61–70.

(168) Hamai, C.; Yang, T.; Kataoka, S.; Cremer, P. S.; Musser, S. M. Effect of Average Phospholipid Curvature on Supported Bilayer Formation on Glass by Vesicle Fusion. *Biophys. J.* **2006**, *90* (4), 1241–1248.

(169) Joshua Salafsky; Jay T. Groves; Steven G. Boxer. Architecture and Function of Membrane Proteins in Planar Supported Bilayers: A Study with Photosynthetic Reaction Centers. *Biochemistry* **1996**, *35* (47), 14773–14781.

(170) Leonenko, Z.; Finot, E.; Cramb, D. AFM Study of Interaction Forces in Supported Planar DPPC Bilayers in the Presence of General Anesthetic Halothane. *Biochim. Biophys. Acta - Biomembr.* **2006**, *1758* (4), 487–492.

(171) Leonenko, Z. V; Finot, E.; Ma, H.; Dahms, T. E. S.; Cramb, D. T. Investigation of Temperature-Induced Phase Transitions in DOPC and DPPC Phospholipid Bilayers Using Temperature-Controlled Scanning Force Microscopy. *Biophys. J.* **2004**, *86* (6), 3783–3793.

(172) Frangopol, P. T.; Cadenhead, D. A.; Tomoaia, G.; Mocanu, A.; Tomoaia-Cotisel, M. The Effect of Procaine on Lipid Domains by Contact Mode Atomic Force Microscopy. *Rev. Roum. Chim.* **2015**, *60* (2-3), 265–273.

(173) He, G.; Sun, R.; Hao, C.; Yang, J.; Wang, M.; Zhang, L. Thermodynamic Analysis and AFM Study of the Interaction of Palmitic Acid with DPPE in Langmuir Monolayers. *Colloids Surfaces A Physicochem. Eng. Asp.* **2014**, *441*, 184–194.

(174) Lorite, G. S.; Nobre, T. M.; Zaniquelli, M. E. D.; de Paula, E.; Cotta, M. A. Dibucaine Effects on Structural and Elastic Properties of Lipid Bilayers. *Biophys. Chem.* **2009**, *139* (2–3), 75–83.

(175) Marquês, J. T.; Viana, A. S.; Almeida, R. F. M. De. Ethanol Effects on Binary and Ternary Supported Lipid Bilayers with Gel/fluid Domains and Lipid Rafts. *Biochim. Biophys. Acta -*

*Biomembr.* **2011**, *1808* (1), 405–414.

(176) Lima, L. M. C.; Giannotti, M. I.; Redondo-Morata, L.; Vale, M. L. C.; Marques, E. F.; Sanz, F. Morphological and Nanomechanical Behavior of Supported Lipid Bilayers on Addition of Cationic Surfactants. *Langmuir* **2013**, *29* (30), 9352–9361.

(177) Nussio, M. R.; Sykes, M. J.; Miners, J. O.; Shapter, J. G. Kinetics Membrane Disruption Due to Drug Interactions of Chlorpromazine Hydrochloride. *Langmuir* **2009**, *25* (2), 1086–1090.

(178) Woods, D. A. Dynamics of Surfactant Adsorption at Solid–Liquid Interfaces, Durham University, 2011.

(179) Churchwell, J. H. TIR-Raman Spectroscopy of Model Supported Lipid Bilayers, Durham University, 2014.

(180) Raman, C. V; Krishnan, K. S. A New Type of Seconday Radiation. *Nature* **1928**, *121* (3048), 501.

(181) Long, D. A. 80TH Anniversary of the Discovery of the Raman Effect: A Celebration. *J. Raman Spectrosc.* **2008**, *39* (3), 316–321.

(182) Woods, D. A.; Bain, C. D. Total Internal Reflection Raman Spectroscopy. *Analyst* **2012**, *137* (1), 35–48.

(183) Atkins, P.; Paula, J. de. *Atkins' Physical Chemistry*, 7th Editio.; Oxford, 2002.

(184) Lee, C.; Bain, C. D. Raman Spectra of Planar Supported Lipid Bilayers. *Biochim. Biophys. Acta (BBA)- Biomembr.* **2005**, *1711* (1), 59–71.

(185) Greene, P. R.; Bain, C. D. Total Internal Reflection Raman Spectroscopy. *Spectrosc. Eur.* **2004**, *16*, 8–15.

(186) Woods, D. A.; Petkov, J.; Bain, C. D. Surfactant Adsorption Kinetics by Total Internal Reflection Raman Spectroscopy. 2. CTAB and Triton X-100 Mixtures on Silica. *J. Phys. Chem. B* **2011**, *115* (22), 7353–7363.

(187) Tyrode, E.; Rutland, M. W.; Bain, C. D. Adsorption of CTAB on Hydrophilic Silica Studied by Linear and Nonlinear Optical Spectroscopy. *J. Am. Chem. Soc.* **2008**, *130* (51), 17434–17445.

(188) Tyrode, E.; Liljeblad, J. F. D. Water Structure Next to Ordered and Disordered Hydrophobic Silane Monolayers: A Vibrational Sum Frequency Spectroscopy Study. *J. Phys. Chem. C* **2013**, *117* (4), 1780–1790.

(189) McKee, K. J.; Meyer, M. W.; Smith, E. A. Plasmon Waveguide Resonance Raman Spectroscopy. *Anal. Chem.* **2012**, *84* (21), 9049–9055.

(190) McKee, K. J.; Meyer, M. W.; Smith, E. A. Near IR Scanning Angle Total Internal Reflection Raman Spectroscopy at Smooth Gold Films. *Anal. Chem.* **2012**, *84* (10), 4300–4306.

(191) Kivioja, A. O.; Jääskeläinen, A.-S.; Ahtee, V.; Vuorinen, T. Thickness Measurement of Thin Polymer Films by Total Internal Reflection Raman and Attenuated Total Reflection Infrared Spectroscopy. *Vib. Spectrosc.* **2012**, *61*, 1–9.

(192) Jubb, A. M.; Verreault, D.; Posner, R.; Criscenti, L. J.; Katz, L. E.; Allen, H. C. Sulfate Adsorption at the Buried Hematite/solution Interface Investigated Using Total Internal Reflection (TIR)-Raman Spectroscopy. *J. Colloid Interface Sci.* **2013**, *400*, 140–146.

(193) Greene, P. R.; Bain, C. D. Total Internal Reflection Raman Spectroscopy of Barley Leaf Epicuticular Waxes in Vivo. *Colloids Surfaces B Biointerfaces* **2005**, *45* (3–4), 174–180.

(194) Praveena, M.; Bain, C. D.; Jayaram, V.; Biswas, S. K. Total Internal Reflection (TIR) Raman Tribometer: A New Tool for in Situ Study of Friction-Induced Material Transfer. *RSC Adv.* **2013**, *3* (16), 5401–5411.

(195) Katoh, K. Contact Angle and Surface Tension Measurement. In *Surface and Interfacial Tension: Measurement, Theory, and Applications*; Hartland, S., Ed.; Marcel Dekker Inc.: New York, N.Y., 2004; pp 368–419.

(196) Thiessen, D. B.; Man, K. F. Surface Tension Measurement. In *The Measurement, Intrumentation, and Sensors: Handbook*; Webster, J. G., Ed.; CRC Press: Boca Raton, FL, 1999; pp 31.1–31.13.

(197) Dukhin, S. S.; Kretzschmar, G.; Miller, R. *Dynamics of Adsorption at Liquid Interfaces: Theory, Experiment, Application*; Elsevier Science B.V.: Amsterdam, 1995.

(198) Israelachvili, J. N. *Intermolecular and Surface Forces*, 3rd Ed.; Academic Press: Burlington, MA, 2011.

(199) Kissa, E. Liquid-Vapour and Liquid-Liquid Boundaries. In *Fluorinated Surfactants and Repellents*; Kissa, E., Ed.; Marcel Dekker Inc.: New York, N.Y., 2001; pp 103–165.

(200) Dragcevic, D.; Bujan, M.; Grahek, Z.; Filipovic-Vincekovic, N. Adsorption at the Air/water Interface in Dodecylammonium Chloride/sodium Dodecyl Sulfate Mixtures. *Colloid Polym. Sci.* **1995**, *273* (10), 967–973.

(201) Kralchevsky, P. A.; Danov, K. D.; Kolev, V. L.; Broze, G.; and A. Mehreteab. Effect of Nonionic Admixtures on the Adsorption of Ionic Surfactants at Fluid Interfaces. 1. Sodium Dodecyl Sulfate and Dodecanol. *Langmuir* **2003**, *19* (12), 5004–5018.

(202) Tajima, K. Radiotracer Studies on Adsorption of Surface Active Substance at Aqueous Surface. III. The Effects of Salt on the Adsorption of Sodium Dodecylsulfate. *Bull. Chem. Soc. Jpn.* **1971**, *44* (7), 1767–1771.

(203) Tajima, K.; Muramatsu, M.; Sasaki, T. Radiotracer Studies on Adsorption of Surface Active Substance at Aqueous Surface. I. Accurate Measurement of Adsorption of Tritiated Sodium Dodecylsulfate. *Bull. Chem. Soc. Jpn.* **1970**, *43* (7), 1991–1998.

(204) Purcell, I. P.; Thomas, R. K.; Penfold, J.; Howe, A. M. Adsorption of SDS and PVP at the Air/water Interface. *Colloids Surfaces A Physicochem. Eng. Asp.* **1995**, *94* (2–3), 125–130.

(205) Stokes, R. J.; Evans, D. F. 5.1 Aggregation of Amphiphilic Molecules to Form Spherical Miceles Illustrates Many Features of Self-Organizing Systems. In *Fundamentals of Interfacial Engineering*; Wiley-VCH Inc.: New York, N.Y., 1997; pp 209–219.

(206) Woodward, R. P. *Surface Tension Measurements Using the Drop Shape Method*; Portsmouth, Va, 2012.

(207) Berthier, J. *Micro-Drops and Digital Microfluidics*, 2nd Ed.; Elsevier Inc.: Oxford, 2013.

(208) Pynn, R. *Neutron Scattering: A Primer*; Los Alamos Science: Los Alamos, N.M., 1990.

(209) Hayter, J. B.; Penfold, J. An Analytic Structure Factor for Macroion Solutions. *Mol. Phys.* **1981**, *42* (1), 109–118.

(210) Hansen, J. P.; Hayter, J. B. A Rescaled MSA Structure Factor for Dilute Charged Colloidal Dispersions. *Mol. Phys.* **1982**, *46* (3), 651–656.

(211) Bradbury, R.; Penfold, J.; Thomas, R. K.; Tucker, I. M.; Petkov, J. T.; Jones, C.; Grillo, I. Impact of Model Perfume Molecules on the Self-Assembly of Anionic Surfactant Sodium Dodecyl 6-Benzene Sulfonate. *Langmuir* **2013**, *29* (10), 3234–3245.

(212) Petkov, J. T.; Tucker, I. M.; Penfold, J.; Thomas, R. K.; Petsev, D. N.; Dong, C. C.; Golding, S.; Grillo, I. The Impact of Multivalent Counterions, Al3+, on the Surface Adsorption and Self-Assembly of the Anionic Surfactant Alkyloxyethylene Sulfate and Anionic/Nonionic Surfactant Mixtures. *Langmuir* **2010**, *26* (22), 16699–16709.

(213) Feigin, L. A.; Svergun, D. I. *Structure Analysis by Small-Angle X-Ray and Neutron Scattering*; Plenum Press: New York, N.Y., 1987.

(214) Brown, D.; Kienzle, P. Neutron activation and scattering calculator https://www.ncnr.nist.gov/resources/activation/ (accessed Feb 18, 2016).

(215) Williams, D. H.; Fleming, I. *Spectrocopic Methods in Organic Chemistry*, 6th ed.; McGraw-Hill Education: Maidenhead, Surrey, 2008.

(216) Kliegman, S.; Eustis, S. N.; Arnold, W. A.; McNeill, K. Experimental and Theoretical Insights into the Involvement of Radicals in Triclosan Phototransformation. *Environ. Sci. Technol.* **2013**, *47* (13), 6756–6763.

(217) Latch, D. E.; Packer, J. L.; Arnold, W. a.; McNeill, K. Photochemical Conversion of Triclosan to 2,8-Dichlorodibenzo-P-Dioxin in Aqueous Solution. *J. Photochem. Photobiol. A Chem.* **2003**, *158* (1), 63–66.

(218) Chen, Z.; Song, Q.; Cao, G.; Chen, Y. Photolytic Degradation of Triclosan in the Presence of Surfactants. *Chem. Pap.* **2008**, *62* (6), 608–615.

(219) Chen, Z.; Cao, G.; Song, Q. Photo-Polymerization of Triclosan in Aqueous Solution Induced by Ultraviolet Radiation. *Environ. Chem. Lett.* **2008**, *8* (1), 33–37.

(220) Wu, Q.; Shi, H.; Adams, C. D.; Timmons, T.; Ma, Y. Oxidative Removal of Selected Endocrine-Disruptors and Pharmaceuticals in Drinking Water Treatment Systems, and Identification of Degradation Products of Triclosan. *Sci. Total Environ.* **2012**, *439* (0), 18–25.

(221) Penfold, J.; Staples, E.; Tucker, I. Neutron Small Angle Scattering Studies of Micellar Growth in Mixed Anionic-Nonionic Surfactants, Sodium Dodecyl Sulfate, SDS, and Hexaethylene Glycol Monododecyl Ether, C12E6, in the Presence and Absence of Solubilized Alkane, Hexadecane. *J. Phys. Chem. B* **2002**, *106* (34), 8891–8897.

(222) *NanoSight NTA 2.2 Analytical Software Manual*; Amesbury, UK, 2011.

(223) Carr, B.; Hole, P.; Malloy, A.; Nelson, P.; Wright, M.; Smith, J. Applications of Nanoparticle Tracking Analysis ( NTA ) in Nanoparticle Research- a Mini-Review. *Eur. J. Parenter. Pharamaceutical Sci.* **2009**, *14* (2), 45–50.

(224) Barron, J. J.; Ashton, C.; Geary, L. *The Effects of Temperature on pH Measurement*; TSP-01; 2; Shannon Free Zone.

(225) Jacquier, J. C.; Desbène, P. L. Determination of Critical Micelle Concentration by Capillary Electrophoresis Application to Organo-Saline Electrolytes. *J. Chromatogr. A* **1996**, *743* (2),

307–314.

(226) Joos, P.; Vollhardt, D.; Vermeulen, M. Interfacial Tension of Sodium Dodecyl Sulfate Solutions at the Hexane-Water Interface. *Langmuir* **1990**, *6* (2), 524–525.

(227) Kegel, W. K.; Aken, G. A. Van; Bouts, M. N.; Lekkerkerker, H. N. W.; Overbeek, J. T. G.; Bruyn, P. L. De. Adsorption of Sodium Dodecyl Sulfate and Cosurfactant at the Planar Cyclohexane-Brine Interface. Validity of the Saturation Adsorption Approximation and Effects of the Cosurfactant Chain Length. *Langmuir* **1993**, *9* (1), 252–256.

(228) Hayter, J. B.; Penfold, J. Determination of Micelle Structure and Charge by Neutron Small-Angle Scattering. *Colloid Polym. Sci.* **1983**, *261* (12), 1022–1030.

(229) Waisman, E. The Radial Distribution Function for a Fluid of Hard Spheres at High Densities. *Mol. Phys.* **1973**, *25* (1), 45–48.

(230) Mukerjee, P.; Yang, A. Y. S. Nonideality of Mixing of Micelles of Fluorocarbon and Hydrocarbon Surfactants and Evidence of Partial Miscibility from Differential Conductance Data. *J. Phys. Chem.* **1976**, *80* (12), 1388–1390.

(231) Laguerre, M.; Hugouvieux, V.; Cavusoglu, N.; Aubert, F.; Lafuma, A.; Fulcrand, H.; Poncet-Legrand, C. Probing the Micellar Solubilisation and Inter-Micellar Exchange of Polyphenols Using the DPPH· Free Radical. *Food Chem.* **2014**, *149*, 114–120.

(232) Benrraou, M.; Bales, B. L.; Zana, R. Effect of the Nature of the Counterion on the Properties of Anionic Surfactants. 1. CMC, Ionization Degree at the CMC and Aggregation Number of Micelles of Sodium, Cesium, Tetramethylammonium, Tetraethylammonium, Tetrapropylammonium, and Tetrabutylammoniu. *J. Phys. Chem. B* **2003**, *107* (48), 13432–13440.

(233) Rodríguez-Pulido, A.; Casado, A.; Muñoz-Úbeda, M.; Junquera, E.; Aicart, E. Experimental and Theoretical Approach to the Sodium Decanoate−Dodecanoate Mixed Surfactant System in Aqueous Solution. *Langmuir* **2010**, *26* (12), 9378–9385.

(234) Akisada, H.; Kuwahara, J.; Koga, A.; Motoyama, H.; Kaneda, H. Unusual Behavior of CMC for Binary Mixtures of Alkyltrimethylammonium Bromides: Dependence on Chain Length Difference. *J. Colloid Interface Sci.* **2007**, *315* (2), 678–684.

(235) Drummond, C. J.; Warr, G. G.; Grieser, F.; Ninham, B. W.; Evans, D. F. Surface Properties and Micellar Interfacial Microenvironment of N-Dodecyl Beta-D-Maltoside. *J. Phys. Chem.* **1985**, *89* (10), 2103–2109.

(236) Pemberton, R. M.; Hart, J. P. Electrochemical Behaviour of Triclosan at a Screen-Printed Carbon Electrode and Its Voltammetric Determination in Toothpaste and Mouthrinse Products. *Anal. Chim. Acta* **1999**, *390* (1–3), 107–115.

(237) Colegate, D. Structure-Kinetics Relationships in Micellar Solutions of Nonionic Surfactants, Durham University, 2009.

(238) Ferré, J.; Rius, F. X. Detection and Correction of Biased Results of Individual Analytes in Multicomponent Spectroscopic Analysis. *Anal. Chem.* **1998**, *70* (9), 1999–2007.

(239) Batchelor, G. K. *An Introduction to Fluid Dynamics*; Cambridge University Press: London, 1967.

(240) Wong, T. C. Micellar Systems: Nuclear Magnetic Resonace Spectroscopy. In *Encyclopedia of*

*Surface and Colloid Science, Volume 5*; Somasundaran, P., Ed.; CRC Press, 2006; p 3742.

(241) Hore, P. J. *Nuclear Magnetic Resonance*, 1st ed.; Oxford University Press: Oxford, 1995.

(242) Momot, K. I.; Kuchel, P. W.; Chapman, B. E.; Deo, P.; Whittaker, D. NMR Study of the Association of Propofol with Nonionic Surfactants. *Langmuir* **2003**, *19* (6), 2088–2095.

(243) Duan, M. S.; Zhao, N.; Össurardóttir, Í. B.; Thorsteinsson, T.; Loftsson, T. Cyclodextrin Solubilization of the Antibacterial Agents Triclosan and Triclocarban: Formation of Aggregates and Higher-Order Complexes. *Int. J. Pharm.* **2005**, *297* (1–2), 213–222.

(244) Akitt, J. W.; Mann, B. E. *NMR and Chemistry: An Introduction to Modern NMR Spectroscopy*, 4th Editio.; Stanley Thornes Ltd: Cheltenham, 2000.

(245) Girvin, M.; Cahill, S.; Harris, R. Chemical Exchange in NMR Spectroscopy http://www.bioc.aecom.yu.edu/labs/girvlab/nmr/course/COURSE_2012/Lecture_ExchangeDynamics_2012.pdf (accessed Jun 21, 2013).

(246) Fujiwara, H.; Kanzaki, K.; Kano, T.; Kimura, A.; Tanaka, K.; Da, Y.-Z. An NMR Shift Reagent Method for the Determination of Micelle/water Partition Coefficients. *J. Chem. Soc. Chem. Commun.* **1992**, No. 10, 736.

(247) Wilson, K. A.; Beck, J. J. Complete Proton and Carbon Assignment of Triclosan via One- and Two- Dimensional Nuclear Magnetic Resonance Analysis. *Chem. Educ.* **2007**, *12*, 1–5.

(248) Maffeo, D.; Velkov, Z.; Misiakos, K.; Mergia, K.; Paulidou, A.; Zavali, M.; Mavridis, I. M.; Yannakopoulou, K. Real-Time Monitoring of Nanomolar Binding to a Cyclodextrin Monolayer Immobilized on a Si/SiO2/novolac Surface Using White Light Reflectance Spectroscopy: The Case of Triclosan. *J. Colloid Interface Sci.* **2011**, *358*, 369–375.

(249) ASTI. Minimizing User Errors in pH Measurements http://www.astisensor.com/minimizing_user_errors_ph.pdf (accessed Feb 26, 2016).

(250) Gottlieb, H. E.; Kotlyar, V.; Nudelman, A. NMR Chemical Shifts of Common Laboratory Solvents as Trace Impurities. *J. Org. Chem.* **1997**, *62* (21), 7512–7515.

(251) Sanders, J. K. M.; Hunter, B. K. *Modern NMR Spectroscopy: A Guide for Chemists*; Oxford University Press: Oxford, 1993.

(252) Krężel, A.; Bal, W. A Formula for Correlating pKa Values Determined in D2O and H2O. *J. Inorg. Biochem.* **2004**, *98* (1), 161–166.

(253) Sivaraman, S.; Sullivan, T. J.; Johnson, F.; Novichenok, P.; Cui, G.; Simmerling, C.; Tonge, P. J. Inhibition of the Bacterial Enoyl Reductase FabI by Triclosan: A Structure−Reactivity Analysis of FabI Inhibition by Triclosan Analogues. *J. Med. Chem.* **2004**, *47* (3), 509–518.

(254) Sigma-Aldrich. Buffer Reference Center http://www.sigmaaldrich.com/life-science/core-bioreagents/biological-buffers/learning-center/buffer-reference-center.html (accessed Mar 19, 2015).

(255) Shapiro, M. J. Structure Assignment with High-Resolution NMR: Experimental Results. In *NMR Spectroscopy Techniques*; Dybowski, C., Lichter, R. L., Eds.; Marcel Dekker Inc.: New York, N.Y., 1987; pp 203–252.

(256) Chen, Z.; Wannere, C. S.; Corminboeuf, C.; Puchta, R.; Schleyer, P. von R. Nucleus-Independent Chemical Shifts (NICS) as an Aromaticity Criterion. *Chem. Rev.* **2005**, *105* (10),

3842–3888.

(257) Heine, T.; Schleyer, P. v. R.; Corminboeuf, C.; Seifert, G.; Reviakine, R.; Weber, J. Analysis of Aromatic Delocalization: Individual Molecular Orbital Contributions to Nucleus-Independent Chemical Shifts. *J. Phys. Chem. A* **2003**, *107* (33), 6470–6475.

(258) Stanger, A. Nucleus-Independent Chemical Shifts (NICS): Distance Dependence and Revised Criteria for Aromaticity and Antiaromaticity. *J. Org. Chem.* **2006**, *71* (3), 883–893.

(259) Gomes, J. A. N. F.; Mallion, R. B. Aromaticity and Ring Currents. *Chem. Rev.* **2001**, *101* (5), 1349–1384.

(260) Lazzeretti, P. Ring Currents. *Prog. Nucl. Magn. Reson. Spectrosc.* **2000**, *36* (1), 1–88.

(261) Wannere, C. S.; Schleyer, P. von R. How Do Ring Currents Affect 1H NMR Chemical Shifts? *Org. Lett.* **2003**, *5* (5), 605–608.

(262) Zana, R. *Dynamics of Surfacatant Self-Assemblies*; Zana, R., Ed.; CRC Press: Boca Raton, FL, 2005.

(263) Fainerman, V. B.; Lylyk, S. V; Aksenenko, E. V; Petkov, J. T.; Yorke, J.; Miller, R. Surface Tension Isotherms, Adsorption Dynamics and Dilational Visco-Elasticity of Sodium Dodecyl Sulphate Solutions. *Colloids Surfaces A Physicochem. Eng. Asp.* **2010**, *354* (1–3), 8–15.

(264) Schultz, Z. D.; Levin, I. W. Vibrational Spectroscopy of Biomembranes. *Annu. Rev. Anal. Chem.* **2011**, *4* (1), 343–366.

(265) Lee, C. Raman Spectroscopy of Supported Lipid Bilayers and Membrane Proteins, University of Oxford, 2005.

(266) Iconomopoulou, S. M.; Voyiatzis, G. A. The Effect of the Molecular Orientation on the Release of Antimicrobial Substances from Uniaxially Drawn Polymer Matrixes. *J. Control. Release* **2005**, *103* (2), 451–464.

(267) Chen, Z.; Chisholm, B. J.; Stafslien, S.; He, J.; Patel, S. Novel, UV-Curable Coatings Containing a Tethered Biocide: Synthesis, Characterization, and Antimicrobial Activity. *J. Biomed. Mater. Res. A* **2010**, *95a* (2), 486–494.

(268) Paloncýová, M.; DeVane, R.; Murch, B.; Berka, K.; Otyepka, M. Amphiphilic Drug-Like Molecules Accumulate in a Membrane below the Head Group Region. *J. Phys. Chem. B* **2014**, *118* (4), 1030–1039.

(269) Feng, Z. V.; Spurlin, T. A.; Gewirth, A. A. Direct Visualization of Asymmetric Behavior in Supported Lipid Bilayers at the Gel-Fluid Phase Transition. *Biophys. J.* **2005**, *88* (3), 2154–2164.

(270) Charrier, A.; Thibaudau, F. Main Phase Transitions in Supported Lipid Single-Bilayer. *Biophys. J.* **2005**, *89* (2), 1094–1101.

(271) Csiszár, A.; Koglin, E.; Meier, R. J.; Klumpp, E. The Phase Transition Behavior of 1,2-Dipalmitoyl-Sn-Glycero-3-Phosphocholine (DPPC) Model Membrane Influenced by 2,4-Dichlorophenol--an FT-Raman Spectroscopy Study. *Chem. Phys. Lipids* **2006**, *139* (2), 115–124.

(272) Domenech, O.; Francius, G.; Tulkens, P. M.; Bambeke, F. Van; Dufrêne, Y.; Mingeot-Leclercq, M.-P. Interactions of Oritavancin, a New Lipoglycopeptide Derived from Vancomycin, with

Phospholipid Bilayers: Effect on Membrane Permeability and Nanoscale Lipid Membrane Organization. *Biochim. Biophys. Acta - Biomembr.* **2009**, *1788* (9), 1832–1840.

(273) Hicks, R. P. To Fully Exploit the Therapeutic Potential of Antimicrobial Peptides, Additional Research Is Required to Develop Improved Bacterial Lipid Membrane Model Systems. *J. Membr. Sci. Technol.* **2012**, *2* (1), e103.

(274) Heerklotz, H. Triton Promotes Domain Formation in Lipid Raft Mixtures. *Biophys. J.* **2002**, *83* (5), 2693–2701.

(275) Lichtenberg, D.; Goñi, F. M.; Heerklotz, H. Detergent-Resistant Membranes Should Not Be Identified with Membrane Rafts. *Trends Biochem. Sci.* **2005**, *30* (8), 430–436.

(276) Maghraby, G. M. M. El; Campbell, M.; Finnin, B. C. Mechanisms of Action of Novel Skin Penetration Enhancers: Phospholipid versus Skin Lipid Liposomes. *Int. J. Pharm.* **2005**, *305* (1–2), 90–104.

(277) Polefka, T. G. Surfactant Interactions with Skin. In *Handbook of Detergents*; Zoller, U., Broze, G., Eds.; Taylor & Francis Group: New York, N.Y., 1999; pp 433–468.

(278) Wertz, P. W.; Abraham, W.; Landmann, L.; Downing, D. T. Preparation of Liposomes from Stratum Corneum Lipids. *J Investig Dermatol* **1986**, *87* (5), 582–584.

(279) Veiga, M. P.; Arrondo, J. L. R.; Goñi, F. M.; Alonso, A. Ceramides in Phospholipid Membranes: Effects on Bilayer Stability and Transition to Nonlamellar Phases. *Biophys. J.* **1999**, *76* (1), 342–350.

(280) Avanti. Phase Transition Temperatures for Glycerophospholipids http://avantilipids.com/tech-support/physical-properties/phase-transition-temps/ (accessed May 12, 2016).

(281) Eis, E. *Spectroscopy of Supported Lipid Bilayers*; Durham, 2015.

(282) O'Brien, R. N.; Quon, D. Refractive Index of Some Alcohols and Saturated Hydrocarbons at 6328 A. *J. Chem. Eng. Data* **1968**, *13* (4), 517.

(283) Staykova, M.; Arroyo, M.; Rahimi, M.; Stone, H. A. Confined Bilayers Passively Regulate Shape and Stress. *Phys. Rev. Lett.* **2013**, *110* (2).

(284) Masukawa, M. K. *Protocols for Fluorescence Microscopy*; Durham, 2015.

(285) Staykova, M.; Holmes, D. P.; Read, C.; Stone, H. A. Mechanics of Surface Area Regulation in Cells Examined with Confined Lipid Membranes. *Proc. Natl. Acad. Sci.* **2011**, *108* (22), 9084–9088.

(286) Özişik, H.; Bayari, S. H.; Sağlam, S.; Angelopoulos, A.; Fildisis, T. Conformational and Vibrational Studies of Triclosan. *AIP Conf. Proc.* **2010**, *1203*, 1227–1232.

(287) *Raman Data and Analysis: Raman Bands*; Villeneuve d'Ascq, France.

(288) Richter, R. P.; Rémi Bérat; and Alain R. Brisson. Formation of Solid-Supported Lipid Bilayers: An Integrated View. *Langmuir* **2006**, *22* (8), 3497–3505.

(289) Woods, D. A.; Bain, C. D. Total Internal Reflection Spectroscopy for Studying Soft Matter. *Soft Matter* **2014**, *10* (8), 1071–1096.

(290) Fermin, D.; Riley, J. Charge in Colloidal Systems. In *Colloid Science Principals, Methods and Applications*; Cosgrove, T., Ed.; John Wiley & Sons, Ltd.: Chichester, 2010; pp 23–44.

(291) Jurkiewicz, P.; Cwiklik, L.; Vojtíšková, A.; Jungwirth, P.; Hof, M. Structure, Dynamics, and Hydration of POPC/POPS Bilayers Suspended in NaCl, KCl, and CsCl Solutions. *Biochim. Biophys. Acta - Biomembr.* **2012**, *1818* (3), 609–616.

(292) Sugiyama, T.; Adachi, T.; Masuhara, H. Crystallization of Glycine by Photon Pressure of a Focused CW Laser Beam. *Chem. Lett.* **2007**, *36* (12), 1480–1481.

(293) Eis, E. *Summary of Results from Fluorescence Microscopy Experiments, Personal Communication*; Durham, 2015.

(294) Yoon, B. K.; Jackman, J. A.; Kim, M. C.; Cho, N.-J. Spectrum of Membrane Morphological Responses to Antibacterial Fatty Acids and Related Surfactants. *Langmuir* **2015**, *31* (37), 10223–10232.

(295) Lapinski, M. M.; Castro-Forero, A.; Greiner, A. J.; Ofoli, R. Y.; Blanchard, G. J. Comparison of Liposomes Formed by Sonication and Extrusion: Rotational and Translational Diffusion of an Embedded Chromophore. *Langmuir* **2007**, *23* (23), 11677–11683.

(296) Mabrey, S.; Sturtevant, J. M. Investigation of Phase Transitions of Lipids and Lipid Mixtures by Sensitivity Differential Scanning Calorimetry. *Proc. Natl. Acad. Sci.* **1976**, *73* (11 ), 3862–3866.

(297) Petrache, H. I.; Dodd, S. W.; Brown, M. F. Area per Lipid and Acyl Length Distributions in Fluid Phosphatidylcholines Determined by 2H {NMR} Spectroscopy. *Biophys. J.* **2000**, *79* (6), 3172–3192.

(298) NHS. Staphylococcal infections http://www.nhs.uk/conditions/Staphylococcal-infections/Pages/Introduction.aspx (accessed Jan 27, 2016).

(299) Tam, N. K. M.; Uyen, N. Q.; Hong, H. A.; Duc, L. H.; Hoa, T. T.; Serra, C. R.; Henriques, A. O.; Cutting, S. M. The Intestinal Life Cycle of Bacillus Subtilis and Close Relatives . *J. Bacteriol.* **2006**, *188* (7), 2692–2700.

(300) Todar, K. Bacillus cereus Food Poisoning http://textbookofbacteriology.net/B.cereus.html (accessed Jan 21, 2016).

(301) Todar, K. Pathogenic E. Coli. In *Todar's Online Textbook of Bacteriology*; 2012; p 4.

(302) Morein, S.; Andersson, A.-S.; Rilfors, L.; Lindblom, G. Wild-Type Escherichia Coli Cells Regulate the Membrane Lipid Composition in a Window between Gel and Non-Lamellar Structures. *J. Biol. Chem.* **1996**, *271*, 6801–6809.

(303) Szabo, E. I.; Amdur, B. H.; Socransky, S. S. Lipid Composition of Streptococcus Mutans. *Caries Res.* **1978**, *12* (1), 21–27.

(304) Marcotte, L.; Barbeau, J.; Edwards, K.; Karlsson, G.; Lafleur, M. Influence of the Lipid Composition on the Membrane Affinity, and the Membrane-Perturbing Ability of Cetylpyridinium Chloride. *Colloids Surfaces A Physicochem. Eng. Asp.* **2005**, *266* (1–3), 51–61.

(305) Cheng, J. T. J.; Hale, J. D.; Elliott, M.; Hancock, R. E. W.; Straus, S. K. The Importance of Bacterial Membrane Composition in the Structure and Function of Aurein 2.2 and Selected Variants. *Biochim. Biophys. Acta - Biomembr.* **2011**, *1808* (3), 622–633.

(306) Suárez-Germà, C.; Montero, M. T.; Ignés-Mullol, J.; Hernández-Borrell, J.; Domènech, Ò. Acyl Chain Differences in Phosphatidylethanolamine Determine Domain Formation and LacY Distribution in Biomimetic Model Membranes. *J. Phys. Chem. B* **2011**, *115* (44), 12778–12784.

(307) Suárez-Germà, C.; Morros, A.; Montero, M. T.; Hernández-Borrell, J.; Domènech, Ò. Combined Force Spectroscopy, AFM and Calorimetric Studies to Reveal the Nanostructural Organization of Biomimetic Membranes. *Chem. Phys. Lipids* **2014**, *183* (0), 208–217.

(308) Seeger, H. M.; Marino, G.; Alessandrini, A.; Facci, P. Effect of Physical Parameters on the Main Phase Transition of Supported Lipid Bilayers. *Biophys. J.* **2009**, *97* (4), 1067–1076.

(309) Picas, L.; Montero, M. T.; Morros, A.; Cabañas, M. E.; Seantier, B.; Milhiet, P.-E.; Hernández-Borrell, J. Calcium-Induced Formation of Subdomains in Phosphatidylethanolamine−Phosphatidylglycerol Bilayers: A Combined DSC, 31P NMR, and AFM Study. *J. Phys. Chem. B* **2009**, *113* (14), 4648–4655.

(310) Kershner, R. J.; Joseph W. Bullard; Michael J. Cima. Zeta Potential Orientation Dependence of Sapphire Substrates. *Langmuir* **2004**, *20* (10), 4101–4108.

(311) Brown, D. A.; London, E. Structure of Detergent-Resistant Membrane Domains: Does Phase Separation Occur in Biological Membranes? *Biochem. Biophys. Res. Commun.* **1997**, *240* (1), 1–7.

(312) Maulik, P. R.; Sripada, P. K.; Shipley, G. G. Structure and Thermotropic Properties of Hydrated N-Stearoyl Sphingomyelin Bilayer Membranes. *Biochim. Biophys. Acta - Biomembr.* **1991**, *1062* (2), 211–219.

(313) Products Containing Triclosan http://www.beyondpesticides.org/programs/antibacterials/triclosan/products-containing-triclosan (accessed Jan 21, 2016).

(314) A List of Products Containing Triclosan. *The Buffalo News*. Buffalo October 2, 2015.

# 7 Information Tables

## 7.1 Molecular Weights

Table 7.1 Molecular weights of the chemicals used in this thesis

| Substance | Molecular weight/ g $mol^{-1}$ |
|---|---|
| TC | 289.54 |
| SDS | 288.38 |
| SL | 222.3 |
| NaOH | 40.0 |
| HCl | 36.46 |
| NaOAc | 82.03 |
| NaCl | 58.44 |
| $Na_2CO_3$ | 105.99 |
| $NaHCO_3$ | 84.0 |
| Tris-base | 121.14 |
| KOH | 56.11 |
| $CaCl_2$ | 110.98 |
| HEPES | 238.30 |
| KCl | 74.55 |
| POPC | 960.07 |
| DMPC | 677.93 |
| Rh-DPPE | 1249.64 |
| POPE | 717.996 |
| POPG | 770.989 |
| Sphingomeylin | 656.505 |
| Cholesterol | 400.637 |

## 7.2 Conversion Tables

Table 7.2 Conversions of the concentration of TC between wt % in water, mg/ml and mol $dm^{-3}$

| Concentration of TC/ wt % | Concentration of TC/ mg/ml | Concentration of TC/ mol $dm^{-3}$ |
|---|---|---|
| 0.1 | 1 | 0.0035 |
| 0.05 | 0.5 | 0.0017 |
| 0.01 | 0.1 | 0.00035 |
| 0.005 | 0.05 | 0.00017 |
| 0.001 | 0.01 | $3.5 \times 10^{-5}$ |

Table 7.3 Conversions of the concentration of SDS between wt % in water, mg/ml and mol $dm^{-3}$

| Concentration of SDS/ wt % | Concentration of SDS/ mg/ml | Concentration of SDS/ mol $dm^{-3}$ |
|---|---|---|
| 2 | 20 | 0.069 |
| 1.5 | 15 | 0.052 |
| 1 | 10 | 0.035 |
| 0.75 | 7.5 | 0.026 |
| 0.5 | 5 | 0.017 |
| 0.25 | 2.5 | 0.0087 |
| 0.1 | 1 | 0.0035 |
| 0.05 | 0.5 | 0.0017 |
| 0.01 | 0.1 | 0.00035 |

Table 7.4 Conversions of the concentration of SL between wt % in water, mg/ml and mol $dm^{-3}$

| Concentration of SL/ wt % | Concentration of SL/ mg/ml | Concentration of SL/ mol $dm^{-3}$ |
|---|---|---|
| 2 | 20 | 0.090 |
| 1.5 | 15 | 0.067 |
| 1 | 10 | 0.045 |
| 0.75 | 7.5 | 0.034 |
| 0.5 | 5 | 0.022 |
| 0.25 | 2.5 | 0.011 |
| 0.1 | 1 | 0.0045 |
| 0.05 | 0.5 | 0.0022 |
| 0.01 | 0.1 | 0.00045 |

# 8 Appendix

## 8.1 Introduction

### 8.1.1 Products sold in the U.S. containing TC

In October 2015, a list of TC containing products was produced by Beyond Pesticides[313] and reported on by local news sources.[314] The list contained:

**Soap:** Dial Liquid Soap; Softsoap Antibacterial Liquid Hand Soap; Tea Tree Therapy Liquid Soap; Provon Soap; Clearasil Daily Face Wash; Dermatologica Skin Purifying Wipes; Clean & Clear Oil Free Foaming Facial Cleanser; DermaKleen Antibacterial Lotion Soap; Naturade Aloe Vera 80 Antibacterial Soap; CVS Antibacterial Soap, pHisoderm Antibacterial Skin Cleanser, Dawn Complete Antibacterial Dish Liquid, Ajax Antibacterial Dish Liquid.

**Dental Care:** Colgate Total; Breeze TC Mouthwash; Reach Antibacterial Toothbrush; Janina Diamond Whitening Toothpaste

**Cosmetics:** Supre Café Bronzer; TotalSkinCare Makeup Kit; Garden Botanika Powder Foundation; Mavala Lip Base; Jason Natural Cosmetics; Blemish Cover Stick; Movate Skin Litening Cream HQ; Paul Mitchell Detangler Comb, Revlon ColorStay LipSHINE Lipcolor Plus Gloss, Dazzle

**Deodorant:** Old Spice High Endurance Stick Deodorant, Right Guard Sport Deodorant, Queen Helene Tea Tree Oil Deodorant and Aloe Deodorant; Nature De France Le Stick Natural Stick Deodorant; DeCleor Deodorant Stick; Epoch Deodorant with Citrisomes; X Air Maximum Strength Deodorant

**Personal products:** Gillette Complete Skin Care MultiGel Aerosol Shave Gel; Murad Acne Complex Kit; Diabet-x Cream; T.Taio sponges and wipes, Aveeno Therapeutic Shave Gel.

**First aid:** SyDERMA Skin Protectant plus First Aid Antiseptic; Solarcaine First Aid Medicated Spray; Nexcare First Aid, Skin Crack Care; First Aid/Burn Cream. HealWell Night Splint; 11-1X1: Universal Cervical Collar with Microban

**Kitchenware:** Farberware Microban Steakknife Set and Cutting Boards; Franklin Machine Products FMP Ice Cream Scoop SZ 20 Microban; Hobart Semi-Automatic Slicer; Chix Food Service Wipes with Microban; Compact Web Foot Wet Mop Heads

**Computer equipment:** Fellowes Cordless Microban Keyboard and Microban Mouse Pad

**Clothes:** Teva Sandals; Merrell Shoes; Sabatier Chef's Apron; Dickies Socks; Biofresh socks

**Children's toys:** Playskool: Stack 'n Scoop Whale, Rockin' Radio, Hourglass, Sounds Around Driver, Animal Sounds Phone, Busy Beads Pal, Pop 'n Spin Top, Lights 'n Surprise Laptop

**Other:** Bionare Cool Mist Humidifier; Microban All Weather Reinforced Hose; Thomasville Furniture; Deciguard AB Ear Plugs; Bauer 5000 Helmet; Aquatic Whirlpools; Miller Paint Interior Paint; QVC Collapsible 40-Can Cooler; Holmes Foot Buddy Foot Warmer; Blue Mountain Wall Coverings; California Paints.; EHC AMRail Escalator Handrails; Dupont Air Filters; Durelle Carpet Cushions; Advanta One Laminate Floors; San Luis Blankets; J Cloth towels; JERMEX mops

## 8.2 Additional information for Chapter 2

### 8.2.1 SANS fitting parameters and fits

Table 8.1 Fitting paramters for SANS data

| SDS | 2 | 1.98 | 1.9 | 1.8 |
|---|---|---|---|---|
| TC | 0 | 0.02 | 0.1 | 0.2 |
| Radius of the inner core (nm) | 16.7 ±0.5 | 17.5 ±0.5 | 15.9 ±0.5 | 21.1 ±0.5 |
| Total radius (nm) | 18.6 ±0.5 | 21.1 ±0.5 | 17.9 ±0.5 | 41.3 ±0.5 |
| Nagg | 120 ±10 | 120 ±10 | 150 ±10 | 600 ±60 |
| electronic charge per micelle (e) | 7.9 | 7.3 | 5 | 11 |
| Ellipticity | 1.21 | 1.17 | 1.31 | 1.02 |
| fract oil | 0 | 0.007 | 0.063 | 0.15 |
| polydispersity | 0.1 | 0.1 | 0.1 | 0.15 |
| core ext | 1 | 1.05 | 0.95 | 1.6 |
| chi squared | 0.203 | 0.449 | 0.174 | 0.322 |
| SF | 0.967 | 0.948 | 0.89 | 0.94 |
| hydration | 2 | 6 | 3 | 12 |

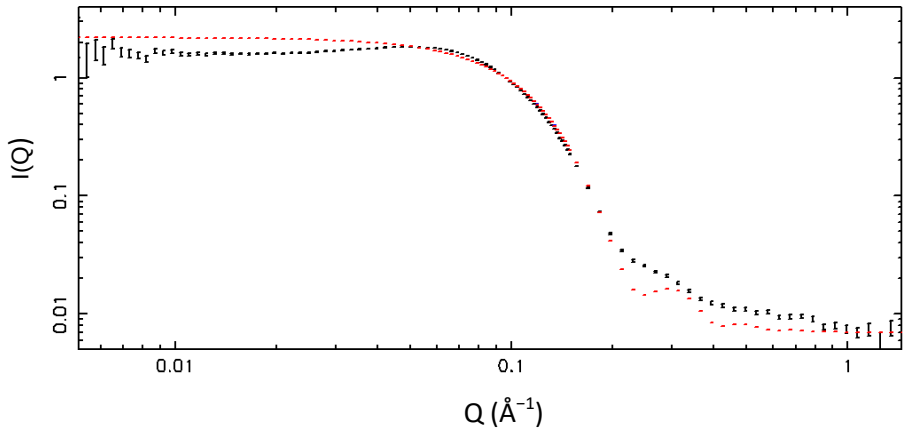


Figure 8.1 Scattering intensity I (Q) in cm$^{-1}$ of 1.98% SDS, 0.02% TC in 0.1 M NaCl, 0.01 M NaOAc (black) against wave vector transfer, Q in Å$^{-1}$ and fitting (red)

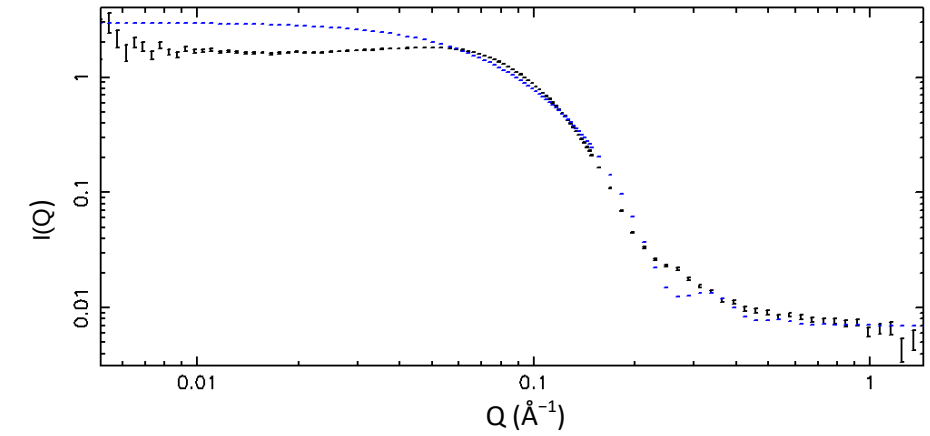


**Figure 8.2 Scattering intensity I (Q) in cm$^{-1}$ of 1.9% SDS, 0.1% TC in 0.1 M NaCl, 0.01 M NaOAc (black) against wave vector transfer, Q in Å$^{-1}$ and fitting (blue)**

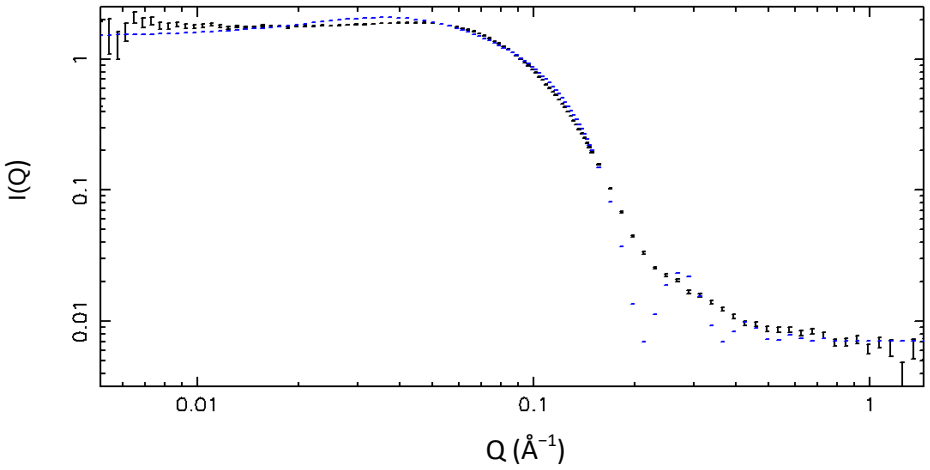


**Figure 8.3 Scattering intensity I (Q) in cm$^{-1}$ of 1.8% SDS, 0.2% TC in 0.1 M NaCl, 0.01 M NaOAc (black) against wave vector transfer, Q in Å$^{-1}$ and fitting (blue)**

### 8.2.2 UV-Vis spectra

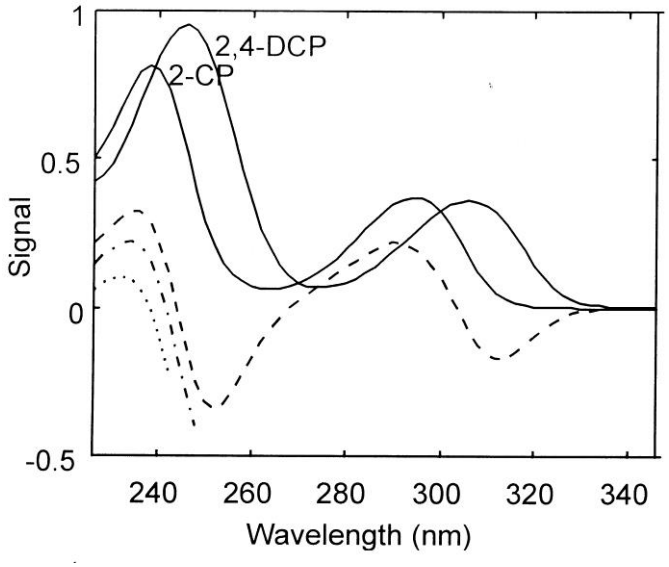


Figure 8.4 Absorbance spectra of 2,4- DCP and 2-chlorophenol (2-CP) in water. Reprinted with permission from Ferré 1998. Copyright 1998 American Chemical Society.[238]

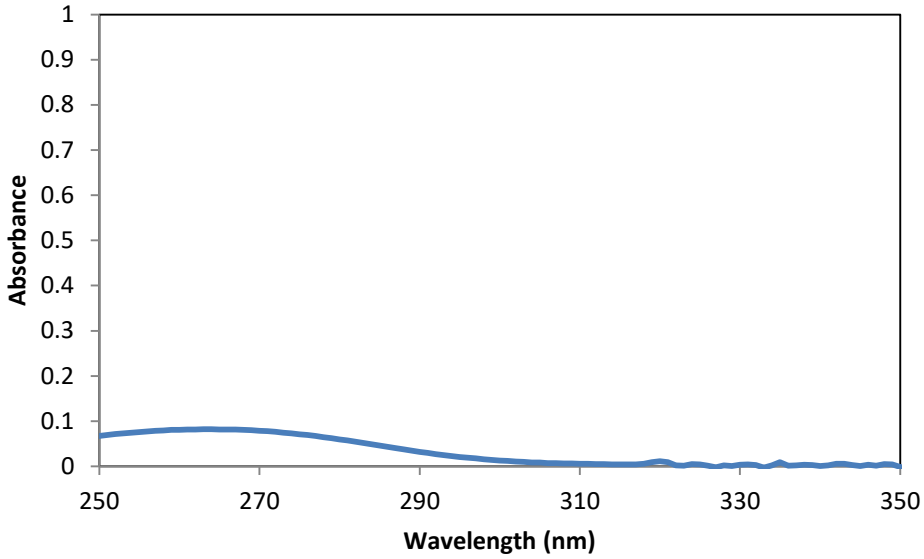


Figure 8.5 Absorbance (A) against wavelength (λ) in nm $C_{12}$TAB at 1 % (blue). Cuvette pathlength was 10 mm.

### 8.2.3 Stopped flow data

Stopped flow analysis was carried out on solutions of TC in surfactant. When these solutions were diluted 50:50 in water, changes in absorbance were observed with time, over about 90 s. As discussed in Section 2.3.4, the movement of surfactant between the bulk and micelles, including complete dissociation and formation of micelles, is less than a second and tends to be between 1 $x10^{-6}$- 1 $x10^{-3}$ s. The process observed as taking around 90 s is most likely to an effect of TC moving out of the micelles into solution, crystallising and crashing out, but requires further investigation.

The absorbance at the maximum was followed and where appropriate, the absorbance at 320 nm was subtracted to account for the increase in absorbance due to scattering. The spectra changed shape with time in different ways when SL was used as compared to SDS (Figure 2.25). The effect will

mostly be due to the pH, which is much higher for the SL solution. When looking at Figure 8.6, there is a difference in the behaviour of the sample where TC is in a 1:30 ratio (0.03% TC) and the other samples where TC is at other ratios that are higher and lower than 1:30. The sample with 0.05% TC (1:20 ratio) is shown for comparison, with the other plots in Figure 8.7. The shape of the change in absorbance remained the same even when fresh samples are made up and tested on different days. From this, there appears to actually be three different types of behaviour. One where there is an initial increase in *A* and then a decrease, another that is the opposite and finally where there is no peak in absorbance with time and just a smooth increase. It may even be that there is a continuum between the behaviour for the 0.03% TC sample above and the behaviour at lower concentrations shown in Figure 8.6.

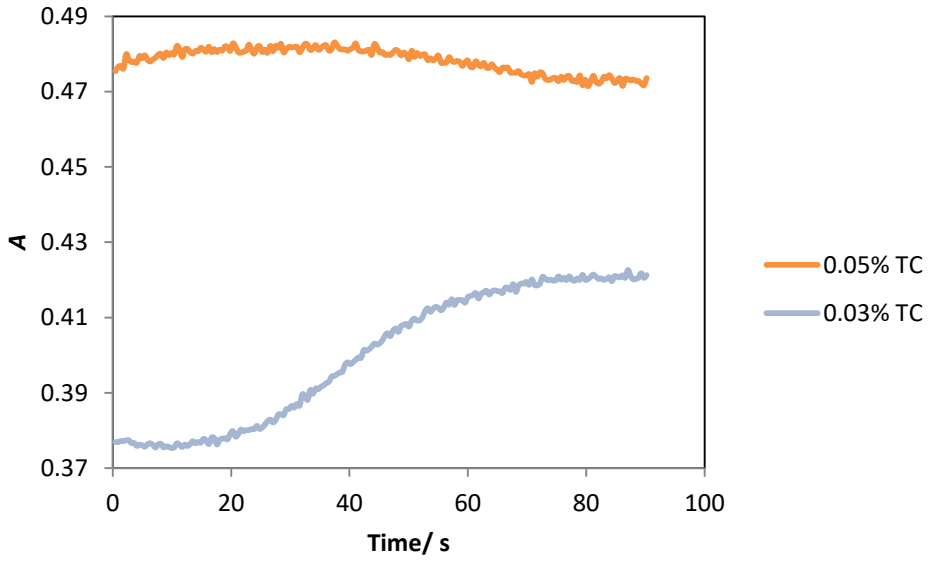


**Figure 8.6 Absorbance (*A*) at 281 nm with the absorbance at 320 nm subtracted against time (s) for samples with 1% SDS and different amounts of TC.**

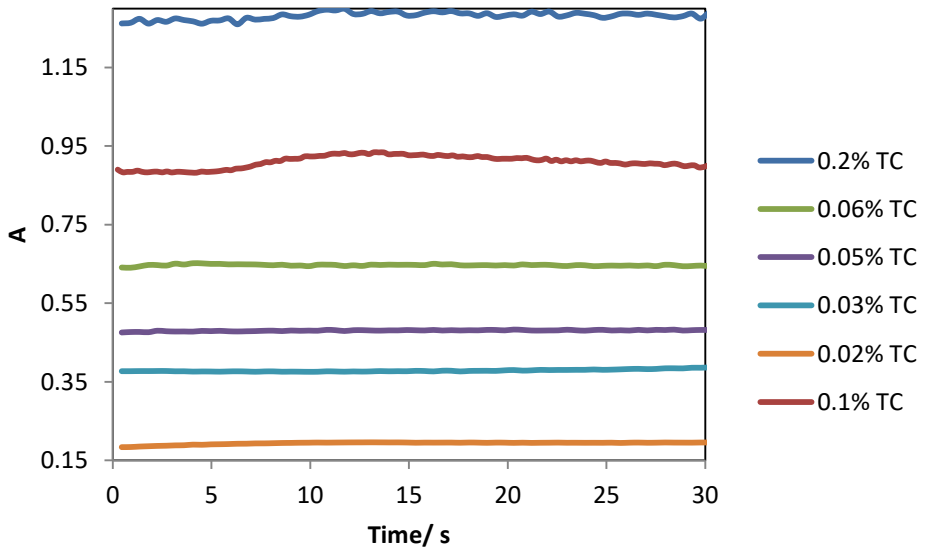


**Figure 8.7 Absorbance (A) at 281 nm with the absorbance at 320 nm subtracted against time (s) for samples with 1% SDS and different amounts of TC.**

When the weight ratio of TC: Surfactant is kept constant in the SDS system at 1:10, similar curves are observed for samples with 1% SDS and 0.5% SDS, but none is apparent for 0.25% SDS (Figure 8.8). Both of these samples remain above the CMC when diluted. It could be that the absorbance of 0.25% is too low to see any detail outside of the errors of the equipment. When the ratio of TC: SL is fixed at 1:10, the curves for samples with SL at 1% and 0.75% are similar, with just an increase in A (Figure 8.9). For 0.5% SL the curve is more similar to 1% SDS, 0.05% TC. For 0.25% SL, the behaviour is different again. This will be because the only TC in the solution is $TC^-_{aq}$ as 0.25% is below the CMC SL.

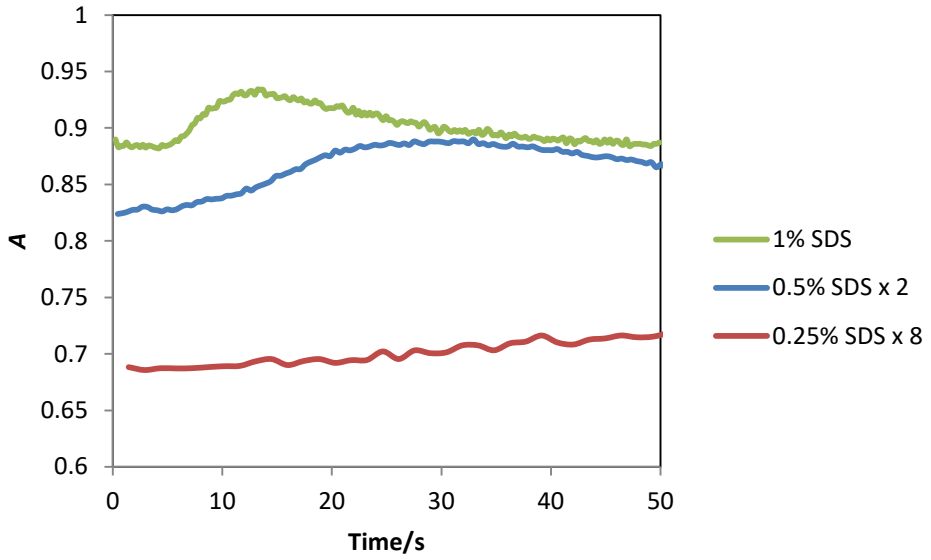


**Figure 8.8 Absorbance (*A*) at 281 nm with the absorbance at 320 nm subtracted against time (s) for samples where the ratio of TC: SDS is fixed at 1:10. The samples with 0.5% and 0.25% SDS have been multiplied by a factor of 2 and 8 respectively for ease of comparison.**

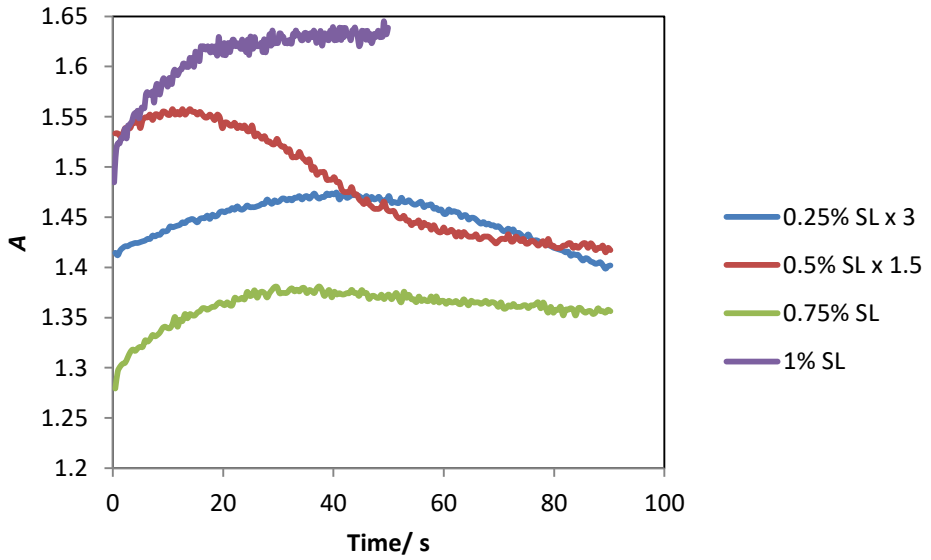


**Figure 8.9 Absorbance (*A*) at 293 nm against time (s) for samples where the ratio of TC: SL is fixed at 1:10. The curves for 0.25% SL and 0.5% SL have been multiplied by appropriate factors for ease of comparison.**

An experiment was also carried out where the concentration of TC was fixed and the concentration of surfactant varied. The traces of absorbance with time were very different with the different concentrations of surfactant (Figure 8.10 and Figure 8.11)

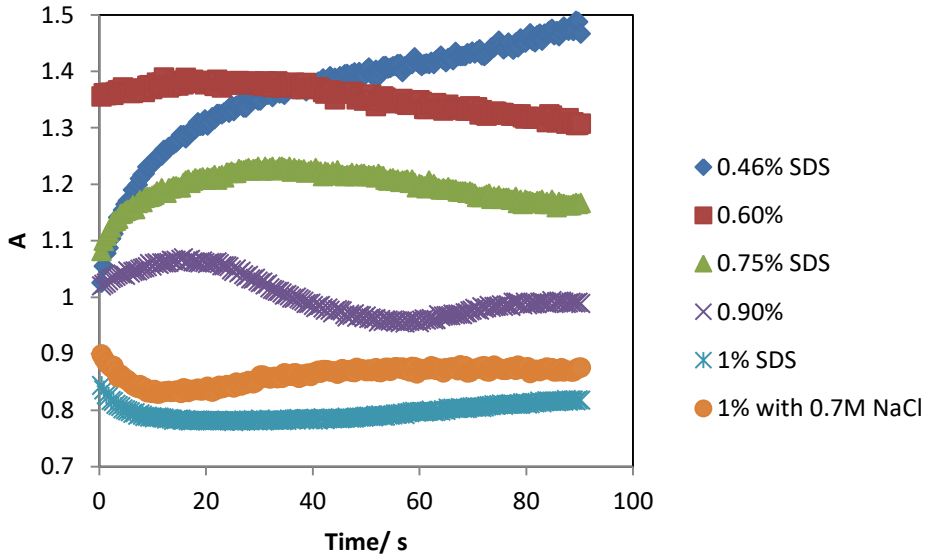


**Figure 8.10 Absorbance (A) at 281nm against time (s) for samples of SDS and TC (0.1%) upon dilution with an equal amount of water. Slit width 1mm.**

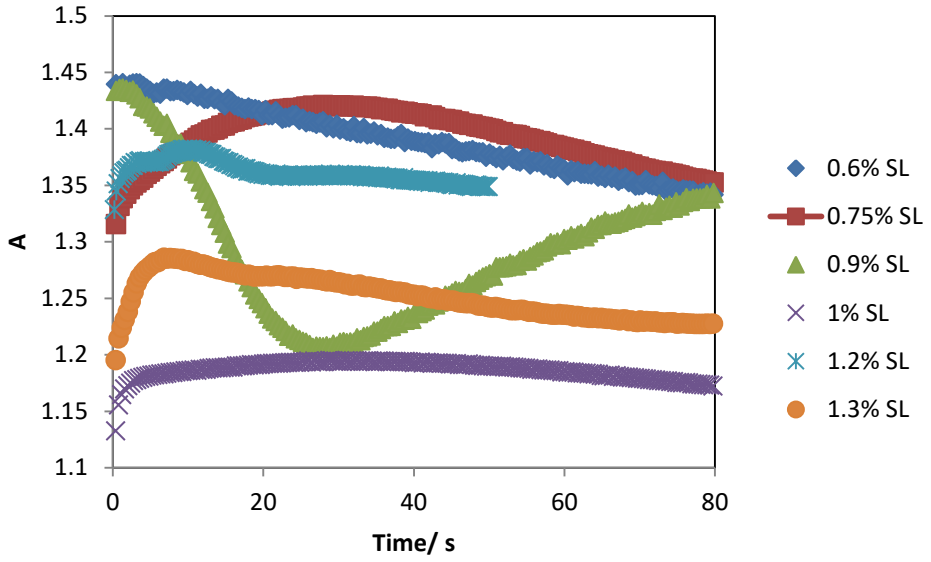


**Figure 8.11 Absorbance (A) at 293 nm against time (s) for samples of SL and TC (0.1%) with mixing. Slit width 1 mm.**

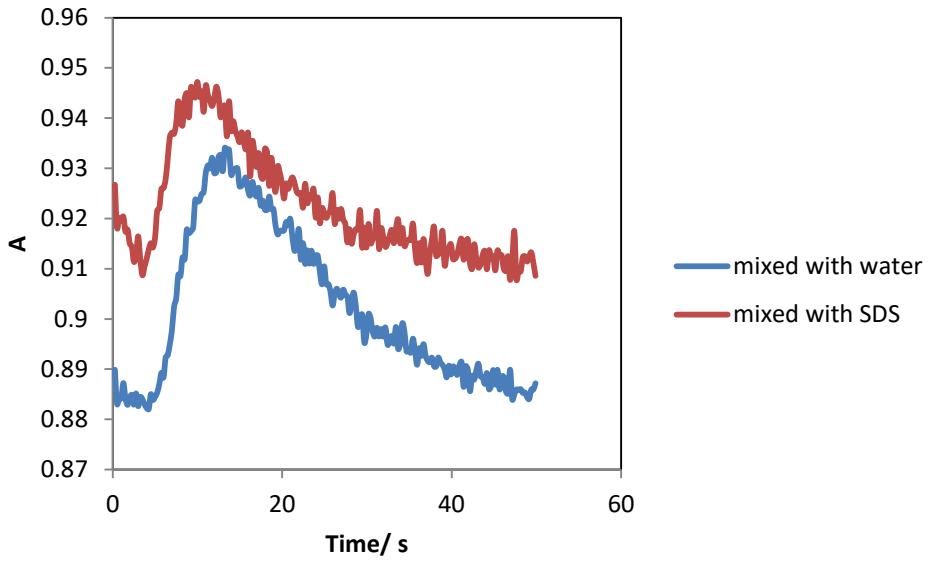


**Figure 8.12 Absorbance (A) at 281 nm with the absorbance at 320 nm subtracted against time (s) for samples with 1% SDS and 0.1% TC equally mixed with either 1% SDS or water.**

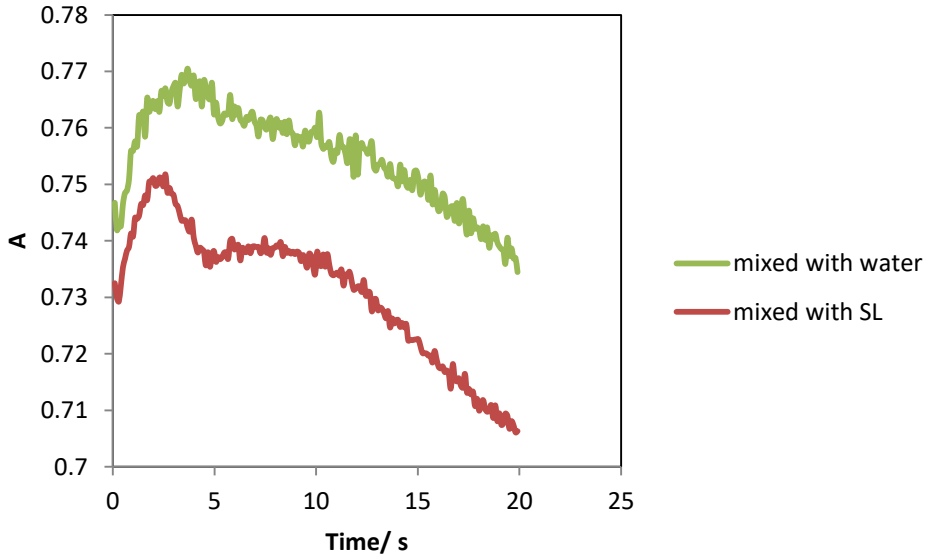


**Figure 8.13 Absorbance (A) at 293 nm against time (s) for samples with 1% SL and 0.05% TC equally mixed with either 1% SL or water**

A few comparisons were carried out when mixing samples with 1% surfactant instead of water, and the trace of absorbance with time. The change in absorption with time was very similar for samples when mixed with either surfactant or water. For 1% SDS, 0.1% TC, when mixed with SDS, the change in absorbance looks nearly identical to mixing with water (Figure 8.12). The main difference is that $A_{max}$-$A_{min}$ is smaller. For 1% SL, 0.05% TC the plots of A with time for samples mixed with either 1% SL or water almost overlay (Figure 8.13). Any difference is more likely due to errors in the experiment rather than different kinetic processes taking place. Surely the TC should equilibrate at a rate faster than can be observed if the rate of transfer between micelle and the bulk is faster than the NMR timescale (see Section 3.3.1).

These results are very much an initial study and a number of factors need to be taken into account before any detailed analysis can take place. Firstly, the reproducibility of this method needs to be improved. A certain amount of scattering will occur in the samples that turn cloudy as the TC crashes out, which should be taken into account. It will be useful to compare this to the UV-Vis spectra of solid TC. Secondly, these data appears to capture a wide variety of different situations and needs to be manipulated so that the individual circumstances can be understood.

After this, models can be developed as to what happens when the TC containing micelles are diluted, both above and below the CMC. For example, it is probable that TC will move between micelles and may form supersaturated micelles before crashing out of solution. This will most likely effect how TC is deposited on the skin, where it will most likely be either as small particulates or as individual molecules.

### 8.2.4 Nanosight analysis of SDS and TC solutions

The particle distribution of SDS and TC samples were studied over several hours after dilution and no great change was seen in any of the dilutions, for example (Figure 8.14).

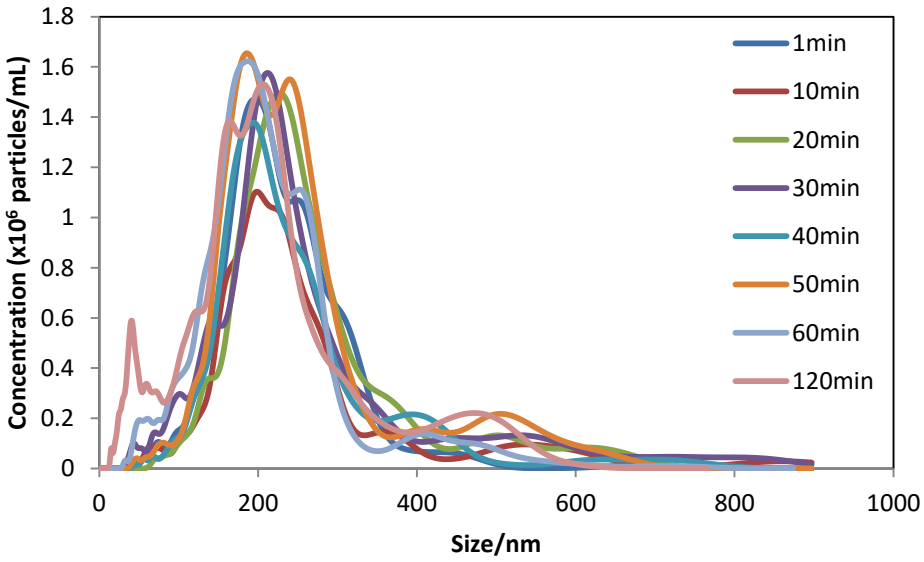


**Figure 8.14 Concentration of particles (x10$^6$/ ml) against particle size in nm for samples of 0.5% SDS, 0.05% TC at certain times after dilution. Each curve is an average of 3 separate measurements.**

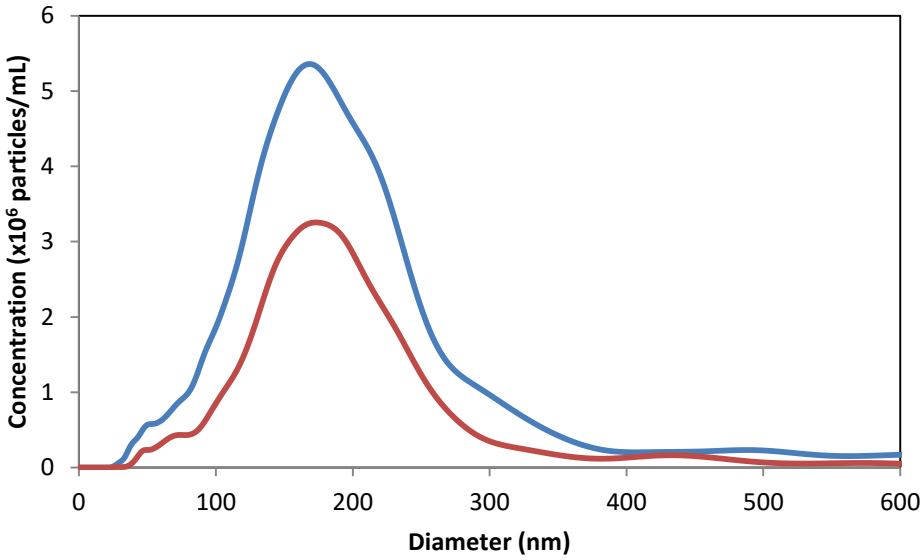


**Figure 8.15 Concentration of particles (x10$^6$/ml) against diameter (nm) for samples with different concentrations of SDS when the molar ratio of SDS: TC is 10:1. The samples have concentrations just above (0.14%, blue) and below (0.1% red) the CMC (0.119%). For the sample with 0.14% SDS, the average was 225 nm, the mode was 168 nm and the concentration was 852 x10$^6$ particles per ml. For the sample with 0.1% SDS, the average was 210 nm, the mode was 168 nm and the concentration was 455 x10$^6$ particles per ml.**

## 8.3 TIR-Raman code

### 8.3.1 Background subtract

```
% A function that subtracts reference background from spectrum of interest.
% Output spectra is given as wavenumber against counts per second.

function [newD]=backgroundsubtract(d,bg)
bg=[bg(:,1),bg(:,2)-min(bg(:,2))];            % Subtracts baseline of
reference background
d=[d(:,1),d(:,2)-min(d(:,2))];                % Subtract baseline of spectra
of interest
f=max(bg(:,2))/max(d(:,2));                   % Finds correction factor
using the water band
f=[1,f];
f=diag(f);
data=d*f;
newD=[data(:,1),data(:,2)-bg(:,2)];           % Includes wavenumber in
output spectra.

newD=[newD(:,1),newD(:,2)./120];              % converts to counts per s

figure(1)
plot(newD(:,1),newD(:,2),'k','LineWidth',1.5)

end
```

### 8.3.2 Background subtract using the silica and water peak

```
A function that subtracts reference background from spectrum of interest.
% Output spectra is given as wavenumber against counts per second.

function [newD]=silicasubtract(d,bg)
```

```
bg=[bg(:,1),bg(:,2)-min(bg(:,2))];            % Subtracts baseline of
reference background
d=[d(:,1),d(:,2)-min(d(:,2))];                % Subtract baseline of spectra
of interest
f=(bg(336, 2))/max(d(336, 2));                   % Finds correction factor
using the intensity of silica band at 1550 cm^-1
f=[1,f];
f=diag(f);
data=d*f;
newD=[data(:,1),data(:,2)-bg(:,2)];           % Includes wavenumber in
output spectra.

newD=[newD(:,1),newD(:,2)./300];

figure(1)
plot(newD(:,1),newD(:,2),'k','LineWidth',1.5)

end
```

### 8.3.3 Fluorescence removal

```
% A function that subtracts fluorescence background from spectrum of
interest.
% Output spectra is given as wavenumber against counts per second.

function [newD]=fluoremove(d)

mdl= LinearModel.fit(d(2:152,1), d(2:152, 2));            % Finds effect of
fl on flat part of spectra
m= mdl.Coefficients{2,1};                % extracts gradient of fit
c= mdl.Coefficients{1,1};                  % extracts intercept
bg=[d(:,1), d(:,1)*m+c];                % creates bg from fl

newD=[d(:,1),d(:,2)-bg(:,2)];           % removes fl bg from data


figure(1)
plot(newD(:,1),newD(:,2),'k','LineWidth',1.5)

end
```

## 8.4 Fluorescence microscopy data

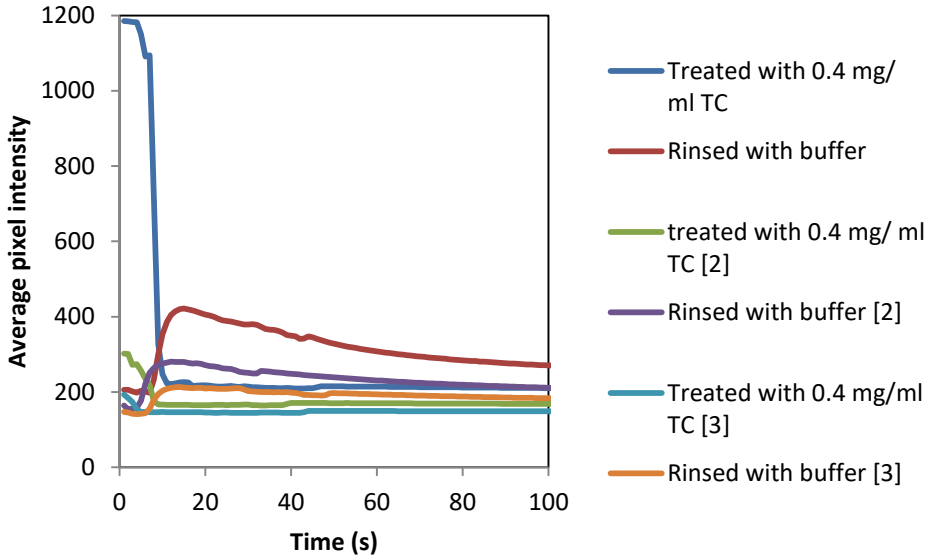


**Figure 8.16 Intensity of fluorescence (mean pixel intensity across the image) against time in s of a POPC Lipid bilayer with 1 mol % Rh-DPPE treated with 0.4 mg/ml TC (blue), and rinsed with buffer after being treated (red). The treatment and rinse was repeated twice more (green and purple), (light blue and orange).**

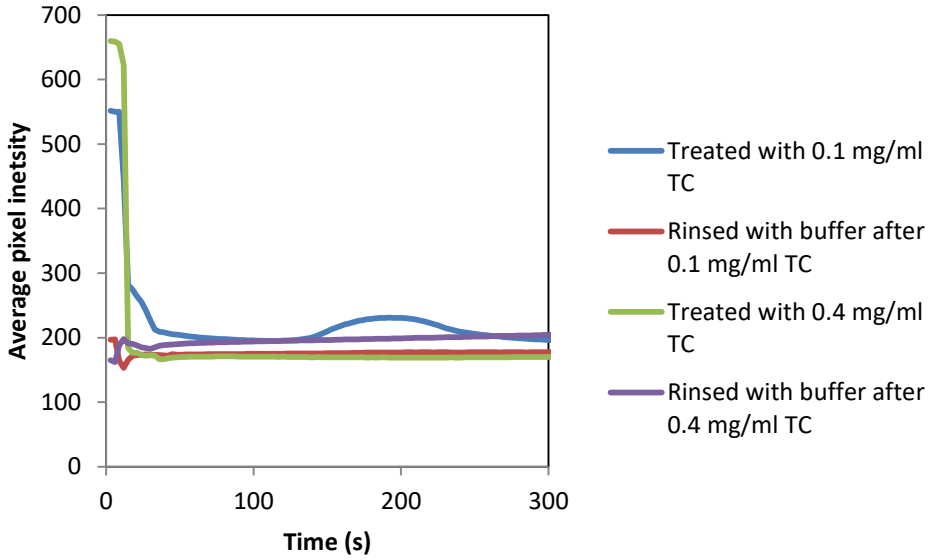


**Figure 8.17 Intensity of florescence (mean pixel intensity across the image) against time in s of a 3:1 POPE/POPG Lipid bilayer with 1 mol % Rh-DPPE treated with 0.1 mg/ml TC (blue), and rinsed with buffer after being treated (red). A fresh bilayer was treated with 0.4 mg/ml TC (green) and rinsed with buffer**

The effect of photobleaching on the fluorescent dye, Rh-DPPE, used in the microscopy experiments was investigated in a DMPC bilayer. Measurements were taken every 3 s for 2 minutes and the fluorescence decreased linearly with the number of images taken. There was no flow of buffer through the cell during this experiment. The expected change in fluorescence intensity during the experiment with 0.1 mg/ml TC and POPC (Figure 4.44), based on the initial intensity of the bilayer before treatment for the 3 experiments carried out overlay the fluorescence intensity plots in Figure

8.20. The change in fluorescence intensity caused by photobleaching is very small compared to the change in intensity caused by TC insertion into the cell.

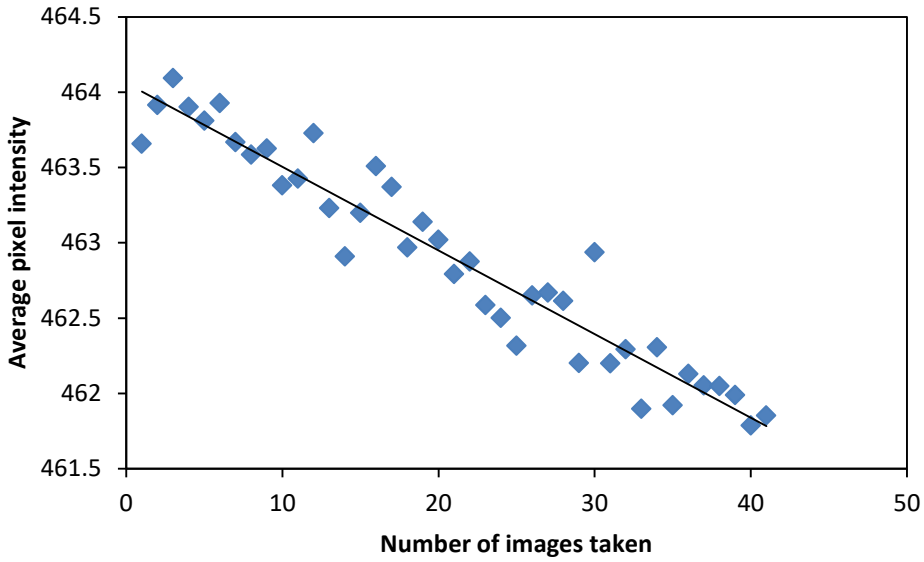


**Figure 8.18 Intensity of florescence (mean pixel intensity across the image) against number of images taken of a DMPC Lipid bilayer with 1 mol % Rh-DPPE**

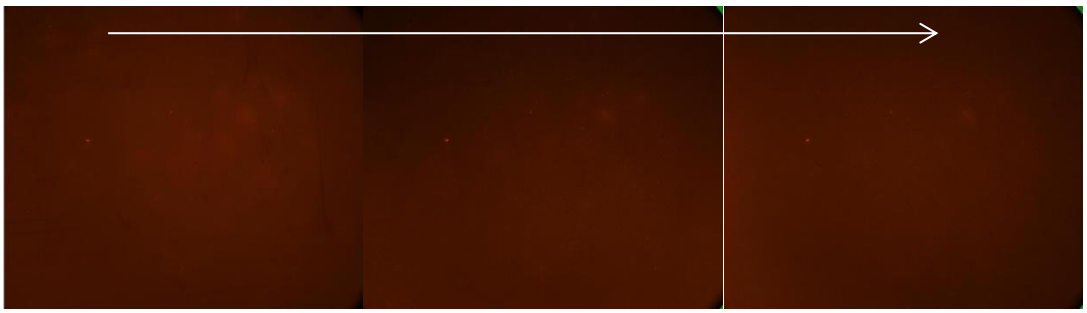

**Figure 8.19 Images of the bilayer treated with 0.1 mg/ mL TC arrow show the experimental progress**

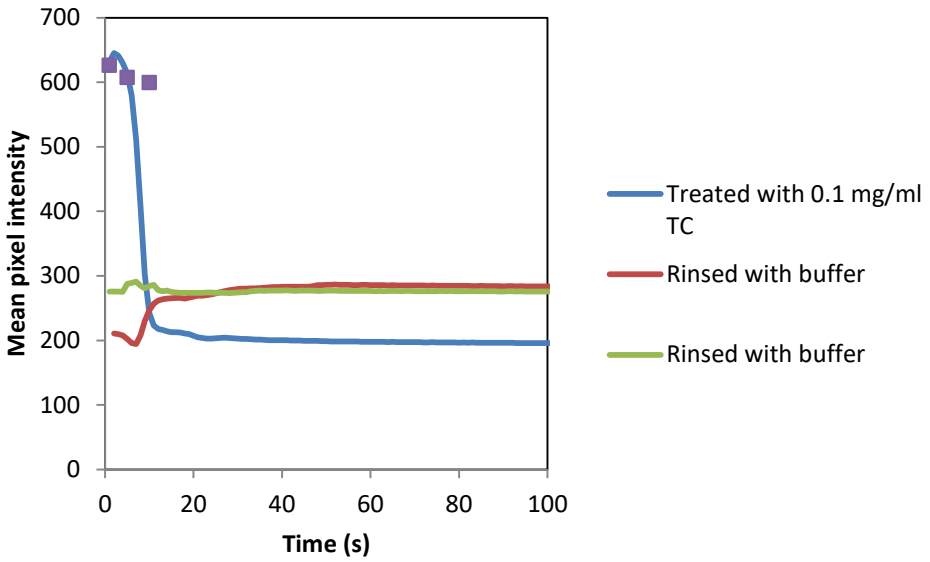


**Figure 8.20 Intensity of fluorescence (mean pixel intensity across the image) against time in s of a POPC Lipid bilayer with 1 mol % Rh-DPPE treated with 0.1 mg/ml TC (blue), and rinsed with pH 7.4 buffer after being treated (red). The bilayer was rinsed with a further half ml of buffer (green).**